LIQUID-PHASE ADSORPTION OF N-PARAFFINS ON TYPE 5A MOLECULAR SIEVES

by

JASEM AHMAD MOHAMAD ALI

Doctor of Philosophy

THE UNIVERSITY OF ASTON IN BIRMINGHAM

DECEMBER 1987

TO

MY PARENTS

MY WIFE

AND MY CHILDREN

THE UNIVERSITY OF ASTON IN BIRMINGHAM

Liquid-Phase Adsorption of n-Paraffins on Type 5A Molecular Sieves

Jasem Ahmad Mohamad Ali

Doctor of Philosophy 1987

SUMMARY

As a basis for the commercial separation of normal paraffins a detailed study has been made of factors affecting the adsorption of binary liquid mixtures of high molecular weight normal paraffins (C_{12}, C_{16}, and C_{20}) from isooctane on type 5A molecular sieves.

The literature relating to molecular sieve properties and applications, and to liquid-phase adsorption of high molecular weight normal paraffin compounds by zeolites were reviewed.

Equilibrium isotherms were determined experimentally for the normal paraffins under investigation at temperatures of 303°K, 323°K and 343°K and showed a non-linear, favourable- type of isotherm. A higher equilibrium amount was adsorbed with lower molecular weight normal paraffins. An increase in adsorption temperature resulted in a decrease in the adsorption value. Kinetics of adsorption were investigated for the three normal paraffins at different temperatures. The effective diffusivity and the rate of adsorption of each normal paraffin increased with an increase in temperature in the range 303 to 343 K. The valuesof activation energy were between 2 and 4 kcal/mole.

The dynamic properties of the three systems were investigated over a range of operating conditions (i.e. temperature, flow rate, feed concentration, and molecular sieve size in the range 0.032×10^{-3} to 2×10^{-3}m) with a packed column. The heights of adsorption zones calculated by two independent equations (one based on a constant width, constant velocity adsorption zone and the second on a solute material balance within the adsorption zone) agreed within 3% which confirmed the validity of using the mass transfer zone concept to provide a simple design procedure for the systems under study. The dynamic capacity of type 5A sieves for n-eicosane was lower than for n-hexadecane and n-dodecane corresponding to a lower equilibrium loading capacity and lower overall mass transfer coefficient. The values of individual external, internal, theoretical and experimental overall mass transfer coefficient were determined. The internal resistance was in all cases rate-controlling.

A mathematical model for the prediction of dynamic breakthrough curves was developed analytically and solved from the equilibrium isotherm and the mass transfer rate equation.

The experimental breakthrough curves were tested against both the proposed model and a graphical method developed by Treybal. The model produced the best fit with mean relative percent deviations of 26, 22, and 13% for the n-dodecane, n-hexadecane, and n-eicosane systems respectively.

KEY WORDS:

Molecular sieve Type 5A, Normal paraffins, Adsorptive separation

ACKNOWLEDGEMENTS

The author wishes to express his deepest gratitude and sincere thanks to Professor GV Jeffreys and Dr CJ Mumford for their supervision, encouragement, valuable guidance, continual help and constructive criticism throughout the course of this work.

Particular gratitude and thanks to Dr RS Al-Ameeri for his kind supervision and help throughout this study.

The author also wishes to thank Dr Abu-Bakr Salem and Dr F Owaysi for their encouragement to start this work.

Special thanks and appreciation to Mr Othman Al-Amree and the entire staff of the Research Laboratory in Kuwait University.

Sincere gratitude and thanks to Dr Sulaiman Shamsodeen and Mr F Mijaly for their help and encouragement.

CONTENTS

PAGE

LIST OF FIGURES

LIST OF TABLES

CHAPTER 1

INTRODUCTION

1.1 INTRODUCTION

Normal paraffins are saturated straight chain hydrocarbons produced mainly from petroleum and natural gas for a variety of applications. Pure normal paraffins in the range C_5 to C_7 are used as solvents. High purity n-paraffins extracted from kerosene (C_7 - C_{12}) find their major uses in biodegradable detergents manufacture, while some are chlorinated and used in several industries e.g. as fire retardents. They also serve as raw material for production of plasticizers, alcohols, fatty acids, and single cell protein. Moreover, paraffin waxes have many applications in different fields.

The normal paraffins are generally available as a mixture blended with other groups of hydrocarbons such as isoparaffins, aromatics, and naphthenes which need to be separated to produce pure normal paraffins, improved octane number gasoline, lube oils of reduced pour point, or dewaxed oils of improved quality. The separation of high molecular weight n-paraffins is therefore a process of considerable commercial importance.

The common techniques used for separation of normal paraffins are urea adduction and molecular sieve adsorption. Other separation methods include fractional distillation, fractional crystallization, elution chromatography, and thin layer chromatography. The choice of one of these methods depends on the type of feed, specifications of the products and other factors which may affect the preference for one of the separation methods.

The recovery of normal paraffins by adsorption on molecular sieves has

become one of the most widely used separation techniques. These synthetic zeolites have the unique property of selectively adsorbing molecules on the basis of size and shape in addition to polarity. Of particular interest are Type 5A molecular sieves, which have the ability to adsorb normal paraffins and olefins, but to exclude aromatic, cyclic, and branched-chain hydrocarbons. The basic unit of the type 5A molecular sieve is a zeolite crystal, a simple cubic crystal with an open structure consisting of a large number of adsorption cavities roughly spherical in shape. The individual adsorption cavities are about 11.5Å in diameter and are connected to adjacent cavities by apertures (pores) having an effective diameter of 5Å . The average zeolite crystal size is about 20,000 Å .

Previous research has shown that considerable molecular sieve studies and developments have been carried out throughout the world. Although molecular sieve adsorption is a technique by which several commercial processes remove straight-chain hydrocarbons from mixtures, relatively little quantitative information has been reported on the liquid phase adsorption of high molecular weight normal paraffins considering both batch and dynamic adsorption processes.

The present study was concerned with the adsorption of liquid binary systems, composed of a high molecular weight normal paraffin (n-dodecane, n-hexadecane, or n-eicosane) and isooctane as solvent, on type 5A molecular sieves to investigate the equilibrium adsorption isotherms, the kinetics of adsorption, and the dynamic properties of adsorption of these systems under different operating conditions. The intention was that the quantitative data and experience obtained will

assist in the selection, optimization and design of such systems.

For this purpose three types of experiment were performed. Equilibrium adsorption experiments were carried out using solutions of different n-paraffin concentrations and determining the amount adsorbed during the equilibrium time which had previously been found . The rate adsorption (kinetics) experiments were performed by calculating the amount adsorbed after various adsorption times in batch system. Dynamic experiments were performed in a packed column constructed to be used in either activation or adsorption cycles. The binary systems were analysed using a digital density meter.

As the present study progressed the following objectives were defined,

a) To obtain data that will be useful for the design of an adsorption system for separation of straight-chain paraffins from branched-chain paraffins.

b) To study the equilibrium adsorption isotherm of high molecular weight n-paraffins, and the effect of temperature on the amount adsorbed on type 5A molecular sieves.

c) To investigate the kinetics of adsorption of n-paraffins by 5A molecular sieves at different temperatures and calculate the diffusivity of these n-paraffins in 5A molecular sieves.

d) To determine the effect of various operating conditions such as flow rate, temperature, feed concentration and particle size on breakthrough curves and dynamic properties of adsorption of liquid binary systems on 5A molecular sieves.

e) To derive a mathematical model for the dynamic system, and compare the predicted breakthrough curveswith the experimental.

The experimental work and theoretical analyses which enabled these objectives to be met are described in Chapters 7 and 8. The significance of the results are discussed in Chapter 9, and future recommendations for continuation of the study of adsorption of high molecular weight normal paraffins are given in Chapter 10.

CHAPTER 2

NORMAL PARAFFINS

2.1 INTRODUCTION

Normal paraffins are straight-chain or branched saturated organic compounds of general chemical formula $C_n H_{2n+2}$. The main sources of normal paraffins are petroleum and natural gas, in which they are present with other hydrocarbon groups and impurities. They can also be produced synthetically from coal. Low molecular weight normal paraffins exist in the gaseous state at ambient temperatures and can be separated from natural gas. Medium normal paraffins, which are present in the liquid phase at ambient temperature, are produced from the kerosine and gas oil fractions obtained by the distillation of hydrocarbon crudes at atmospheric pressure. Heavy normal paraffins which are solid at ambient temperature, are obtained from lubricating oil fractions having various average boiling points, from distillation residues resulting from the vacuum distillation of hydrocarbon crudes.

The term paraffin waxes is used for mixtures of various hydrocarbon groups, especially paraffins and cycloalkanes, that are solid at ambient temperature. Paraffin waxes are classified into either of two groups according to their crystal structure. Macrocrystalline paraffin waxes are mixtures which consist chiefly of saturated, normal C_{18} - C_{30} hydrocarbons and smaller amounts of iso-alkanes and the cycloalkanes. In addition to normal hydrocarbons, microcrystalline paraffin waxes contain large amounts of isoalkanes and naphthanes with long alkyl side-chains. The major part of these waxes consists of C_{40} - C_{55} compounds (1).

2.2 PHYSICAL PROPERTIES

Normal paraffins possess a wide range of physical properties depending upon their molecular weights. These compounds are available in a gaseous, liquid, or

solid state at ambient conditions. The normal paraffins which contain one to four carbon atoms are gases, 5 to 16 are liquids, and higher than 16 are solids termed paraffin waxes. Some important physical properties of n-paraffins, which are liquid or solid at ambient temperature are listed in Table 2.1, indicating that n-pentane is already liquid and n-hexadecane solid at ambient temperature.

According to Etessam and Sawyer , the relationship between the melting point and the molecular weight for n-alkanes is: (quoted in ref. 1)

$$\text{m.p.} = 415 \frac{M}{M+95} - 273 \qquad 2.1$$

where m.p. is the melting point in ^{o}C and M the molecular weight.

Ivanovsky established a relation between the melting point and the density.

$$10^3 \, d_4^{90} = 716 + 0.75 \, \text{m.p} \qquad 2.2$$

where d_4^{90} is the density at $90^{o}C$ relative to that of water at $4^{o}C$.

Liquid paraffins have a melting point lower than 318K ($45^{o}C$). Commercial liquid paraffins contain 92-99.5% weight of normal paraffins(6). The quality of liquid paraffins depends mainly on the structure and properties of n-alkanes and the nature and quantity of impurities. Branching of the carbon chain at identical molecular weights, results in a significant decrease in the melting point, since high melting points are inseparable from high symmetry of the crystals, and this condition will be satisfied above all in the case of straight chain alkanes. The melting points of various normal and branched paraffins are presented in Table 2.2. These demonstrate, for example that among $C_{26}H_{54}$ alkanes, the melting point of n-hexacosane is

Table 2.1 Structure and physical constants of n-alkanes

Hydrocarbon	Formula	Temperature K (@ 1 atm)		Density (kg/m^3) @ 293 K	Refractive Index @ 293 K
		Melting Point	Boiling Point		
n-Butane	C_4H_{10}	134.5	272.5	.602 (1)	
n-Pentane	C_5H_{12}	143.5	309	.625	1.3577
Octane	C_8H_{18}	216.2	398.7	702.6	1.3974
Nonane	C_9H_{20}	219.3	423.8	717.7	1.4054
Decane	$C_{10}H_{22}$	243.3	447.1	730.1	1.4119
Undecane	$C_{11}H_{24}$	247.4	468.9	740.2	1.4172
Dodecane	$C_{12}H_{26}$	263.3	489.3	748.7	1.4216
Tridecane	$C_{13}H_{28}$	267.0	508.4	756.3	1.4256
Tetradecane	$C_{14}H30$	278.5	526.6	762.7	1.4290
Pentadecane	$C_{15}H_{32}$	283.0	543.6	768.4	1.4319
Hexadecane	$C_{16}H_{34}$	291.1	559.8	773.3	1.4345
Heptadecane	$C_{17}H36$	295.0	574.9	776.7 (2)	1.4367
Octadecane	$C_{18}H_{38}$	301.0	589.1	776.7 (2)	1.4388
Nonadecane	$C_{19}H_{40}$	305.0	604.5	777.6 (2)	1.4350
Eicosane	$C_{20}H_{44}$	309.4	615.1	777.7 (2)	1.4360
Heneicosane	$C_{22}H_{46}$	313.4	631.4	778.2 (2)	1.4352
Docosane	$C_{22}H_{46}$	317.4	640.0	778.2 (2)	-
Hexacontane	$C_{60}H_{122}$	371.5-372.3	-	-	-
Heptacontane	$C_{70}H_{142}$	378.0-378.5	-	-	-
Hectane	$C_{100}H_{202}$	388.1-388.4	-	-	-

(1) At the boiling point. (2) At the melting point.

Table 2.2 Melting points of various normal and branched paraffins found in waxes

Hydrocarbon	Melting point ^{o}K
$C_{24} H_{50}$	
n-Tetracosane	324.5
2-Methyltricosane	315.0
2.2-Dimethyldocosane	307.6
5-n-Butyleicosane	281.0
$C_{26} H_{54}$	
n-Hexacosane	329.4
5-n-Butyldocosane	293.8
7-n-Butyldocosane	276.2
9-n-Butyldocosane	274.3
11-n-Butyldocosane	273.0
$C_{28} H_{58}$	
10-Nonylnonadecane	268.0
$C_{44} H_{90}$	
22-Methyltritetracontane	339.6

329.4K (56.4°C) as compared to 273K (0°C) for ll-n-butyldocosane[1]. The boiling points of identical molecular weight straight-chain and branched alkanes also differ, but to a much smaller degree than the melting points. In the C_{24} - C_{28} range, the boiling point of the branched alkanes is lower by only 4°C to 15°C than that of the corresponding n-alkanes (depending on the number, length and position of the side chains)[1]. No definite relationship can be established between the viscosities of normal and branched paraffinic hydrocarbons. While alkanes with one side chain often have lower viscosities than those of the corresponding normal alkanes, the viscosity of alkanes with two or three side chains is higher than that of the corresponding normal alkane. Paraffin liquids at ambient temperature and melts of paraffins solid at ambient temperature behave as Newtonian systems. Specific volume versus temperature data for normal C_{20}, C_{24}, C_{26}, C_{28}, C_{32} and C_{36} alkanes are plotted in Figure 2.1. In the case of C_{24}, C_{26}, C_{28}, and C_{32} alkanes, the solid-phase transition takes place at some °C below the melting point. The curve for C_{20} displays no solid-phase transition, while the curve for C_{36} exhibits two such transitions[1].

2.3 CHEMICAL PROPERTIES

Normal alkanes are saturated and neutral compounds fairly resistant to the action of chemicals. A more detailed study of the chemical properties of alkanes, however, led to the recognition that they are far from being totally inert to chemicals. Their most important reactions are steam cracking for production of hydrogen, pyrolysis for production of olefins, chlorination and other substitution reactions.

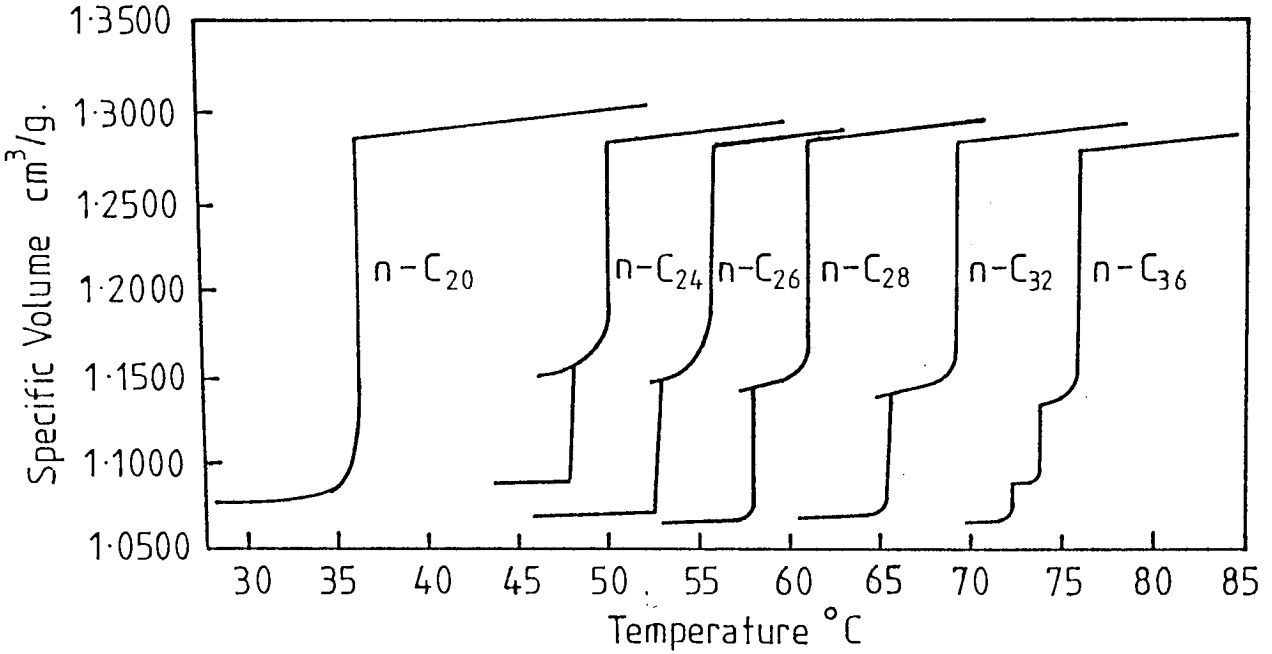

Figure 2.1 Specific volume versus temperature for some n-alkanes

2.4 SEPARATION OF N-PARAFFINS

2.4.1 Introduction

The separation of normal paraffins is important in several industrial processes, for example:

(a) Production of n-paraffins from petroleum distillates for further uses.

(b) Removal of n-paraffins for improvement of products as in the octane improvement of gasoline, pour point reduction of lube oils and dewaxing of oils for improvement of their quality.

Several methods are used for normal paraffins recovery. The choice of method depends on the type of feed, specification of the products and other factors which may affect the preference of one of the separation methods[2].

The common techniques used for separation of n-paraffins are urea adduction and molecular sieve adsorption. Each of these processes exhibits a selectivity according to the size of molecules. The normal or straight-chain molecules of paraffins have smaller radii than other hydrocarbons and hence can selectively enter the openings in urea adduct or zeolite crystals and become occluded in their cavities. Urea adduction has been used extensively but has some disadvantages. For example breaking of the adduct can easily occur and some non-normal paraffins may also participate in adduct formation[3]. These disadvantages do not exist in the case of adsorption by molecular sieves. Other separation methods include fractional distillation, fractional crystallization, elution chromatography, and thin layer chromatography[1]. Brief summaries of these separation methods are given below:

2.4.2 Separation by Fractional Distillation

Separation by distillation is based on the differing boiling points of the components. Application is therefore limited, since the boiling points of successive members of the normal paraffin series are very close to one another, particularly in the case of compounds containing more than 25 C-atoms. Therefore, preparative separation by distillation is effective mainly in the case of lower than C_{20} n-alkane.

Distillation is difficult to apply to iso-alkanes and cycloalkanes, since the boiling points of the members of these two homologous series overlap. Evidently separation by distillation is much less effective in the case of microcrystalline paraffin waxes than in the case of liquid paraffins and macrocrystalline paraffin waxes.

2.4.3 Separation by Fractional Crystallization

Fractional crystallization is a successful method for the separation of microcrystalline paraffin waxes based on differential solubility. Ketones, halogenated hydrocarbons and different gasoline grades have been used as solvents. Fractional crystallization yields fractions of both macrocrystalline and microcrystalline paraffin waxes differing in molecular structure and molecular dimensions. At higher temperatures of crystallization fractions containing higher molecular weight and less branched alkanes, as well as cycloalkanes with long side chains, will crystallize. With successive lowering of the temperature, the fractions will contain more and more iso-alkanes and cycloalkanes with shorter side chains; simultaneously the average molecular weight of the fractions will decrease.

2.4.4. Separation by Urea Adduct Formation

X-ray studies have shown that the long chains of n-alkanes as well as long chains of iso and cycloalkanes, if present, are enclosed in the tubular channels of the adduct, and this results in a hexagonal urea lattice. Urea crystallizes in the hexagonal system only when an adduct is formed, its normal crystal being tetragonal. Adduct formation between n-alkanes and urea takes place in solutions of the former in gasoline, benzene or halogenated hydrocarbons when solid urea or an aqueous or alcoholic urea solution is added. When solid urea is applied a small amount of a wetting agent, i.e. water, alcohol or some other substance with a similar effect, is necessary. Adduct formation is inhibited by resins, bituminous substances, sulphur compounds, etc. Therefore, it is important to remove such substances from the material before adduct formation, by elution chromatography or some other method.

Adduct formation is an equilibrium reaction, the equilibrium being dependent on temperature, concentration of urea and adduct-forming components, and the nature of the solvent. Adduct formation is exothermic; the heat of reaction is the higher the longer the alkane chain. Hence the stability of the adduct is greater the longer the adduct-forming molecule chain. Short-chain n-alkanes only form adducts at low temperatures and these products will readily decompose. Therefore use of adduct formation by urea is preferable in cases including the separation of long n-paraffin chain compounds.

As an alternative to urea, thiourea can also be used successfully for studying the chemical composition of complex mixtures of hydrocarbons and their derivatives. Thiourea forms adducts most readily with branched compounds.

2.4.5 Separation by Elution Chromatography

For chemical group analysis of liquid paraffins and macro and microcrystalline paraffin waxes, column chromatographic separation methods are used. Silica gel or active alumina is preferably used as adsorbent. The ratio of adsorbent to sample is between 20 : 1 and 30 : 1. The sample is introduced in the form of a dilute solution in gasoline or hexane. The succession of the eluents is that of the increasing polarity, e.g. mixture of hexane and benzene, benzene, methanol and chloroform. This method allows separation of saturated hydrocarbons, and mono-, bi- and tricyclic aromatics with satisfactory sharpness.

2.4.6 Separation by Thin Layer Chromatography

Separation of macro- and microcrystalline paraffin waxes by thin layer chromatography was developed, among others, by Dietscht and Sucker(1). They used a 250 μm silica gel support layer impregnated with 40% urea. To avoid recrystallization of the urea, a small amount of sorbite was applied. The paraffin wax to be studied was applied in a 1% solution in benzene, at 50 to 60°C and the solvent used was a mixture of carbon tetrachloride and ethanol saturated with urea. By using a suitable solvent composition and temperature (around 50°C), they succeeded in obtaining satisfactory separation of the paraffin wax with respect to chain length and degree of branching. By using appropriate conditions and simultaneous runs with reference standard material, they could determine the ratio of n- and iso-alkanes in macrocrystalline paraffin waxes.

2.4.7 Separation of n-paraffins by Adsorption Processes

Introduction

The recovery of n-paraffins by adsorption on molecular sieves has become one of the most widely used separation techniques. These synthetic zeolites have the unique property of selectively adsorbing molecules on the basis of size and shape in addition to polarity. Linde Type 5A molecular sieves have the ability to adsorb normal paraffins and olefins but to exclude branched-chain, cyclic, and aromatic hydrocarbons. The product from the adsorption process is of high purity, i.e. >96%, and operating costs are lowest in comparison with other separation processes.

Feedstock

Feedstocks for n-alkane manufacture are petroleum distillates with boiling ranges corresponding to the desired carbon atom number products. A general requirement in feedstocks is for the n-alkane content to be 15-30 wt%, maximum sulfur content 300-600 p.p.m. and maximum nitrogen content 20 p.p.m. To eliminate polymerization in the course of adsorption, the maximum permissible olefin content in the feedstock is limited to 1-2 wt%[1]. The acid sites on the molecular sieves should alternatively be neutralized by treating the sieves with ammonia or an organic amine in the absence of polar solvent to inhibit cation exchange [2].

To meet these requirements, it is often necessary to subject the feedstock to preliminary refining. Water should be removed from the feed by passage of the feed through a guard bed of molecular sieves of 3Å or larger pore size[2].

Commercial Processes

The technological process consists essentially of four stages:

adsorption

flushing

desorption

regeneration of the adsorbent

Adsorption may be conducted in the liquid phase, in the vapour phase, or in a mixed phase. Flushing is performed with some non-adsorbable gas or with the solvent used in desorption. The purpose of flushing is to remove substances other than n-alkanes deposited on the surface of the molecular sieve particles and in the spaces between the particles. Desorption can be accomplished by increasing the temperature, decreasing the pressure, passing an inert medium through the bed, displacement with a more strongly sorbed material, displacement with a less strongly sorbed material, or combinations of these methods (4).

Many commercial processes for separation of n-paraffins with molecular sieves are carried out in the vapour phase such as the Isosive, Ensorb, British Petroleum, Texaco Selecting Finishing (TSF) Shell and Parex processes. The Molex process is operated in the liquid phase (2).

2.5 USES AND APPLICATIONS

The potential uses of liquid paraffins and paraffin waxes are large and very diverse.

2.5.1 Production of Protein

Yeasts with high protein and vitamin content can be obtained from straight chain hydrocarbons by means of appropriate cultures of microorganisms. The essential feature of the process is similar to the manufacture of conventional pressed yeast. The main difference between the two processes is that the carbohydrate starting

material supplies the carbon and hydrogen, as well as the major part of the oxygen required for the build-up of the protein from an aqueous solution. However, the hydrocarbons are insoluble in water and have to be processed in the form of an emulsion. The total oxygen requirement must be provided by the air that is blown through the emulsion. Nitrogen is introduced in the form of ammonia added to the air blown through the usual starting material which consists of C_{10}-C_{20} n-alkanes [1].

Petroleum yeast (single cell protein, SCP) is a dry, powder-like product, its protein content varying between 60 and 65%. Petroleum yeast can be used solely for animal feed. Usually 20% of protein yeast could be mixed with the feed, in the case of fish feed even up to 75% was accepted. Feeding tests were carried out for several generations of cattle, sheep, goats, horses, etc. Neither carcinogenic nor any other detrimental effects were observed.

2.5.2 Production of Olefins

Olefins can be obtained from paraffin oils or paraffin waxes by a thermal cracking process or by dehydrochlorination of chlorinated paraffins. The olefins produced have many applications as starting materials for the petrochemical industry. Owing to their double bond they are more reactive then alkanes. Valuable products can be obtained by their polymerization, alkylation, hydration, etc.

2.5.3 Manufacture of Chlorinated Paraffins

Three types of chlorination processes are used industrially. Catalytic chlorination is used especially for gaseous hydrocarbons. It is carried out in a solvent, mainly carbon tetrachloride. The homogeneous-phase catalysts used are substances

that yield readily dissociating compounds with chlorine, e.g. iodine, sulfur, iron chloride or zinc chloride.

A second type of processes is thermal chlorination of high paraffin petroleum fractions and paraffin waxes melting in the 50 to 60°C temperature range. Photochemical chlorination process is also one of the chlorination processes that can be achieved by radiation energy. The absorption range of chlorine is 2500 - 4500 A; it is thus capable of utilizing UV and UV-spectrum of visible light.

Chlorinated paraffins are oily, viscous liquids at ambient temperature, and soluble in petroleum, petroleum products and organic solvents. The solubility is dependent upon the chlorine content. Monochloroparaffin is used for alkylation of benzene, phenol and naphthalene in the manufacture of detergents, lubricant additives (detergents, dispersing agents, oxidation inhibitors) and textile finishing agents. Large quantity of chlorinated paraffins are used in plastic processing, textile industry, leather and paint industries.

2.5.4 Paraffin Wax Uses

Paraffin waxes are widely used in various fields as summarized below,

a) applications in the paper industry,

b) applications in the household chemicals (polishes, creams, candles, etc.,

c) application in cosmetics

d) application in the food industry and in agriculture (cheese-coating, poultry processing, fruit preservation, etc.),

e) miscellaneous applications (matches, textiles, electrical industry,

pencil manufacture, wax emulsions for building construction, etc.),

Detailed applications are discussed in references (2, 5).

CHAPTER 3

MOLECULAR SIEVES

3.1 INTRODUCTION

Molecular sieves are a type of zeolite, a crystalline material having within each crystal a system of precisely-arrayed cavities and pores. Natural zeolites are impractical for commercial use due to their scarcity and high degree of chemical and physical variability. Molecular sieves are synthetically-produced, crystalline metal alumina-silicates that have been activated for adsorption by removing their water of hydration. Highly porous adsorbents are thus formed with a stable lattice framework. This lattice framework, possesses a unique property of selectively adsorbing molecules on the bases of their size, configuration, polarity, and other physical characteristics(7). The other commercial adsorbents which include the activated carbons, activated clay, inorganic gels such as silica gel and activated alumina do not possess an ordered crystal structure, as in the zeolite structure, and consequently the pores are non-uniform. Figure 3.1 illustrates the pore distribution of various molecular sieves and two other adsorbents.(8)

Molecular sieves have pores of uniform size which are uniquely determined by the unit structure of the crystal. Depending on the size of these pores, molecules may be readily adsorbed, slowly adsorbed or completely excluded. This sieve-like selectivity, based on molecule size plus a selective preference for polar or polarizable molecules, and a high capacity over a wide range of operating conditions, give molecular sieves a high level of adsorption efficiency. The above mentioned characteristics of molecular sieves are used in many industrial applications.

3.2 HISTORICAL BACKGROUND

Zeolites are naturally occuring minerals and, were discovered two centuries ago by Baron Cronstedt who observed that certain mineral crystals when

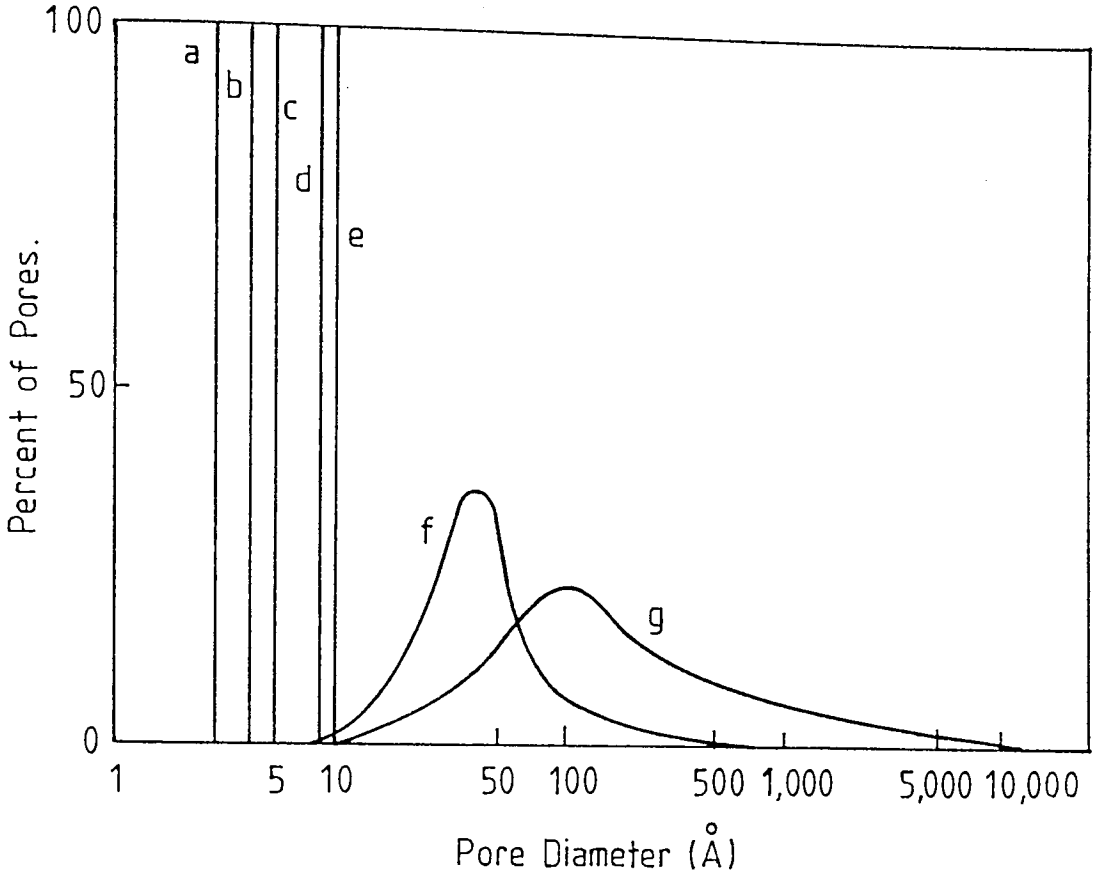

Figure 3.1 Typical pore size distribution, illustrating that molecular sieves have precise pore diameters.

LEGEND:

(a) Linde molecular sieve type 3A

(b) Linde molecular sieve type 4A

(c) Linde molecular sieve type 5A

(d) Linde molecular sieve type 10X

(e) Linde molecular sieve type 13X

(f) Typical silica gel

(g) Typical activated carbon

heated appeared to melt and boil at the same time (9, 10). Therefore, he coined the term zeolite from Greek Zeo, to boil, and lithes, stone. In 1926, J W McBain first spoke of Zeolites as "molecular sieves", thus suggesting that they could be used to separate one size molecule from another. Barrer and his group pointed out such potential applications for molecular sieves as the separation of normal from isoparaffins and polar from nonpolar molecules. In 1948, a group of Union Carbide Corporation research workers under the direction of R M Milton, set out to synthesize zeolites in the laboratory(11). In 1954, Linde Air Co., introduced synthetic zeolites under the trade name 'Molecular Sieves'(12) and in 1959, the Davison Chemical Division of W R Grace and Co., initiated production and distribution of crystalline alumino silicates under the trade mark of 'Microtrap'(10).

Since then, the continuously increasing number of industrial applications has resulted in substantially increased production capacity and the introduction of a large variety of Molecular Sieve products.

3.3 TYPES OF MOLECULAR SIEVE

Various types of molecular sieves were synthesized to overcome the disadvantages of natural zeolites. Commercial molecular sieves are supplied in a pellet or bead form which contains about twenty percent clay binder.

The clay binder which is present in the pellets is claimed to act merely as an inert diluent with no significant effect on the sorptive properties(13).

Among the types that have been found to be most commercially useful are the type 3A, 4A, 5A, 10X and 13X. Table 3.1 illustrates the basic types of commercially available molecular sieves with some of their properties(11). The size and position of the exchangeable cations may affect the free aperature size in any

particular type of molecular sieve. In the type A crystal, the effective diameter of the

TABLE 3.1 Basic types of commercially available molecular sieves

Basic Type	Nominal Pore Diameter, Å	Available Form	Cation	Theoretical SiO_2/Al_2O_3
3A	3	Powder, 1/8", 1/16" Pellets, 4x8, 8x12 beads	K^+	2/1
4A	4	Powder, 1/8", 1/16" Pellets, 4x8, 8x12 beads, mesh	Na^+	2/1
5A	5	Powder, 1/8", 1/16" Pellets, 4x8, 8x12 beads, mesh	Ca^{++}	2/1
10X	8	Powder, 1/8", 1/16" Pellets	Ca^{++}	2.5/1
13X	10	Powder, 1/8", 1/16" Pellets, 4x8, 8x12 beads, mesh	Na^+	2.5/1
Y	7 to 9	Powder, 1/8", 1/16" Extrudates	Varying	3 to 6/1
AW-300	3 to 4	1/8", 1/16" Pellets	Mixed	10/1
AW-500	4 to 5	1/8"1/16" Pellets 4x8, 8x12 beads	Mixed	4 to 6/1
Mordenite	7 to 9	Powder 1/8", 1/16" Pellets, mesh	Na^+ or H^+	10/1

opening is 3, 4, and 5 angstroms when the cations are predominantly potassium, sodium, and calcium, respectively(14). According to the free aperature size and the guest molecule effective size adsorption will take place . Table 3.2 shows the sieving effects of some molecular sieves and the molecules which may be adsorbed or excluded.

3.4 ZEOLITE CRYSTAL STRUCTURE

Because of the importance of a knowledge of the structure of zeolite, many research studies have been reported (15, 16, 17). The properties and structure of synthetic zeolite type A were first reported by Brick et. al., in 1956(16, 17). Here, a description of the lattice framework of the 5A sieves is presented.

Structurally the zeolites are "framework" alumino-silicates which are based on an infinitely extending three-dimensional network of $A10_4$ and SiO_4 tetrahedra linked to each other by sharing all of the oxygen atoms. Electrical neutrality is achieved by the inclusion of alkali or alkaline earth ions such as Na^+, K^+, Ca^{++}, St^{++} or Ba^{++} (16). The framework contains channels and interconnected voids which are occupied by the cation and water molecules. The cations are quite mobile and may usually be exchanged, to varying degrees, by other cations.

The composition of the Type A zeolite is expressed by the structural formula $Me_{12/n}$ $[(A10_2)_{12}(SiO_2)_{12}]$. NH_2O where Me represents exchangeable cations of charge n.

As shown in the schematic drawings of Figure 3.2, the sodalite cage encloses a cavity(ß-cage) which has eight, six-membered oxygen rings (6MR) and six, four-membered oxygen rings (4MR). The diameter of a 6MR is 23Å and that of the ß-cage is 6.6Å. In the 5A zeolites, the framework consists of a tetrahedral

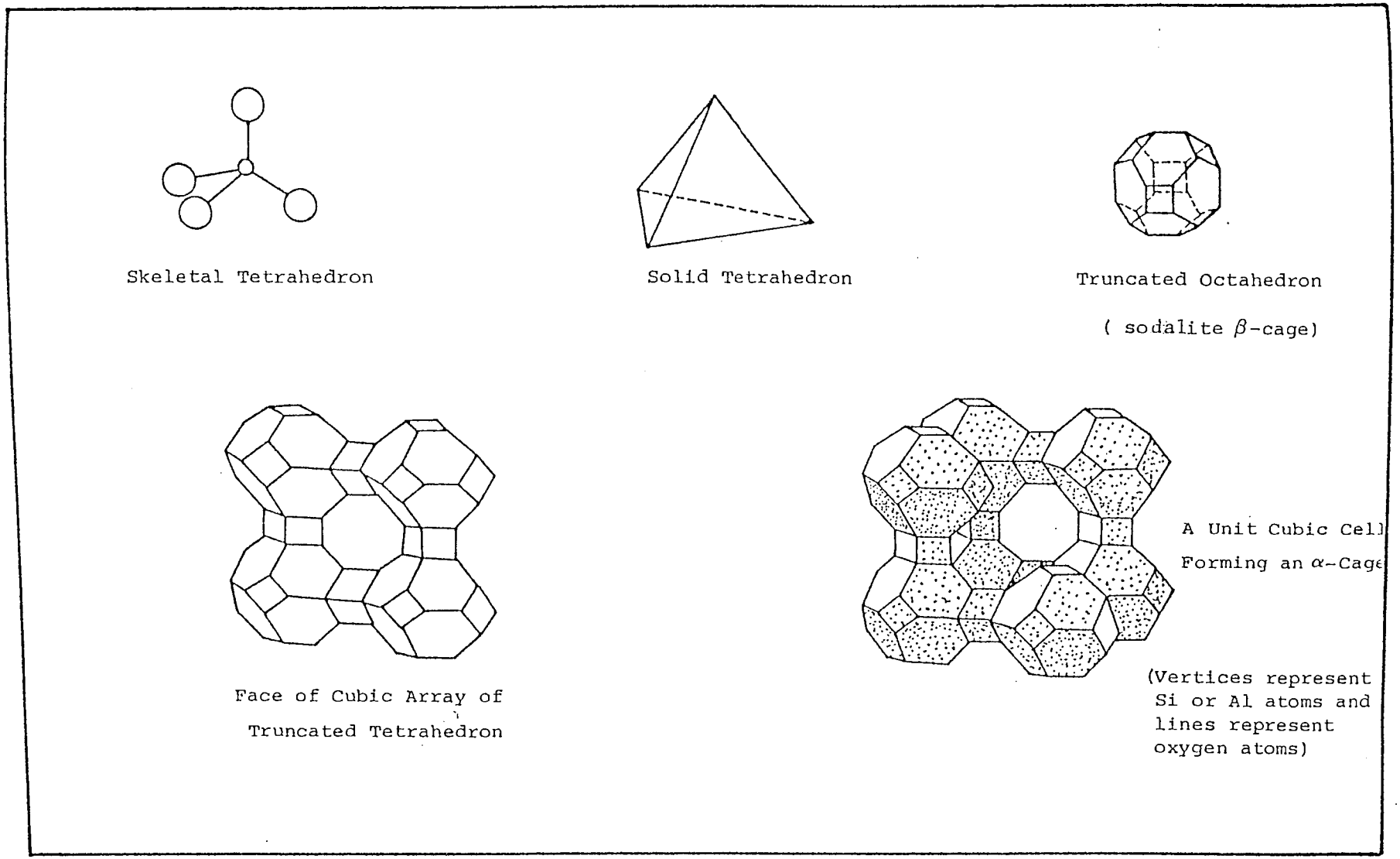

Figure 3.2 Molecular sieve Type 5A - Zeolite framework

arrangement of eight sodalite cages linked by twelve 4MR, all of which together define a roughly spherical cavity (α-cage) of 11.4Å in diameter.

This arrangement of the sodalite cages leads to the formation of six, eight-membered oxygen rings (8MR), which are the entrances to the α-cage. These 8MR apertures form the links between other $\alpha\beta$ cages. The size of the 8MR apertures is of importance because it determines the maximum dimensions of the molecules that can enter the crystal lattice. Aperture openings are a direct function of the Si/Al ratio and the type of cations. The Si/Al ratio determines the number of cations in a unit cell, and the size of the cation, which is associated with the 8MR, fixes the diameter of the aperture. The cation in the crystal can be replaced (normally to the extent of about 75%) by other cations without disturbing the basic structure of the crystal.

By appropriate choice of framework structure, Si/Al ratio and cationic form, adsorbents with widely different adsorptive properties may be prepared.

Table (3.1) shows the basic types of commercially available molecular sieve with the nominal pore diameter, the available form, the cation, and the theoretical SiO_2/Al_2O_3 for each type [11]. Among the types that have been found to be most commercially useful are Type 4A and Type 13X which have the following unit cell formulae:

Type 4A : $Na_{12}[(AlO_2)_{12}(SiO_2)_{12}] \cdot 27H_2O$

Type 13X : $Na_{86}[(AlO_2)_{86}(SiO_2)_{106}] \cdot 276H_2O$

In both cases the sodium ion can be exchanged to form other useful products. The size and position of the exchangeable cations may affect the free aperture size in any particular type of molecular sieve. Thus, the replacement of sodium ions in Type 4A with calcium ions produces Type 5A, with a free aperture

size of 4.2 angstroms (18).

The Linde 5A zeolite is of primary interest for this study. The unit cell of the type 5A molecular sieve is:

$$Ca_{4.5}Na_3\,[(AlO_2)_{12}\,(SiO_2)_{12}]\,.30H_2O$$

There are 60% calcium ions and 40% sodium ions which result in an aperture of 4.2Å in diameter. This allows molecules with effective diameters up to 5Å to squeeze through the apertures into α-cages (17).

Normal paraffin molecules which have an effective diameter of 4.86Å can easily penetrate the crystal lattice and be adsorbed on the surface of an α-cage. Larger molecules of the branched paraffins and aromatic hydrocarbons cannot enter the lattice because their effective diameter is larger than 5Å.

In the zeolite diffusion process, the diffusing molecule first enters the crystal through the interstitial space to an empty or partially filled α-cage, where it is adsorbed on the surface.

Some molecules may by-pass a partially filled cavity and seek out an empty one while others may displace adsorbed molecules, thus facilitating further penetration of the crystal. The intercrystalline void spaces within the pellet are of the same magnitude as the crystal size, which is about 20,000Å, and are referred to as macropores. The macropores occupy about 31% of the total particle volume (19).

3.5 MOLECULAR SIEVE PROPERTIES

Molecular sieves are alkaline in nature - having a pH range in water slurry of 9.0 to 10.5 - most types are stable in solutions that fall within a pH range of 5 to 12, and a few are stable in solutions having a pH as low as 3. In vapour

phase processes only the gases that will hydrolize to form strong acids will readily react with them. Molecular sieves types A and X are stable to heat. A temperature of about 700°C is required to decompose the crystal structure. Beside the ability of molecular sieves to selectively adsorb according to molecule size, due to size of the pores, they have a strong affinity for polar molecules, so they will adsorb polar molecules in preference to non-polar molecules, even though both molecules are of similar size. Molecular sieves show a marked affinity for chemically unsaturated molecules, so molecules of this type can be separated from saturated molecules of approximately the same size as in the separation of ethane from ethylene using 4A molecule sieves. Table 3.2 illustrates some examples of molecular separation by different molecular sieves(18).

The unique adsorption characteristics of molecular sieves as compared to other common adsorbents are shown in Figure 3.3. Molecular sieves have large surface area, in the order of 700-800 m^2/gram and the zeolite pellets which are the main commercial product are made of microcrystals of zeolites about 1.0 micron in diameter embedded in a dried clay binder (20). The basic unit of the type-5A molecular sieve is a zeolite crystal with an open structure consisting of a large number of adsorption cavities roughly spherical in shape. The crystal density of hydrated type A zeolite was found to be 1.99 ± .004 g/cc. As generally prepared the type A zeolite crystals are cubic with edges averaging 1-5 micron in length (16).

The individual adsorption cavities are about 11.5Å in diameter and are connected to adjacent cavities by apertures having an effective diameter of 5Å. The unit cell has a dimension of 12.3Å. Physical properties of some commercial molecular sieves are shown in Table 3.3.

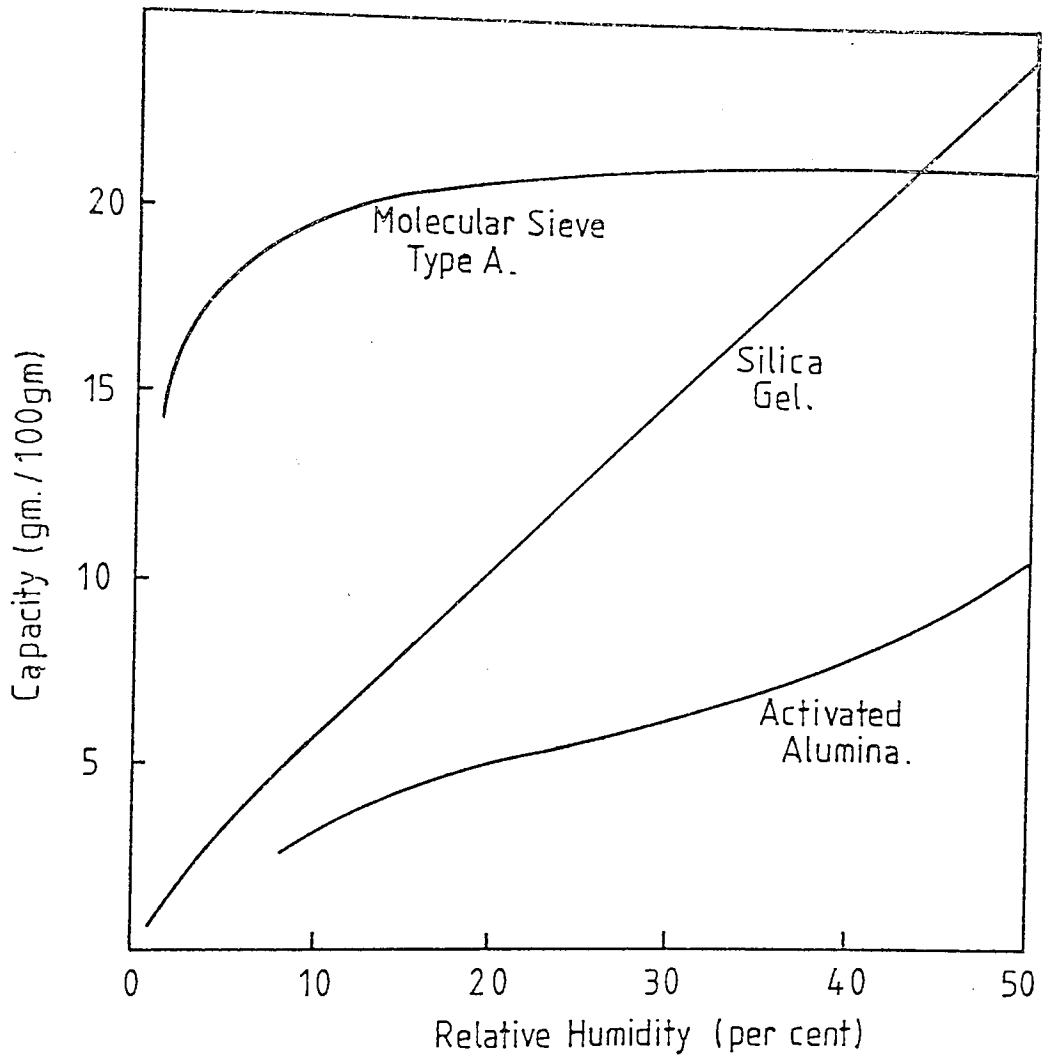

Figure 3.3 Water vapour adsorption on different adsorbents at 25°C

Table 3.2 Sieving effects of some molecular sieves toward different molecules

Basic Type	Nominal Pore Diameter, Å	Molecules Adsorbed*	Molecules Excluded
3A	3	Molecules with an effective diameter <3Å, including H_2O and NH_3	Molecules with an effective diameter >3Å, e.g. ethane
4A	4	Molecules with an effective diameter <4Å, including ethanol, H_2S, CO_2, SO_2,	Molecules with an effective diameter >4Å, e.g. propane
5A	5	Molecules with an effective diameter <5Å, including n-C_4H_9OH*, n-C_4H_{10}*, C_3H_8 to $C_{22}H_{46}$, R-12.	Molecules with an effective diameter >5Å, iso compounds and all 4 carbon rings
10X	8	Iso paraffins and olefins, C_6H_6, molecules with an effective diameter <8Å	Di-n-butylamine and larger
13X	10	Molecules with an effective diameter <10Å	Molecules with an effective diameter >10Å, e.g., $(C_4F_9)_3N$

* Each type adsorbs listed molecules plus those of preceding type.

3.6 COMMERCIAL MANUFACTURE:

In the commercial manufacture of molecular sieve Type A sodium silicate, aluminium trihydrate and sodium hydroxide are automatically batch weighed into mix tanks and stirred until homogeneous. The resulting gel is pumped into crystallization tank where it is maintained under closely controlled conditions. The progress of crystallization is monitored by several quality control techniques. The crystal slurry is filtered and washed. If calcium or other cations are to be substituted for sodium in the crystal, the filter cake is transferred to a heated tank where it is mixed with a solution of the appropriate metal salt. The exchange forms are washed

Table 3.3 Physical properties of typical "Linde molecular sieves" type A and type X

Type	Pellet Size, m x 10^3	Bulk Density, kg/m^3	Particle Diameter m x 10^3	Crush Strength kg	Heat of Adsorption, kJ/kg H_2O	Equilib. H_2O Capacity @ 298K wt%
3A	1.6	641.3	1.5 - 2.0	2.91	4186.8	20
3A	3.2	641.3	3.0 - 3.5	6.58	4186.8	20
4A	1.6	657.3	1.5 - 2.0	4.72	4186.8	20
4A	3.2	657.3	3.0 - 3.5	9.53	4186.8	20
5A	1.6	700.0	1.5 - 2.0	2.63	4186.8	21.5
5A	3.2	700.0	3.0 - 3.5	5.72	4186.8	21.5
13X	1.6	609.2	1.5 - 2.0	5.45	4186.8	28.5
13X	3.2	609.2	3.0 - 3.5	11.35	4186.8	28.5

and filtered.

To form pellets, crystals from the filter are mixed with specially selected clay binders and fed through an extruder. The pellets are then dried, screened, and fired in a rotary kiln to drive out the water and activate the molecular sieves (11).

3.7 USES OF MOLECULAR SIEVES

Due to the ability of commercial manufacturers to produce various types of molecular sieves with different adsorbing, catalyzing and ion exchanging properties, they have found wide-spread industrial applications and uses as adsorbents, catalysts and ion exchangers.

3.7.1 Molecular Sieves As Adsorbents:

Molecular sieves are of the most important adsorbents today because of the following unique adsorptive properties(18):

a) Selective adsorption of molecules based on molecular dimensions, so on using Type 5A molecular sieve with a free aperture size of 4.2Å, only the molecules of dimension less than 5Å will be squeezed and entered the crystal, e.g n-paraffins and olefins molecules, while aromatics and branched molecules will be excluded.

b) Highly preferential adsorption of polar molecules. The very strong adsorptive forces in molecular sieves are due primarily to the cations which are exposed in the crystal lattice. These cations act as sites of strong localized positive charge which electro-statically attract the negative and of polar molecules. For example, molecular sieve will adsorb carbon monoxide in preference to argon.

Under the influence of the localized, strong positive charge on the cations, molecules can have dipoles induced in them. The polarized molecules are then adsorbed strongly due to the electrostatic attraction of the cations. The more unsaturated the molecule, the more polarizable it is and the more strongly it is adsorbed. Thus molecular sieves will effectively remove acetylene from olefins, and olefins from saturated hydrocarbons.

c) Highly hydrophilic surface.

d) Variation of properties by ion exchange.

The most important applications of molecular sieves in industry as an adsorbent can be classified as the following operations:

* Recovery of normal paraffins from kerosene using 5A molecular sieve. The separation of para-xylene, which is used in the manufacture of polyester, from mixed xylenes and ethyl benzene is now successfully performed on a large scale by employing molecular sieves. Pressure-swing adsorption process using molecular sieves now separates oxygen of 95% purity from air in a cheaper and more efficient way than conventional cryogenic separation routes.

* Purification of gases and liquids for many applications use molecular sieves. They are now widely used for "sweetening" liquified petroleum and natural gas. Molecular sieves (especially type 13X) can be used for mercaptan removal from light petroleum fractions. The removal of mercaptans, sulfides and disulfides from an oil of 240 - 360°C boiling range by 5A and 13X sieves at 222 - 277°C was studied by Pavlyuchenko et al [21]. Nitrogen compounds can be removed from feeds such as gasoline by passage through a bed of molecular sieves of pore sizes from about 7 to 13 angstroms which preferably have been preloaded with an organic nitrogen base such as pyridine, methyl

pyridine, etc. [22]. Type 13X molecular sieve is used for purification of air prior to liquefaction by adsorbing carbon dioxide and water vapour.

* Molecular sieves are used in drying due to their high ability to produce low effluent water concentrations (water concentrations as low as 35 parts per billion are obtainable in dynamic drying service over a wide range of operating conditions).

Prior to liquefaction of natural gas, it must be processed to remove such components as carbon dioxide and water which can freeze out and plug cryogenic heat exchangers during liquefaction[23].

In some drying operations it is difficult to remove water without the other components of the feed which is considered as a serious problem in cases where product composition is critical. The co-adsorption problem can be solved easily by selecting a molecular sieve type with a critical pore diameter small enough to prevent all stream components except water from being admitted to the active inner surfaces of the adsorption cavities. This prevents the co-adsorption of materials other than water while providing maximum capacity for water and effluent water concentrations of one to ten parts per milion[18].

Molecular sieve type 3A, which has a pore size of 3.0Å, has found wide use in the drying of olefinic gases and liquids because all hydrocarbons are excluded from its adsorption cavities.

For the drying of pipeline natural gas at the front end of low temperature hydrocarbon recovery plants, molecular sieve type 4A, compared with silica gel desiccant offers (1) a two to three times higher design water loading, (2) longer desiccant life because heavy hydrocarbons coadsorption is eliminated, and (3) increased downstream hydrocarbon recovery because of both the sponging effect of the unadsorbed heavier hydrocarbons and the increased operating pressure resulting

from the lower pressure drop through the smaller molecular sieve bed[24].

Other non-regenerable molecular sieve applications include the drying of refrigerant, in house and industrial refrigeration units, the scavenging of moisture from pigments, metal based paints and formulations for rubber and urethanes, the control of ambient humidity in the encapsulation, packaging, and shipping of electronic components and other moisture sensitive parts[18].

3.7.2 Molecular Sieve Catalysis

Type X and type Y are large pore molecular sieves of primary interest in catalysis. The activity and selectivity of both types can be modified by cation exchange, decationization and metal loading. These catalysts are different from conventional catalysts in several important respects[18]:

a) their ionic surfaces provide unusually strong carbonium ion activity,

b) their exchangeable cations facilitate the introduction of catalytic metals in the highest degree of dispersion,

c) they are completely crystalline with uniform, internal pores of molecular dimensions.

An example of the high activity and good selectivity of molecular sieve catalysts is catalytic cracking in petroleum refining[25, 26].

Compared with conventional silica alumina cracking catalysts, 15 to 20% higher gasoline yields are typically obtained with the molecular sieve containing catalysts.

Isomerization with unpromoted molecular sieve catalyst can be used to upgrade low octane n-paraffins and thereby increase gasoline yield in petroleum refining[27].

Molecular sieve catalysts can also be used in hydrocracking to increase refinery gasoline yield. It's performance has been excellent from both a product selectivity and a deactivation rate standpoint. The catalyst's ability to crack in the presence of nitrogen and sulfur compounds, and to undergo multiple bed regenerations with little loss in activity, has been a major factor in the success of the process[28].

3.7.3 Zeolites as Ion Exchangers

Zeolites are capable of exchanging cations. It has been seen earlier that by exchanging cations, the window diamters are controlled. Synthetic ion exchange zeolites, however, are not as well developed commercially as zeolite adsorbents or catalysts. Some potential applications of zeolite as cation exchangers include removal of ammonium ions from sewage and agricultural waste, isolation of radio-active by-products of nuclear reactions for collection or disposal, ion-sieving, and separation of isotopes etc.

CHAPTER 4

ADSORPTION THEORY

4. ADSORPTION THEORY

Adsorption is a common mass transfer operation used in drying and in gas and liquid purification processes. A distinction is made between two types of adsorption phenomena, physical adsorption and chemisorption. Chemisorption comprises an irreversible process and is the result of chemical interaction between the solid and the adsorbed substance; it has an important role in catalytic processes.

4.1 PHYSICAL ADSORPTION

Physical adsorption is a reversible phenomenon and is the result of intermolecular forces of attraction between molecules of the solid adsorbent and the adsorbate.

The forces attracting the fluid molecules to the solid surface are relatively weak. The adsorbed substance does not penetrate within the crystal lattice of the solid and does not dissolve in it but remains entirely upon the surface. In the case of the highly porous adsorbents, such as molecular sieves, the adsorbed substance will penetrate into the cavity through apertures or pores. Equilibrium between the solid surface and the gas molecules is usually rapidly attained and because the energy requirements are small is easily reversible. The amount of physical adsorption decreases rapidly as the temperature is raised and is generally very small at any temperature above the critical temperature of the adsorbed component.

Physical adsorption is not highly dependent on the irregularities in the nature of the surface, but is usually directly proportional to the surface area. Almost all adsorptive separation processes depend on physical adsorption.

4.2 FORCES AND ENERGIES OF ADSORPTION

Two forces are involved in physical adsorption namely van der Waal's forces, which are always present, and electrostatic interactions comprising polarization, dipole, and quadrupole interactions. The electrostatic contributions are only significant in the case of adsorbents such as zeolites which have an ionic structure[29]. In zeolite adsorbents the electrostatic contribution may vary according to the type of molecule adsorbed. These molecules have been classified into groups according to the effect of the electrostatic forces [30]. Group A molecules are substances, such as permanent gases and alkanes, which do not interact any more strongly with molecular sieves than with other sorbents such as activated carbon and silica gel. Group B molecules have π - electron bonding, for example, aromatics such as benzene. Group D molecules have permanent dipole groups, for example, alcohols and amines. The group D molecules interact most strongly, and group A molecules least strongly, with zeolite.

4.3 ADSORPTION EQUILIBRIA

The distribution of solute between liquid and solid phases in an adsorbent - solute-solvent system at equilibrium at a specific constant temperature is commonly termed an adsorption isotherm. Adsorption equilibrium data are presented and correlated by plotting the quantity of solute adsorbed per unit weight of adsorbent, G, as a function of the equilibrium concentration of solute remaining in solution, C[35]. Three major classes of isotherms can be characterized according to their different effects upon column performance[31]. They include "favourable"

equilibria for which the isotherm is convex upwards as shown in Figure 4.1, "unfavourable" equilibria for which the curve is concave upwards, and the linear isotherm.

For systems in which the equilibrium isotherm is linear or unfavourable the mass transfer zone broadens continuously as the front propagates through the column. Such behaviour is commonly referred to as dispersive or "proportionate pattern" since the width of the mass transfer zone increases in direct proportion to the distance travelled through the column.

When the isotherm is favourable a completely different type of behaviour is observed. In the initial region the mass transfer front spreads as it progresses, but after some distance from the inlet it continues to progress as a stable mass transfer zone with no further change in shape. The distance required to approach the constant-pattern limit depends on the degree of non linearity of the isotherm and on the kinetics of sorption. For many practical systems this distance is very small. The assumption of a constant pattern is therefore a very useful design approximation since the calculation of the form of the mass transfer front under constant pattern conditions is very simple[29].

Gleuckauf and Coates [32] point out that if the isotherm is favourable the height of the adsorption zone decreases as it moves through the bed. However, this "self-sharpening" characteristic is counteracted by a finite rate of mass transfer and axial diffusion so that, in practice, zones of nearly constant height are often observed[33].

Several mathematical formulations to describe adsorption equilibria have been widely adopted. They include the isotherm model originally proposed by

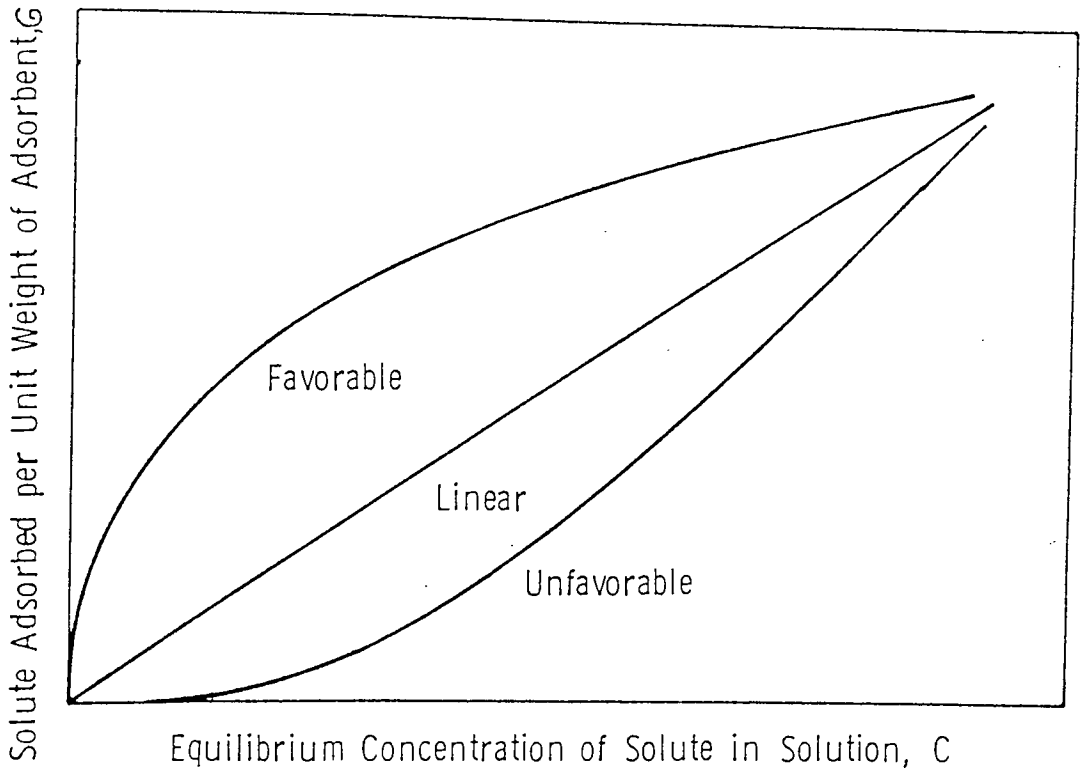

Figure 4.1. Basic types of adsorption isotherms

Langmuir,[34].

$$G = a_m \frac{bC}{1 + bC} \qquad 4.1$$

that of Freundlich, [35]

$$G = K C^{\frac{1}{n}} \qquad 4.2$$

and that of Brunauer, Emmett and Teller, [35]

$$G = \frac{a_m AC}{(C_s - C)\,[1 + (A-1)\,C/C_s]} \qquad 4.3$$

where

a_m = ultimate uptake capacity of adsorbent, mol/kg

G = adsorption value, mol/kg

b = Langmuir energy term, litres/mol

K = adjustable curve-fitting constant

n = adjustable curve-fitting

A = BET energy term, $\frac{\text{litres}}{\text{mol}}$

C_S = saturation concentration of solute in solution, mol/litre

In 1967 Eltekov and Kiselev[36] suggested an equation for pore filling in the form of multilayers referred to as Brunauer - Emmett-Teller (BET) and expressed as:

$$G_1 = \frac{a_{m1}\,\beta\,(f-1)\,x_1\,(1-x_1)}{1 + (\beta f - 1)\,x_1} \qquad 4.4$$

where,

a_{m1} = the maximum amount of component 1 filling the cavities of 1g of zeolite mol/kg.

f = a function characterizing the collective interactions occurring in the zeolite-solution system.

ß = coefficient of mutual displacement of the molecule of the components

x_1 = mole fraction of component 1 in solution after adsorption

G_1 = adsorbed amount of component 1 mol/kg

The adsorbed amount of normal paraffin in the present study was calculated using Gibb's Equation (37).

$$G_1 = \frac{n}{m_s} (x_o - x_1) \qquad 4.5$$

where,

n = total number of moles in solution

m_S = weight of molecular sieve

x_o = initial mole fraction of component 1 in solution

x_1 = equilibrium mole fraction of component 1

Equation 4.4 has been used in cases where the pores of the adsorbent are only partially occupied by the adsorbable component over a fairly wide concentration range, the rest of the adsorbing area remaining free. Therefore it was used to

represent adsorption isotherms in the present study.

Due to the absence of molecules of isooctane solvent in the zeolite cavities in the systems under investigation, because the critical diameter of the isooctane molecule is greater than the effective pore diameter, it may be assumed that $\beta \simeq 1$[36].

4.4 HEAT OF ADSORPTION

The heat of adsorption provides a direct measure of the strength of the bonding between sorbate and the adsorbent surface. The greatest values of adsorption heat observed in physical adsorption are for molecular sieves (zeolites) which arise from the interactions of active cations in zeolite crystals with adsorbate hydrocarbon molecules.

When molecules with π - bonds, as in aromatic hydrocarbons, or polar functional groups, are adsorbed by porous crystals of zeolite sieves, they interact very strongly with the exchange cations of zeolite cavities [38].

For the sorption of small dipolar molecules such as H_2O and NH_3 on zeolite adsorbents the electrostatic contribution may be very large, giving rise to unusually high heats of adsorption (25-30 kcal/mole)[29]. Usually all processes of physical adsorption are exothermic since the adsorbed molecule has at most two degrees of translational freedom on the surface and since the rotational freedom of the adsorbed species must always be less than that of the fluid phase molecule, the entropy change on adsorption

$$\Delta S = S_{ads} - S_{fluid} \qquad 4.6$$

is necessarily negative.

In order for significant adsorption to occur, the free energy change on adsorption (ΔF) must also be negative and since:

$$\Delta F = \Delta H - T\Delta S \qquad 4.7$$

this requires ΔH to be negative, resulting in exothermic adsorption(29).

Three heats of adsorption are of relevance,

a) The isothermal integral heat of adsorption.

This is the total heat involved in the adsorption process from zero adsorbate loading to some final adsorbate loading (filling rate) at a constant temperature.

b) The differential heat of adsorption.

This is the change in integral heat of adsorption with a change in adsorbate loading. It is dependent upon pressure (or concentration), temperature, and adsorbate coverage or loading (14).

c) The isosteric heat of adsorption, obtained from the application of the thermodynamically derived Clausius-Clapeyron type equation to experimentally measured equilibrium data.

$$q_{iso}^{G} = -R\left[\frac{\partial \ln X}{\partial \frac{1}{T}}\right] \qquad 4.8$$

At a constant adsorbent loading the equilibrium concentration X is plotted as a function of the inverse absolute temperature on semi logarithmic coordinates, and the slopes of the straight-line isosteres yield the isosteric heats. From pairs of isotherms at different temperatures (T_1 and T_2) the isosteric heat may be calculated by Equation 4.9 which is a result of integrating of Equation 4.8.

$$q_{iso}^{G} = 4.58 \frac{T_1 T_2}{T_2 - T_1} \log \frac{X_2}{X_1} \qquad 4.9$$

where X_1 and X_2 are the equilibrium concentrations at temperatures T_1 and T_2 respectively and at constant adsorbate loading (G) for each adsorbate.

The superscript G in Equations 4.8 and 4.9 is an indication that the isosteric heat of adsorption must be calculated at a fixed coverage of adsorption. Thus,

if q_{iso}^{G}

is assumed to be independent of temperature, Equation 4.8 suggests that a plot of 1n X versus1/T will produce a straight line of slope

q_{iso}^{G}/R.

4.5 KINETICS OF ADSORPTION

The rate of physical adsorption at a surface is generally high so that in a porous adsorbent the overall rate of adsorption is always controlled by the resistances to mass or heat transfer, rather than by the intrinsic sorption kinetics[29]. However to relate the dynamically varying solids and solution-phase concentrations of solute at any time and position in an adsorption column, it is necessary to fully understand the kinetics of solute transport. Consequently, the mechanisms of such transport must be considered in detail.

The overall diffusion process associated with a zeolite particle represents the combined effects of

(i) diffusion through the boundary layer of fluid surrounding the adsorbent particle (film or external diffusion)

(ii) diffusion within the pores of the particle (pore diffusion)

(iii) diffusion along the surface of the pores (pore-surface diffusion)

(iv) adsorption on the internal pore surfaces (adsorption).

This is illustrated in Figure 4.2[35]

For measurement of diffusion of a diffusing single component, in bi-disperse systems, such as beds of porous zeolite crystals at constant pressure, the following equation is generally used for small values of time [39].

$$\frac{G_t - G_o}{G_\infty - G_o} = 6\left(\frac{D_e}{\pi a^2}\right)^{\frac{1}{2}} \sqrt{t} \qquad 4.10$$

where:

G_∞ = the amount adsorbed at equilibrium

G_t = the amount adsorbed at time t

G_o = the amount adsorbed at time 0

D_e = diffusivity (or diffusion constant, coefficient), cm^2/sec

a = radius of the particle

Thus, by plotting the term on the left side in Equation 4.10 versus $\sqrt{t}$, the diffusivity can be directly evaluated from the slope. The experimental data can be obtained from kinetic sorption experiments.

One of the most striking characteristics of zeolitic diffusion is its strong dependence on temperature. Diffusion rate generally increases exponentially with temperature as expressed by the Arrhenius type of relationship,

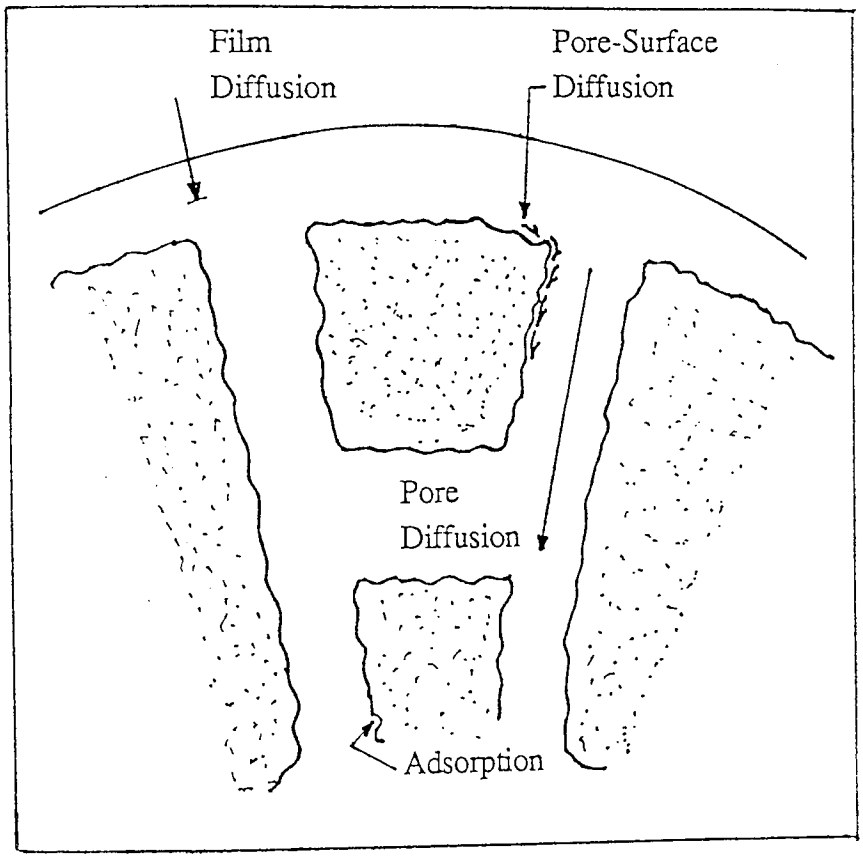

Figure 4.2 Adsorption on a porous adsorbent particle

$$D = D_o e^{-E/RT} \qquad 4.11$$

where

E = the activation energy

D_O = constant

Equation 4.11 can be written in linear form

$$\ln D = \ln D_o - E/RT \qquad 4.12$$

Plotting $\ln D$ versus $\frac{1}{T}$ yields a straight line of slope = E/R

from which the activation energy E can be estimated without prior determination of diffusivity D. If one considers the plots of G_t/G_∞ against time at each of two different temperatures T_1 and T_2, and measures the times t_1 and t_2 taken for G_t/G_∞ to reach the same value at each of the two temperature then,

$$D_1 t_1 = D_2 t_2 \qquad 4.13$$

Accordingly

$$\ln \frac{t_1}{t_2} = \ln \frac{D_2}{D_1} = \frac{E}{R}\left[\frac{1}{T_1} - \frac{1}{T_2}\right] \qquad 4.14$$

$$E = 4.58 \frac{T_1 \ T_2}{T_2 - T_1} \log \frac{t_1}{t_2} \qquad 4.15$$

This method is applicable for any distribution of crystal shapes and sizes.

CHAPTER 5

ADSORPTION DESIGN THEORY

5.1 INTRODUCTION

The design of an adsorption system to accomplish a desired degree of separation requires prediction of the rates of adsorption either by:

(a) The prediction of the complete breakthrough curve where it is possible to describe the unsteady state process of fixed-bed adsorption by a generalized differential equation based on a material balance around an increment of bed height. This method is discussed in Chapter 8.

or, (b) The mass-transfer zone concept or adsorption zone approach in which a total resistance is expressed in terms of an amount of unused adsorbent, which must be added to the adsorbent equilibrium requirement. This concept, originally suggested by Michaels for fixed-bed ion-exchange columns[40], provides a simple and effective method for considering rate phenomena in fixed-bed adsorption systems.

5.2 BREAKTHROUGH CURVES

In fixed bed, dynamic adsorption systems, a fluid feed that is rich in the sorbable component flows through a bed containing absorbent particles. An adsorption zone moves through the bed in the direction of the feed flow. Upstream from this zone the bed is essentially saturated with adsorbate and the concentration of solute in the solvent is the same as the feed concentration. Downstream, the bed is essentially free from adsorbate and the solvent is solute-free. When the adsorption zone reaches the end of the bed, the concentration of solute in the effluent rises, in a characteristic S-shape "breakthrough" curve, to the feed concentration at which point the bed is completely saturated with adsorbate. The point at which the concentration of

solute in the effluent rises to five percent of the feed concentration is termed the "breakthrough point'. The 'exhaustion point' of the bed is reached when the effluent concentration reaches 95 percent of the feed concentration. At any given time, the adsorption zone is defined as that portion of the bed over which the concentration changes from five percent to 95 percent of the feed concentration. An idealized breakthrough curve is shown in Figure 5.1.

5.3 ADSORPTION ZONE APPROACH

The adsorption zone approach is based on the important assumption that once the adsorption zone is established, the height and velocity of the zone remain constant as it moves through the bed. Gleuckauf and Coates[32] pointed out that if the equilibrium curve is concave to the fluid-phase concentration axis, the height of the adsorption zone decreases as it moves through the bed. However, this "self-sharpening" characteristic is counteracted by a finite rate of mass transfer and axial diffusion so that, in practice, zones of nearly constant height are often observed. This approach is also limited by the following important assumptions:

(i) The bed is uniformly packed;

(ii) the adsorbent temperature and initial adsorbate loading are uniform throughout the bed;

(iii) the feed rate, feed temperature and feed composition are constant;

(iv) there are no radial temperature, concentration or flow gradients;

(v) the temperatures of both the fluid and adsorbent are essentially equal;

(vi) the fluid does not undergo a phase change;

(vii) adsorption heat effects are negligible; and

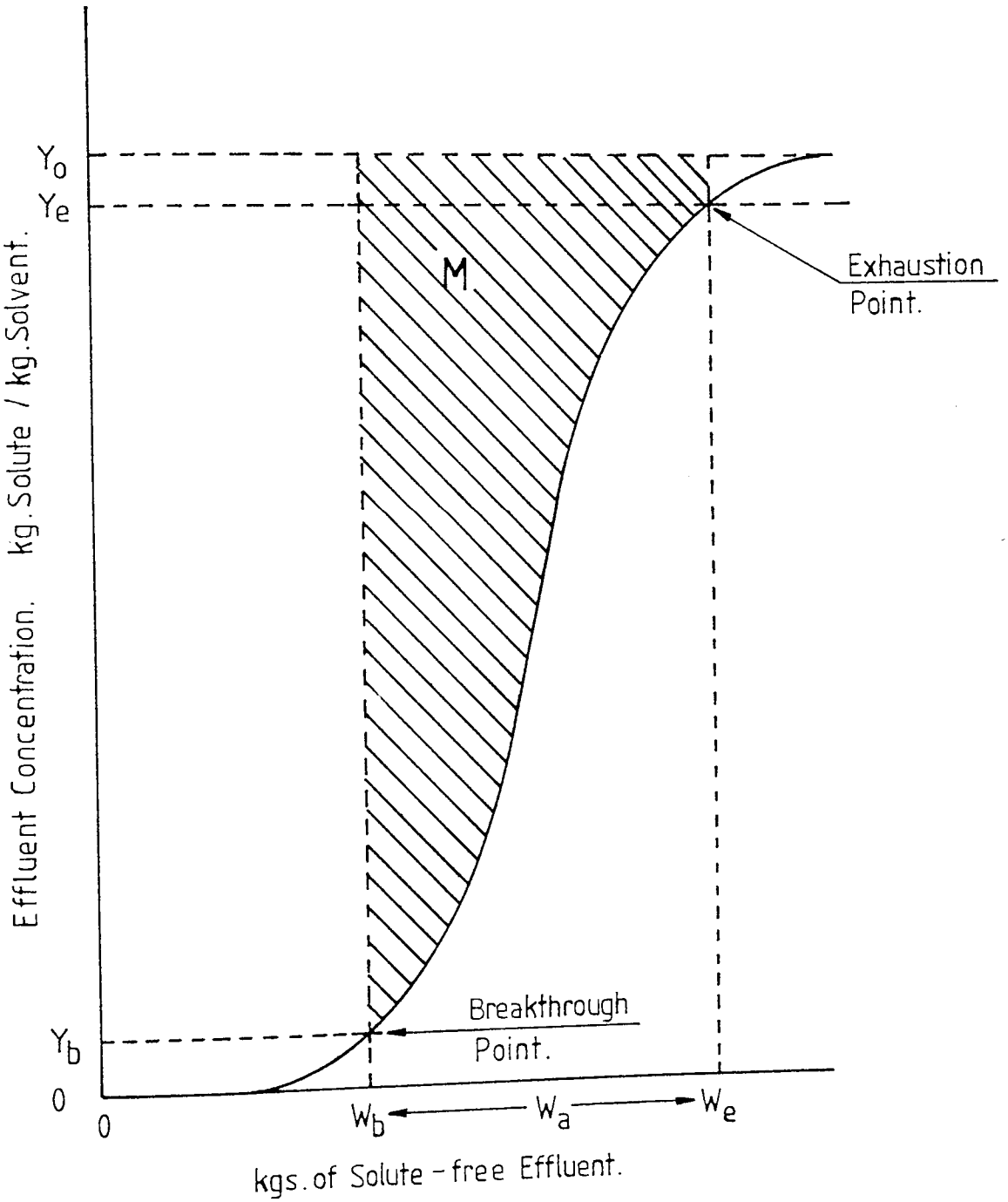

Figure 5.1 Idealised breakthrough curve

(viii) chemical reactions do not occur.

5.3.1 The Height of the Adsorption Zone

The height of the adsorption zone can be calculated from experimental breakthrough data by two independent equations. These equations are derived in detail in Appendix A. The first equation is based on a constant width, constant velocity adsorption zone and a zone formation time which is proportional to the fractional saturation of the adsorbent within the zone at the breakthrough point. The zone height Z_a, is expressed as:

$$Z_a = Z \frac{W_a}{W_e - (1 - f) W_a} \qquad 5.1$$

where,

Z = Total bed height, m.

W_a = Solute-free effluent collected between the breakthrough and the exhaustion points, kg.

W_e = Total solute-free effluent collected up to the exhaustion point, kg.

f = Fractional ability of adsorbent within the adsorption zone to adsorb additional solute.

The second equation for determining the zone height is based on a solute material balance within the adsorption zone, and is expressed as:

$$Z_a = \frac{Q_a}{A \rho_b \ f \ (T.D.C.)} \qquad 5.2$$

where,

Q_a = Quantity of solute adsorbed between the breakthrough and exhaustion points, kg.

A = Cross-sectional area of column, sq.m.

ρ_b = Bulk density of solute-free adsorbent, kg/cu.m.

T.D.C.= Loading of adsorbent in equilibrium with fluid of feed concentration, kg. solute/kg. adsorbent or Total Dynamic Capacity

Agreement between Equations 5.1 and 5.2 will confirm the validity of the assumptions considered in Equation 5.1. The height of the adsorption zone can also be derived from the expression for the rate of mass transfer in the adsorption zone. The zone height, as a function of the overall mass-transfer coefficient, number of transfer units, and flow rate, is given by:

$$Z_a = \frac{G_s}{K_y a} \int_{Y_b}^{y_e} \frac{dY}{Y-Y^*} = \frac{G_s N_t}{K_y a} \qquad 5.3$$

where,

G_S = Superficial mass flow rate of solute-free solvent, $\frac{\text{kg solvent}}{\text{(hr.)(sq.m.)}}$

$K_y a$ = overall mass-transfer coefficient, $^{kg}/_{(hr)(m^3)}$

N_t = Number of overall transfer units based on a weight ratio driving force in the fluid phase.

Y = Concentration of fluid stream at any point in the adsorption zone, kg solute/kg solvent.

Y_e = Concentration of fluid stream at exhaustion point,

kgsolute/kg.solvent.

Y_b = Concentration of fluid stream at breakthrough point, kg.solute/kg.solvent.

Y^* = Concentration of fluid stream at equilibrium with adsorbent at any point in the adsorption zone, kg.solute/kg.solvent.

Equation 5.3, which is derived in Appendix A, is based on the assumption that $K_y a$ is a constant throughout the adsorption zone. Implicit in this assumption is isothermal behavior. To determine the overall mass-transfer coefficient from Equation 5.3 it is necessary to have experimental equilibrium data to calculate N_t and the calculated zone height from Equation 5.1 or 5.2.

5.3.2 Determination of Bed Dynamic Capacities from S-Curves

For any fixed-bed unit operating at constant fluid flow rate for which the S-curve has been determined as in Figure 5.2, it is clear that the total dynamic capacity of the bed can be calculated by graphical integration of the relation.

$$\text{T.D.C.} = \left[Y_o \int_{w=o}^{w=\infty} \frac{Y_o - Y}{Y_o} \, dW \right] / m_s \qquad 5.4$$

where

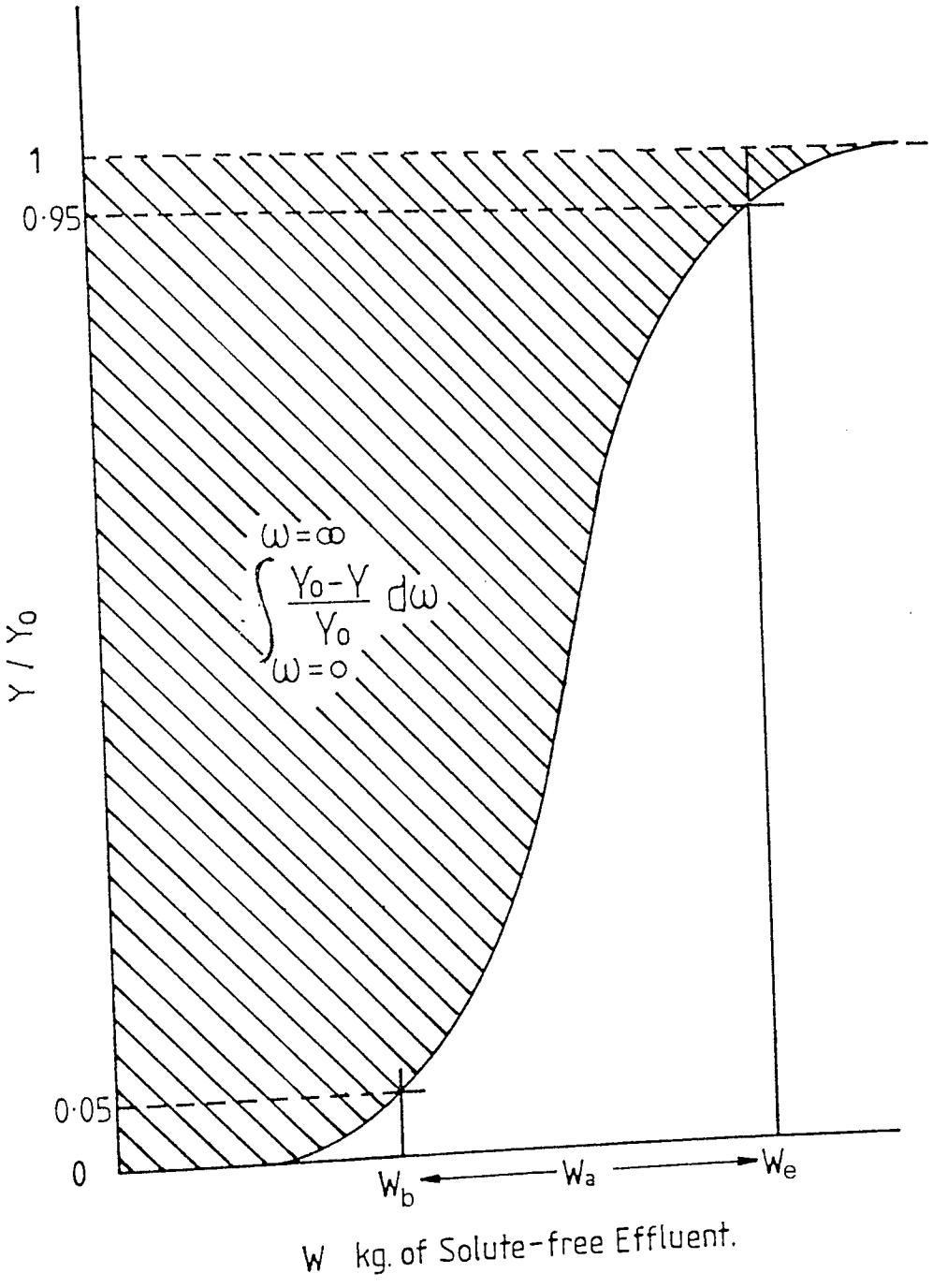

Figure 5.2 Breakthrough curve used in determination of total dynamic capacity

$$\int_{w=0}^{w=\infty} \frac{Y_o - Y}{Y_o} dW = \text{Area above breakthrough curve between.}$$

w = o and w at Y/Yo = 1.0

Y_o = Feed concentration kg solute/kg solvent.

m_s = Weight of molecular sieve kg.

5.3.3. Determination of Breakthrough Dynamic Capacity by Zone-Height Method (40)

If an adsorption fixed-bed is operated to the break-through point i.e., operated until the concentration of solute in the effluent reaches 5% of its value in the feed - the only portion of the bed not essentially exhausted will be the band at the bottom of the bed corresponding to the mass transfer zone. Since this region is partly saturated with adsorbate, the break-through capacity of the bed may be determined from the relation

$$\text{B.D.C.} = \text{T.D.C.} \left(\frac{Z - (1 - f) Z_a}{Z} \right) \qquad 5.5$$

where, Z = Bed height, m.

Z_a = Height of mass-transfer zone, m.

f = Fractional ability of adsorbent within the adsorption zone to adsorb additional solute.

The height of the mass-transfer zone is a measure of the rate of adsorption under a fixed average concentration driving force.

The variables influencing this height are, therefore, those which affect the resistance to mass transfer, that is, temperature, adsorbent particle size, feed concentration, and liquor velocity. Since the process occurring in the zone is not significantly influenced by the exhausted adsorbent below it, or the fresh adsorbent above it, the zone height should be independent of both the over-all height of the bed and bed cross-sectional area. Thus, if the zone height is known for a given adsorption process under conditions of specified temperature, influent solute concentration, adsorbent particle size, and fluid flow rate, the capacity of a bed of any desired height and cross section can be calculated from Equation 5.5 for the specified conditions. It is clear that as long as mass transfer zone heights are relatively small, they can be calculated by the methods outlined above from the S curve data obtained from simple, laboratory size columns. If fluid velocity is the only variable to be considered, a single column will suffice for the construction of a plot of zone height as a function of fluid velocity, from which a practical adsorption unit can be designed [40].

5.3.4 Analysing Mass-Transfer Waves

The mass transfer front, or wave, is the fluid concentration or adsorbent loading profile of the adsorbable component over the mass transfer zone[41]. The fact that real mass-transfer waves are S-shaped is evidence of resistance to mass transfer. The greater the resistance, the longer is the wave. As mass transfer resistance decreases, the wave becomes shorter. In the ideal case the curve becomes a vertical, straight line (zero length). The "ideal" mass-transfer wave is called the stoichiometric wave or front.

At breakthrough under ideal conditions, the concentration of sorbable component in the effluent would change instantaneously from Y_B to Y_E, and the entire bed would be loaded to equilibrium capacity. Breakthrough under the ideal conditions of no mass-transfer resistance is defined as the stoichiometric breakthrough. The time at which stoichiometric breakthrough occurs is termed the stoichiometric time, and designated θ_S.

All real mass-transfer waves can be analysed in terms of an equivalent stoichiometric front.

In Figure 5.3 the area below the wave (a, g, d, e, a) reflects unused adsorbent capacity. The ratio of the area above the wave (a, g, d, b, a) to the total area of a rectangle (a, b, d, e, a) is the fraction of used adsorbent in the mass transfer zone. A vertical straight line drawn through the mass transfer wave at g- such that the area a, f, c, b, a, is equal to the area a, g, d, b, a - yields an equivalent stoichiometric front for the particular system. Then the entire rectangle h, f, c, k, h corresponds to adsorbent at its equilibrium loading Y_E, and is defined as the equivalent equilibrium section. It is specified in terms of the length of equivalent equilibrium section, LES. The area f, e, d, c, f corresponds to adsorbent at its initial loading, X_O, and by definition, it is equivalent unused bed, or, briefly, the unused bed. It is specified in terms of the length of unused bed.

5.4 LENGTH OF UNUSED BED (LUB)

This method produces a useful approximation in cases where neither the fluid or solid phase mass transfer coefficients are available. The solid-phase coefficient particularly is not usually available for most industrial developments.

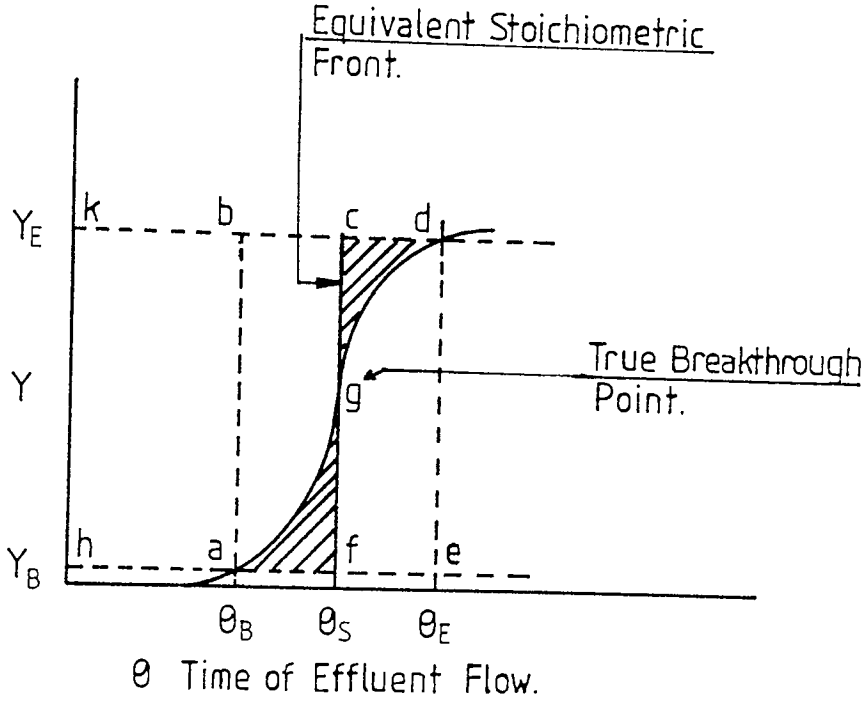

Figure 5.3 Mass transfer fronts

The LUB concept is of considerable value in the design of molecular sieve processes. Collins defined the length of unused bed (LUB) as an additional quantity of adsorbent added to compensate for the presence of a mass transfer zone during dynamic adsorption (41). The length of unused bed is expressed by the equation:

$$LUB = \frac{(\theta_s - \theta_B)}{\theta_s} Z \qquad 5.6$$

where

Z = Adsorbent bed length.

θ_B = Time at which breakthrough occurs

θ_S = Time at which the stoichiometric breakthrough occurs.

Equation 5.6 is derived in Appendix A.

The LUB depends on many factors including particle size of the molecular sieve, temperature, properties of the material being sorbed and other material presorbed on the sieves, and the activity of the sieves.

The LUB concept is a useful method for design purposes in the case of a favourable adsorption equilibrium.

5.5 DEGREE OF SATURATION

Knowledge of the percentage approach to saturation at the breakpoint is one

requirement for the design of a fixed-bed adsorber. Considering an adsorption column Z m. tall and of unit cross-sectional area, it contains $Z\,\rho_b$ kg adsorbent, where ρ_b is the apparent packed density of the solid in the bed. If this were all in equilibrium with the entering fluid, and therefore completely saturated at an adsorbate concentration X_S kg adsorbate/kg adsorbent, the adsorbate weight would be $Z\rho_b X_S$ kg. At the breakpoint, the adsorption zone of height Z_a m is still in the column at the bottom, but the rest of the column, $Z - Z_a$ m, is substantially saturated. At the breakpoint, therefore, the adsorbed solute is $(Z - Z_a)\,\rho_b\,X_S + Z_a\,\rho_b\,(1 - f)X_S$ kg. The degree of saturation of the column at the breakpoint is therefore[42]:

$$\text{Degree of saturation} = \frac{(Z - Z_a)\,\rho_b X_S + Z_a\,\rho_b\,(1 - f)X_S}{Z\,\rho_b\,X_S} = \frac{Z - f\,Z_a}{Z} \qquad 5.7$$

5.6 MASS TRANSFER COEFFICIENTS

The overall resistance to mass transfer in molecular sieves can be envisaged to be comprised of at least three individual resistances to diffusion :

1. external film resistance;
2. pore diffusion resistance;

and 3. intracrystalline (zeolite) diffusion resistance.

Schumacher [43] considered that during the initial portions of the breakthrough curve, adsorption will take place in crystals near the surface of the pellet and that the external film resistance will be controlling. This would appear to be a reasonable assumption. Conversely, during the final portion of the breakthrough

curve, the adsorbent is almost saturated and a molecule may have to diffuse a distance into the pellet before being adsorbed, in which case pore diffusion or intracrystalline diffusion may control the rate of mass transfer. Thus, it is likely that the $K_y a$ calculated from Equation 5.3 is not constant but represents an average value for the entire adsorption zone.

The particles generally have a bidisperse pore structure as indicated in Figure 5.4. During physical adsorption, the resistance to mass transfer of solute from the fluid to the adsorbed state on the solid can be considered to be composed of (29)

a The external fluid film resistance, and

b diffusional resistances to solute mass transfer through the fluid within the pores of the solid.

5.6.1 The External Film Mass Transfer Coefficient

Each particle in the bed is assumed to be surrounded by a laminar sublayer, through which mass transfer occurs by molecular diffusion. The thickness of the laminar sublayer, and hence the mass transfer coefficient, is determined by the hydrodynamic conditions. It is convenient to correlate mass transfer rates in terms of an effective mass transfer coefficient (k_f) defined according to a linear driving force equation(29):

$$\frac{\partial \bar{q}}{\partial t} = k_f a\,(C - C^*) = \frac{3k_f}{R_p}\,(C - C^*) \qquad 5.8$$

where

a is the external surface area per unit particle volume. ($3/R_p$ for spherical particles) and $\bar{q}$ is the adsorbed phase concentration averaged over a particle.

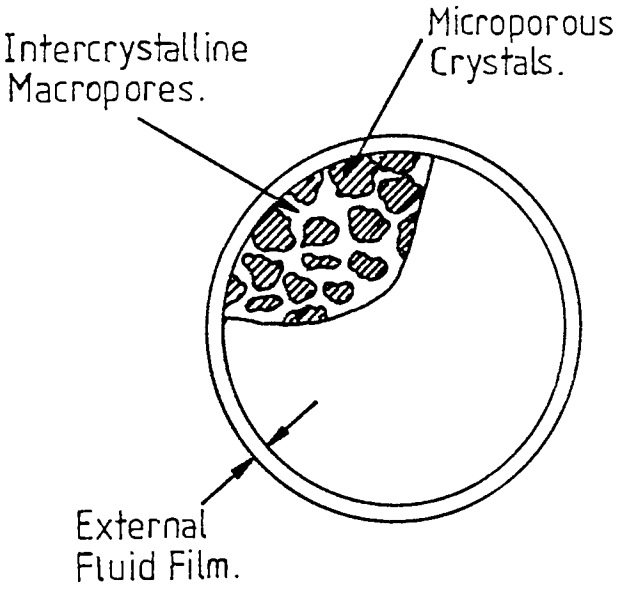

Figure 5.4 Schematic diagram of composite adsorbent pellet showing the three principal resistances to mass transfer

C* is the fluid concentration at the exterior surface of the solid.

In the case under discussion the concentration of sorbate throughout the solid is uniform and is related to C* through the sorption isotherm.

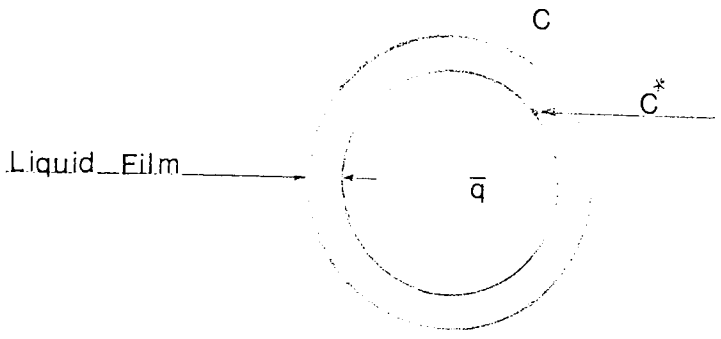

The appropriate dimensionless group characterizing film mass transfer is the Sherwood number, defined by

$$Sh = 2 R_p k_f / D_m \qquad 5.9$$

which is the analog of the Nusselt number for heat transfer. A simple analysis of heat conduction from an isolated spherical particle surrounded by a stagnant fluid leads to the conclusion that the limiting value of Nusselt number for low Reynolds number flows is 2.0, and by analogy this should also be the lower limit for the Sherwood number. At higher Reynolds numbers convective effects become significant and a correlation of the form Sh = f (Sc, Re) is to be expected.

Experimental mass transfer data at low Reynolds numbers show a great deal of scatter, but most of the reported Sherwood numbers fall somewhat below the limit of 2.0 predicted from the Ranz-Marshall correlation which was derived from the

results of an experimental study of mass transfer rates for freely falling solid spheres, and which has been widely applied to packed beds.

$$Sh = \frac{2\,k_f R_p}{D_m} = 2.0 + 0.6\,Sc^{1/3}\,Re^{1/2} \qquad 5.10$$

Wilson and Geankoplis suggested the following correlation for liquids, (29)

$$.0015 < Re < 55, \quad Sh = \frac{1.09}{\varepsilon}\,Re^{0.33} Sc^{0.33} \qquad 5.11$$

$$55 < Re < 1050, \quad Sh = \frac{0.25}{\varepsilon}\,Re^{0.69}\,Sc^{0.33} \qquad 5.12$$

where

$$Sc = \frac{\mu}{\rho_f\,D_m}$$

$$Re = \frac{\rho_f\,U\varepsilon\,(2R_p)}{\mu}$$

U = interstitial velocity of fluid

D_m = molecular diffusivity

ρ_f = density of fluid

μ = viscosity of the fluid

R_p = adsorbant radius

ε = voidage of adsorbent bed

5.6.2 Solid-phase Mass-Transfer Coefficient

Diffusion which results from a concentration gradient within the individual

sorbent particle is called particle phase, solid-phase, sorbent-phase, or internal diffusion.

For spherical symmetry, the rate is

$$\frac{\delta Y}{\delta t} = D_p\left(\frac{\delta^2 Y}{\delta r^2} + \frac{2}{r}\frac{\delta Y}{\delta r}\right) \qquad 5.13$$

where

D_p = the particle-phase diffusivity

Y = the dimensionless solid-phase concentration at an internal radius r

t = adsorption time.

This equation is often approximated by the linear-driving force relation of Glueckauf and Coates (32).

$$\frac{dY}{dt} = \varphi_p\, k_p\, a\, (Y^* - Y) \qquad 5.14$$

where

Y = the dimensionless concentration of the solute of interest averaged over the entire particle

Y* = the value that would be in equilibrium with the instantaneous fluid-phase concentration outside the particle.

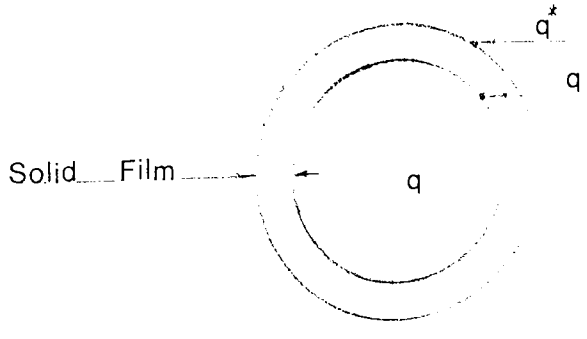

φ_p = factor obtained by comparing the true slope of the curve of particle uptake vs time with the slope given by Equation (5.14) at Y = 0.5

a = the outersurface interfacial area of contacting system (solid plus fluid), or $\frac{6(1-\varepsilon)}{d_p}$

$k_p = \frac{10\, D_p}{d_p(1-\varepsilon)} \equiv$ solid-phase mass transfer coefficient

The rate equation can, also, be expressed in terms of a hypothetical solid film coefficient $k_p a$ and solid-phase concentration driving force $(q^* - q)$

$$\frac{\delta q}{\delta t} = k_p \frac{a}{1-\varepsilon} (q^* - q) \qquad 5.15$$

where

q^* = the concentration of the sorbed phase in equilibrium with C,

q = the mean concentration of sorbed phase averaged over the pellet

according to Satterfield[44] as:

$$D_{pore} = D_m \varepsilon_p / \tau \quad \text{for a liquid} \qquad 5.17$$

where

ε_p = the internal porosity of the particle

τ = the tortuosity

D_m = molecular diffusion

The product k_p a is related to the diffusivity and the effective spherical particle diameter d_p through the equation:

$$k_p a = \frac{60\, \varepsilon_p\, D_m}{d_p^2\, \tau} \qquad 5.18$$

5.6.3 Overall Mass Transfer Coefficient

At different times during the period when the pellet is exposed to a sorption wave, both the external film and the internal diffusional resistance are important in determining the overall rate of transfer. When the sorption wave reaches a pellet and the fluid concentration around it begins to increase, the external film is important. Thus neglect of the external film in calculations will result in the prediction of a sharper breakthrough curve than that occurring in practice.

During the latter stages of an adsorption process the transfer rate is usually controlled by internal diffusion. Hence a method is required of adding both internal and external effects, which lead to the concept of overall mass transfer coefficient for the adsorption processes. Treybal treated overall mass transfer coefficient as follows(42).

In representing the overall mass-transfer coefficient $K_y a$ based on a, the outside surface of the solid particles, the rate of solute transfer over the differential height of adsorber dZ, Figure 5.5, can be written in the usual manner as (42).

$$L_S dX = G_S dY = K_y a\,(Y - Y^*)\,dZ \qquad 5.19$$

where

L_S = solid mass velocity mass/(cross-sectional area of column)(time)

G_S = solute-free fluid mass velocity "

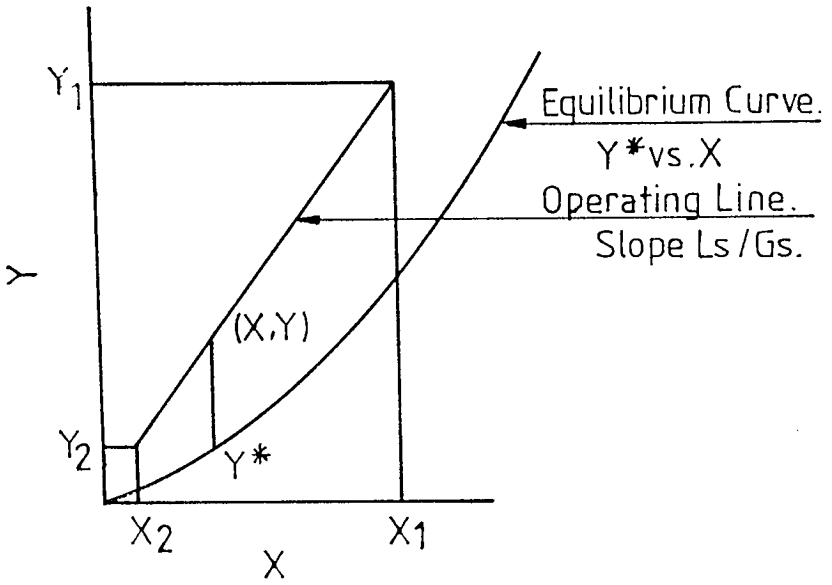

Figure 5.6 Operating line and equilibrium curve

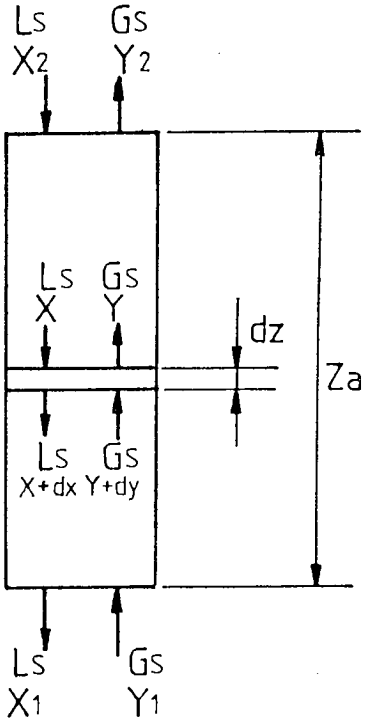

Figure 5.5 Active adsorption height

Y^* = the equilibrium composition in the liquid corresponding to the adsorbate composition X.

The driving force $Y - Y^*$ is then represented by the vertical distance between operating line and equilibrium curve Figure 5.6. Rearranging Equation 5.19 and integrating defines the number of transfer units N_t,

$$N_t = \int_{Y_2}^{Y_1} \frac{dy}{(Y - Y^*)} = \frac{K_y a}{G_s} \int_{o}^{Z_a} dZ = \frac{K_y a}{G_s} Z_a \qquad 5.20$$

The value of integral in Equation 5.20 is usually evaluated graphically, as illustrated in Appendix B, and the active height Z_a determined using Equations 5.1 or 5.2. The overall mass transfer coefficient can be calculated from knowledge of the individual mass transfer coefficients applying the expression

$$\frac{1}{K_y a} = \frac{1}{k_y a} + \frac{1}{k_p a} \qquad 5.21$$

CHAPTER 6
PREVIOUS INVESTIGATIONS

6. PREVIOUS INVESTIGATIONS

In 1924, Weigel and Steinhoff (45) first reported that zeolite crystals can selectively adsorb molecules of certain dimensions and configurations from a mixture of different types of molecules. Subsequently much literature have been published concerning the unique characteristics of this interesting class of adosorbents as summarized in Chapter 3.

Many studies have been reported on adsorption of normal paraffins on molecular sieves (46, 47, 48, 49, 50, 51, 37, 52, 43). These studies covered the adsorption of light, middle, and some heavy normal paraffins, and included both vapour-phase and liquid-phase adsorption processes.

A considerable amount of research has been done on the vapour-phase adsorption of pure and binary normal paraffins (56, 57, 58, 59, 60). The published articles for the liquid-phase adsorption process of normal paraffins relate to ,

a) Binary solution composed of single adsorbable normal parraffin and non-adsorbable solvent(53).

b) Binary solution composed of two adsorbable normal paraffins(54).

c) Ternary solution composed of two adsorbable normal paraffins and one non-adsorbable solvent(7).

The experimental studies carried out to investigate the adsorption processes covered both batch and the dynamic systems.

6.1 BATCH SYSTEM STUDIES

A method was described in 1962, by O'Connor, et-al(55), for the determination of normal paraffins in C_{20} to C_{32} paraffin waxes. Adsorption of the

normal paraffins was accomplished by refluxing an iso-octane solution of the wax in the presence of pelleted molecular sieves, Type 5A. To demonstrate that the rate of adsorption is dependent upon the molecular weight of normal paraffin, 2 grams each of normal paraffins C_{20}, C_{28}, and C_{32}, were dissolved in 100 ml of iso-octane and refluxed with 40 grams of sieves. As the molecular weight increased, the rate of adsorption became slower. When the molecular weight and solution concentration were held constant, the rate of adsorption was dependent upon the quantity of adsorbent available; the greater the quantity of adsorbent, the higher the adsorption rate. In another study[61] it was illustrated that no cyclic or branched chain hydrocarbons could be adsorbed by 5A molecular sieve, where a synthetic blend was prepared, using n-decylcyclohexane, 2-methyldecane, and n-tridecane dissolved in isopentane, to be adsorbed by molecular sieves, Type 5A. Examination of the unadsorbed residue by gas chromatography showed that n-tridecane was adsorbed but n-decylcyclohexane and 2-methyldecane were not adsorbed.

Burgess, et-al[62] studied the adsorption of normal paraffins within the C_4-C_{20} range in specially treated type 5A molecular sieves and tested the relations of Langmuir, Bering and Serpinskii to illustrate the maximum number of molecules which can be present within a sieve cavity. They reported that, the maximum number of molecules decreases with increasing molecular weight, down to values of 1.2 ± 0.5 for C_{10}, and 0.75 ± 0.5 for C_{20}. In the C_{10} - C_{20} range, the only interaction forces are those between the single hydrocarbon molecule and the sieve wall; with smaller molecules, C_8 to C_1, molecule - molecule interactions will also contribute to the total energy of the system. The results of Burgess (and, as discussed later in Chapter 9, those of the present work with C_{12}, C_{16} and C_{20} normal paraffins) do not agree with

the prediction by Barrer (63) that, with increasing carbon number, the isosteric heats of sorption should rise at a constant rate.

The liquid-phase adsorption of normal paraffins C_7, C_{10}, C_{12}, and C_{14} on Linde Type 5A molecular sieve has been investigated, by Sundstrom and Krautz(46), to determine the effect of molecular size, temperature, and concentration on the equilibrium loading for single and binary systems. Their study showed irregularity of the variation of the equilibrium loading with molecular weight, which was inconsistent with the regular decrease of equilibrium loading with increasing molecular weight of normal paraffins described in other literature (52) (and as discussed later for normal paraffins C_{12}, C_{16} and C_{20} in the present work). The equilibrium loading of normal dodecane at temperature 30°C was shown to be 12.4gm/100gm sieve (in good agreement with the result of 13.6gm/100gm sieve subsequently reported in Chapter 9).

In the case of a single system the equilibrium loading capacity decreased with increasing temperature, and the adsorptive capacity of the molecular sieves was not measureably changed by the presence of non-adsorbable material. In the binary systems the normal paraffins with lower molecular weight were preferentially adsorbed. The selectivity followed the order:

$$n\text{-}C_6 > n\text{-}C_{10} > n\text{-}C_{12} > n\text{-}C_{14}$$

In a study on NaY and HY zeolite(58) aromatic compounds were selectively adsorbed in preference to paraffins and naphthenes. Smaller aromatic compounds were adsorbed in preference to larger aromatic compounds. Satterfield and Cheng reported that for molecules of the same size the sieving effect has no role in adsorption but physiochemical adsorption and steric effects can play an important role in this selectivity.

In another study(64), Satterfield and Cheng investigated the diffusion

rates of mesitylene (1,3,5 trimethyl benzene) and of mesidine (2,4,6-tr aniline) in NaY at two temperatures, 0°C and 30°C. The estimated diffusion coefficients were at 0°C 15.4 x 10^{-13} sq.cm./sec. for mesitylene and 0.187 x 10^{-13} sq. cm./sec. for mesidine. Since the steric properties of these two compounds, molecular size and shape, are essentially the same, they attributed the difference in the diffusion rate to the fact that the presence of the polar group, $-NH_2$, in mesidine greatly reduced its rate of diffusion compared with that of mesitylene, in zeolites composed of positive (cation) and negative (alumino) ions. Therefore, a strong electrostatic field must exist in their pores. This electrostatic field is strong enough to cause substantial shifts of bonding electrons in adsorbed molecules and the strong interaction between the zeolite and the diffusing molecules. As a result of this interaction, molecules with higher polarity would be expected to have lower mobility in the zeolite channels and thus a slower diffusion rate.

Falkovich, et al studied the adsorption of normal paraffins C_{10}, C_{14}, C_{16}, C_{17}, C_{20}, C_{24}, and C_{28} from isooctane solutions on particular granules of CaA zeolite at temperatures of 20, 100 and 150°C[52]. It was concluded that over a fairly wide concentration range the cavities of CaA zeolite are only partially occupied by the adsorbate molecules, the rest of the adsorbing area remaining free. Therefore the usual equations cannot be used, since these equations assume equilibrium between the adsorbed and bulk binary solutions. An equation for molecular adsorption from binary solutions in the form:

$$G_1^n = \frac{a_m (f-1)\, x\, (1-x)}{1 + (f-1)\, x} \qquad 6.1$$

was used.

where a_m is the maximum amount of component adsorbed filling the cavities of 1gm of zeolite, and f is a function characterizing the collective interactions occurring in the zeolite-solutions system.

Equilibrium data showed that the above equation fits the adsorption isotherms satisfactorily. It was shown also that both f and a_m decrease with increasing temperature, due to increasing molecular mobility in the cavities and a weakening of intermolecular bonds. Adsorption capacity decreased as the chain length of the normal paraffin molecule increased.

Falkovich, et al the authors of the previous investigation, studied the kinetics of adsorption of some normal paraffins C_{10}, C_{14}, C_{16}, and C_{17} by CaA zeolite at 20, 100, and 150°C(37). The kinetic data for each binary system were illustrated in terms of the ratio G_t/G as a function of $\sqrt{t}$, where G_t is the amount of the adsorption at time t, and G is the equilibrium amount of adsorption obtained from the isotherm for equilibrium adsorption.

They calculated the effective diffusion coefficient, the total diffusion coefficient, and the apparent activation energies. From them it was concluded that the effective diffusion coefficient for adsorption at 20°C depends only slightly on the length of the hydrocarbon chain in a normal paraffin; with increasing temperature the diffusion rate increased rapidly, and that the apparent activation energies were 3-4 kcal/mol at moderate temperature and 10-15 kcal/mole at higher temperatures indicating a change in the nature of the diffusion.

Liquid-phase adsorption of normal paraffins, C_5, C_6, C_7, and C_8 from benzene on Linde 5A molecular sieve was carried out, by Gupta, et. al., (57). The dynamic adsorption of normal heptane showed that the time to reach equilibrium

decreased with increasing temperature. Adsorption isotherms showed an initial increase in equilibrium loading with concentration followed by a relatively large range of concentration over which the equilibrium loading was nearly constant and then a further increase at still higher concentration. They reported that the reason for this upward increase in equilibrium loading at high paraffin concentrations was probably associated with adsorption on external surfaces and not with intracrystalline adsorption. The effect of temperature was a maximum for normal pentane and reduced for higher paraffins, and the effect of concentration on the equilibrium loading increased with increase in molecular weight for a particular temperature.

Yakimova et. al.[65] investigated the influence of temperature on the kinetics of liquid-phase adsorption of normal paraffins on zeolite CaA in the temperature range -20 to 100°C. From kinetic curves for the adsorption of normal nonane from a mixture with toluene at various temperatures there was clearly an appreciable rise in the rate of adsorption with increasing temperature. They reported the existence of a threshold temperature, below which normal paraffin molecules would not effectively penetrate into the primary structure of zeolite, at a temperature of -20°C.

Hassan[7], studied the adsorption of normal paraffins C_6, C_8, C_9, C_{10}, C_{12}, and C_{14} dissolved in non-adsorbable solvent, benzene on 5A molecular sieve crystals. The experiments were performed to generate adsorption isotherm and adsorption rate data. The results of this study showed that at 25°C the ternary systems having two adsorbable solutes, exhibited adsorption isotherms which were not irreversible i.e. the equilibrium loadings of the liquid normal paraffins in 5A zeolites were dependent on the liquid phase concentration. This was not the case with single solutes adsorbed from binary liquid solutions which exhibited irreversible adsorption.

Al-Zaid[66] performed a detailed study of the feasibility of adsorptive

purification of slack waxes from traces of aromatic compounds using type 13X molecular sieves to achieve ≤ 0.01% aromatics in the product. Equilibrium isotherms were determined for aromatic compounds such as cumene, dodecylbenzene, naphthalene, 1-methylnaphthalene, and others at 303°K and 343°K. Lower molecular weight, or more compact, molecules were preferentially adsorbed. An increase in adsorption temperature resulted in a decrease in the adsorption value. The isosteric heat of adsorption and the kinetics of adsorption for different aromatic compounds were studied. The diffusivity decreased significantly when a long alkyl chain was attached to the benzene ring e.g. in dodecylbenzene; molecules with small cross-sectional diameter such as cumene were adsorbed most rapidly. The sorption rate increased with temperature. Studies performed with individual aromatic compounds demonstrated the affinity of type NaX molecular sieves to adsorb aromatics in the concentration range 3% - 5%.

6.2. DYNAMIC SYSTEM STUDIES

Numerous studies have been made of adsorption of normal paraffins using a dynamic flow system which has wide commercial applications in the field of normal paraffins separation. The liquid-phase adsorption of normal hexane from cyclohexane, benzene, and isooctane was studied, by Schumacher and York[43], in a fixed bed of Type 5A molecular sieves at atmospheric pressure from a 5 to 20% normal hexane feed at flow rates between 4 and 60 feet per hour. They reported the effect of flow rate, adsorbent particle size, temperature, feed concentration, and solvent system on the height of the adsorption zone and overall mass transfer coefficient. The design method followed in this work was the adsorption zone approach suggested by

Michaels[40]. The height of the adsorption zone was calculated by two methods. The first is based on a constant width, constant velocity adsorption zone. The second equation is based on a solute material balance within the adsorption zone. The zone height, Z_a, is expressed in two equations respectively as:

$$Z_a = Z W_a/[W_e - (1-f) W_a] \qquad 6.2$$

$$Z_a = Q_a/A \rho_b X_S f \qquad 6.3$$

where Z is the total bed height, W_a is the solute-free effluent collected between the breakthrough and exhaustion points, W_e is the total solute-free effluent collected up to the exhaustion point, f is the fractional ability of adsorbent within the adsorption zone to adsorb additional solute, Q_a is the quantity of solute adsorbed between the breakthrough and exhaustion points, A is the cross-sectional area of the column, ρ_b is the bulk density of solute-free adsorbent, and X_S is the equilibrium loading of the adsorbent. They reported good agreement between the experimental zone heights calculated by Equations 6.2 and 6.3 which justified the assumption of an adsorption zone of constant width and speed. The zone height was dependent on flow rate, particle size, feed concentration, and solvent system, but nearly independent of temperature.

Roberts and York[19] measured the rate of adsorption of normal paraffins C_6, C_{12}, C_{16}, and C_{18}, in packed column, from binary liquid solutions consisting of an adsorbable normal paraffin and non-adsorbable solvent (benzene) using 5Å molecular sieve. The purpose of their research was to study the mechanism of mass transfer in adsorption by molecular sieves. They divided the mass transfer resistances into:

a. The external diffusion which is the same as in any other mass

transfer from a fluid to a solid.

b. Diffusion in the macropores which takes place by bulk diffusion rather than by Knudsen diffusion. The macropore diffusion rate is determined by the mutual diffusivity of the solvent solute pair, the tortuosity factor of the pellet, the pellet size, and the solute concentration.

c. The zeolite diffusion, for which the diffusing molecule is influenced much more strongly by the crystal lattice than by other molecules of its own kind whether gas or liquid. The zeolite diffusion resistance should be a function of only the adsorbate, zeolite lattice structure, and temperature.

The authors reported that several experiments have been carried out to determine zeolite diffusion constants at 25°C for normal paraffins (C_6, C_{12}, C_{16}, and C_{18}). The results showed that the zeolite diffusion constant decreased by only 30% as the chain length increased from 6 to 12 carbon atoms, but was 100 times greater for C_{12} than for C_{16}, which supports the contention of O'Connor and Norris (1960) that paraffins containing more than 14 carbon atoms are adsorbed only very slowly at room temperature.

Two studies have been described by Antonson and Dranoff [68,69] of the adsorption of ethane on type 4A and 5A molecular sieve particles. In the first part of the work they investigated the rate controlling process in the adsorption of ethane from helium by Linde type 4A molecular sieve pellets. They tested their system applying a mathematical model presented by Rosen [70] which was a result of solution of equations, the basic material balance equation which describes the average composition at any axial position in the bed on the assumption of neglecting longitudinal dispersion, the linear adsorption isotherm equation, and the rate equation considering the combined effect of a liquid film and solid diffusion into spherical

particles. The solution involved analytical and numerical techniques to yield C/C_o as a function of time and position in the packed bed. The predicted breakthrough curves fitted the experimental data well, indicating the usefulness of the intraparticle diffusion model in characterizing this process. The temperature dependence of the diffusivity could be well represented by an Arrhenius relation with activation energy of 6.4 kcal/g-mole.

In the second study, these authors investigated the relative importance of macropore and micropore diffusion in the adsorption of ethane by type 4A and 5A molecular sieves. Intraparticle diffusion coefficients were found by comparing experimental breakthrough curves with the theoretical curves of Rosen. Analysis of the diffusivities and their dependence on particle size indicated that diffusion within the crystal micropore controls the rate in 4A pellets, while a combined macropore-micropore process is involved in the 5A pellets.

6.3 MATHEMATICAL MODELS

Numerous studies have been done by many authors to develop mathematical models for dynamic adsorption processes, which facilitate prediction of breakthrough curves, and thus, process efficiency. The prediction of breakthrough curves for a dynamic adsorption process starts with solving the conservation equation subject to boundary conditions, together with the appropriate adsorption rate equation consistent with the equilibrium isotherm. The various mathematical models differ only in the form of the rate expression and the choice between the conservation equation for the case considering axial dispersion and the case neglecting it.

Thomas [71] published a theory of fixed bed performance for application to ion exchange columns. It was assumed that the rate was controlled by the ion

exchange step, the rate equation being:

$$\frac{\partial q}{\partial t} = k\ [\ C\ (q_{\infty} - q) - \frac{1}{K}\ q\ (Co - C)] \qquad 6.4$$

where k is the forward velocity constant of the exchange, q_{∞} is the concentration equivalent to total quantity of exchangeable ion in the exchange resin,C, q are fluid and solid concentrations of an exchange component and K is an equilibrium constant for ion exchange.

Equation 6.4 can be rewritten:

$$\frac{\partial (q/q_{\infty})}{\partial t} = k\ C_o \left[\frac{C}{C_o} (1 - \frac{q}{q_{\infty}}) - \frac{1}{K} \frac{q}{q_{\infty}} (1 - \frac{C}{C_o}) \right] \qquad 6.5$$

By defining time and distance parameters

$$T = k\ C_o\ (t - \frac{z}{u}) \qquad 6.6$$

$$X = \frac{k\ q_{\infty}\ z}{mu} \qquad 6.7$$

$$m = \frac{\varepsilon}{1 - \varepsilon}$$

the conservation equation and rate equation can be simplified to yield respectively:

$$\left(\frac{\partial(C/C_o)}{\partial X}\right)_T = - \left(\frac{\partial(q/q_\infty)}{\partial T}\right)_X \qquad 6.8$$

$$\frac{\partial(q/q_\infty)}{\partial T} = \frac{C}{C_o}\left(1 - \frac{q}{q_\infty}\right) - \frac{1}{K}\frac{q}{q_\infty}\left(1 - \frac{C}{C_o}\right) \qquad 6.9$$

Equation 6.8 and 6.9 can be solved by the method of Thomas to yield

$$C/C_o = \frac{J\left(\frac{X}{K}, T\right)}{J\left(\frac{X}{K}, T\right) + \left[1 - J\left(X, \frac{T}{K}\right)\right]} \quad \exp\left[\left(\frac{1}{K} - 1\right)(T - X)\right] \qquad 6.10$$

The function J is defined as

$$J\left(\alpha, \frac{1}{K}\right) = 1 - \int_o^\infty \exp\left(-\frac{1}{K} - \alpha\right) I_o\left(2\sqrt{\frac{X}{K}}\right) dX \qquad 6.11$$

Where I_o is modified Bessel function of zero order. The numerical value of T(X, 1/K) have been calculated from this model for a wide range of parameters and the results were presented in graphical form by Hiester and Vermeulen [12].

Hougen and Marshall [72] developed an analytical method to predict the breakthrough curve for isothermal conditions where a linear equilibrium relation exists between the adsorbate content of the ideal gas and of the solid. They considered the

situation where mass transfer through the fluid film is the rate controlling step, and the sorbate of low concentration. Under these conditions they developed the following pair of partial differential equations:

$$\frac{\partial W}{\partial t} = b\left(\frac{Y}{C} W\right) \qquad 6.12$$

and

$$-\left(\frac{\partial Y}{\partial x}\right) = a\,(Y - CW) \qquad 6.13$$

where

W = adsorbate content of solid kg/kg of solid

t = time, hr.

Y = adsorbate content of fluid stream, kg/kg of fluid (adsorbate-free basis)

b = ßC

x = longitudinal distance in bed measured in direction of flow, m.

$$ß = \frac{G}{\rho_B H_d}$$

G = mass velocity of adsorbate free fluid flowing, kg/(sq.m.)(hr.)

ρ_B = bulk density of solid, kg/cu.m.

H_d = the height of a transfer unit =

$$\frac{G}{a_v k_G P_f M_G}$$

a_v = external area of solid particles, sq.m./cu.m.

k_G = mass transfer coefficient

P_f = pressure factor for diffusion, which for dilute gases is equal to total pressure T.

M_G = molecular weight of adsorbate free gas

$$a = \frac{1}{H_d}$$

C = equilibrium constant

The solution for Equations 6.12 and 6.13 was developed for the special condition where Y is constant at x = 0 for all values of t and W is zero at t = o for all values of x. This solution is expressed as follows:

$$\frac{Y}{Y_o} = 1 - e^{-bt} \int_o^{ax} e^{-ax} J_o(2i\sqrt{btax})\, d(ax) \qquad 6.14$$

where

$$i = \sqrt{-1}$$

and

J_O = Bessel function of the first kind and zero order

Y_O = mass of adsorbate per unit mass of entering gas (adsorbate free basis)

Antonson and Dranoff[73] modified the linear equilibrium spherical particle model of Rosen by replacing the linear equilibrium isotherm with the Langmuir isotherm. They obtained a single integro-differential equation which could not be solved analytically because of non linearity. Hence finite difference techniques offered the alternative.

Hasanain, et. al[74] developed a model to describe the adsorption of

gases and vapours on solids in packed beds by using the assumption that the controlling mass transfer resistance is due primarily to diffusion in the spherical solid particles, the equilibrium relationship is described by the generalized isotherm equation proposed by Radke and Prausnitz, Equation 6.15, and neglecting the axial dispersion effects.

$$q^* = aC/(1 + \alpha C^{1-ß}) \qquad 6.15$$

where

q^* = adsorbate concentration in the solid phase at the fluid-solid interface in equilibrium with the bulk gas concentration,

C = adsorbate concentration

a, α and ß = empirical constants in the Radke-Prausnitz equation

Many other models have been presented and summarized by Ruthven[29] which includes all the conditions considered by numerous authors.

CHAPTER 7

EXPERIMENTAL INVESTIGATION

7 EXPERIMENTAL INVESTIGATION

Both batch and continuous flow experiments were conducted with molecular sieves. The batch experiments were carried out to study the equilibrium isotherms and kinetic adsorption of the normal paraffins under investigation. The continuous flow experiments were done to investigate the dynamic behaviour and the dynamic properties of adsorption of the normal paraffins C_{12}, C_{16}, and C_{20} under different operating conditions.

7.1 BATCH EXPERIMENTS

Batch adsorption experiments were performed using sealed cylindrical stainless tubes of the type shown in Figure 7.1, each of 60 cm^3 capacity.

An electrically-heated water bath provided with a temperature controller and shaker maintained the adsorption system at a constant temperature during each experiment with an accuracy of $\pm$ 0.1°C. The shaking plate was perforated to retain the tubes as illustrated in Figure 7.2.

7.1.1 Equilibrium Isotherm Experiments

Equilibrium isotherm experiments were carried out to determine the equilibrium loading of molecular sieve Type 5A and to determine adsorption isotherms for the normal paraffins, n-dodecane, n-hexadecane, and n-eicosane at three different temperatures 30°C, 50°C and 70°C.

Solution Preparation

Several solutions of individual normal paraffins (solute) with isooctane (solvent) were prepared with different concentrations. The weight percentage and

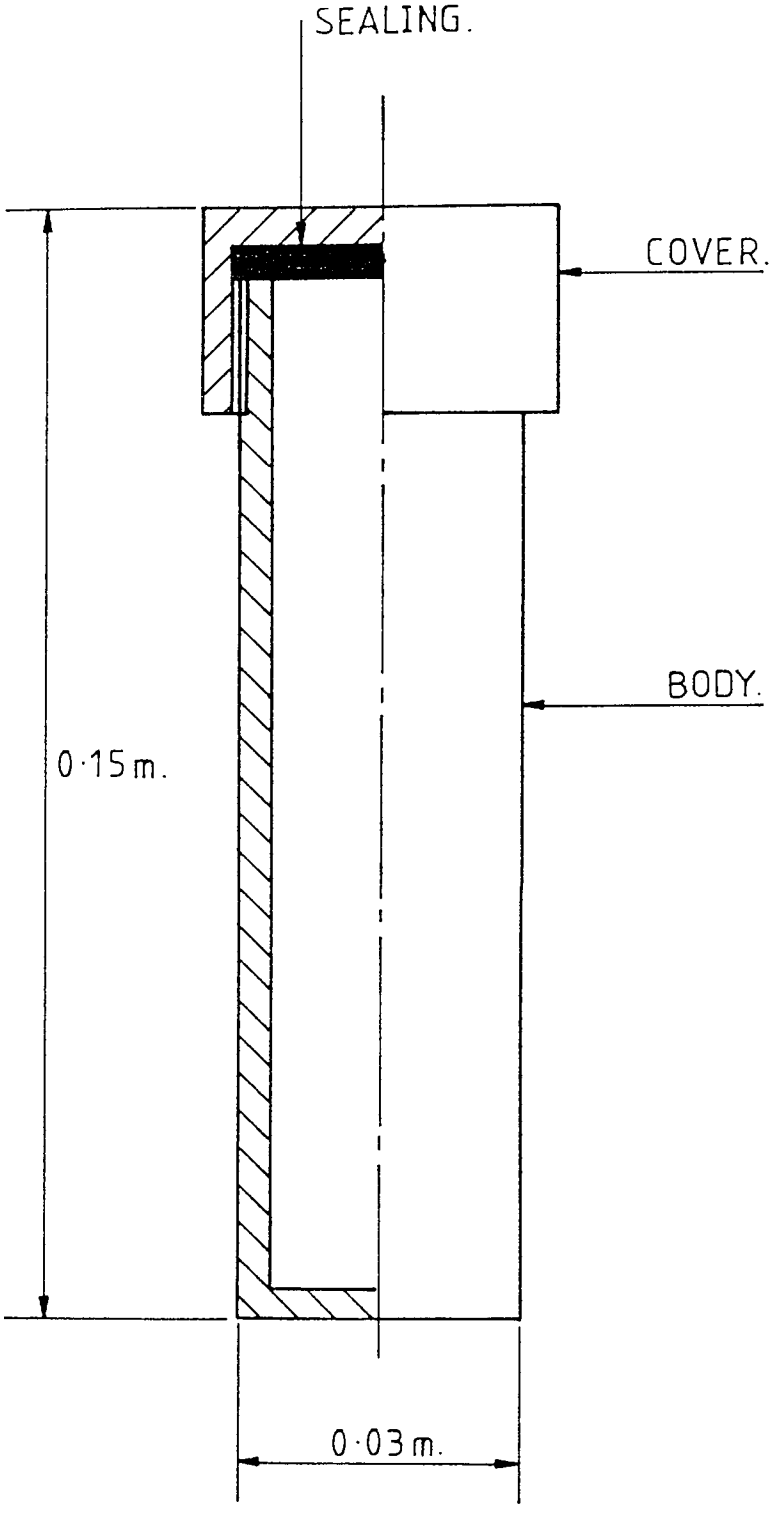

Figure 7.1 Batch adsorption tube

Figure 7.2 Thermostatic water bath for batch experiments

mole fraction of each normal paraffin in each of the different solutions are listed in Table 7.1. The solutions were prepared in a volumetric flask of 50 cm^3 volume. The flask was weighed empty, after addition of the normal paraffin, and again after addition of isooctane. The solution in the flask was mixed by continuous shaking until all the normal paraffin had dissolved and a homogeneous solution was obtained.

The specifications and physical properties of the normal paraffins and isooctane are shown in Table 7.2.

Experimental Procedure

10 ml of normal paraffin solution of known concentration was introduced into a numbered stainless steel tube. A known quantity, about 1 g, of freshly-prepared dry activated molecular sieve, in the form of 1/8 inch pellets containing 20% inert clay binder, was poured quickly into the tube which was then closed firmly.

Each closed tube was placed in the shaking plate in the water bath at the selected adsorption temperature of 303, 323, or 343°K for a specific time to attain equilibrium. Preliminary experiments were first performed for each normal paraffin system to determine the equilibrium time, that is the time after which no more adsorption occurred, at the different temperatures. These equilibrium times are shown in Table 7.3.

After allowing the equilibrium time, the sample from each tube was analysed with a digital density meter, and the amount of normal paraffin adsorbed was calculated for each system as shown in Appendix B.

Table 7.1 Concentration Range of Original Solutions

N-Dodecane		N-Hexadecane		N-Eicosane	
%Wt	Mole-fraction	%Wt	Mole-fraction	%Wt	Mole-fraction
1.07	0.0072	0.57	.0029	1.04	.0042
1.62	0.0109	1.12	.0057	1.22	.0050
2.11	0.0143	1.66	.0084	1.64	.0067
3.10	0.0210	2.23	.0114	1.99	.0081
3.86	0.0262	2.68	.0136	2.23	.0091
4.37	0.0297	3.28	.0168	2.49	.0102
4.87	0.0332	3.58	.0184	3.12	.0128

Table 7.2 Physical Properties of n-paraffins and isooctane

Name	Formula	Molecular wt.	Spec.G.(d_4^{20})	Description
N-Dodecane	$C_{12}H_{26}$	170.34	.748	Purity > 98% (GC)
N-Hexadecane	$C_{16}H_{34}$	226.45	.773	Purity > 98% (GC)
N-Eicosane	$C_{20}H_{42}$	282.56	.791	Purity > 97% (GC) M.P. 36-38°C
Iso-Octane	C_8H_{18}	114.23	.690	Purity > 99.5%

Table 7.3 Equilibrium Time at Different Temperatures

	Equilibrium Time (Hrs) At		
Normal Paraffin	303°K	323°K	343°K
N-Dodecane	40	26	15
N-Hexadecane	63	40	20
N-Eicosane	70	45	25

7.1.2 Kinetic Adsorption Experiments

Kinetic adsorption experiments were performed to investigate the adsorption rate of each of the normal paraffins, n-dodecane, n-hexadecane, and n-eicosane at three different temperatures, 303°K, 323°K, and 343°K, from binary solutions in isooctane (solvent). The adsorbent comprised Type 5A molecular sieve in the form 1/8 inch pellets as described in section 7.2.1.

Solution Preparation

Solutions were prepared containing a concentration of 0.01 mole fraction of each normal paraffin. Each solution was prepared in a volumetric flask of 500 cm^3 capacity. The estimated volumes of isooctane and normal paraffin were well-mixed to form the solution of 0.01 mole-fraction concentration. The precise concentration of each solution was then determined analytically using the density-meter.

The estimated volumes were calculated from the mole fraction definition

$$\text{Mole-fraction} = \frac{\dfrac{V_{np} \times \rho_{np}}{M_{np}}}{\dfrac{V_{np} \times \rho_{np}}{M_{np}} + \dfrac{V_{iso} \times \rho_{iso}}{M_{iso}}} \qquad 7.1$$

or in final form:

$$V_{np} = 0.0274 \frac{M_{np}}{\rho_{np}} \qquad 7.2$$

where

V_{np} = volume of normal paraffin cm^3

ρ_{np} = density of normal paraffin g/cm^3

V_{iso} = volume of isooctane = 450 cm^3

ρ_{iso} = density of isooctane g/cm^3

M_{np} = molecular weight of normal paraffin

M_{iso} = molecular weight of isooctane

Mole fraction = 0.01

The values were all measured at 20°C. The values of densities and molecular weights are listed in Table 7.2.

Experimental Procedure

Fifteen clean, dry, and numbered stainless steel tubes were prepared. 10 cm^3 of a solution, e.g. normal dodecane in isooctane, of 0.01 mole-fraction concentration was introduced into each tube.

1.0 gram of freshly-dry, activated molecular sieve was poured quickly into each tube. The covers were closed firmly and the tubes placed in the water bath which was maintained at the desired adsorption temperature. The contact time was calculated from the moment of contacting the molecular sieves with the solution. After specific time intervals of 2, 8, 15, 30, 60, 120, 180, 240, 300, 360, 690, 900, 1090, 1380 and 2130 minutes each tube was taken out of the bath, opened quickly and the solution decanted into a numbered test tube. The solution concentration was then determined using the density-meter. The same procedure was repeated for the three normal paraffins at the three adsorption temperatures.

7.1.3 Molecular Sieve Activation

Molecular sieves have a high affinity for polar molecules particularly water and can be used, in general, for drying and removing water from gases and liquids. Activation of Type 5A molecular sieve was achieved in the batch system according to the following sequence:

a) Fifteen Pyrex glass crucibles were cleaned, numbered, and weighed with their covers.

b) About one gram of molecular sieve, in the form of 1/8 inch pellets, was introduced into each crucible.

c) After removing their covers the crucibles were placed in an oven for five hours at temperatures of 723°K (450°C) to drive off water present in the pores of the molecular sieve.

d) At the end of the activation time, each crucible was covered quickly and transferred to a dessicator for cooling. Figure 7.3.

e) Each crucible was taken out of the dessicator, weighed, and the molecular sieve poured into solution for adsorption determination.

The difference between the weights (e) and (a) represented the weight of activated molecular sieve.

7.2 DYNAMIC FLOW SYSTEM EXPERIMENTS

Twenty eight dynamic flow experiments were carried out for three liquid systems. Each system was composed of a normal paraffin (n-dodecane, n-hexadecane, or n-eicosane) dissolved in isooctane. These systems were subjected to the adsorption process in a column packed with Type 5A molecular sieves. The experiments were performed to study the effects of different operating conditions namely temperature, flow rate of the fluid, feed concentration, size of molecular sieves, and type of normal paraffins on the breakthrough curve and upon the dynamic properties of each system. The range of operating conditions used in the experiments are listed in Table 7.4.

A description of the materials, apparatus, and procedures are presented in the following sections.

Figure 7.3 Activation of molecular sieves for batch experiments

About 1g of Type 5A molecular sieve in the form of 1/8 inch pellets was placed in each pyrex crucible and inserted into the electric furnace at approximately 730^{o}K

Table 7.4 Experimental Operating Variables

Temperature ^oK	Feed Conc. mole-fraction	Flow rate m^3/sec	Molecular sieve size (x 10^3) m
303	.01	6.1×10^{-8}	1 - 2
323	.02	5×10^{-8}	0.5 - 1
343	.03	2.78×10^{-8}	0.032 - 0.5

Table 7.5 Physico-chemical Properties of Type 5A Molecular Sieves[14, 18]

Property	Value
Nominal Pore Diameter, Angstroms	5
Unit cell composition	$Ca_{4.5}\ Na_3\ [(A10_2)_{12}\ (SiO_2)_{12}].30\ H_2O$
Pellet particle size, m	3.175×10^{-3}
Density, kg/m^3	690
Water content, wt%	<1.5
Inert binder, wt%	20.0
Porosity, %	43
Crushing strength, kg	5.63
Heat of adsorption, $kJ/_{kg}\ H_2O$	4186.8
Specific Heat, $kJ/_{kgK}$	1.09
Type of Crystal	Simple Cubic
Adsorption Capacity for water vapour % wt*	21.5

* lbs. $H_2O/_{100lbs}$ activated adsorbent at 17.5 mm Hg& 25°C.

7.2.1 Materials

The materials used in the dynamic experiments comprised normal paraffins, isooctane, and 5A molecular sieve.

a) Normal Paraffins and Isooctane

The normal paraffins studied in the flow system corresponded with those in the batch system, and the solvent was isooctane with the same properties as summarised in Table 7.2. The binary solutions consisting of normal paraffin (solute) and isooctane (solvent) were prepared with the required specific concentration in bottles of 2500cm^3 capacity.

b) Molecular Sieve Adsorbent

Type 5A molecular sieve was used in the form of 1/8 inch cylindrical pellets. The average pellet length was approximately 0.48 x 10^{-2}m. The crystalline sieves themselves were evenly distributed within the macroporous clay matrix, and formed about 80% of the total weight of the pellet.

The physico-chemical properties of Type 5A molecular sieves are illustrated in Table 7.5.

7.2.2. Experimental Apparatus

The dynamic adsorption experiments were performed in an experimental apparatus designed and constructed to permit the measurement of breakthrough curves for the adsorption of normal paraffin from a binary liquid phase solution on activated 5A molecular sieve particles at constant specific temperatures.

A schematic diagram of the experimental apparatus is shown in Figure 7.4. As illustrated in Figure 7.5 and Figure 7.6 the apparatus consisted essentially of two sections, an adsorption section and a molecular sieve activation section, but

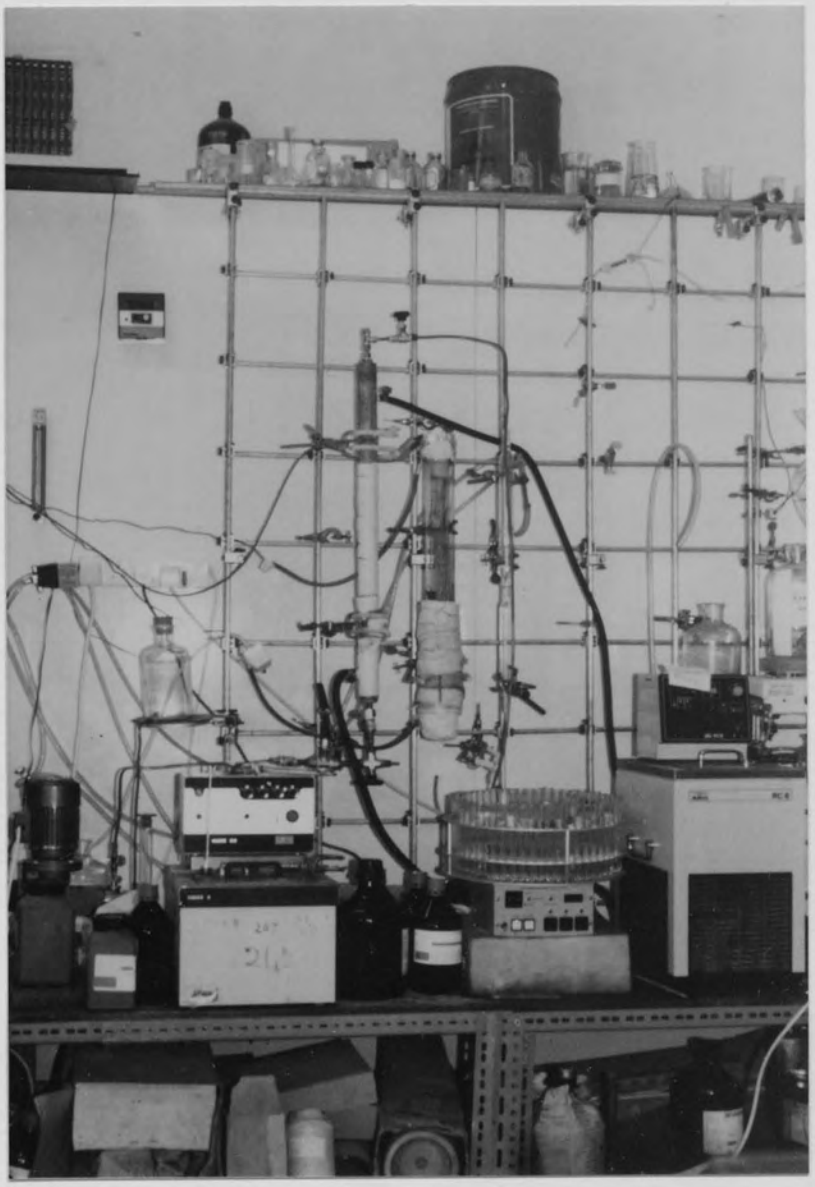

Figure 7.5 General arrangement of dynamic adsorption apparatus

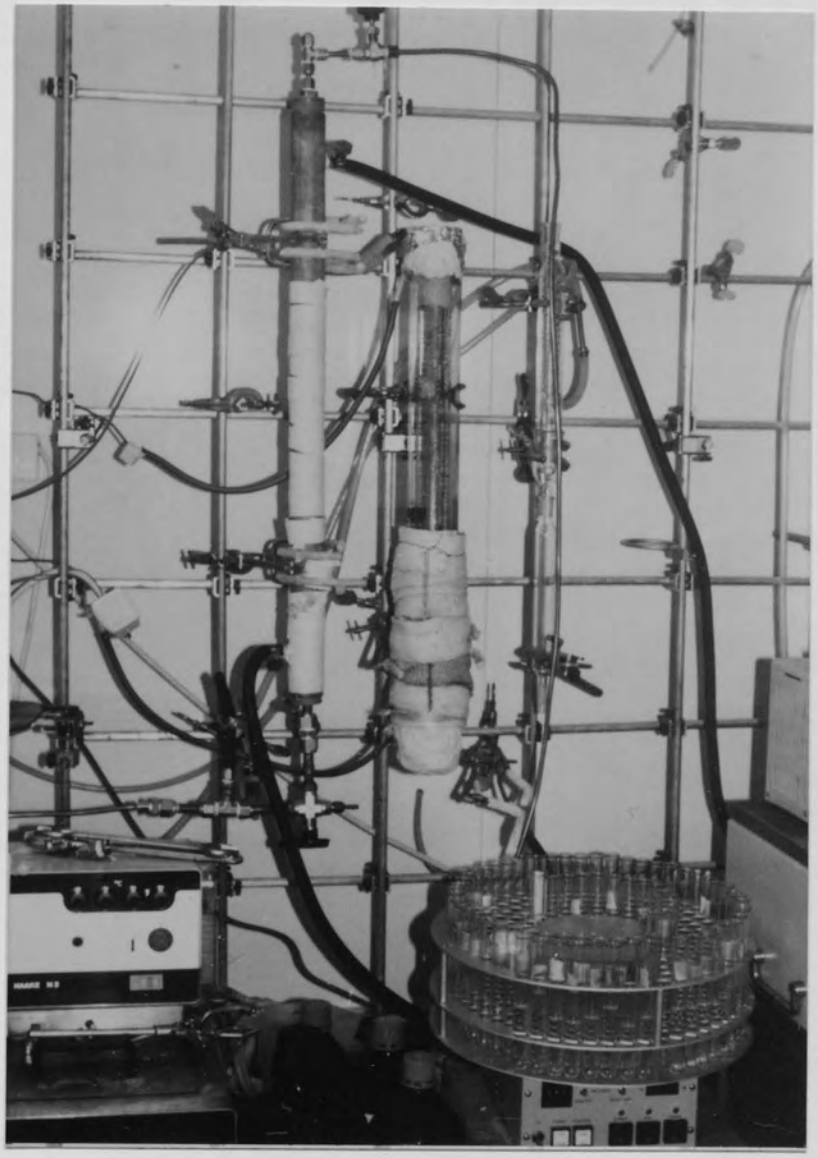

Figure 7.6 Adsorption and activation columns

using a common column.

a) Adsorption Section

The adsorption section was mainly composed of the following parts:

* Glass container of one litre capacity to supply the feed pump with solution to be adsorbed.

* Pulsation pump to supply the required flow rate of fluid. The flow rate could be controlled by changing the stroke of pumping through a graduated flow controller knob. The graduation was expressed as efficiency in the range of 0 to 120. A calibration curve was determined for the pump, relating the efficiency with the actual flowrate, as shown in Figure 7.7.

* Adsorption column A diagram of the adsorption column is shown in Figure 7.8. The column was constructed of brass which, because it has a higher conductivity than glass, assisted in the attainment of isothermal conditions for the adsorption process. It was also robust. The column was of 0.0169 m internal diameter,0 .019 m external diameter, and 0.688 m high. A stainless steel screen was inserted at the bottom of the column for supporting the contents of the column. The top and the bottom ends of the column were connected to flexible nuts to facilitate connection and disconnection of the column ends to other parts of the apparatus during the different stages of loading molecular sieve, activation of molecular sieve, the adsorption process, unloading of used molecular sieve, and cleaning the column.

A packed section of inert beads, glass beads of 0.0015 to 0.002 m diameter, preceded the molecular sieve bed in the adsorption column. This performed several functions:

i) To distribute the flow of the fluid entering the adsorption column;

ii) To preheat the inlet fluid and raise its temperature to the required

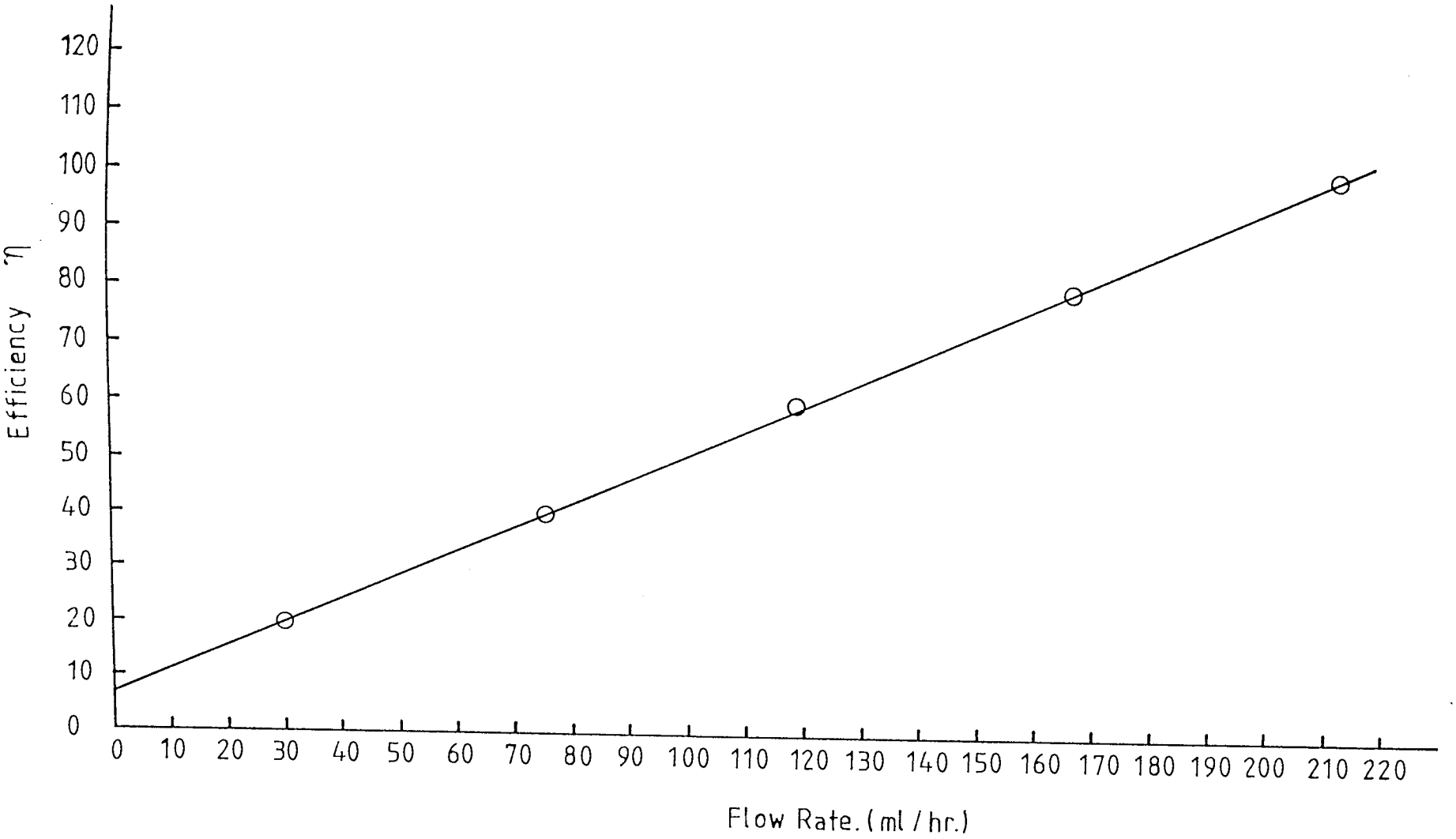

Figure 7.7 Calibration curve of the reciprocating pump

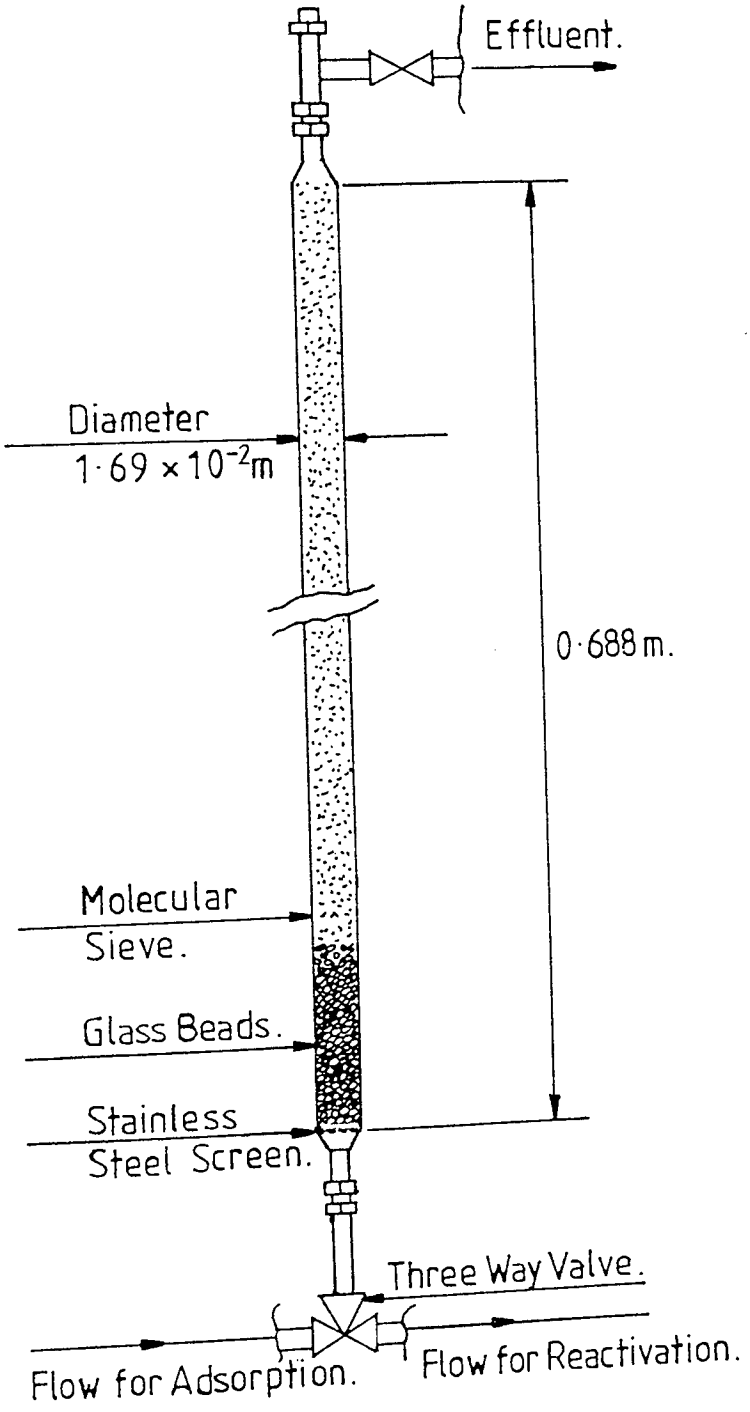

Figure 7.8 Adsorption column
Bead size (1-2) $x10^{-3}$m
Bead height 0.2m

adsorption temperature;

iii) To change the height of molecular sieve bed by the insertion of different heights of the inert beads.

* Adsorption Temperature Control System

To maintain a constant adsorption temperature the column was provided with a cylindrical pipe jacket. The jacket was connected to a circulating water supply. This was pumped from a controlled temperature water bath, with temperature control to $\pm 0.1^{o}C$.

b) Molecular Sieve Activation Section

The activation method developed for this study in which the molecular sieve remained in the column had the advantage of keeping the activated molecular sieve under vacuum and reducing the time of contacting with air to a minimum, (i.e. to the time for pressure adjustment only). This decreased the possibility of deactivation of the molecular sieve compared with the method used by earlier workers (66, 67) in which the activated molecular sieves were inevitably exposed to atmosphere during transfer from an oven to the adsorption column.

Activation of the molecular sieve used in the dynamic experiments was achieved using the following equipment.

* The adsorption column previously described.

* Two concentric glass tubes. The inner tube was of 0.04 m I.D. and the outer one of 0.07 m I.D. and each was 0.69 m high. The inner tube was wrapped with an electrical heating coil to provide the heat necessary for activation of the molecular sieve. The tubular heating coils were insulated by the outer glass tube. The ends of the tubes were plugged with insulating material.

*An electrical controller-regulated for temperature control.

The activation temperatures were measured and controlled using a thermocouple connected to an electrical controller-regulator.

*Vacuum pump:

A, BS 2511/12 RPM 1425 vacuum pump ex Edwards, U.K., was used to achieve the required vacuum for activation. It was connected to the base of the adsorption column via a three-way valve and glass flask to prevent any liquid or solid particles entering the pump. A vacuum gauge was provided to measure the vacuum attained in the column.

7.2.3 Experimental Procedure

The experimental procedure for the dynamic adsorption experiments included preparation of the molecular sieve, its activation and the adsorption process itself.

a) Preparation of molecular sieve

The following procedures were followed to ensure uniformity of the adsorbent in successive experiments.

* Molecular sieves (zeolite type 5A, 1/8 inch pellet) was crushed using a mortar and pestle.
* The crushed molecular sieves were then sieved, using a Fritsch sieve shaker, to provide the following fractions:

  $> 2.0 \times 10^{-3}$m, $1.0 - 2.0 \times 10^{-3}$m, $0.5 - 1.0 \times 10^{-3}$m, $0.032 - 0.5 \times 10^{-3}$m and $<0.032 \times 10^{-3}$m.
* Fractions of sizes $1.0 - 2.0 \times 10^{-3}$m, $0.5 - 1.0 \times 10^{-3}$m, and $0.032 - 0.5 \times 10^{-3}$m were removed and stored for use. The fraction of

sizes > 2. x 10^{-3}m was recrushed.

b) Activation of molecular sieves

Activation of the molecular sieves was carried out according in the following stages:

* The requisite quantity of molecular sieve of desired specific size was weighed for a specific run.
* The height of the adsorption column which would be occupied by a certain weight of molecular sieves of specific size range was estimated experimentally. This was simply done by filling a separate tube of similar diameter and measuring the height corresponding to a known weight. For example 0.638 x 10^{-2}m column height would be occupied by 1gm of molecular sieve of size range 1.0 - 2.0 x 10^{-3}m and 0.251 x 10^{-2}m column height would be occupied by 1gm of glass beads. The estimated weight of glass beads was introduced into the adsorption column using a funnel, followed by the weighed amount of molecular sieves.
* The lower end of the adsorption column was connected to the three way valve 5, which was connected to the vacuum pump 18 through the liquid trap 22 as shown in Figure 7.4.
* The vacuum pump 18 was switched on and valve 19 was closed. The vacuum drawn was indicated by the vacuum gauge 20 down to 15μm.
* Evacuation of the column commenced by opening the three - way valve to the vacuum pump side.
* The column temperature controller 23 was switched on and the set point was fixed at 618^{o}K.

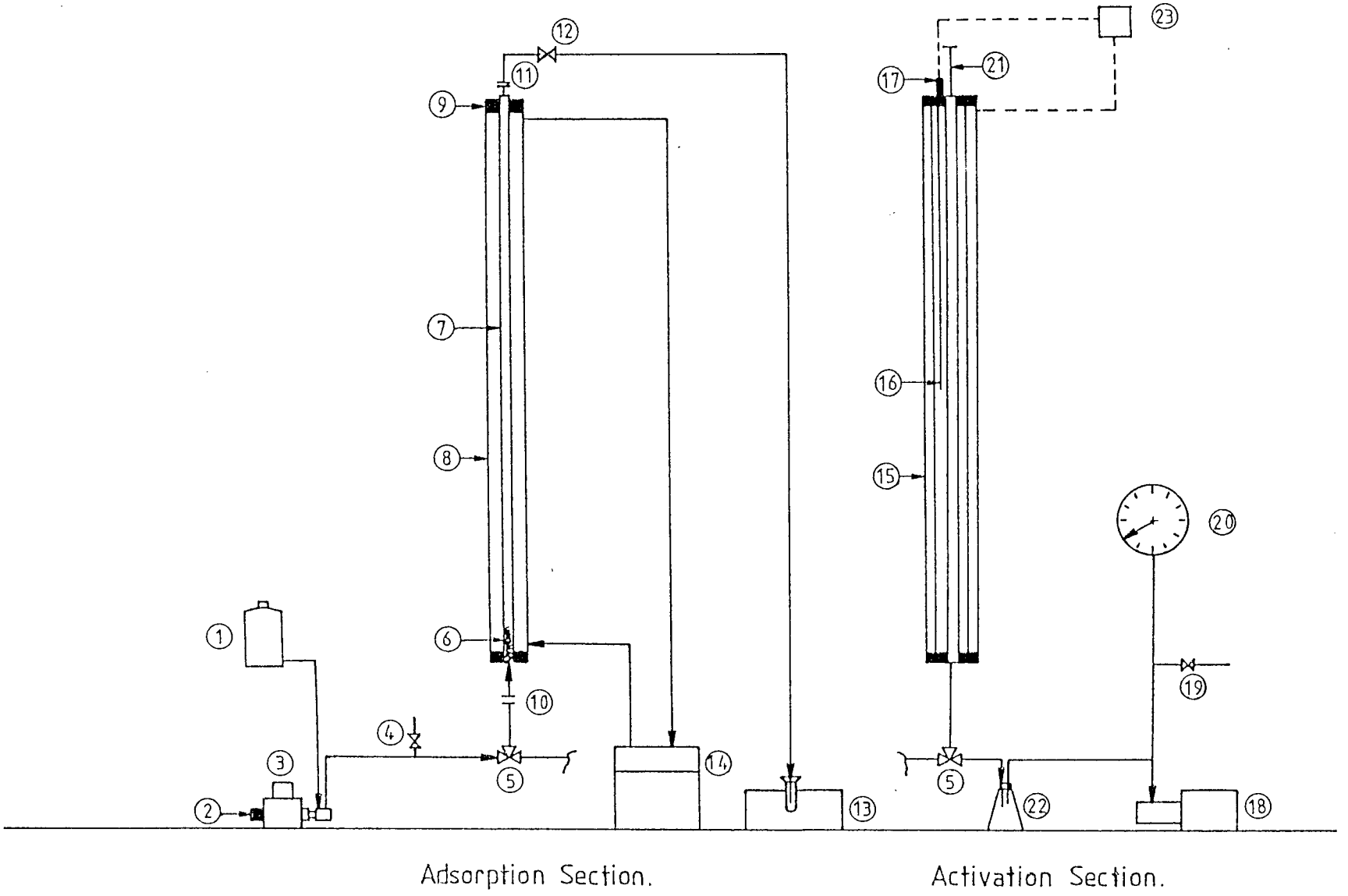

Figure 7.4 Schematic diagram of apparatus for dynamic experiments

KEY TO NUMBERS OF FIGURE 7.4

1	One litre glass container
2	Flow controller
3	Feed pump
4, 12, 19	Valves
5	Three way valve
6.	Glass beads
7	Adsorption column
8	Outer column
9	Rubber cork
10, 11	Flexible connections
13	Automatic sample collector
14	Water batch circulator
15	Outer glass tube
16	Inner glass tube
17	Thermocouple
18	Vacuum pump
20	Vacuum guage
21	Blind connection
22	Liquid trap
23	Temperature controller

* After four hours of activation the column was closed using the three way valve, valve 19 was opened gradually to atmosphere, and the vacuum pump and temperature controller were switched off.

c) Adsorption Process Procedures

After activation of the molecular sieves in the column and cooling, the column was removed from the activation section and transferred to the adsorption section. The adsorption procedure was carried out according to the following steps (with reference to Figure 7.4).

* The adsorption column 7 was fixed within the outer column 8 by the two rubber corks 9.
* The adsorption column was opened to atmosphere through the three-way valve.
* The three-way valve was connected to the fluid pumping line.
* The plugged connection 21 was disconnected and replaced by a connection with valve 12 which was in turn connected to a copper pipe leading to an automatic sample collector with numbered sample tubes 13
* The water bath circulator 14 was switched on and the temperature controller of the bath was set to the desired adsorption temperature for the experiment.
* The flow controller 2 of the feed pump 3 was adjusted to give the required flow rate.
* The pump was switched on and connection 4 opened to vent any air bubbles in the line as illustrated in Figure 7.9.
* Three way valve 5 was opened in the direction of the adsorption column, and connection 4 was closed to admit fluid to the packed column. The effluent was collected in the sample tubes.

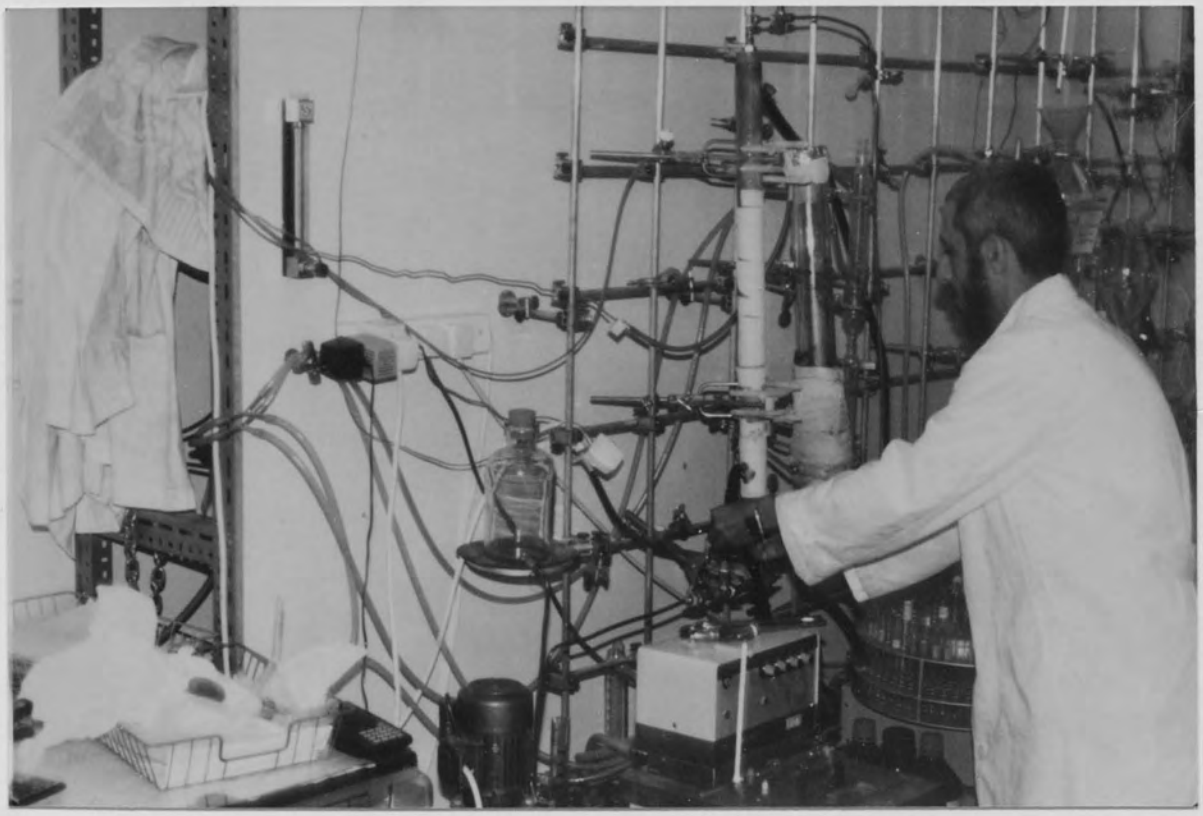

Figure 7.9 Air bubble removal

* The automatic sample collector was arranged to move each five minutes.
* The samples were analysed using the density meter.
* The time was measured directly using stop watch.
* Breakthrough curves were constructed from all the experiment results.

7.3 ANALYTICAL TECHNIQUE

Initially an attempt was made to analyse the binary systems composed of isooctane and normal paraffin using a digital refractometer. However considerable difficulty arose in obtaining reliable analyses at low concentrations of normal paraffin in the binary solution. The potential for using a density meter was realised after comparing the difference in densities of normal dodecane and isooctane that is 0.0587, with the difference in refractive indices of 0.0306.

Analysis of prepared solutions of low concentration using the density meter and the refractometer confirmed the preference for the density meter for reproducible readings. The DMA 40 Digital Density Meter was used for analysis of binary solutions in both batch and continuous flow experiments. The precision of the instrument was $\pm$ 1 x 10^{-4} g/cm^3.

7.3.1 Measuring Principle of the DMA 40 Digital Density Meter

The DMA 40 Digital Density Meter simplifies the accurate determination of the density of liquids and gases by reducing the procedure to the electronic measurement of a time period. The measuring principle is based on the variation of the natural frequency of a hollow oscillator when filled with different liquids. The mass, and thus the density or concentration, of the liquid changes this natural

frequency due to a gross mass change of the oscillator caused by the introduction of the liquid. As shown in Figure 7.10, the oscillator consists of a hollow elastic glass tube which is electronically excited in an undamped harmonic fashion. The direction of oscillation is perpendicular to the plane of the U-shaped sample tube. The frequency of the oscillator is only influenced by that fraction of the volume of liquid which is actually in the vibrating part of the sample tube.

7.3.2 Description of the Density Meter

The borosilicate glass (Duran 50) oscillator (sample tube), is mounted in the centre of a double walled cylinder fused at both ends. The space between the sample tube and inner wall of the cylinder is filled with a gas of high thermal conductivity. A thermostatically controlled, liquid flows between the outer and inner wall of this cylinder, Figure 7.10. For this study a circulator (C400, Techne) was connected to the Density meter and filled with water. The temperature stability of the system was $\pm$ 0.02°C. This design enabled the instrument to attain temperature equilibrium in the shortest possible time.

The filling of the sample tube could be observed through the window on the front plate. A built-in pump provided a stream of filtered air to dry out the sample tube after cleaning. The electronic part of the instrument provided for excitation of the oscillator (sample tube) at constant amplitude. The built-in quartz crystal timer permitted accurate determination of the period of oscillation in about 2 seconds. Although measurements were made continuously, the last resulting figure was always displayed by means of a buffer (short memory circuit).

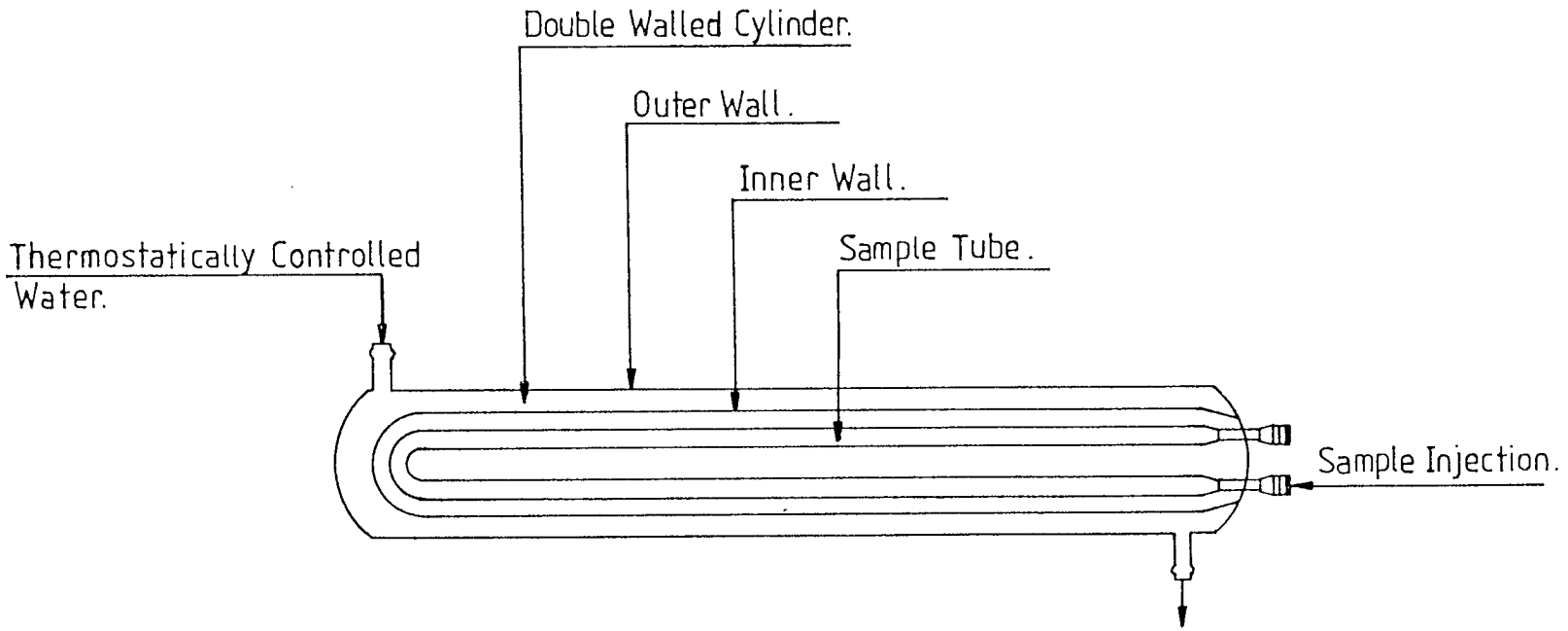

Figure 7.10 Sample tube and double-walled cylinder.
Sample tube was a hollow elastic glass tube,
electronically-excited; capacity 0.7cm^3

7.3.3 Operation of the Instrument

The sample tube starts to oscillate automatically when the power is turned on. After a certain time, depending on the sample density, the display shows a number which represents the period of oscillation. The measurement is continuously repeated on the sample until it is removed. The displayed value may drift until temperature equilibrium is reached, but should then only fluctuate a maximum of ± one digit with a well-thermostated sample tube (i.e. with a temperature control better than ± 0.05°C). If greater variations are encountered, then either complete temperature equilibrium of the measuring cell has not been reached, or the sample has not been correctly loaded or some phenomenon such as degassing is occurring in the sample.

7.3.4 Analytical Procedure

Analysis of the three binary systems, normal paraffin + isooctane, studied was by the Density Meter described above. Standard binary solutions were prepared by mixing weighed portions of each pure component in a 50 milliliter flask. The solutions were weighed on a Mettler analytical balance with an accuracy of ± 0.0003 grams.

The period of oscillation of these standard solutions was measured and used to prepare a calibration curve of mole fraction normal paraffin versus period of oscillation for each binary system. These calibration curves are shown as Figures 1, 2, and 3 in Appendix C. For calibration of the instrument, the oscillation period of pure isooctane at constant temperature of 25°C was used as reference for analysis of all samples.

The following procedures were carried out to analyse specific samples after calibration of the instrument and cleaning the sample tube:

a) Approximately 0.7 cm^3 of liquid sample was injected into the lower opening of the sample tube using a plastic tipped hypodermic syringe. The filling was observed through the window in the front panel after turning on the illumination. Figure 7.11 illustrates the injection step.

b) The hypodermic syringe was left in position after completely filling the sample tube and the illumination was switched off.

c) When temperature equilibrium was attained after approximately 40 seconds, i.e. a stable reading was observed, the oscillation time period (T_{sample}) was taken.

d) The sample was withdrawn into the syringe, and the sample tube was rinsed with alcohol.

e) The air pump was switched on, the air hose was connected to the upper inlet of the sample tube, and the flow of the air was continued until the displayed value repeated itself several times, which was representing T_{air}.

f) The air pump was switched off, and T_{air} was compared with its original value to ensure complete removal of all solvent or any other contamination.

Figure 7.11 Injection of sample into the density meter

CHAPTER 8

MATHEMATICAL MODELLING

8.1 MATHEMATICAL MODELLING

Sorption systems may be designed to operate with fixed beds which, whilst they are mechanically-simple, operate in an unsteady-state mode. This may require relatively complex mathematical models to predict the amount of sorbent required for a given duty.

The problem of predicting sorbate concentration as a function of time and distance along a fixed bed has received increasing attention over the last thirty years, many solutions being offered for different operating conditions. The complexity of the mathematical solutions increased where more effects are considered. Clearly it is necessary to understand the importance of any effect before including it in any analysis. Nevertheless, a considerable number of models have been developed as summarised in Chapter 6. The model used here for the dynamic adsorption of a liquid phase system follows that of Hougen and Marshall [72], for adsorption of an ideal gas. The differential mass balance equations for an element of the adsorption column and for an adsorbent particle within such an element provide the starting point for development of a mathematical model to describe the dynamic behaviour of the system. The following approximations are introduced to simplify the analysis.

(1) The feed stream is assumed to consist of a dilute mixture containing only a single adsorbable component.

(2) The system is assumed to be isothermal and the pressure drop through the column is neglected.

(3) The fluid velocity is taken to be uniform across any section

of the column, and axial dispersion is neglected (plug flow assumption).

(4) The size of the adsorbent particles is assumed to be sufficiently small that changes in the fluid phase concentration over a single particle may be neglected.

(5) Equilibrium between fluid phase and adsorbed phase is assumed to be linear.

(6) It is assumed that the rate of removal of solute from the fluid phase by the solid adsorbent is controlled by the mass transfer of the solute molecule through a liquid film to the solid adsorbent.

Considering an element of the bed, as shown in Figure 8.1, the materials balance relationship for the packed bed may be expressed as:

$$\text{Input} = \text{Output} + \text{Adsorption} + \text{Accumulation} \qquad 8.1$$

For the case of constant velocity of the fluid across the bed, and neglecting longitudinal diffusion, the following mathematical formulations can be written for the system.

Fluid phase sorbate balance:

$$\text{Input} = U A \varepsilon C$$

$$\text{Output} = U A \varepsilon C + \frac{\delta(UA\varepsilon C)}{\delta x} dx$$

$$\text{Input} - \text{Output} = - \frac{\delta(UA\varepsilon C)}{\delta x} dx$$

$$\text{Accumulation} = \frac{\delta(AC\varepsilon\, dx)}{\delta t}$$

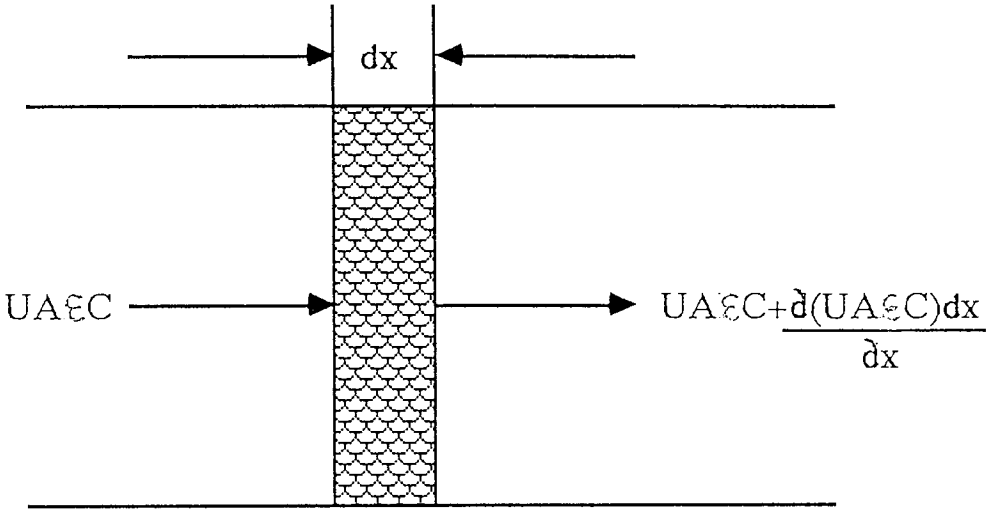

Figure 8.1. Mass conservation of sorbate in a fixed bed

Loss by adsorption = N_S A (l-ε) a_p dx = N_S A dx a_Z

Solid phase sorbate balance:

Input - Output = O

$$\text{Accumulation} = \frac{\delta[(1-\varepsilon)A\, q\, dx]}{\delta t}$$

Loss by adsorption = - N_S A (l-ε) a_p dx

Considering fluid and solid phase together

$$\text{Input - Output} = -\frac{\delta(UA\varepsilon C)}{\delta x}dx$$

$$\text{Accumulation} = \frac{\delta[(1-\varepsilon)Aq\, dx]}{\delta t} + \frac{\delta(\varepsilon\, AC\, dx)}{\delta t}$$

Loss by adsorption = O

where:

A = the cross-sectional area of empty column

a_p = the external area of granule per unit volume of granule

a_Z = the external area of granule per unit volume of fixed bed

C = the molar concentration of sorbate in the fluid

q = the concentration of sorbate in the solid

N_S = the flux of sorbate per unit of external area of granules

ε = the intergranular voidage

U = the intergranular fluid velocity

x = the distance along the column

t = time

Equating in accordance with Equation (8.1), the case of fluid and solid taken together yields:

$$-\frac{\delta(UA\varepsilon C)}{\delta x}\,dx = \frac{\delta[(1-\varepsilon)\,Aq\,dx]}{\delta t} + \frac{\delta(\varepsilon AC\,dx)}{\delta t}$$

Cancellation of common terms and dividing through by ε gives:

$$U\left(\frac{\delta C}{\delta x}\right)_t + \frac{1-\varepsilon}{\varepsilon}\left(\frac{\delta q}{\delta t}\right)_x + \left(\frac{\delta C}{\delta t}\right)_x = O$$

Let

$$m = \frac{\varepsilon}{1-\varepsilon}$$

$$U\left(\frac{\delta C}{\delta x}\right)_t + \frac{1}{m}\left(\frac{\delta q}{\delta t}\right)_x + \left(\frac{\delta C}{\delta t}\right)_x = O \qquad 8.2$$

which is the conservation equation for a fixed bed. For an isothermal plug flow system with equilibrium governed by a linear isotherm and the mass transfer rate controlled by external fluid film resistance, the breakthrough curve for a step change in feed concentration at time zero is given by the solution of Equation (8.2) with the following Equations:

$$q = K\,C^* \qquad 8.3$$

which represents the linear isotherm where:

C* = the concentration of the solute in the fluid phase, which is assumed to be in equilibrium with q.

K = the slope of the isotherm

The rate Equation can be expressed as

$$\frac{\delta q}{\delta t} = k_f a_p (C - C^*) \qquad 8.4$$

which represents the mass transfer controlled by external film resistance.

where:

k_f = the external fluid film mass transfer coefficient $^{m}/_{sec}$

a_p = the external area of granule per unit volume of granule, upon which the theoretical coefficient was based.

For spherical particles

$$a_p = \frac{3}{R_p}$$

where

R_p = the average radius of the particles m

Combining Equations 8.3 and 8.4

$$\frac{\delta q}{\delta t} = \frac{3k_f}{R_p}\left(C - \frac{q}{K}\right) \qquad 8.5$$

By defining time and distance parameters,

$$Z = \frac{3k_f}{R_p}\left(t - \frac{X}{U}\right) \qquad 8.6$$

Time parameter

$$Y = \frac{3k_f}{U R_p m} X \qquad 8.7$$

Distance parameter

the rate Equation 8.5 and the conservation Equation 8.2 can be simplified.

If C is regarded as a function of Z and Y

i.e. $C = F(Y,Z)$

$$dC = \left(\frac{\delta C}{\delta Y}\right)_Z dY + \left(\frac{\delta C}{\delta Z}\right)_Y dZ \qquad 8.8$$

$$\left(\frac{\delta C}{\delta X}\right)_t = \left(\frac{\delta C}{\delta Y}\right)_Z \left(\frac{\delta Y}{\delta X}\right)_t + \left(\frac{\delta C}{\delta Z}\right)_Y \left(\frac{\delta Z}{\delta X}\right)_t \qquad 8.9$$

$$\left(\frac{\delta Y}{\delta X}\right)_t = \frac{3\,k_f}{U\,R_p\,m} \qquad 8.10$$

$$\left(\frac{\delta Z}{\delta X}\right)_t = -\frac{3\,k_f}{R_p\,U} \qquad 8.11$$

Substituting 8.10 and 8.11 into 8.9, yields

$$\left(\frac{\delta C}{\delta X}\right)_t = \frac{3k_f}{U\,R_p\,m}\left(\frac{\delta C}{\delta Y}\right)_Z - \frac{3k_f}{R_p\,U}\left(\frac{\delta C}{\delta Z}\right)_Y \qquad 8.12$$

Also,

$$\left(\frac{\delta C}{\delta t}\right)_X = \left(\frac{\delta C}{\delta Y}\right)_Z \left(\frac{\delta Y}{\delta t}\right)_X + \left(\frac{\delta C}{\delta Z}\right)_Y \left(\frac{\delta Z}{\delta t}\right)_X \qquad 8.13$$

$$\left(\frac{\delta Y}{\delta t}\right)_X = O \qquad 8.14$$

$$\left(\frac{\delta Z}{\delta t}\right)_X = \frac{3k_f}{R_p} \qquad 8.15$$

Substituting Equation 8.14 and 8.15 into Equation 8.13 yields,

$$\left(\frac{\delta C}{\delta t}\right)_X = \frac{3k_f}{R_p}\left(\frac{\delta C}{\delta Z}\right)_Y \qquad 8.16$$

In the same manner regarding q as a function of Y and Z i.e. $q = \varphi(Y,Z)$.

$$dq = \left(\frac{\delta q}{\delta Y}\right)_Z dY + \left(\frac{\delta q}{\delta Z}\right)_Y dZ$$

$$\left(\frac{\delta q}{\delta t}\right)_X = \left(\frac{\delta q}{\delta Y}\right)_Z \left(\frac{\delta Y}{\delta t}\right)_X + \left(\frac{\delta q}{\delta Z}\right)_Y \left(\frac{\delta Z}{\delta t}\right)_X \qquad 8.17$$

From Equation 8.6 and 8.7

$$\left(\frac{\delta Y}{\delta t}\right)_X = O \qquad \left(\frac{\delta Z}{\delta t}\right)_X = \frac{3k_f}{R_p}$$

$\therefore$ Equation 8.17 becomes,

$$\left(\frac{\delta q}{\delta t}\right)_X = \frac{3k_f}{R_p}\left(\frac{\delta q}{\delta Z}\right)_Y \qquad 8.18$$

Substituting Equations 8.12, 8.16 and 8.18 into the conservation Equation 8.2.

$$U\left[\frac{3k_f}{U R_p m}\left(\frac{\delta C}{\delta Y}\right)_Z - \frac{3k_f}{R_p U}\left(\frac{\delta C}{\delta Z}\right)_Y\right] + \frac{1}{m}\left[\frac{3k_f}{R_p}\left(\frac{\delta q}{\delta Z}\right)_y\right] +$$

$$\frac{3k_f}{R_p}\left(\frac{\delta C}{\delta Z}\right)_Y = O$$

$$\therefore \left(\frac{\delta C}{\delta Y}\right)_Z = -\left(\frac{\delta q}{\delta Z}\right)_Y \qquad 8.19$$

Substituting Equations 8.12, 8.16 and 8.5 into conservation Equation 8.2 gives:

$$\left(\frac{\partial C}{\delta Y}\right)_Z = -\left(C - \frac{q}{K}\right) \qquad 8.20$$

From Equations 8.19 and 8.20

$$\left(\frac{\delta q}{\delta Z}\right)_Y = C - \frac{q}{K} \qquad 8.21$$

In order to solve Equations 8.20 and 8.21 under the following boundary conditions

At $t = O$ $C = O$ $q = O$ for all X

$Z = O$	$C = O$	$q = O$	for all Y
$X = O$	$C = Co$		for all t
$Y = O$	$C = Co$		for all Z

Involves application of the Laplace Transformation to Equation 8.20

$$L\left(\frac{\delta C}{\delta Y}\right) = \frac{d\bar{C}}{dY} = -\left(\bar{C} - \frac{\bar{q}}{K}\right)$$

where $\bar{C} = L(C)$

$\bar{q} = L(q)$

$$\frac{d\bar{C}}{dY} = -\left(\bar{C} - \frac{\bar{q}}{K}\right) \qquad 8.22$$

Apply Laplace Transformation to Equation 8.21

$$L\left(\frac{\delta q}{\delta Z}\right)_Y = \left(\bar{C} - \frac{\bar{q}}{K}\right)$$

$$L\left(\frac{\delta q}{\delta Z}\right)_y = S\bar{q} - q(O)$$

According to initial boundary conditions $q(O) = O$

$$\therefore \quad S\bar{q} = \bar{C} - \frac{\bar{q}}{K}$$

$$S\bar{q} + \frac{\bar{q}}{K} = \bar{C}$$

$$\bar{q} = \frac{\bar{C}}{S + \frac{1}{K}} \qquad 8.23$$

Substituting Equation 8.23 into Equation 8.22

$$\frac{d\bar{C}}{dY} = -\left[\bar{C} - \frac{1}{K}\left(\frac{\bar{C}}{S + \frac{1}{K}}\right)\right]$$

$$= -\bar{C}\left[1 - \frac{1}{KS + 1}\right]$$

$$= -\bar{C}\left[\frac{KS + 1 - 1}{KS + 1}\right] = -\bar{C}\frac{KS}{KS + 1}$$

$$\therefore \quad \frac{d\bar{C}}{dY} = -\bar{C}\frac{KS}{KS + 1} \qquad 8.24$$

Integrate Equation 8.24:

$$\int_{\frac{Co}{S}}^{\bar{C}} \frac{d\bar{C}}{\bar{C}} = - \frac{K S}{K S + 1} \int_{O}^{Y} dY$$

where from the boundary conditions

$$\text{At} \qquad Y = O \qquad C = C_O$$

$$\therefore \qquad \bar{C} = \frac{Co}{S}$$

$$\therefore \qquad \ln \frac{\bar{C}}{\frac{Co}{S}} = - \frac{K S}{K S + 1} Y$$

$$\therefore \qquad \bar{C} = \frac{Co}{S} e^{\frac{- K S}{(K S + 1)} Y} \qquad 8.25$$

From Equations 8.23 and 8.25

$$\bar{q} = \frac{1}{S + \frac{1}{K}} \left[\frac{Co}{S} e^{\frac{- K S}{K S + 1} Y} \right]$$

$$\bar{q} = \frac{Co\ e^{\left[-\frac{S}{(S+\frac{1}{K})}Y\right]}}{S\,(S+\frac{1}{K})} = \frac{Co\ e^{-\left[1-\frac{\frac{1}{K}}{S+\frac{1}{K}}\right]Y}}{S\,(S+\frac{1}{K})}$$

$$\bar{q} = Co\ e^{-Y}\ \frac{e^{\left[\frac{Y}{K\,(S+\frac{1}{K})}\right]}}{S\,(S+\frac{1}{K})} \qquad 8.26$$

The inverse Laplace Transformation of Equation 8.26

$$q = L^{-1}\,\bar{q} = Co\,e^{-Y}\ L^{-1}\ \frac{\left[e^{(Y/K(S+\frac{1}{K}))}\Big/ S+\frac{1}{K}\right]}{S} \qquad 8.27$$

$$L^{-1}\ \frac{\left(e^{Y/K(S+\frac{1}{K})}\right)\Big/ S+\frac{1}{K}}{S} = \int_{o}^{Z} f(Z)\,dZ \qquad 8.28$$

$$f(Z) = L^{-1}\ \frac{e^{\left[Y/K(S+\frac{1}{K})\right]}}{S+\frac{1}{K}}$$

Using the shift property of the Laplace Transform

$$f(Z) = e^{-\frac{Z}{K}} \; L^{-1} \; \frac{e^{Y/KS}}{S}$$

From Laplace Transform Tables

$$L^{-1} \frac{e^{Y/KS}}{S} = Jo\left(2\sqrt{-\frac{Y}{K}Z}\right) = Jo\left(2i\sqrt{\frac{Y}{K}Z}\right)$$

where

$$i = \sqrt{-1}$$

Jo = Bessel function of the first kind and zero order

$$\therefore f(Z) = e^{\frac{-Z}{K}} \, Jo\left(2i\sqrt{\frac{Y}{K}Z}\right) \qquad 8.29$$

Substitute Equation 8.29 into 8.28

$$L^{-1} \frac{e^{Y/K(S+\frac{1}{K})} \Big/ S + \frac{1}{K}}{S} = \int_0^Z e^{\frac{-Z}{K}} \, Jo\left(2i\sqrt{\frac{Y}{K}Z}\right) dZ \qquad 8.30$$

From Equation 8.27 and 8.30

$$q = Co \; e^{-Y} \int_0^Z e^{\frac{-Z}{K}} \, Jo\left(2i\sqrt{\frac{Y}{K}Z}\right) dZ \qquad 8.31$$

$$\left(\frac{\delta q}{\delta Z}\right)_Y = Co\ e^{-Y}\ e^{\frac{-Z}{K}}\ Jo\ (2i\sqrt{\frac{Y}{K}Z})$$

Using Equation 8.19

$$\left(\frac{\delta C}{\delta Y}\right)_Z = -\left(\frac{\delta q}{\delta Z}\right)_Y$$

yields,

$$\left(\frac{\delta C}{\delta Y}\right)_Z = -\ Co\ e^{-Y}\ \ e^{\frac{-Z}{K}}\ Jo\ (2i\sqrt{\frac{Y}{K}Z}) \qquad 8.32$$

Integration of Equation 8.32 with respect to Y,

$$\int_{Co}^{C} dc = -\int_{o}^{Y} Co\ e^{-Y}\ e^{\frac{-Z}{K}}\ Jo\ (2i\sqrt{\frac{Y}{K}Z})\ dY$$

$$\therefore\ C = Co - \int_{o}^{Y} Co\ \ e^{-Y} e^{\frac{-Z}{K}}\ Jo\ (2i\sqrt{\frac{Y}{K}Z})\ dY$$

$$Jo\ (2i\sqrt{\frac{YZ}{K}}) = Io\ (2\sqrt{\frac{YZ}{K}})$$

where:

Io = the Bessel function of zero order for an imaginary argument.

$$\therefore\ C = Co - Co \int_{o}^{Y} e^{-\frac{Z}{K}} e^{-Y}\ Io\left(2\sqrt{\frac{YZ}{K}}\right) dY$$

$$\frac{C}{Co} = 1 - \int_{o}^{Y} e^{-\left(\frac{Z}{K}+Y\right)}\ Io\left(2\sqrt{\frac{YZ}{K}}\right) dY \qquad 8.33$$

Equation 8.33 describes the concentration profile of the effluent of the adsorption column as a function of the parameters Z and Y. To express Equation 8.33 as a function of time and column height it is necessary to substitute the following expressions into Equation 8.33:

$$Y = \frac{3k_f}{U\ Rp\ m}\ X$$

$$dY = \frac{3k_f}{U\ Rp\ m}\ dX$$

$$Z = \frac{3k_f}{Rp}\left(t - \frac{X}{U}\right)$$

$$\therefore \frac{C}{Co} = 1 - \frac{3k_f}{U\,Rp\,m} \int_o^L \left\{ e^{\frac{3k_f}{Rp}\left[\frac{1}{K}(t - \frac{X}{U}) + \frac{X}{Um}\right]} \right.$$

$$\left. Io\left(\frac{6k_f}{Rp} \sqrt{\frac{X(t - \frac{X}{U})}{UmK}} \right) \right\} dX \qquad 8.34$$

For the condition $t \geq \frac{L}{U}$

L represents the height of the bed.

The application of Equation 8.34 for the prediction of breakthrough curves, is discussed in Chapter 9 and the results compared with experimental data. The detailed analysis is also shown there.

CHAPTER 9

RESULTS AND DISCUSSION OF RESULTS

9 RESULTS AND DISCUSSION OF RESULTS

The experimental data and calculated results are illustrated in this chapter and in Appendix B. Sample calculations and summaries of all derived quantities are given in Appendix B. The discussions and interpretation of the results are presented in detail in this chapter. For convenience the experimental results and discussion are considered in three sections, namely: the equiiibrium adsorption isotherms, the kinetics of adsorption, and the dynamic adsorption studies.

9.1 THE EQUILIBRIUM ADSORPTION ISOTHERMS

The equilibrium adsorption loading experiments were carried out with binary solutions and cylindrical 1/8 inch pellets of 5A zeolites, in the liquid phase only at three different temperatures 303 K, 323 K and 343 K.

As mentioned in Chapter 4, the forces involved in physical adsorption include both dispersion-repulsion forces and electrostatic interactions comprising polarization, dipole, and quadrupole interactions. When the solution of n-paraffin component is contacted with the active type 5A molecular sieve, the molecules of n-paraffin component will be distributed among the zeolite cavities together with the solvent molecules. The molecules of n-paraffin penetrate into the cavities through the pores and become adsorbed due to interactions with the cations in cavities of zeolite crystals.

These interactions may be specific or non-specific. The specific interactions can be characterized by the energy which arises from field-dipole or field gradient-quadrupole interactions of the sorbate molecules. Non-specific interactions are related to dispersion, repulsion and polarization contributions.

For non-polar molecules such as n-paraffins, only the non-specific interactions can contribute to the energy of adsorption.

Figures 9.1 to 9.3 show the equilibrium adsorption isotherm curves for normal dodecane, normal hexadecane, and normal eicosane respectively. The points represent the experimental data determined by the Gibbs equation 4.5; the curves were calculated from an equation proposed by Eltekov and Kiselev (36) for pore filling in the form of multilayers referred to as the Brunauer-Emmett-Teller (BET) equation and expressed as Equation 4.4.

Figures 9.1 to 9.3 demonstrate that Equation 4.4 fits the adsorption isotherms satisfactorily and the limiting amounts of adsorption (G_m) as determined experimentally, ie. points on the isotherm curves, are in a good agreement with the values (a_m) calculated from Equation 4.4 and shown in Table 9.1.

The general trend of the isotherm curves shows an initial linear increase in equilibrium loading with concentration followed by a relatively large range of concentration over which the equilibrium loading is nearly constant. It is clear that the isotherms are favourable, approaching irreversible adsorption. At the same concentration, the equilibrium loading decreases with increasing temperature.

A comparison of these figures shows that the effect of temperature on the change of equilibrium loading is maximum for normal dodecane and reduces for higher paraffins.

Figure 9.4 illustrates a plot of the amounts adsorbed at saturation

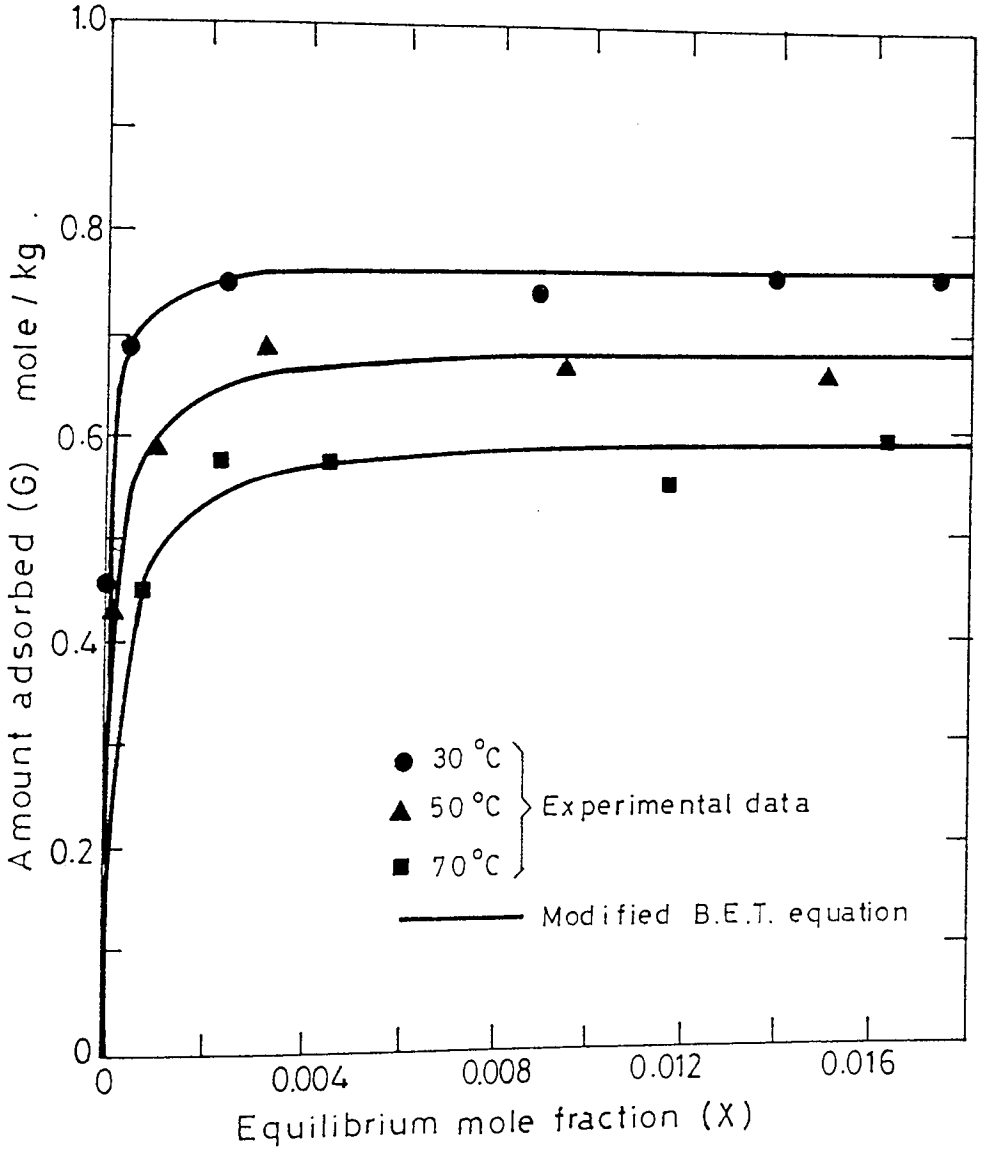

Figure9-1: Adsorption isotherms of n-dodecane

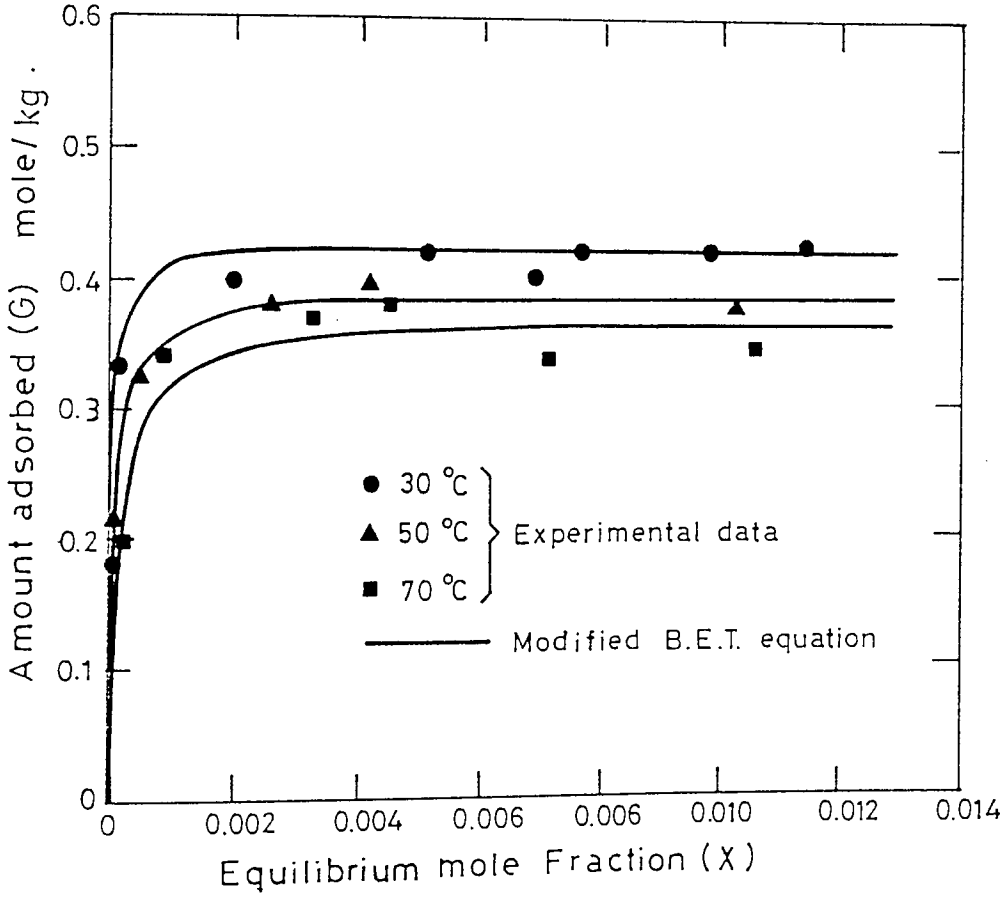

Figure 9·2 : Adsorption isotherms of n-hexadecane

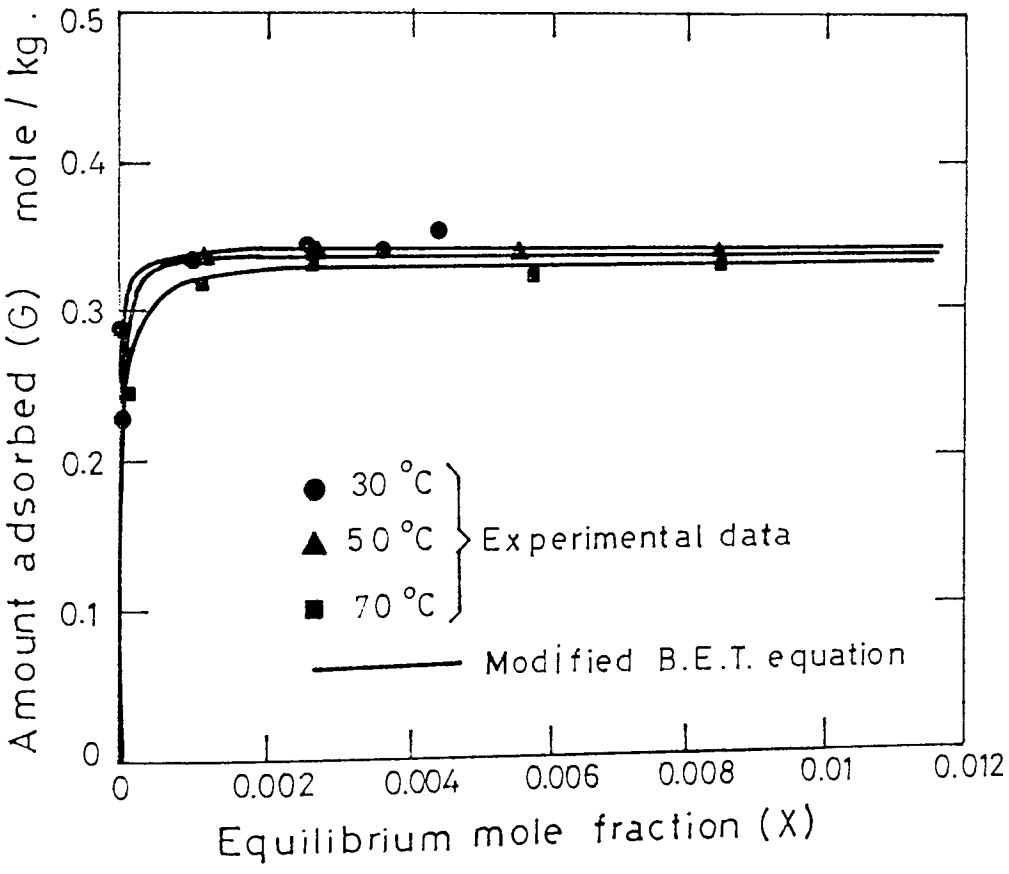

Figure 9·3: Adsorption isotherms of n-eicosane

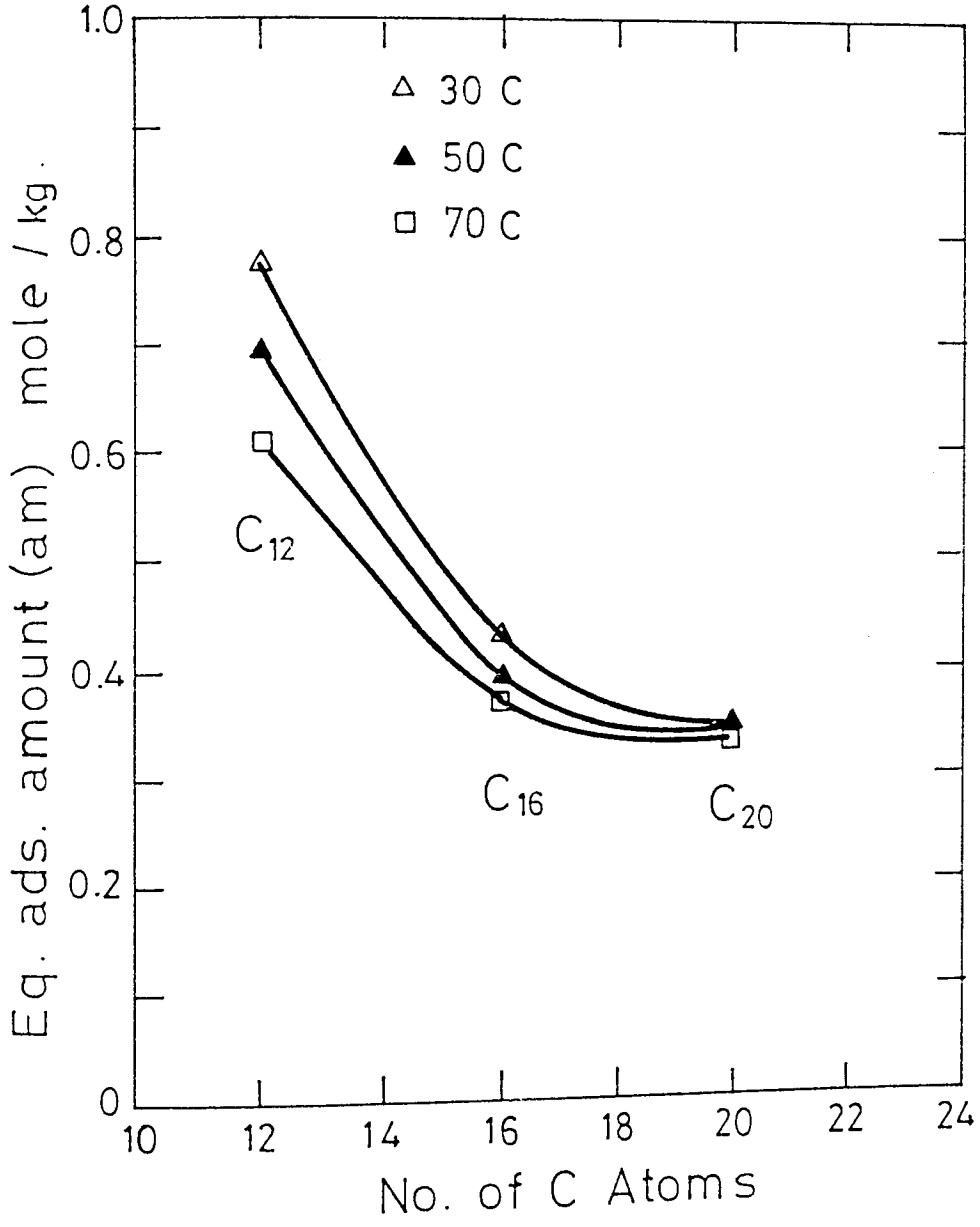

Figure 9·4 : Plot of max. value adsorbed vs. n-paraffin carbon atoms.

(maximum loading) versus the number of carbon atoms in the normal alkane chain at different temperatures. As demonstrated by this figure, the temperature effect decreased with increased length of n-paraffin chain. The difference between the maximum amount adsorbed at 303°K and 343°K is 0.18 mole/kg, 0.06 mole/kg, and 0.02 mole/kg for n-dodecane, n-hexadecane, and n-eicosane respectively. This is attributed to increased molecular mobility in the cavities of molecular sieve and weakened intermolecular bonds with increasing temperature.

The results of equilibrium loading for normal dodecane are in a good agreement with those of Sundstrom and Krautz (46), who have reported a loading of 12.4 gm/100 gm sieve at 303°K compared with a loading in this study of 13.2 gm/100 gm sieve at same temperature.

At the same condition of adsorption temperature and liquid concentration, the equilibrium loading decreased with the increase in molecular weight, ie. the lower molecular weight paraffin was preferentially adsorbed. For example, at an adsorption temperature of 323°K and solution equilibrium concentration of 0.004 mole fraction the equilibrium loading for normal dodecane was 0.67 mole/kg sieve, while it was 0.38 mole/kg sieve and 0.335 mole/kg sieve for normal hexadecane and normal eicosane respectively.

Gupta et al (57) reported a similar trend for adsorption of normal paraffins C_5, C_6, C_7 and C_8 where at 18°C and at an equilibrium concentration of 1.6 mole/l the equilibrium loading for the normal paraffins were 2.03, 1.62, 1.43 and 1.34 mole/kg sieve respectively. This emphasizes the violation of Traube's rule, as reported by previous authors, that higher molecular weight adsorbate

should be preferentially adsorbed.

The preferential adsorption of lower molecular weight normal paraffins on 5A molecular sieves arises because both physiochemical adsorption and steric effects are important in the zeolites. Since type 5A molecular sieves have a pore opening of 5Å and normal paraffins have a critical diameter of 4.9Å , steric effects will play an important role. For shorter chain compounds, ie. lower molecular weight normal paraffins, steric effects will be less in comparison to larger chain compounds (57).

Table 9.1 lists calculated values of limiting amount of adsorbate filling the cavities of 1gm of molecular sieve (a_m), separation coefficient (f), and equilibrium adsorption time (t) for the normal paraffins under investigation at different temperatures. It can be seen that the logarithm of the separation coefficient (log f) for the three normal paraffins and at different temperatures are higher than 2, which gives an indication of the high selectivity of adsorption of these normal paraffins from isooctane solution by Type 5A molecular sieve.

The values of a_m, f, and t decreased with increase in the temperature due to increasing molecular mobility, a weakening in their bonds with the cavity surfaces, and an increase in the effect of the force field due to the solution. The increase in temperature also results in more rapid diffusion of the molecules in the molecular sieve cavities with a consequent reduction in time for the physical interactions to occur.

Table 9.1 Calculated equilibrium adsorption values

Temperature °K	n-Dodecane				n-Hexadecane				n-Eicosane			
	a_m* mole/kg	f**	log f	t*** hr	a_m mole/kg	f	log f	t hr	a_m mole/kg	f	log f	t hr
303	0.7735	16879	4.2	40	0.428	28775	4.5	63	0.345	47286	4.7	70
323	0.6936	6161	3.8	26	0.394	10206	4.0	40	0.3415	46481	4.6	45
343	0.609	3547	3.5	15	0.372	6612	3.8	20	0.3363	12830	4.1	25

* Maximum amount of adsorbate filling the cavities of 1gm of geolite

** Separation coefficient

*** Equilibrium adsorption time

Heat of Adsorption

The isosteric heats of adsorption of normal paraffins n-C_{12}, n-C_{16} and n-C_{20} in Table 9.2 were derived from adsorption isosteres in Figures 9.5 to 9.7 respectively at three different temperatures 303, 323 and 343°K. Equation 4.8 suggests that a plot of ln x versus 1/T will produce a straight line, ie. adsorption isostere, of slope q^{G}_{iso}/R

The calculations of isosteric heats are illustrated in Appendix B.

The effect of temperature on sorption equilibria in the region 303-343°K is presented in the form of graphs relating the isosteric heat of sorption ($-q_{iso}$) with fractional loading (θ) for individual n-paraffins, at a temperature of 323°K. Values of q_{iso} were calculated from the Clausius-Clapeyron Equation 4.9 using X_{303} and X_{343} as shown in the sample calculation. The results are illustrated in Figure 9.8, the lines indicating the main trends.

The values of heat of adsorption of normal paraffins C_{12}, C_{16} and C_{20} decreased with increasing molecular weight at any one value of θ (eg. $\theta = .8$). A similar trend has been observed by Burgess et al (62) with 5A sieve in the normal paraffin molecular weight region (C_{10} - C_{20}) at temperature of 623°K.

Barrer and Ibbitson (63) discussed the effect of molecular weight on the heat of sorption in molecular sieves. Their observation with Chabazite showed that q_{iso} increased by ~ 3 kcal/mole per CH_2 group in the series methane to n-heptane.

Table 9.2 Values of isosteric heats and amount of n-paraffins adsorbed

n-paraffin	n-Dodecane			n-Hexadecane			n-Eicosane		
Amount adsorbed	0.3	0.4	0.55	0.2	0.3	0.35	0.25	0.3	0.31
Heat of adsorption kcal/gm mole	7.0	8.2	15.9	4.5	9.4	14.5	5.4	7.2	7.2
kJ/gm mole	29.1	34.4	66.6	18.8	39.3	60.7	22.6	30.1	30.1

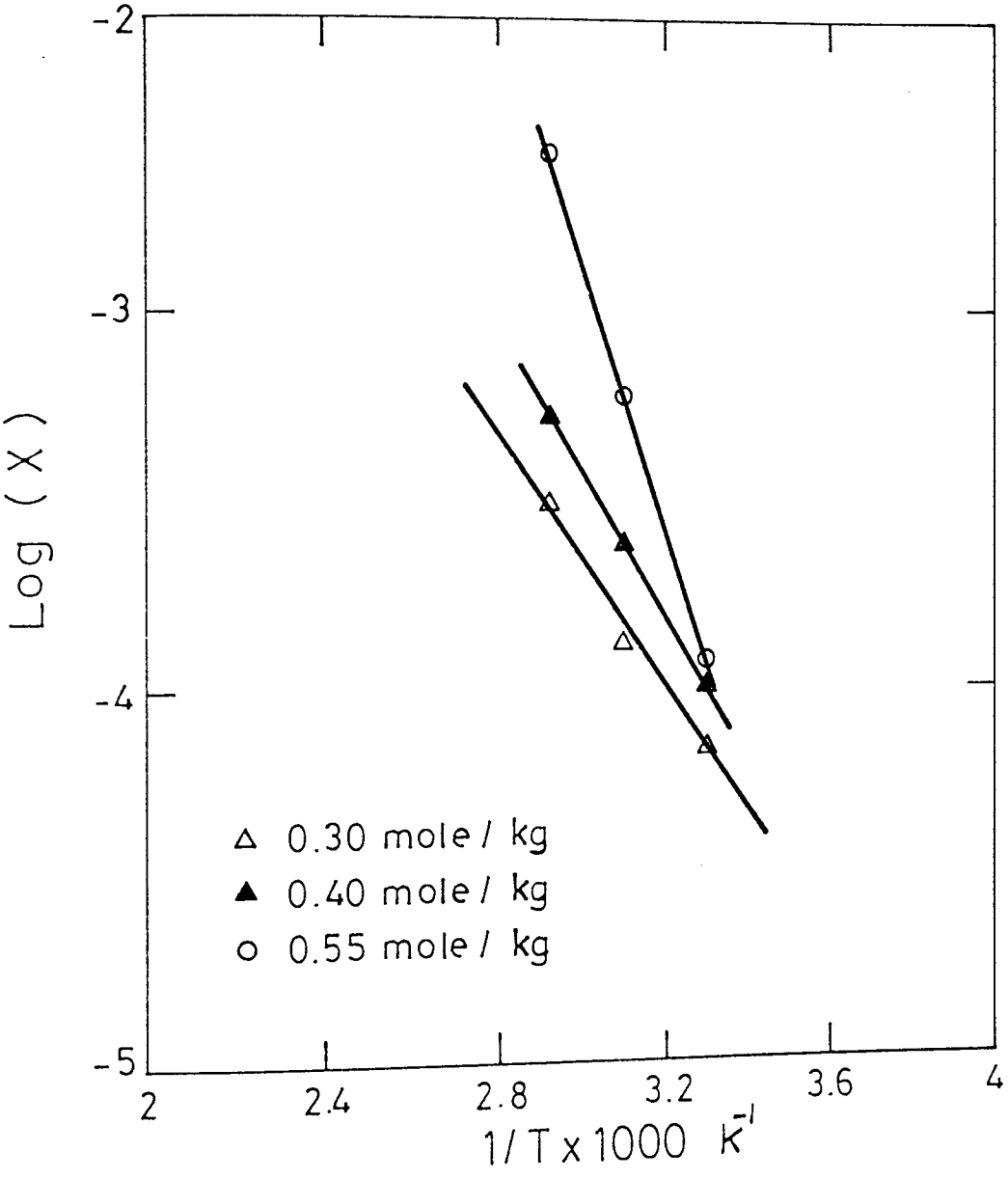

Figure 9·5: Isostere of n-dodecane

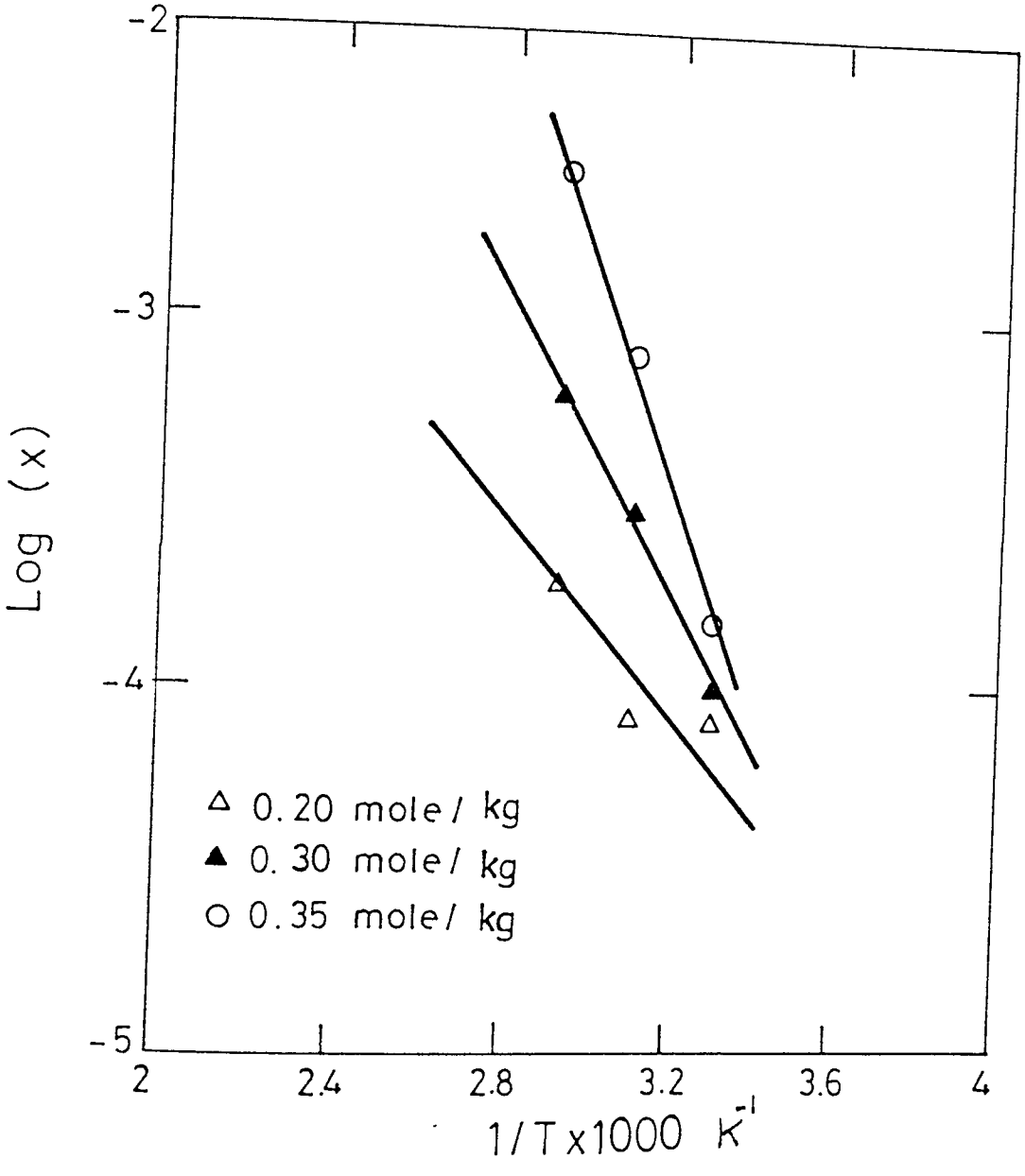

Figure 9.6 : Isostere of n-hexadecane.

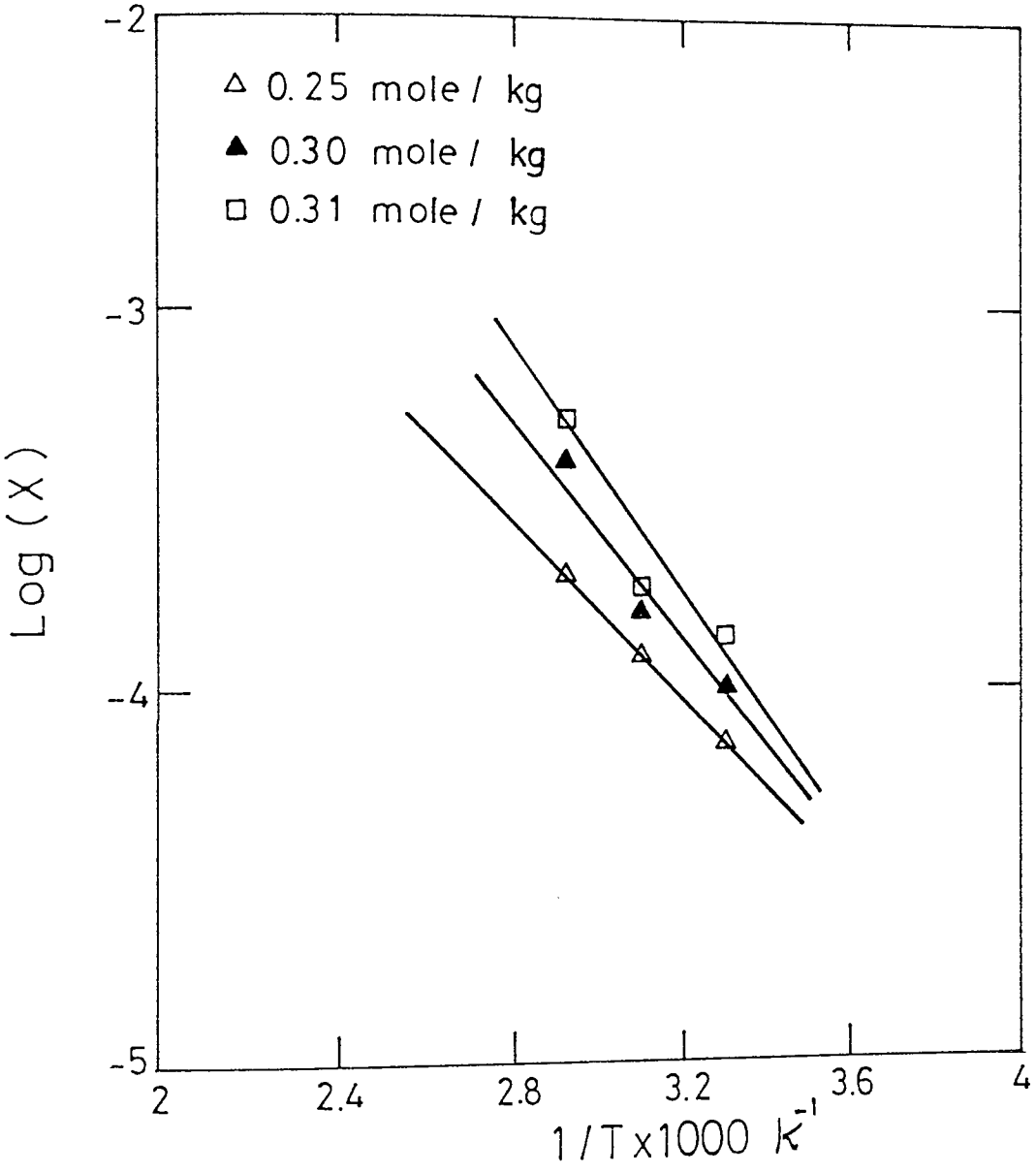

Figure 9.7: Isostere of n-eicosane.

With other types of adsorbing surfaces, the heat of sorption also rises for the n-paraffin series. The work of Peterson and Redlich (60) has also been said to indicate that q_{iso} rises with molecular weight in 5A sieves.

The results from a study by Burgess et al did not agree with the prediction by Barrer that, with increasing carbon numbers, the isosteric heats of adsorption should rise at a constant rate. The non applicability of Barrer's prediction in case of zeolites was discussed by Burgess et al (62).

Barrer's prediction, that the heat of adsorption would rise continuously with increasing molecular weight, was based on the assumption that all additional CH_2 groups would have equal access to the sieve wall. Whilst this may be true in urea complexes, a limiting effect may be expected in zeolites. The reason for this is that the additive behaviour of heat of adsorption continues as long as every part of a hydrocarbon molecule can interact, without complication, with a suitable sorption site on the sieve wall, the energy of stabilisation only then being fully available. Thus deviations are likely to be associated with the shape of the molecule itself, and, in particular, with the coiled configuration adopted by paraffins such as C_8 and above. The carbon atoms of such a long-chain molecule can only approach the wall after a partial uncoiling, which may involve up to 0.5-1.0 kcal/mole per CH_2 group. The loss of this energy offsets the gain in stability due to the interaction with the wall. The importance of the proximity of CH_2 groups to the walls would be more marked in sieves with narrow entrances such as 5A molecular sieves. This effect could explain why the increase in heat of adsorption with carbon number in 5A sieves does not continue beyond ~ C_8.

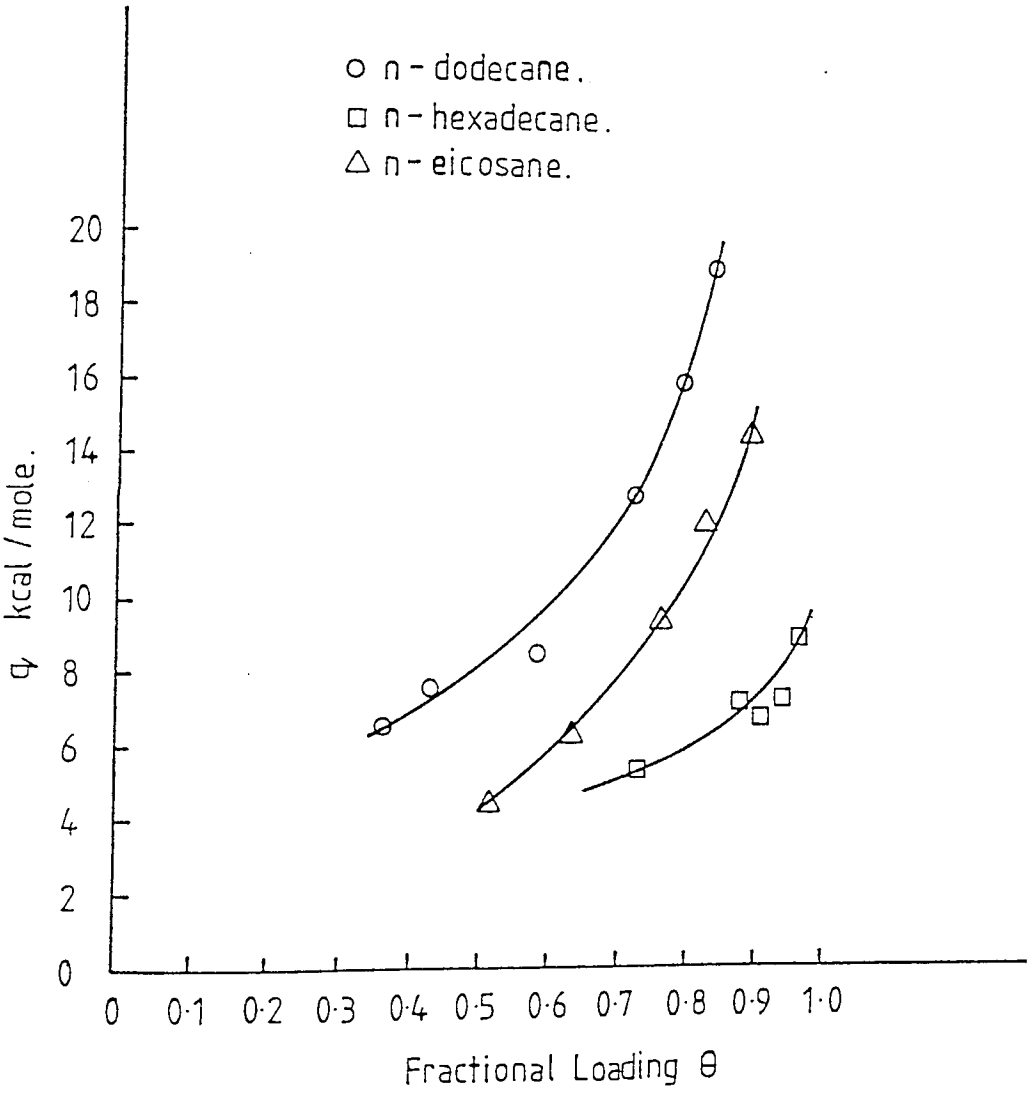

Figure 9.8 Variation of q_{iso} with fractional loading for sorption of n-paraffins on 5A molecular sieves at $323^{o}K$

An increase in heat of adsorption with coverage is observed for the three n-paraffins under investigation, as illustrated in Figure 9.8 and this is commonly attributed to the effect of intermolecular attraction forces. This agrees with the major trends confirmed by Burgess et al, that the dependence of heat of adsorption on loading is increasingly steep (C_9 - C_{20}) for 5A sieves.

9.2 THE KINETICS OF ADSORPTION

The rate experiments were conducted by methods mentioned in Chapter 7, with 5A molecular sieves in the form of 1/8 inch pellets. The kinetics of adsorption in this study were concerned with the adsorption rate of normal paraffins, n-dodecane, n-hexadecane, and n-eicosane at three different temperatures, 303, 323 and 343°K from a binary solution composed of normal paraffin (solute) and isooctane (solvent).

The effective diffusivities were calculated for all systems using Barrer and Brook equation 4.10. The activation energies were determined from the variation of effective diffusivity with 1/T, by applying Eyring's equation 4.11. The sample calculations are illustrated in Appendix B.

9.2.1 The Adsorption Kinetic Curves

The adsorption kinetics curves were represented by plotting the relative adsorption of solute (G_t/G_∞) (where G_t is the adsorption at time t, G_∞ is the

equilibrium adsorption) at time t versus $\sqrt{t}$. This relationship expresses the degree of saturation of the sorption capacity at any given time.

Figures 9.9 to 9.11 illustrate adsorption kinetics of n-dodecane, n-hexadecane, and n-eicosane respectively at temperatures 303, 323, and 343°K.

These figures show the effect of temperature on adsorption kinetics for the normal paraffins. The rate of adsorption increased with increasing temperature. The equilibrium time was according to the following table.

Temperature °K	(Equilibrium time hr)		
	n-C_{12}	n-C_{16}	n-C_{20}
303	17	20	28
323	14	18	23
343	8	10	11

The rate of adsorption at 343°K was rapid and equilibrium was reached within several hours as shown in the above table. The time of equilibrium was increased with molecular weight of n-paraffins and decreased with increasing temperature. The decrease of the equilibrium time with temperature could be due to the temperature-dependence of the energy of interactions. Increasing the temperature enhanced the mobility of the molecules towards the molecular sieves pores. This accelerated the interactions between the bonds of adsorbate molecules and the electrostatic charge of the zeolite crystals resulting in a more rapid approach to

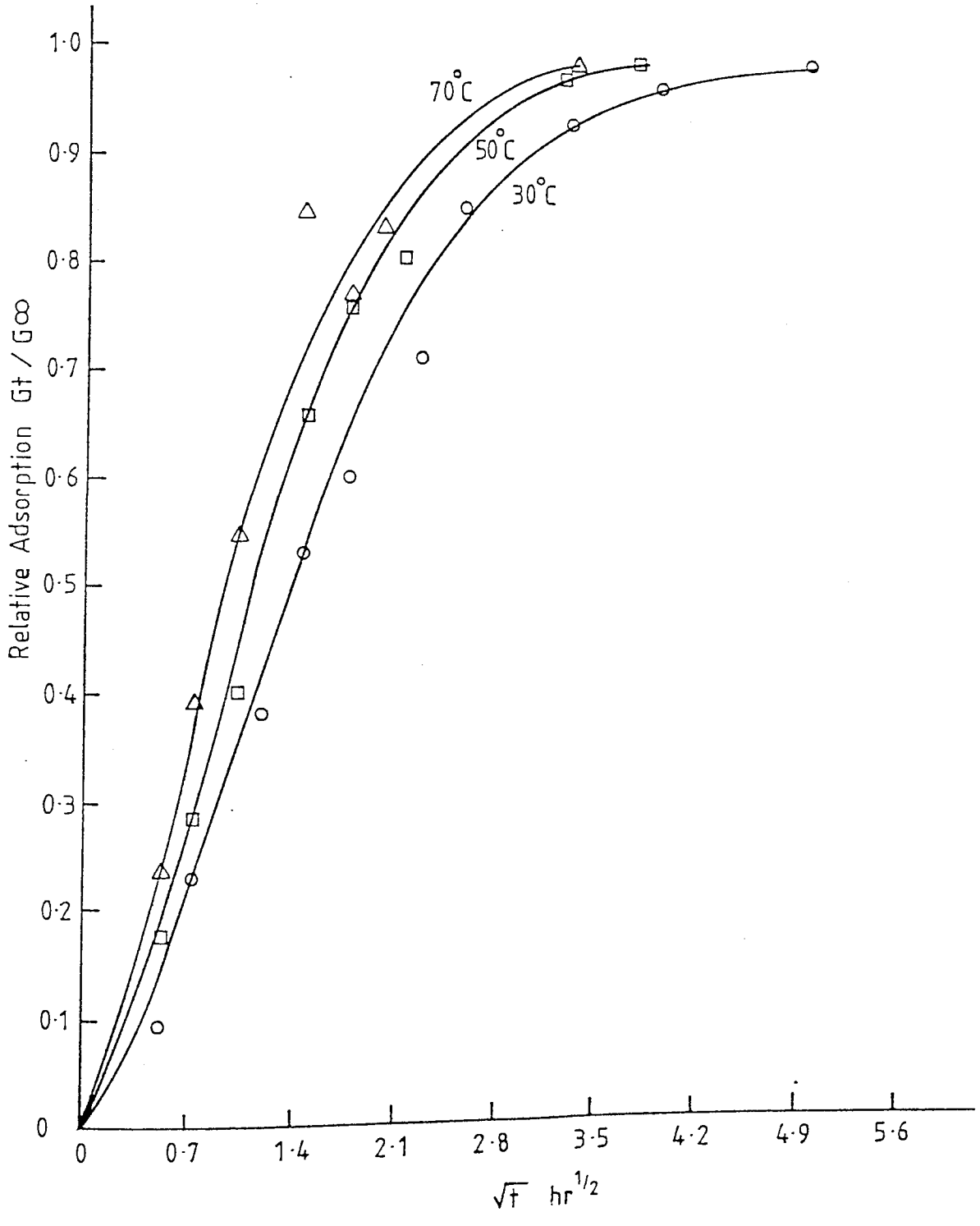

Figure 9.9 Kinetics of adsorption of n-dodecane from isooctane solutions at various temperatures

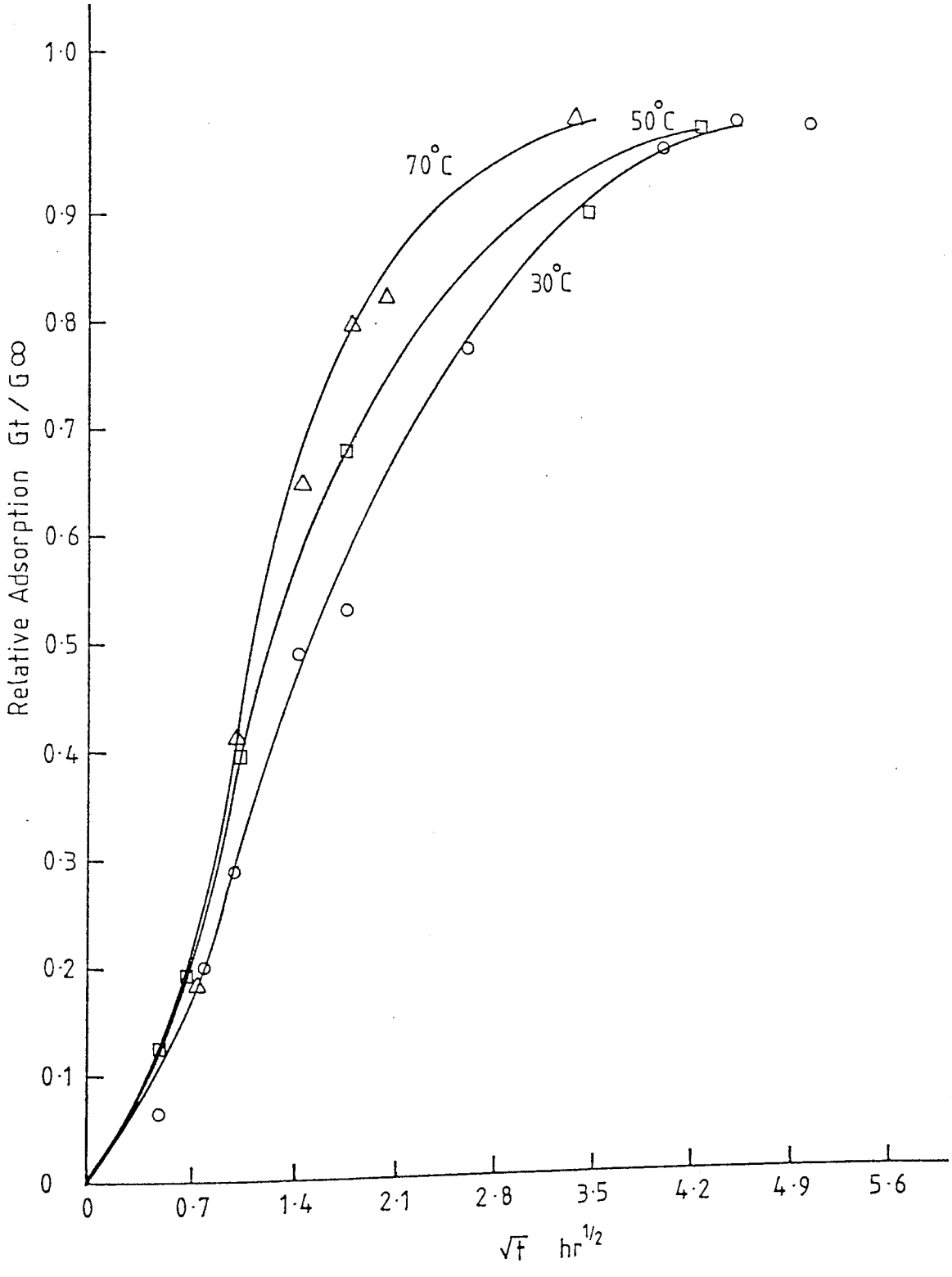

Figure 9.10 Kinetics of adsorption of n-hexadecane from isooctane solution at various temperatures

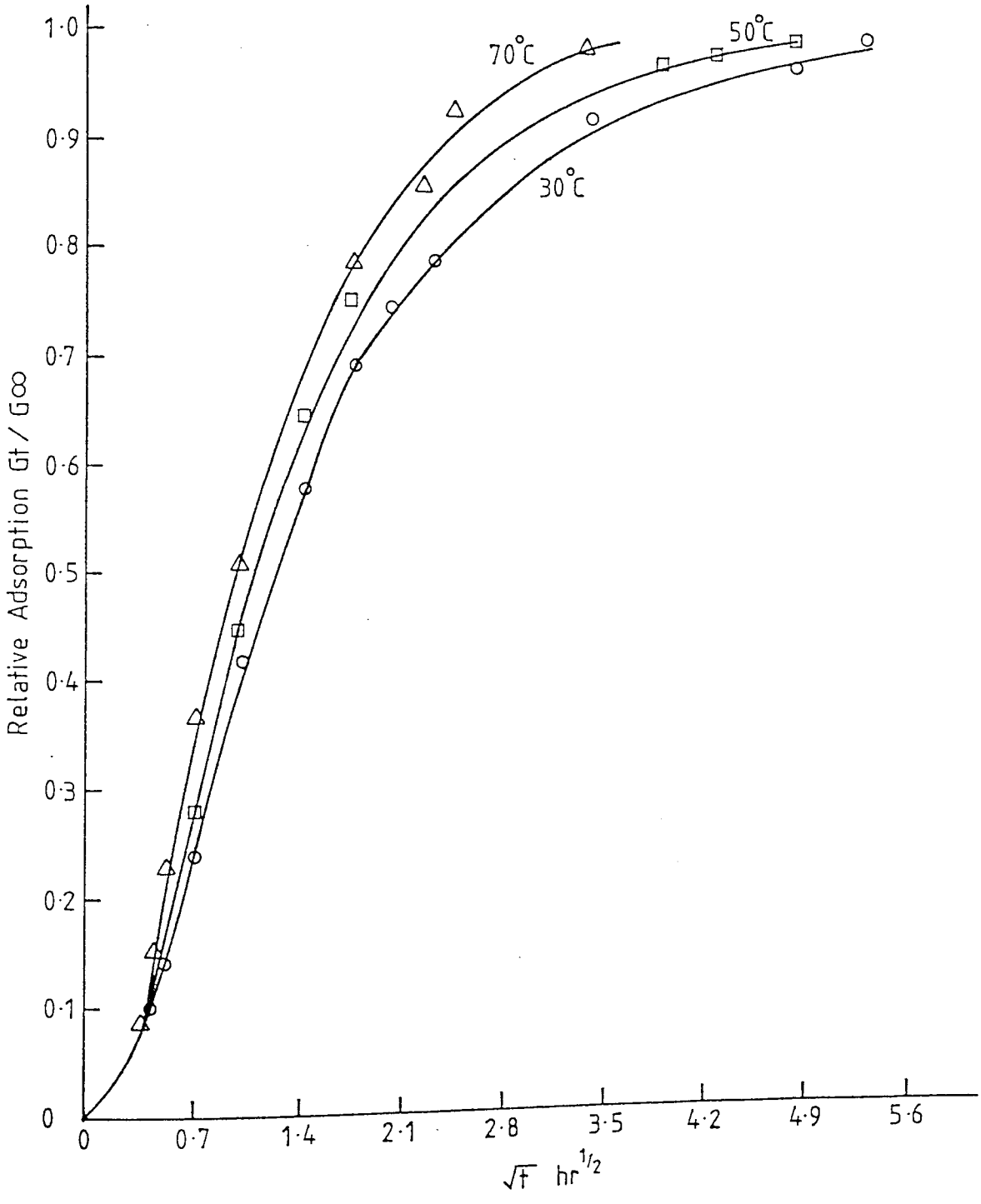

Figure 9.11 Kinetics of adsorption of n-eicosane from isooctane solution at various temperatures

equilibrium.

In isotherm adsorption studies it was concluded that the equilibrium amount adsorbed decreased with increasing temperature for the n-paraffins considered in this work.

For optimum conditions of adsorption of n-paraffins in industrial applications it is important to consider the effects of temperature on both rate of adsorption, to reduce the time of process cycle, and maximum amount to be adsorbed in each cycle.

9.2.2 The Effective Diffusivity D_e

Kinetic data for sorption of gases and liquids in zeolites are generally correlated in terms of diffusion coefficients calculated from experimental sorption curves.

Previous studies (13) have revealed a complex pattern of behaviour which indicated that the diffusion mechanism depends upon the relative sizes of the diffusing molecule and the zeolite micropore. The effective diffusivities of normal paraffins were tabulated in Table 9.3 at various temperatures 303, 323 and 343°K. There is a general rise in effective diffusivity with increasing temperature. This can be attributed to the increasing mobility of the molecules in the solution. Also, in the case of adsorption of n-paraffins by molecular sieve 5A, where the orifice size and the critical diameter of molecules are close to one another, adsorption occurs with a high activation energy. To overcome the energy barrier a molecule has to

Table 9.3 Effective Diffusivities of normal paraffins at different adsorption temperatures

n-Paraffin		303°K		323°K		343°K	
	$\sqrt{t}$ ($hr^{1/2}$)	G_t/G_∞	De ($x10^{10}$)m^2/sec	Gt/G_∞	De ($x10^{10}$)m^2/sec	G_t/G_∞	De ($x10^{10}$)m^2/sec
C_{12}	.35	.09	.055	.01	.075	.14	.144
	.70	.22	.086	.27	.127	.37	.234
	1.05	.37	.107	.47	.172	.57	.252
	1.40	.52	.110	.63	.173	.72	.222
	1.75	.66	.121	.76	.158	.82	.184
	2.10	.76	.118	.84	.143	.88	.159
	2.45	.84	.100	.90	.113	.93	.122
	2.80	.89	.084	.94	.095	.97	.101
C_{16}	0.70	.17	.049	.20	.068	.21	.075
	1.05	.32	.078	.41	.128	.44	.147
	1.40	.48	.098	.58	.144	.64	.175
	1.75	.59	.095	.69	.130	.78	.168
	2.10	.68	.094	.76	.118	.87	.153
	2.45	.76	.082	.84	.098	.92	.119
	2.80	.83	.074	.89	.085	.96	.098
C_{20}	0.70	.24	.098	.28	.139	.33	.186
	1.05	.42	.134	.47	.172	.53	.218
	1.40	.56	.138	.62	.167	.68	.198
	1.75	.69	.130	.72	.144	.79	.171
	2.10	.75	.115	.80	.130	.86	.150
	2.45	.81	.092	.85	.103	.91	.117
	2.80	.85	.077	.89	.086	.95	.097
	3.15	.89	.067	.93	.073	.98	.081

possess appreciable reserves of kinetic energy which increase with a rise in temperature. In addition small deformations of the zeolite crystalline lattice are possible with a rise in tempreature which cause an increase in the dimensions of orifices which eases penetration of n-paraffin molecules into adsorption cavities.

The same trend was noted by other authors (62). Figures 9.12 to 9.14 demonstrate the change of effective diffusivity with relative adsorption (G_t/G_∞) for n-dodecane, n-hexadecane, and n-eicosane respectively at various temperatures 303, 323 and 343°K. Clearly the three n-paraffins behaved in a similar manner. Their diffusivities increased gradually to approach an intermediate maximum then fell off gradually to a minimum at equilibrium. The maximum diffusivities associated with their relative adsorption are listed in the following table:

Temperature °K	n-dodecane		n-hexadecane		n-eicosane	
	Max D_e ($x10^{12}$) m^2/sec	G_t/G_∞	Max D_e ($x10^{12}$) m^2/sec	G_t/G_∞	MaxD_e ($x10^{12}$) m^2/sec	G_t/G_∞
303	12.2	0.63	9.9	0.56	13.8	0.55
323	17.3	0.60	14.3	0.57	17.1	0.55
343	24.6	0.55	17.6	0.7	21.5	0.55

The irregular behaviour of diffusivity as molecular weight of the n-paraffins increased has a parallel in the report of Gorring (15) that the diffusivity of normal

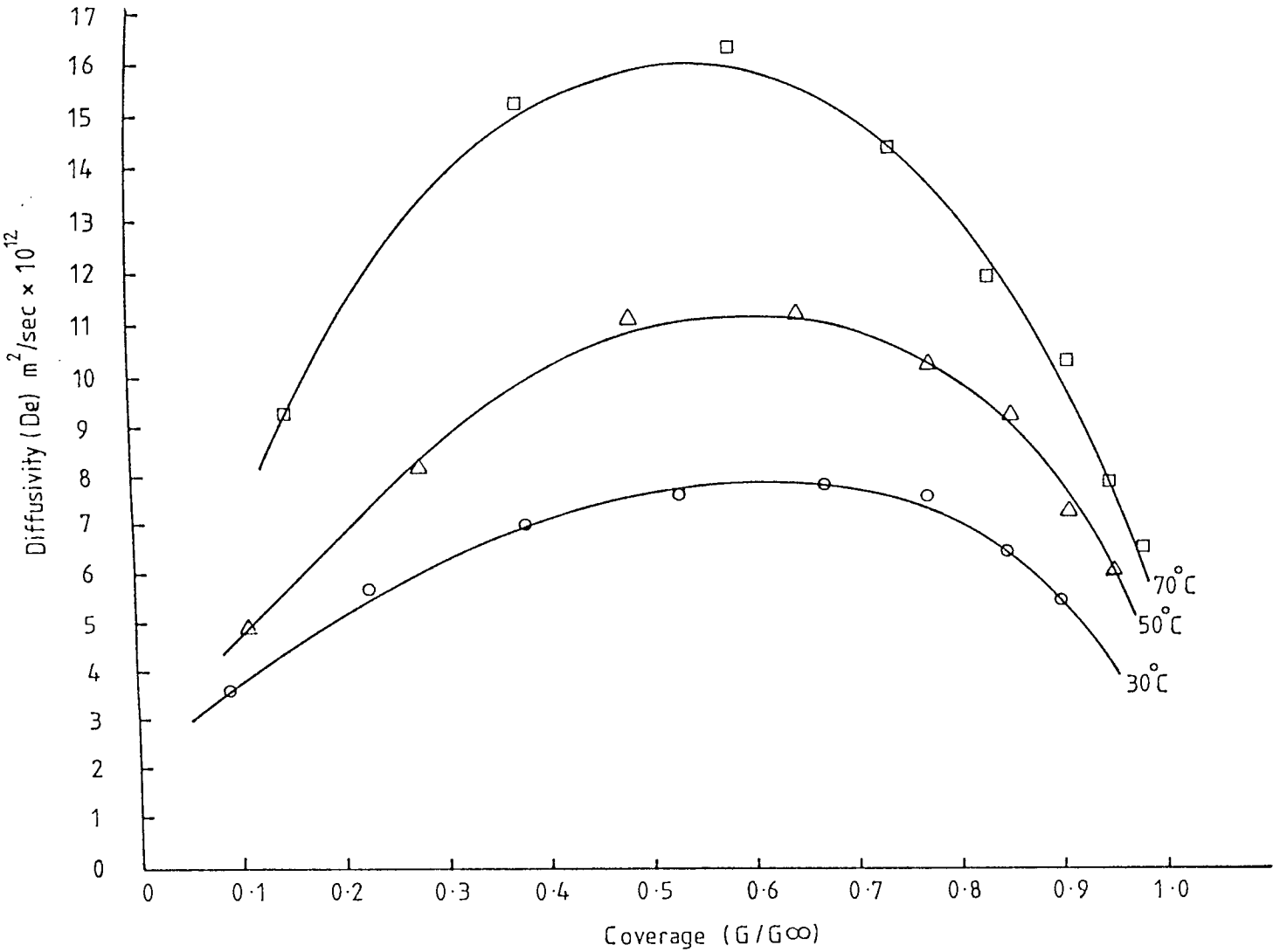

Figure 9.12 Diffusivity versus fractional coverage of n-dodecane

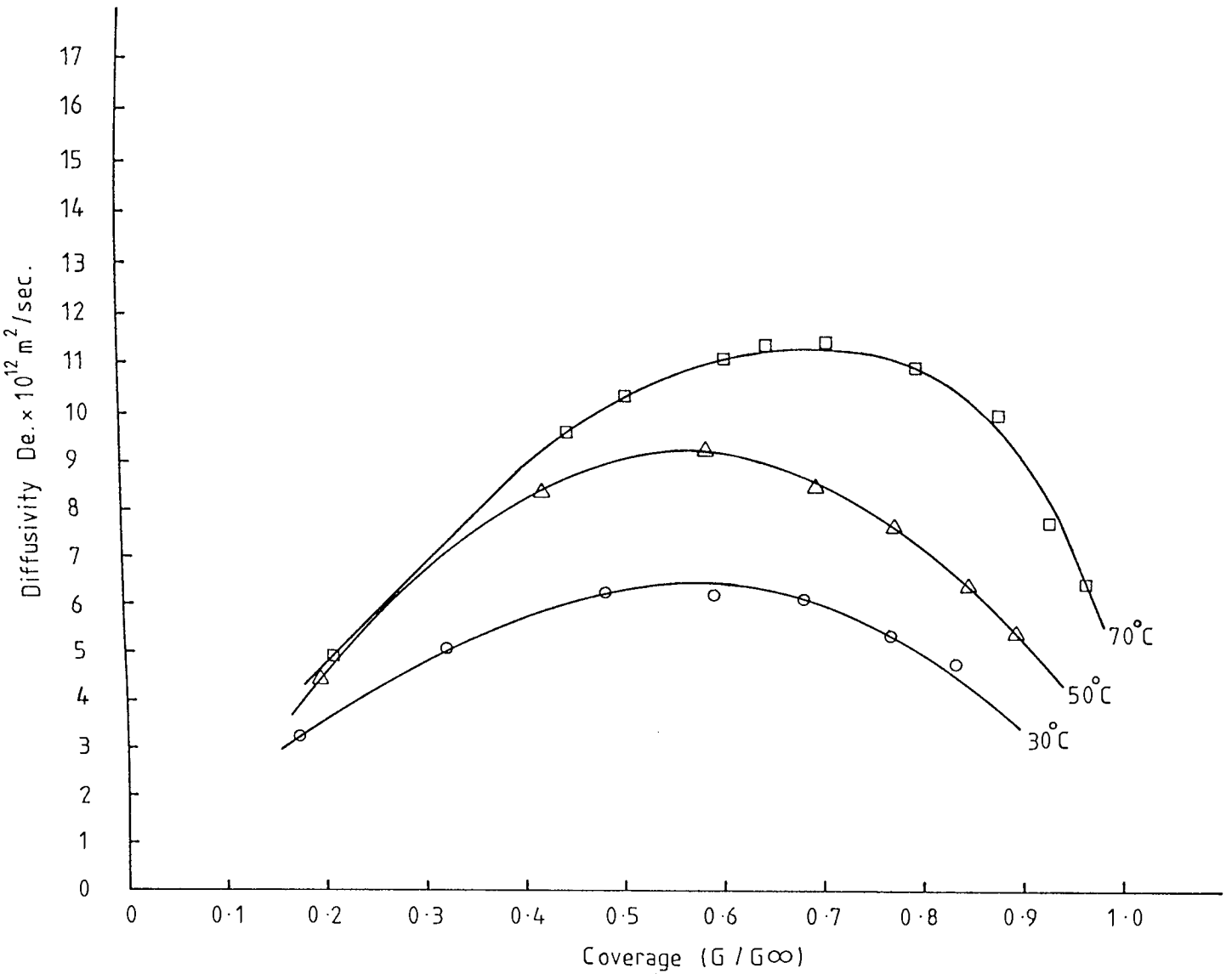

Figure 9.13 Diffusivity versus fractional coverage of n-hexadecane

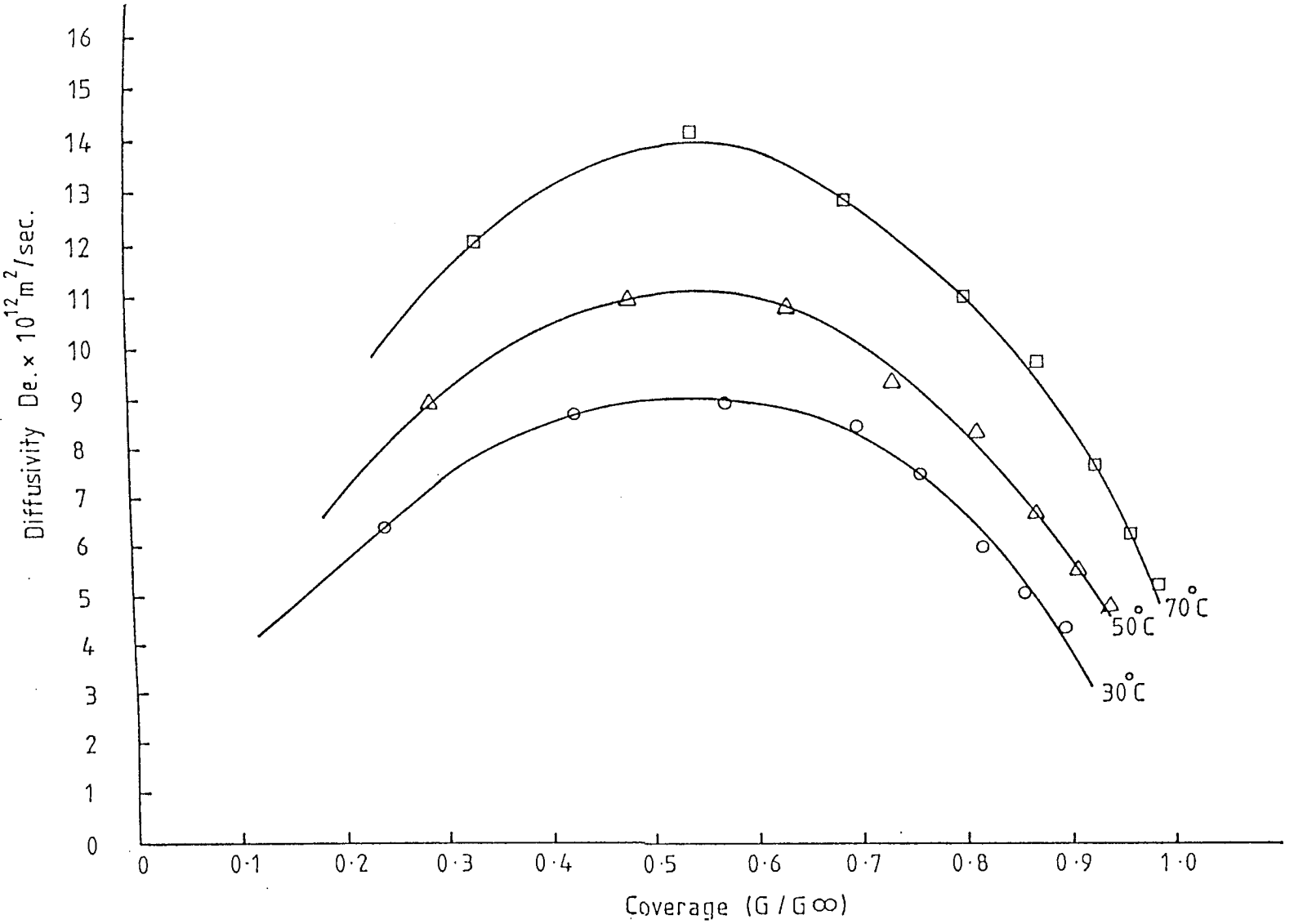

Figure 9.14 Diffusivity versus fractional coverage of n-eicosane

paraffins in Zeolite T dropped to a minimum with an increase in molecular weight up to C_8, then rose to a maximum up to C_{12}, dropping again with the member C_{14}. The results were interpreted in terms of a "window effect" in which maxima and minima were related to degrees of fit of the diffusing molecule relative to crystal dimensions.

This phenomena was interpreted by Gorring for diffusion of n-paraffin in potassium T zeolite as follows: The length of the n-octane molecule corresponds almost exactly to the free length of the erionite cage defined by the alumino silicate framework. The close sheathing of the n-octane molecule by the hexagonally shaped erionite cage yields a configuration where the molecule just fits the cavity. It is a low-energy trap defined by the cage with the primary energy barrier to diffusion deriving from the 8-membered rings forming the cage exit/entry ports. Entrapment in the cage leads to low mobility for "just-fitting" molecules such as n C_7-C_8. Molecules larger than n C_8 are too long to entirely fit into the erionite cage and must assume a configuration with part of the molecule extending through at least one 8-membered ring constituting the aluminosilicate framework. This extension through an 8-ring is conceived to result in a partial surmounting of the energy barrier by virtue of molecular size alone. Channelization of the n-paraffin through the 8-ring results in high selectivity to successful forward translation via both a lowered energy barrier and an imposed molecular orientation in the direction required for migration . Thus, larger molecules can have enhanced mobility.

Figures 9.15 to 9.17 show the variation of D_e with $\sqrt{t}$ at different

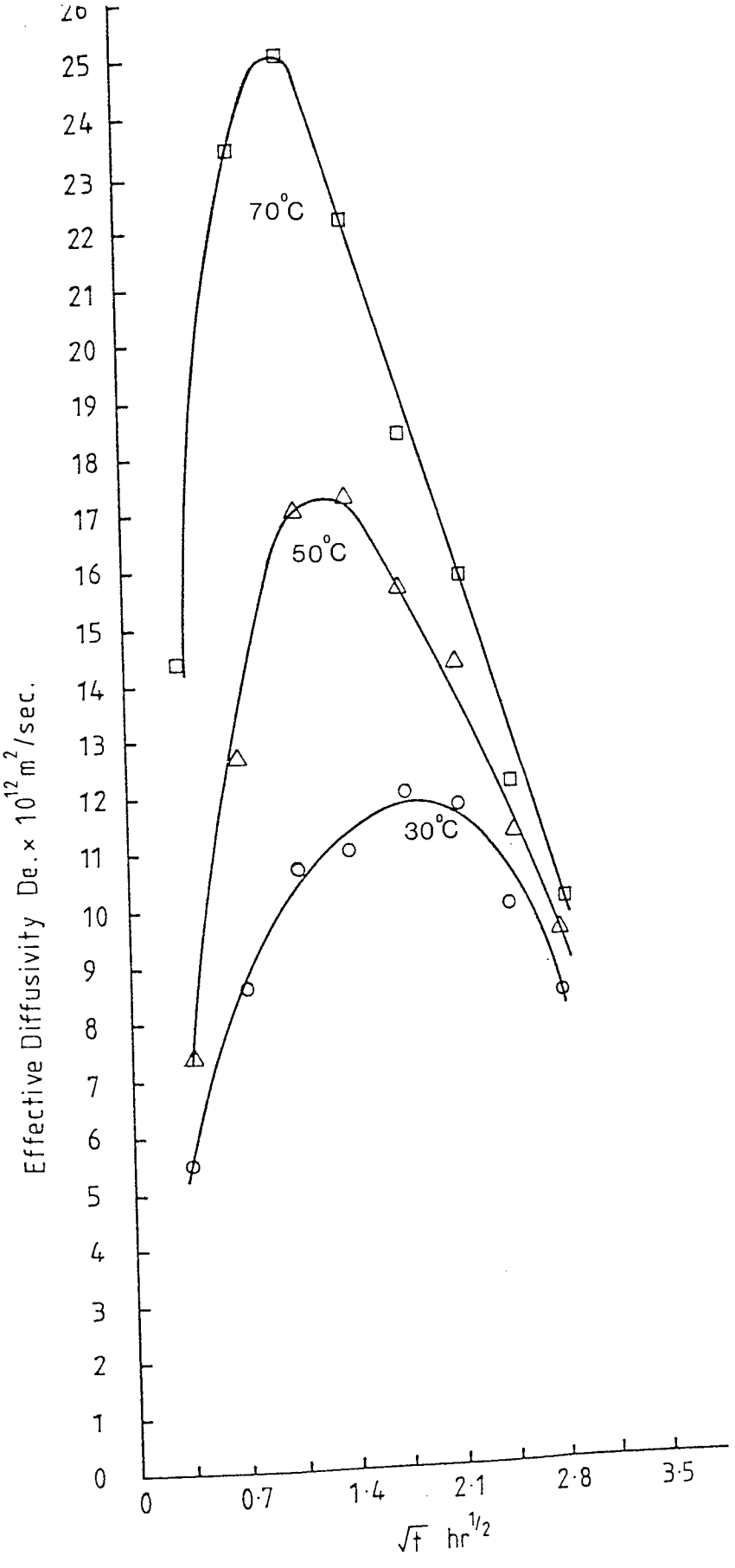

Figure 9.15 Variation of effective diffusivity for n-dodecane with adsorption time at temperatures 303, 323 and 343°K

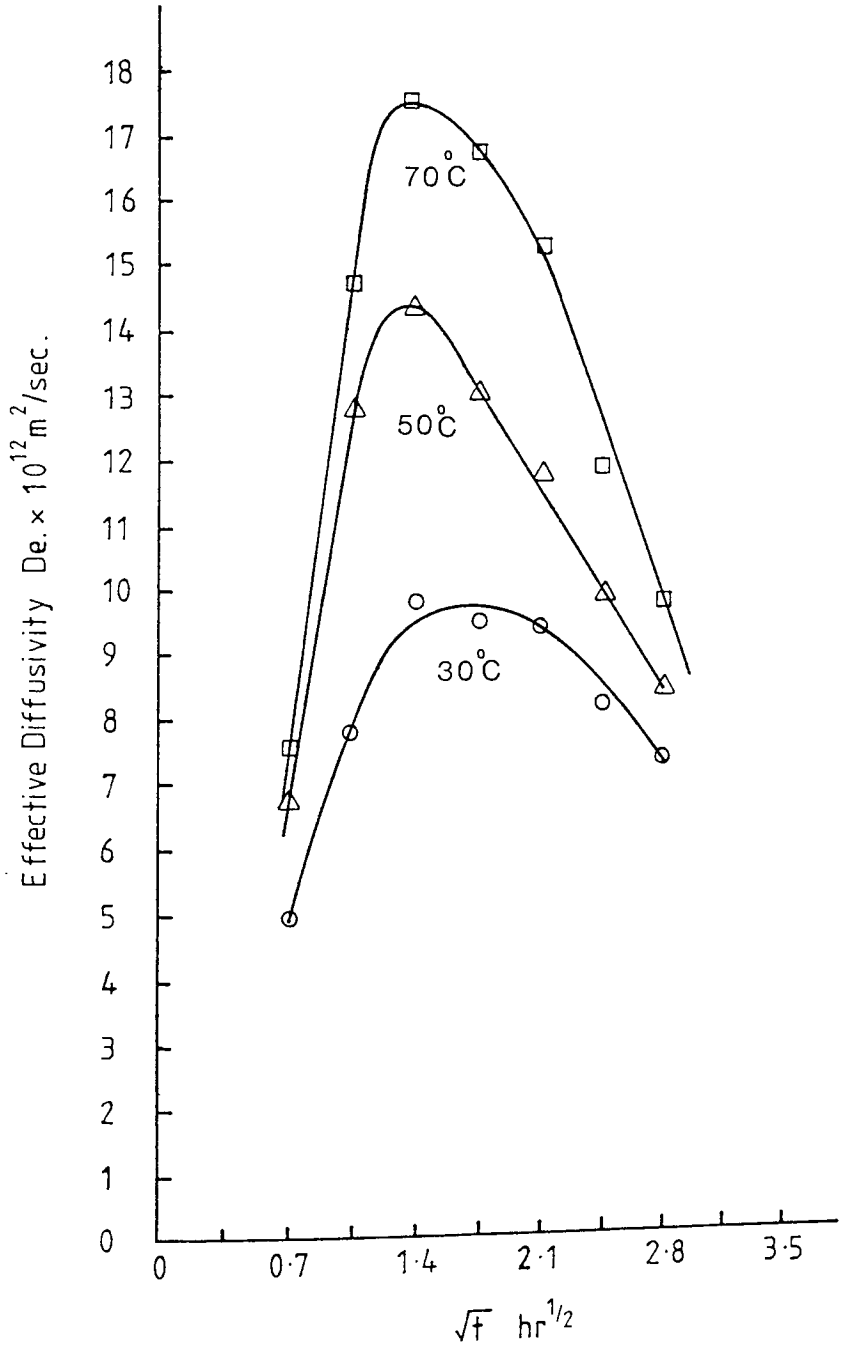

Figure 9.16 Variation of effective diffusivity for n-hexadecane with adsorption time at temperatures 303, 323 and 343°K

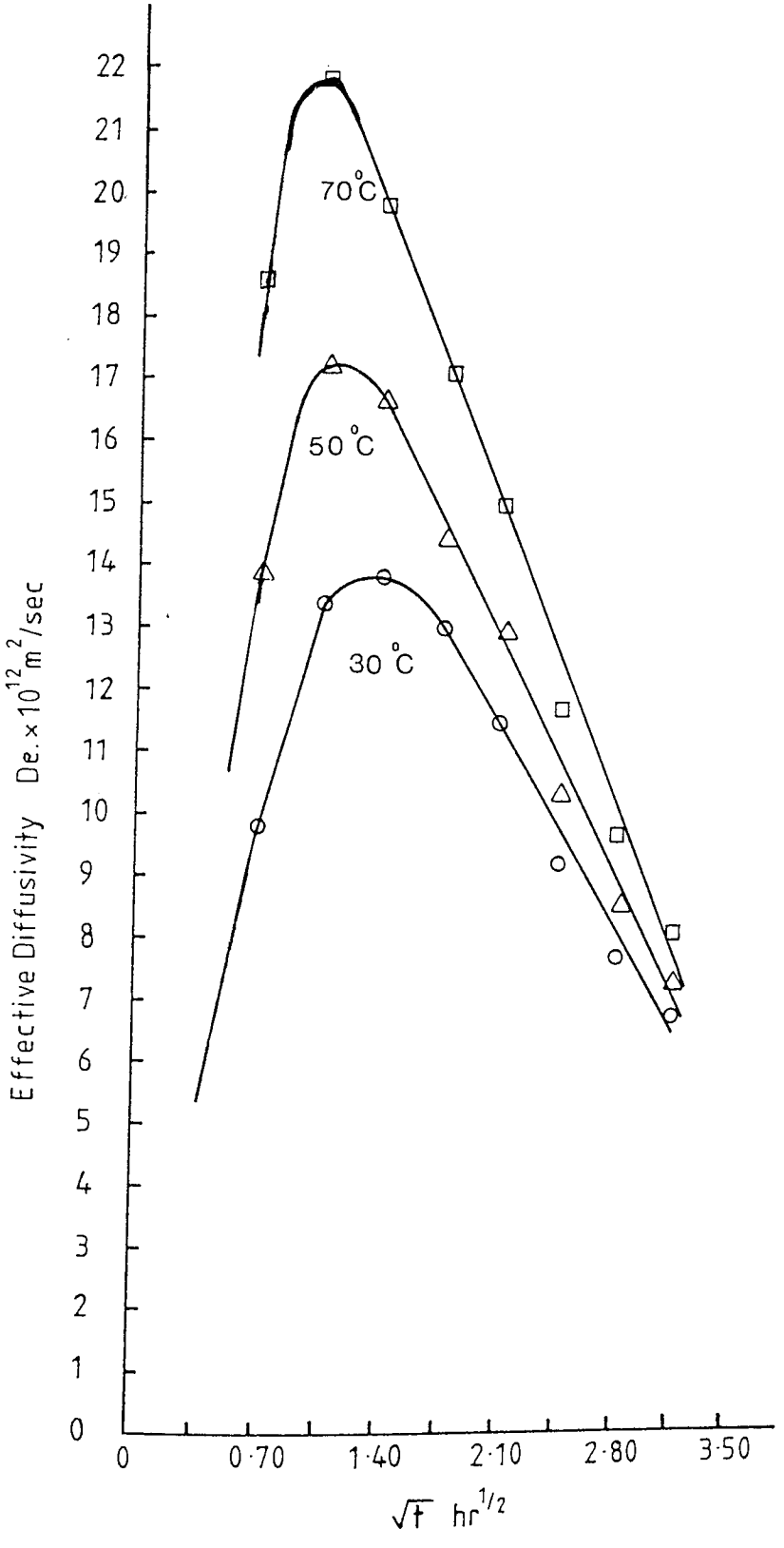

Figure 9.17 Variation of effective diffusivity for n-eicosane with adsorption time at temperatures 303, 323 and 343°K

temperatures for n-paraffins C_{12}, C_{16} and C_{20} respectively. The diffusion coefficient at first increases, then remains constant for definite period as the zeolite cavities are filled. This definite period is longest at lowest temperatures and shortest at high temperature for the three normal paraffins. The diffusivity finally decreases rapidly near the equilibrium point. Similar behaviour has been observed elsewhere (37).

9.2.3 Activation Energy E

The activation energies of normal paraffins under investigation were calculated from the differences in the logarithm of adsorption time, t, with the reciprocal of the difference of absolute temperatures, $T_1 = 303°K$ and $T_2 = 343°K$, at different relative adsorption G_t/G_∞, applying Equation 4.15 as shown in the sample calculation in Appendix B.

Table 9.4 illustrates values of activation energy of normal paraffins C_{12}, C_{16} and C_{20} at various values of relative adsorption, G_t/G_∞. The activation energy was lower than the heat of adsorption, as is required by adsorption theory since the energy barrier for movement from site to site on a surface is not as great as the energy required to leave the surface.

Falkovich et al (37) have reported activation energies, for normal paraffins C_{10}, C_{14}, C_{16} and C_{18} on particular granules of CaA zeolite at low range temperatures 300°K of 12.5, 14.6 and 16.7 kJ/mole for C_{10}, C_{14} and C_{16}, and C_{18} respectively which are within the range of the present study results.

Al-Zaid (66) reported the activation energy of dodecybenzene, for

diffusion in molecular sieve type 13X, as 24.0 kJ/mole which is higher than the values of activation energies of adsorption of normal paraffins by molecular sieve type 5A, although the critical diameter of normal paraffins are near to the pore diameter of 5A zeolite crystal. This can be attributed to the stronger interactions of dodecylbenzene molecules with the electrostatic charges of the molecular sieve sites, compared with n-paraffin molecule interactions with these sites, since they are non-polar molecules.

Table 9.4 Activation energies of n-paraffins for diffusion in molecular sieve type 5A in the temperature range 303-343°K

n-Paraffin	Activation energies kJ/mole		
	$G_t/G_\infty = 0.25$	$G_t/G_\infty = 0.5$	$G_t/G_\infty = 0.75$
n-Dodecane	16.0	8.8	6.8
n-Hexadecane	6.9	5.3	8.3
n-Eicosane	10.7	4.8	5.2

9.3 DYNAMIC FLOW SYSTEM RESULTS

The experimental data and calculated results are tabulated in Tables 9.5 to 9.12. Sample calculations and summaries of all derived data are given in

Appendix B, Section 3, based upon Experimental Run (1).

The dynamic system results are presented and discussed in the following sections.

9.3.1 Breakthrough Curve

Experimental breakthrough curves were plotted for twenty eight experimental runs using different systems under various operating conditions. Runs 1 to 11 involved the adsorption of dodecane, runs 12 to 19 the adsorption of hexadecane, and runs 20 to 28 the adsorption of eicosane.

A typical experimental breakthrough curve is shown in Figure 9.18. The shape of this curve and of all the experimental curves obtained as shown in Figures 9.19 to 9.33 was a smooth, S-shape but with some deviations from the idealized breakthrough curve shown in Figure 5.1. The deviation of the breakthrough curve from ideality, for the systems studied, increased with the higher normal paraffins ie. in the case of hexadecane the deviation was greater than with normal dodecane but less than with normal eicosane. The ideal case curve is perfectly symmetrical about its mid-point ($C/C_O = 0.5$). A measure of the asymmetry of the breakthrough

curve is indicated by the f values. For an ideal curve, f, the fractional ability of the adsorbent within the adsorption zone to adsorb additional solute, is 0.5. For the experimental breakthrough curve of the normal dodecane system in Run 1, for which the operating conditions were similar to those in Runs 15 and 23 for n-hexadecane and n-eicosane respectively, the value of f was 0.48, with a percentage

deviation of 4%. For the n-hexadecane and n-eicosane systems values of f were 0.45 and 0.4 with percentage deviations of 10% and 20% respectively.

Table 9.5 Experimental data for normal Dodecane - isooctane system

Run	Sieve Weight kg	Temperature °K	Initial Conc Mole-fraction	Flow Rate (V_t) (x 10^8)m^3/S	Average Sieve Size d_p (x 10^3) m
1	0.0662	323	0 .012	5.0	1.5
2	0.0662	343	0.012	5.0	1.5
3	0.0662	303	0.012	5.0	1.5
4	0.0702	323	0.012	5.0	0.75
5	0.0662	323	0.012	2.78	1.5
6	0.0662	323	0.012	6.1	1.5
7	0.0726	323	0.012	5.0	0.266
8	0.0662	323	0.021	5.0	1.5
9	0.0662	323	0.028	5.0	1.5
10	0.0223	323	0.012	5.0	1.5
11	0.0358	323	0.012	5.0	1.5

Table 9.6 Experimental data for normal hexadecane isooctane system

Run	Sieve Weight kg	Temperature °K	Initial Conc Mole-fraction	Flow Rate (V_t) (x 10^8)m^3/S	Sieve Size Average d_p(x 10^3) m
12	0.067	343	0.0064	5.0	1.5
13	0.067	303	0.0064	5.0	1.5
14	0.0358	323	0.01	5.0	1.5
15	0.066	323	0.01	5.0	1.5
16	0.066	323	0.01	2.78	1.5
17	0.066	323	0.01	6.1	1.5
18	0.066	323	0.02	5.0	1.5
19	0.066	323	0.01	5.0	0.75

Table 9.7 Experiemntal data for normal eicosane - isooctane system

Run	Sieve Weight kg	Temperature °K	Initial Conc Mole-fraction	Flow Rate (V_t) (x 10^8)m^3/S	Sieve Size Average d_p(x 10^3) m
20	0.036	323	0.01	5.0	15
21	0.036	303	0.01	5.0	1.5
22	0.036	343	0.01	5.0	1.5
23	0.066	323	0.01	5.0	1.5
24	0.066	323	0.01	6.1	1.5
25	0.066	323	0.02	5.0	1.5
26	0.066	323	0.01	5.0	0.75
27	0.045	323	0.01	5.0	1.5
28	0.066	323	0.01	2.78	1.5

TABLE 9.8 Calculated results - normal dodecane - isooctane system

Run	Bed Density ρ_b kg/m^3	Feed Density ρ_f kg/m^3	Feed Viscosity μ (x 10^4)N/m^2	Molecular Diffusion D_m (x 10^8)m^2/sec	Reynolds No. Re	Schmidt No. Sc	Mass Trans Coefficient k_f (x 10^7)m/sec
1	760.7	668.7	3.64	0.2507	0.614	217	155.1
2	775.9	650.5	3.0	0.3221	0.725	143	183.4
3	775.9	684.4	4.74	0.1805	0.483	384	124.7
4	784.6	668.7	3.64	0.2507	0.307	217	252.8
5	775.9	668.7	3.64	0.2507	0.341	217	127.8
6	775.9	668.7	3.64	0.2507	0.75	217	165.6
7	834.7	668.7	3.64	0.2507	0.109	217	512.3
8	775.9	669.3	3.69	0.2507	0.606	220	155.3
9	775.9	669.7	3.73	0.2507	0.600	222	155.3
10	775.9	668.7	3.64	0.2507	0.614	217	155.1
11	775.9	668.7	3.64	0.2507	0.614	217	155.1

TABLE 9.9 Calculated results - normal hexadecane - isooctane system

Run	Bed Density ρ_b kg/m^3	Feed Density ρ_f kg/m^3	Feed Viscosity μ (x 10^4)N/m^2	Molecular Diffusion D_m (x 10^8)m^2/sec	Reynolds No. R_e	Schmidt No. Sc	Mass Trans Coefficient k_f (x 10^7)m/sec
12	775.9	650.4	3.02	0.2850	0.720	163	169.2
13	775.9	684.2	4.8	0.1597	0.477	439	114.7
14	775.9	668.9	3.72	0.2217	0.601	251	142.9
15	775.9	668.9	3.72	0.2217	0.601	251	142.9
16	775.9	668.9	3.72	0.2217	0.334	251	117.6
17	775.9	668.9	3.72	0.2217	0.733	251	152.5
18	775.9	669.7	3.87	0.2217	0.579	261	142.9
19	784.6	668.9	3.72	0.2217	0.301	251	227.3

TABLE 9.10 Calculated results - normal eicosane - isooctane system

Run	Bed Density ρ_b kg/m^3	Feed Density ρ_f kg/m^3	Feed Viscosity μ (x 10^4)N/m^2	Molecular Diffusion D_m (x 10^8)m^2/sec	Reynolds No. R_e	Schmidt No. S_c	Mass Trans Coefficient k_f (x 10^7)m/sec
20	775.9	668.9	3.86	0.2091	0.579	276	137.5
21	775.9	684.6	5.07	0.1506	0.451	492	110.3
22	775.9	650.8	3.14	0.2687	0.693	180	162.7
23	775.9	668.9	3.86	0.2091	0.579	276	138.0
24	775.9	668.9	3.86	0.2091	0.706	296	146.8
25	775.9	669.9	4.15	0.2091	0.539	297	137.6
26	784.6	668.9	3.86	0.2091	0.289	276	218.6
27	775.9	668.9	3.86	0.2091	0.579	276	137.5
28	775.9	668.9	3.86	0.2091	0.322	276	113.2

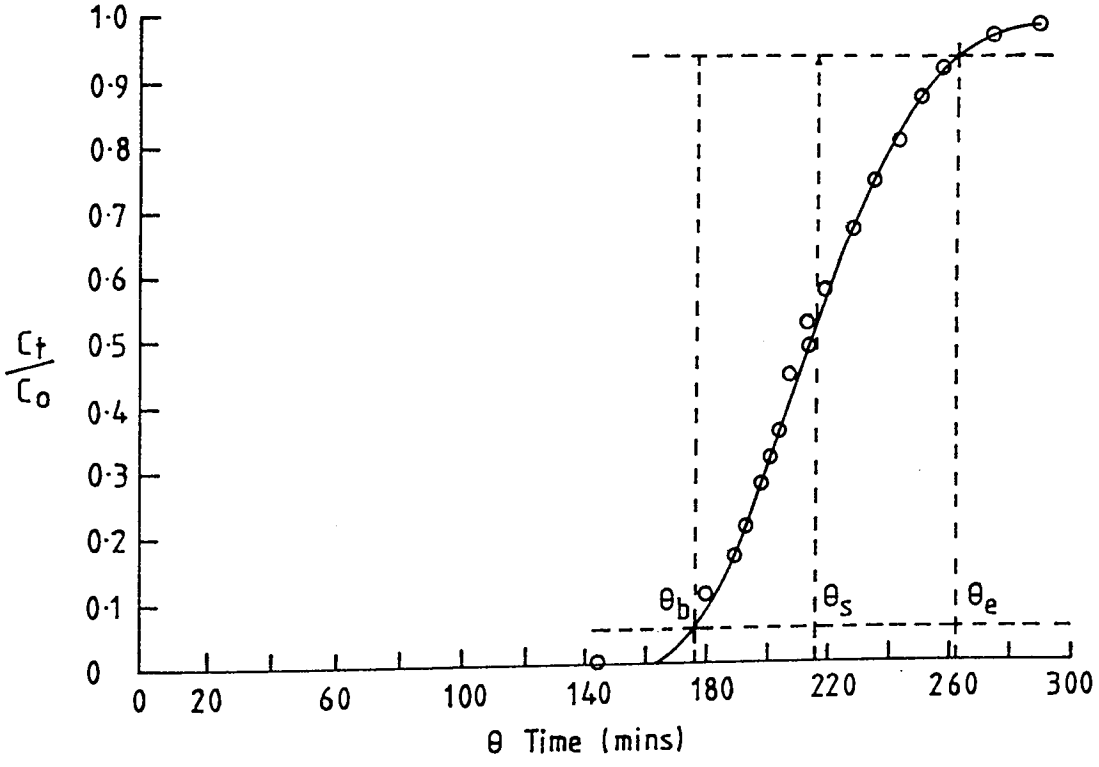

Figure 9.18 Experimental breakthrough curve (Run 1)

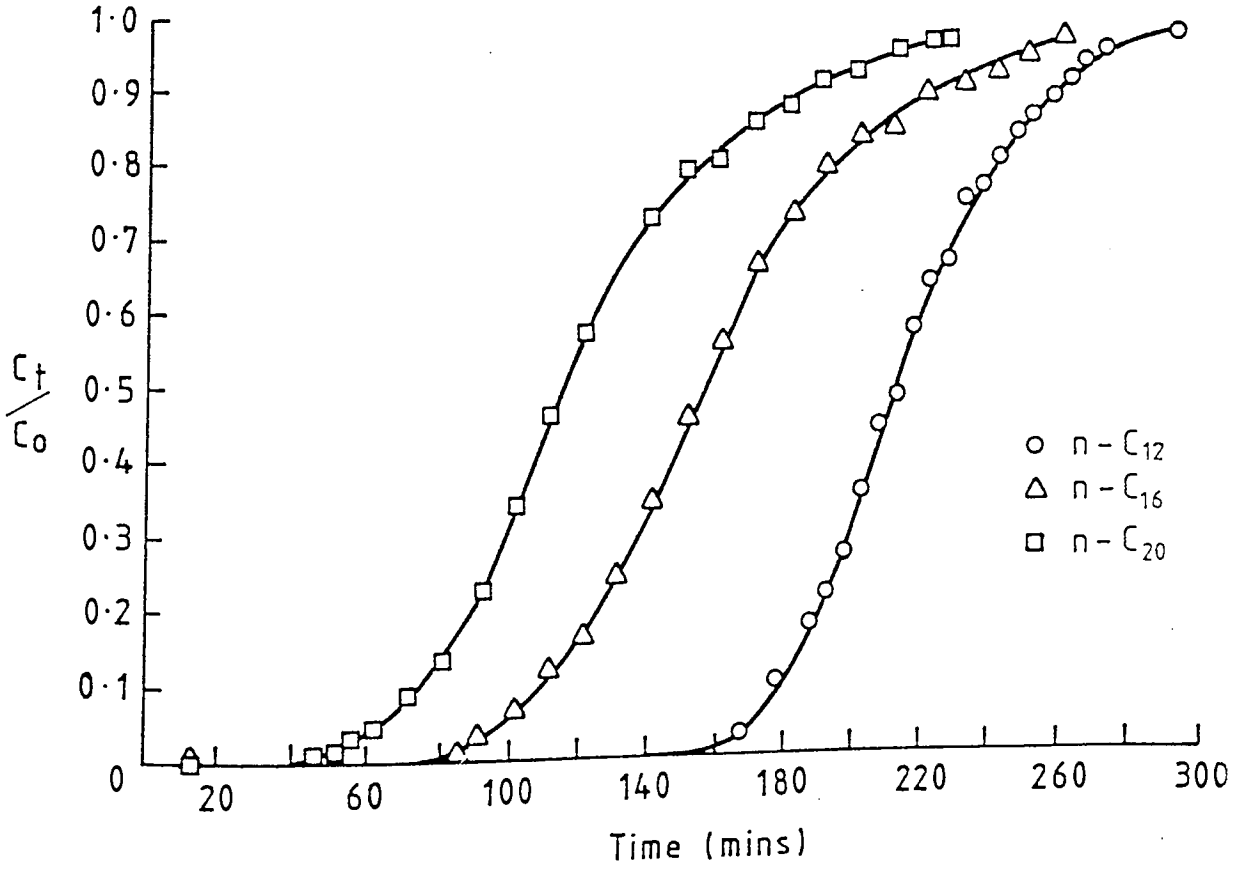

Figure 9.19 Breakthrough curves of n-paraffins at 323^{O}K

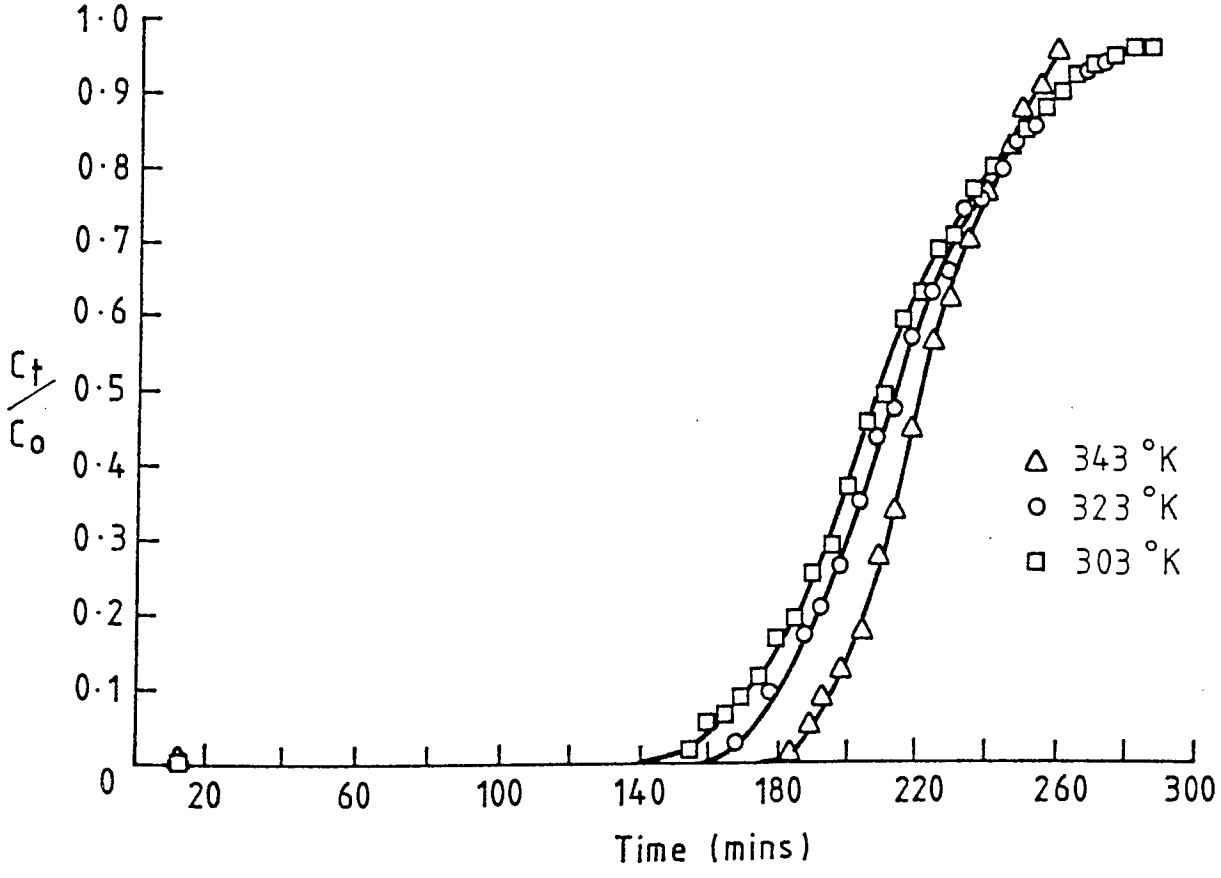

Figure 9.20 Effect of temperature on breakthrough curve of n-dodecane

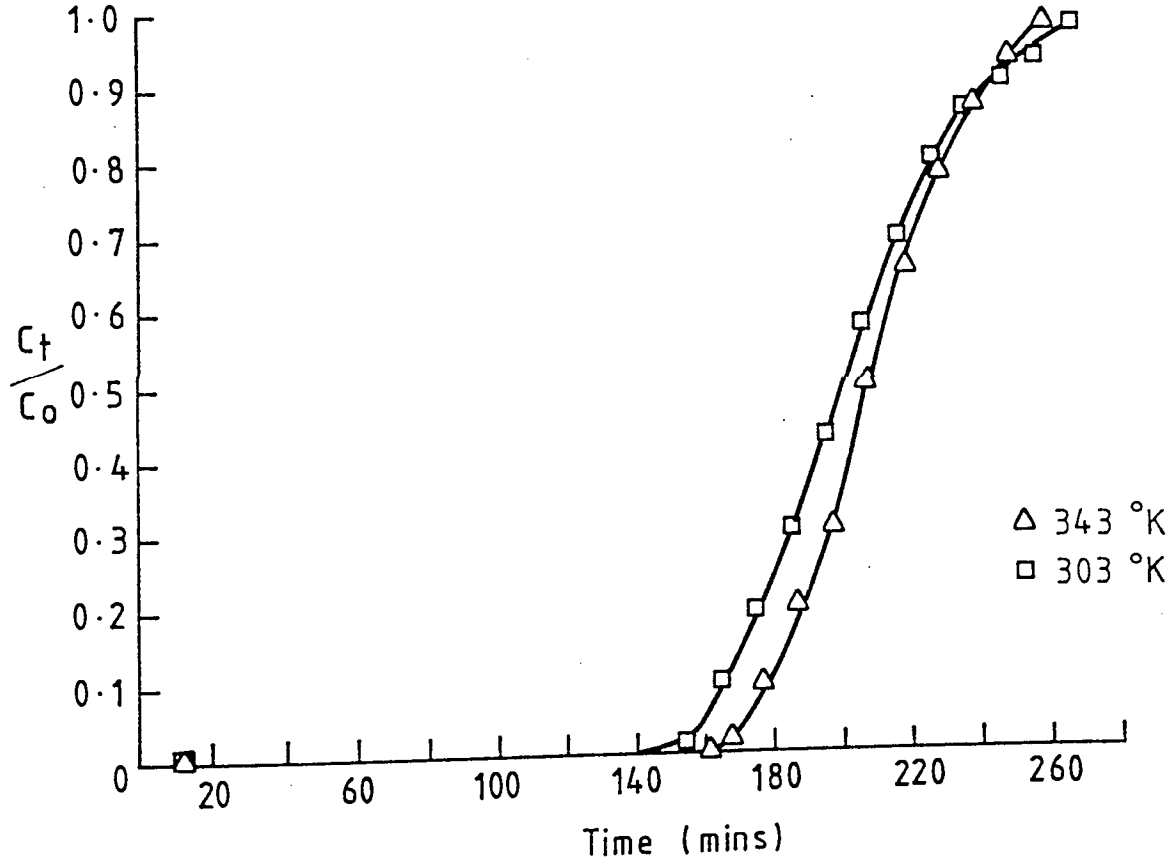

Figure 9.21 Effect of temperature on breakthrough curve of n-hexadecane

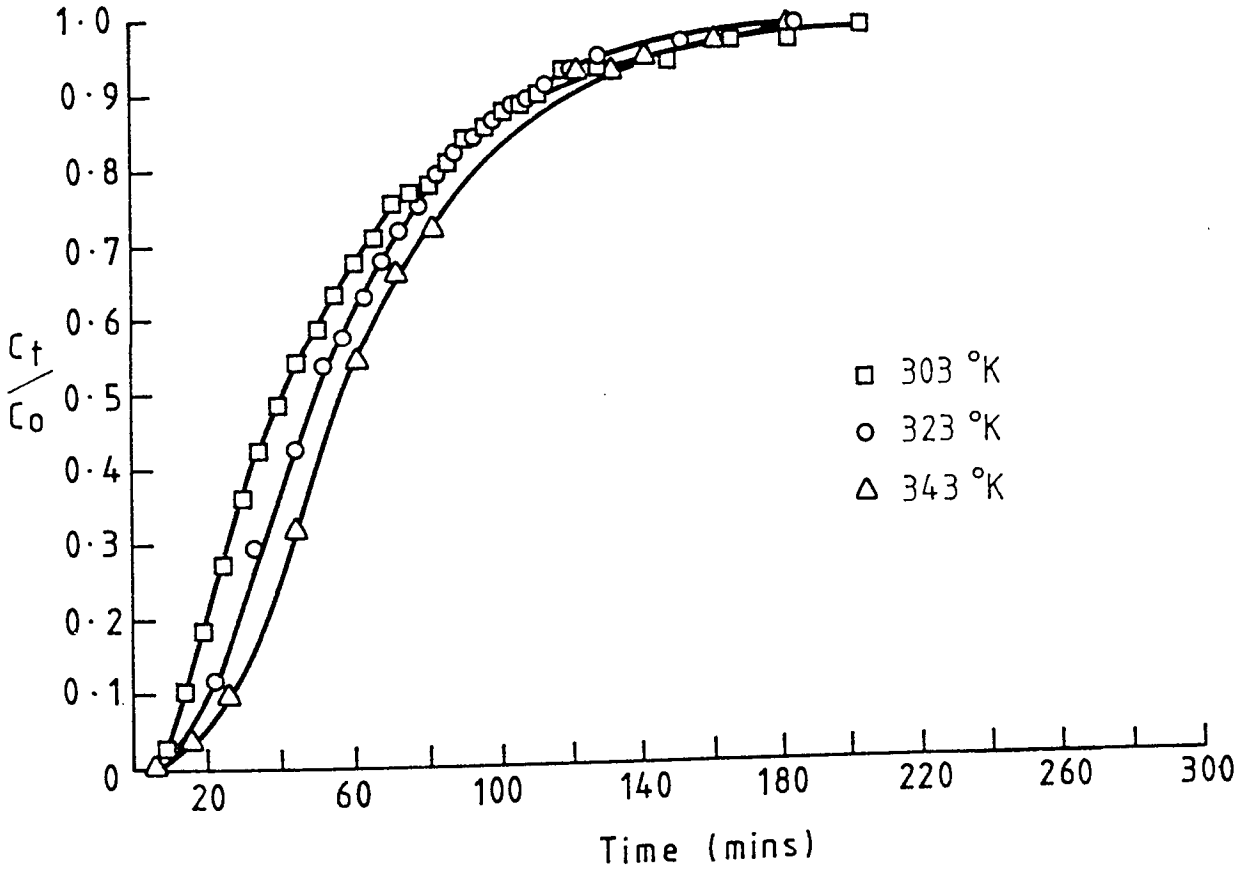

Figure 9.22 Effect of temperature on breakthrough curve of n-eicosane

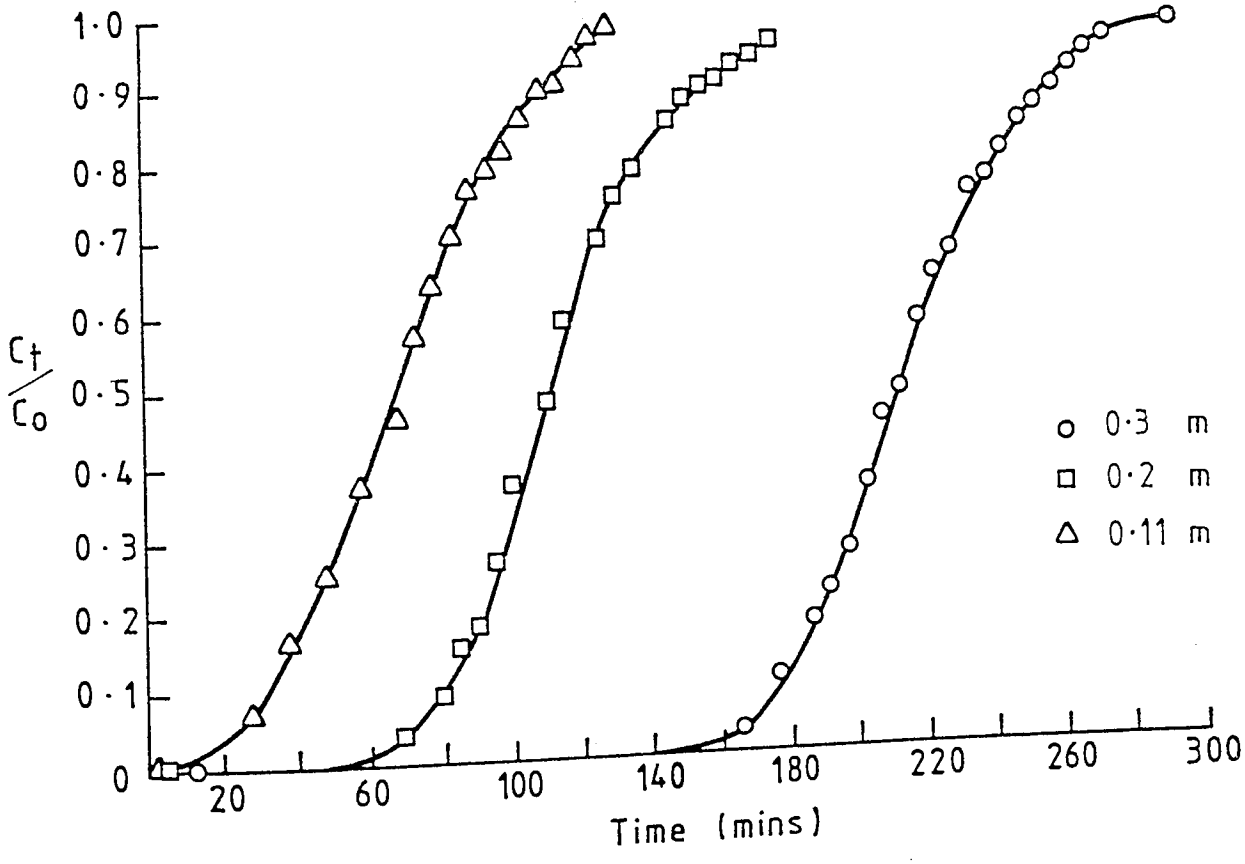

Figure 9.23 Effect of bed height on breakthrough curve of n-dodecane

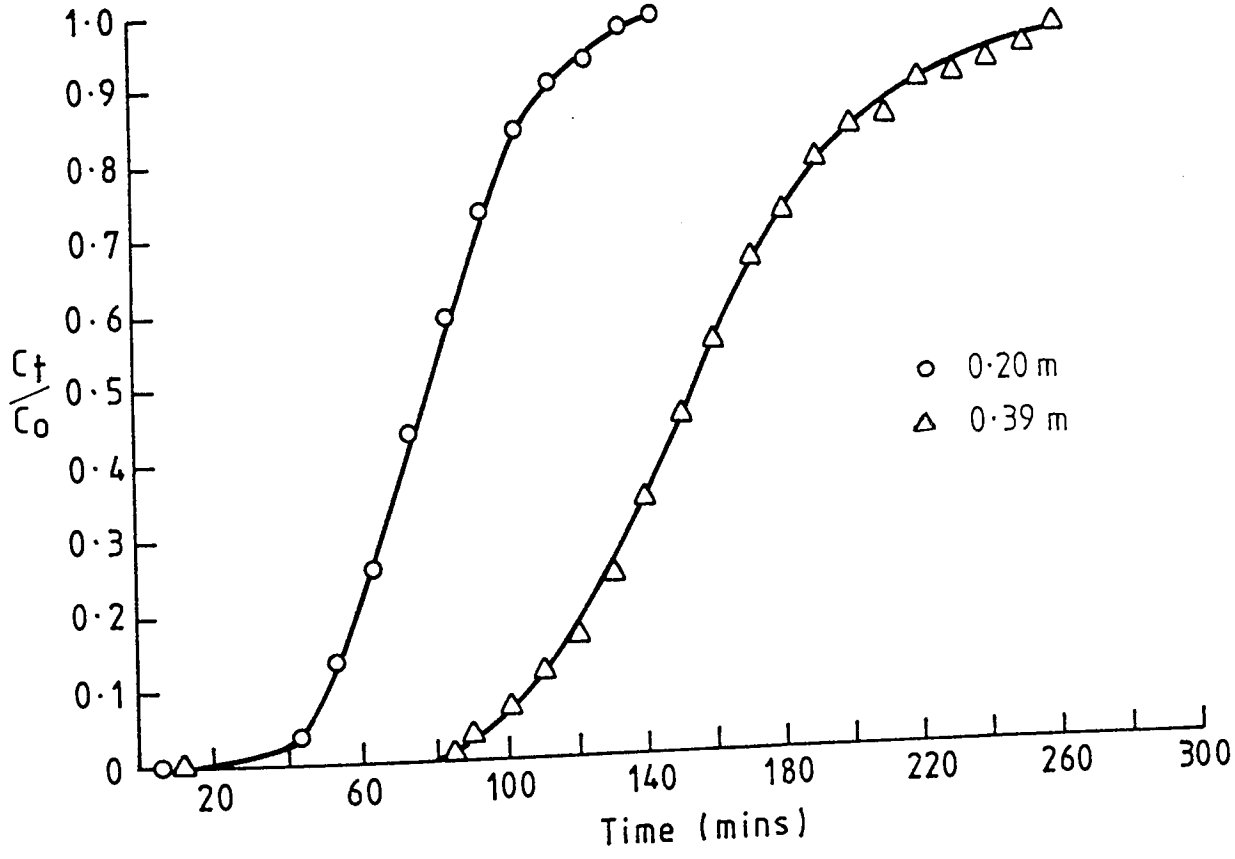

Figure 9.24 Effect of bed height on breakthrough curve of n-hexadecane

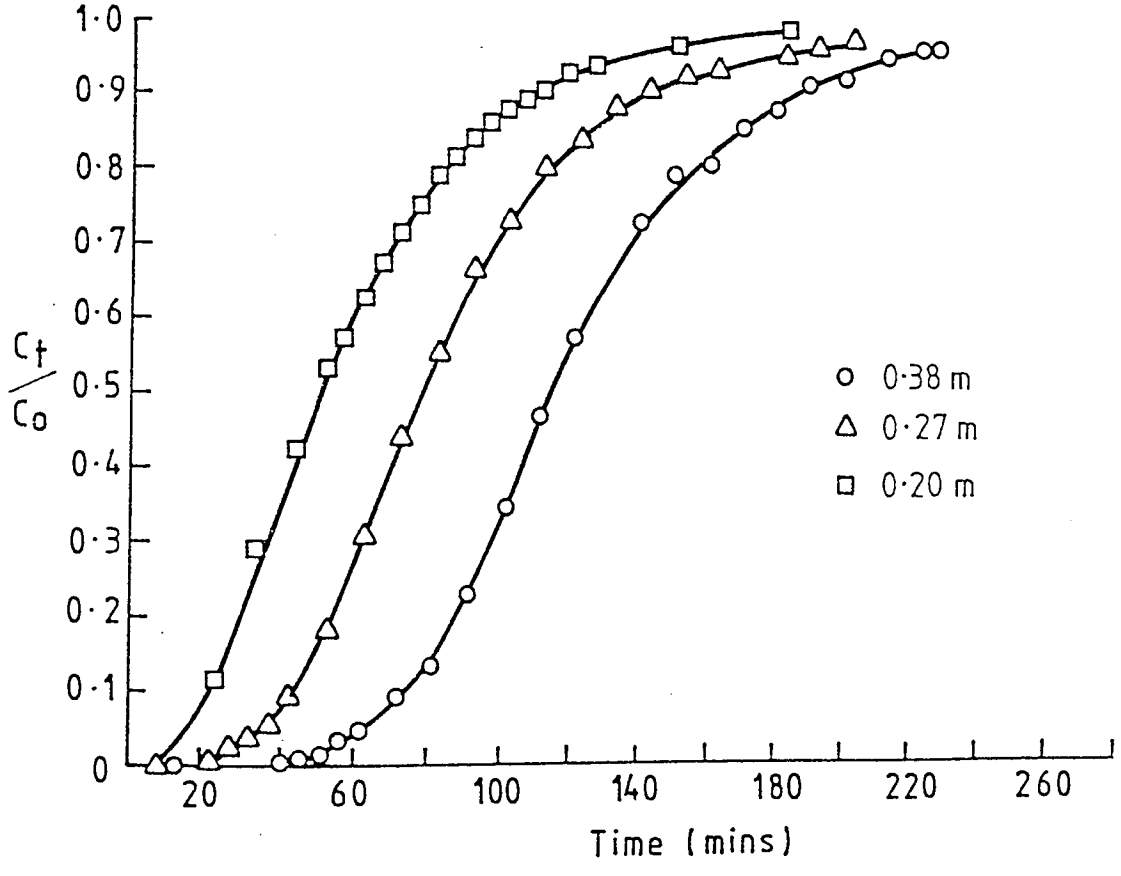

Figure 9.25 Effect of bed height on breakthrough curve of n-eicosane

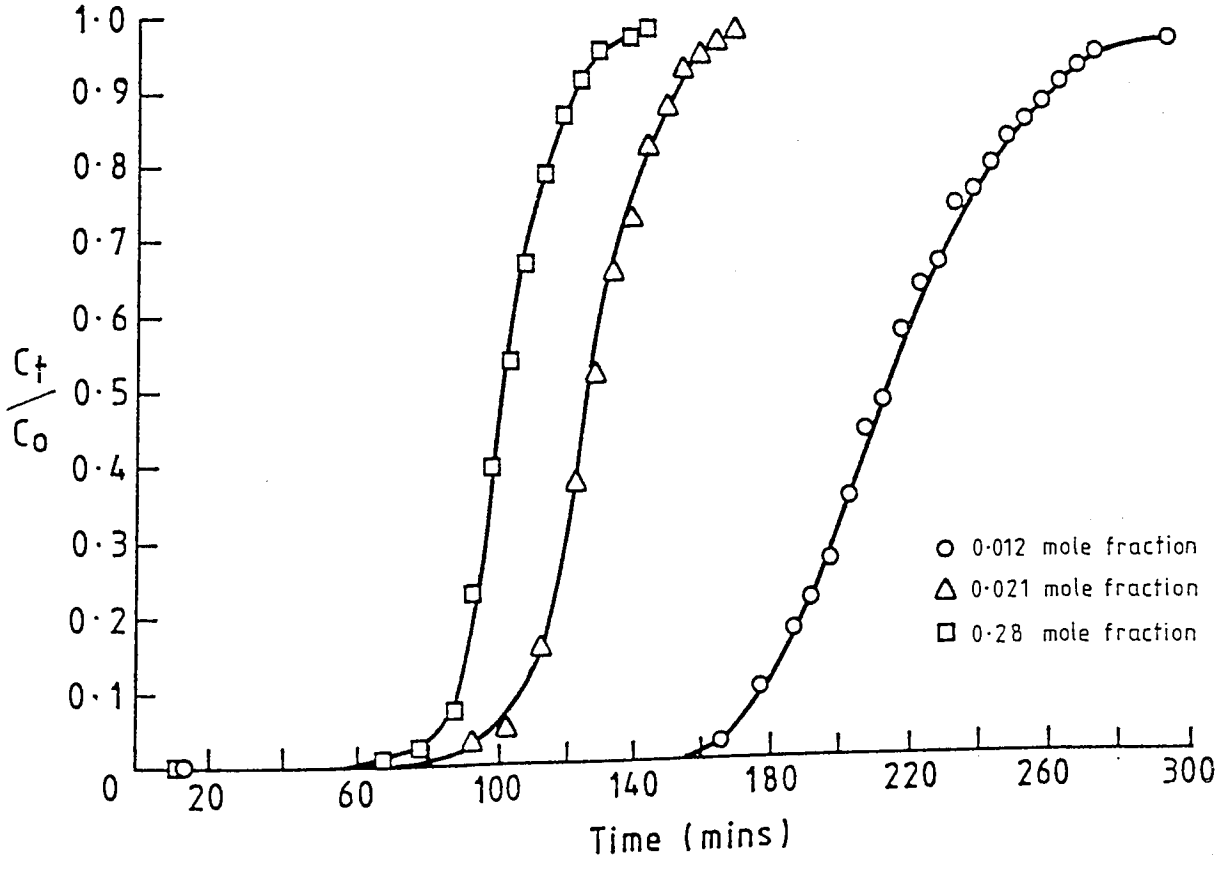

Figure 9.26 Effect of feed concentration on breakthrough curve of n-dodecane

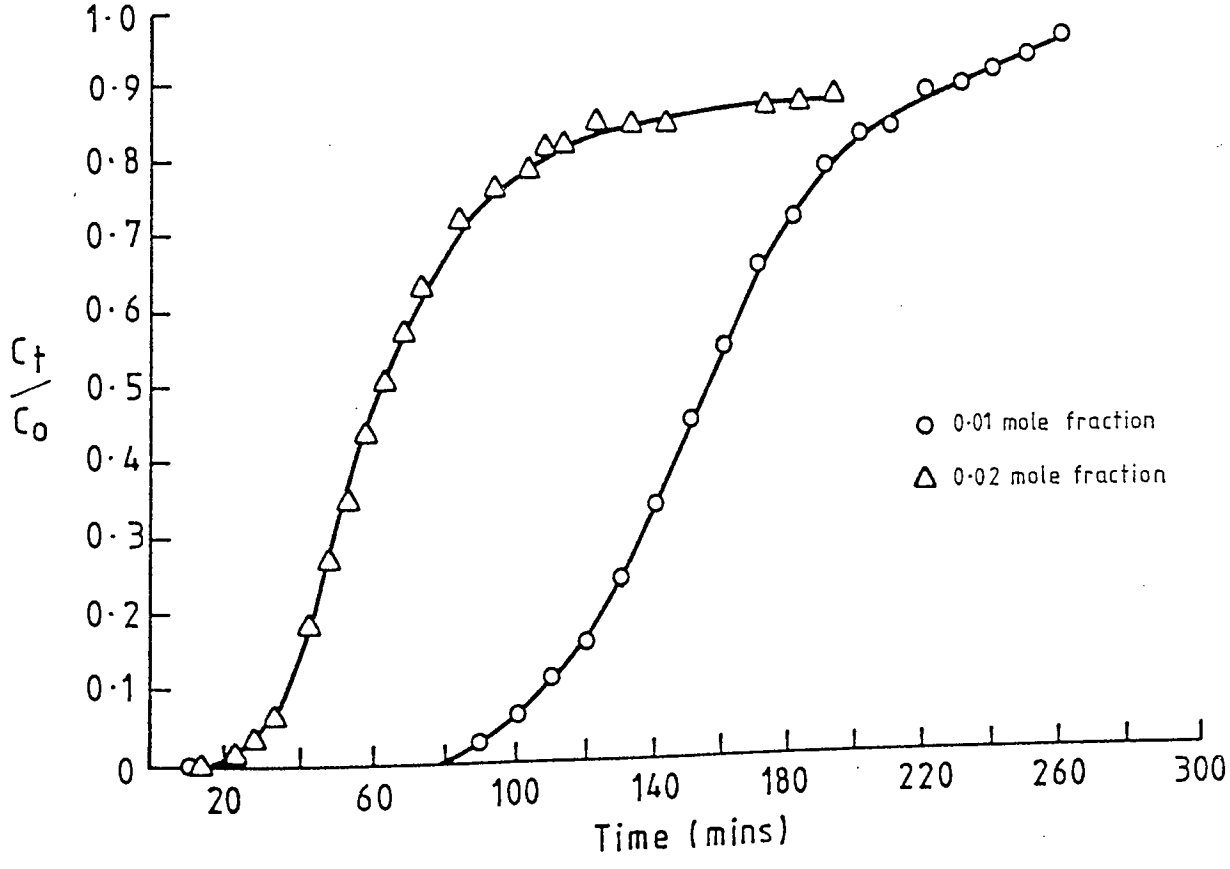

Figure 9.27 Effect of feed concentration on breakthrough curve of n-hexadecane

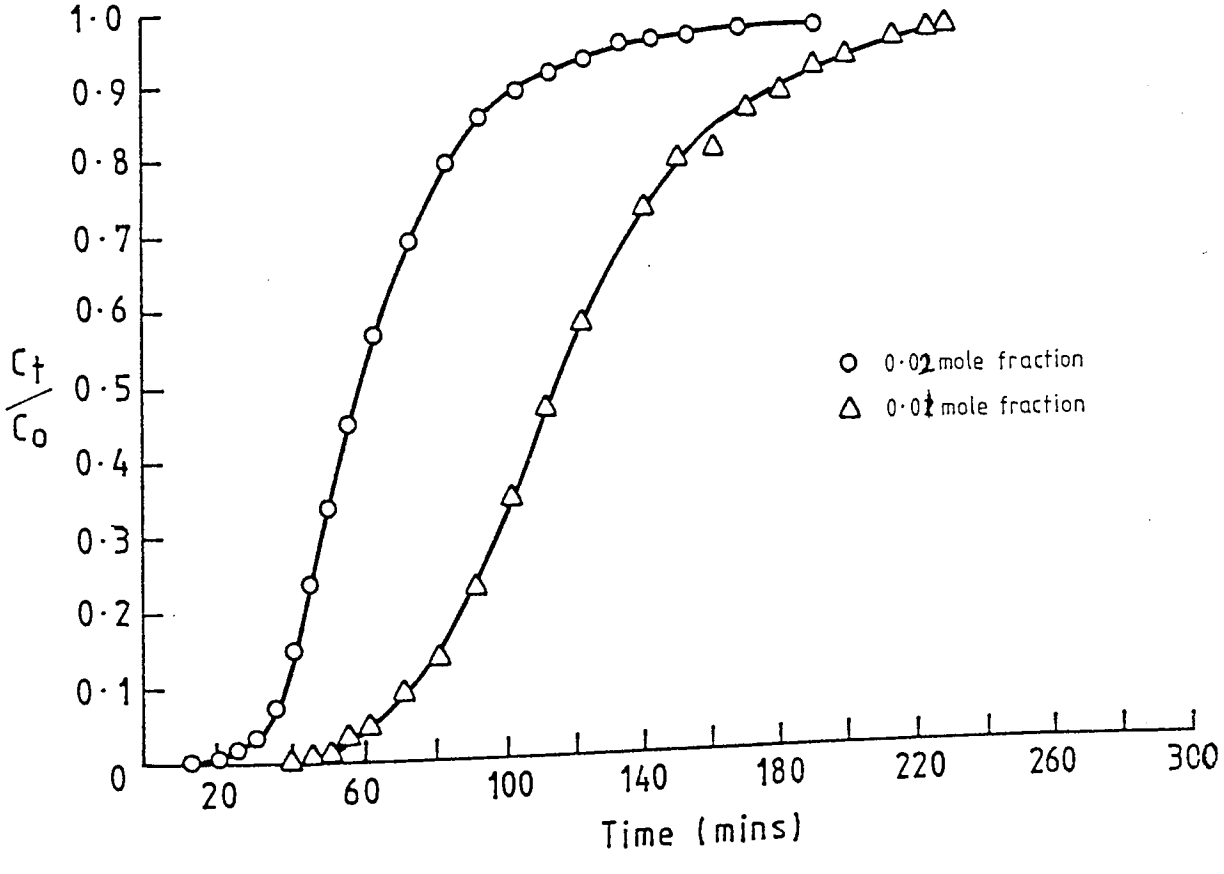

Figure 9.28 Effect of feed concentration on breakthrough curve of n-eicosane

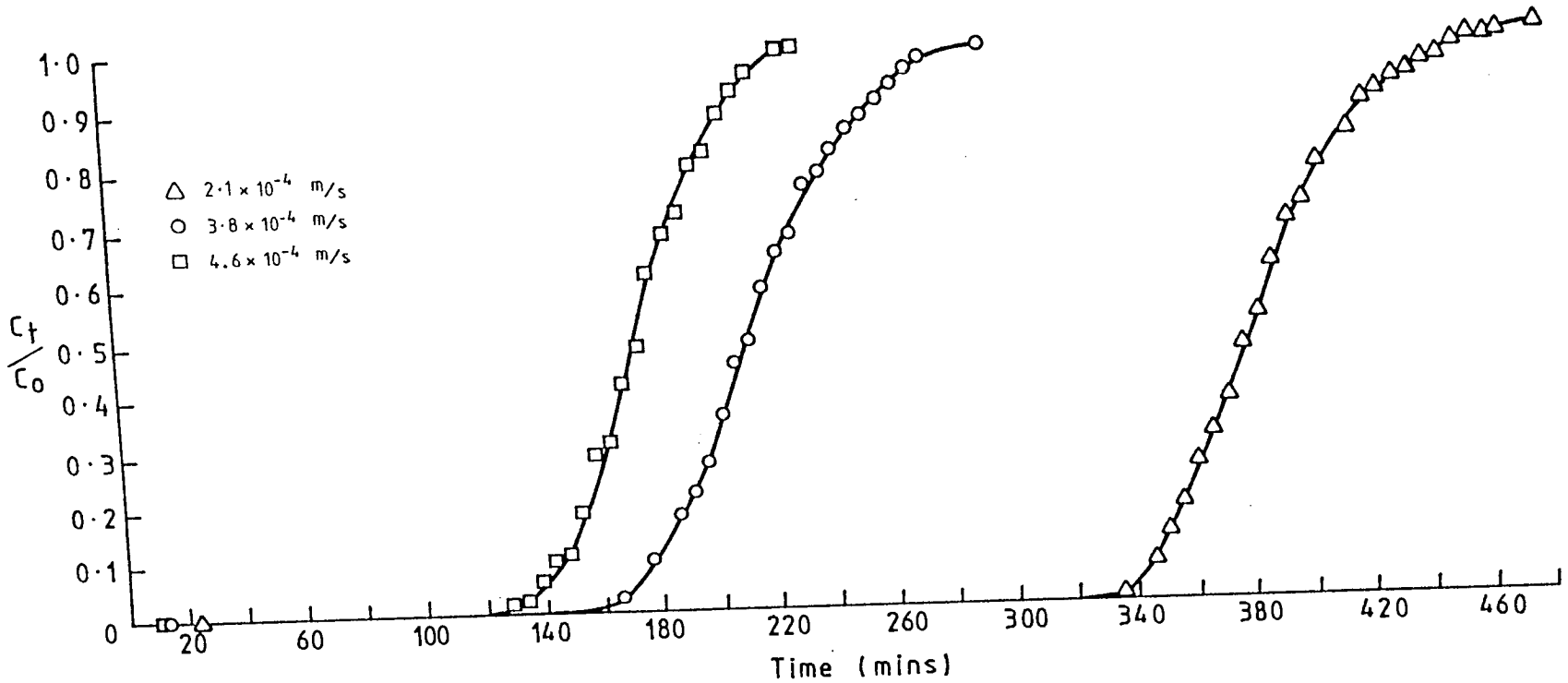

Figure 9.29 Effect of superficial velocity on breakthrough curve of n-dodecane

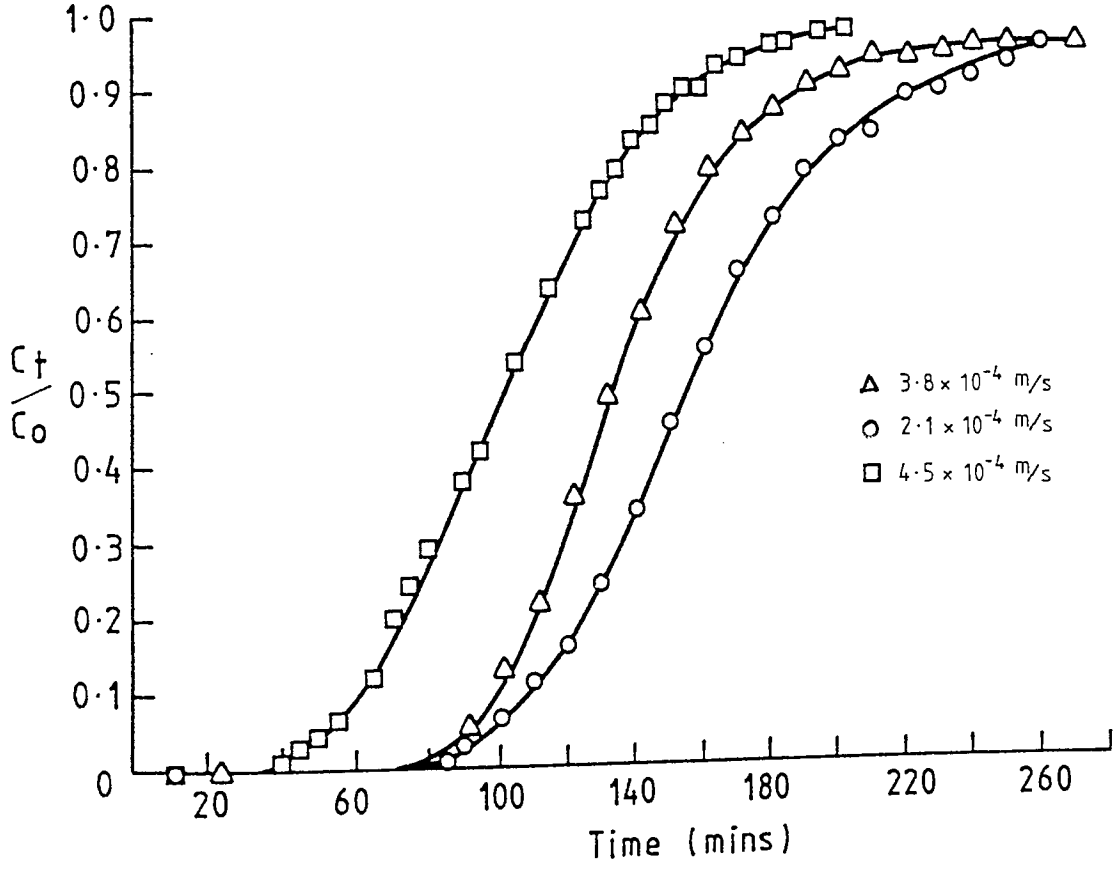

Figure 9.30 Effect of superficial velocity on breakthrough curve of n-hexadecane

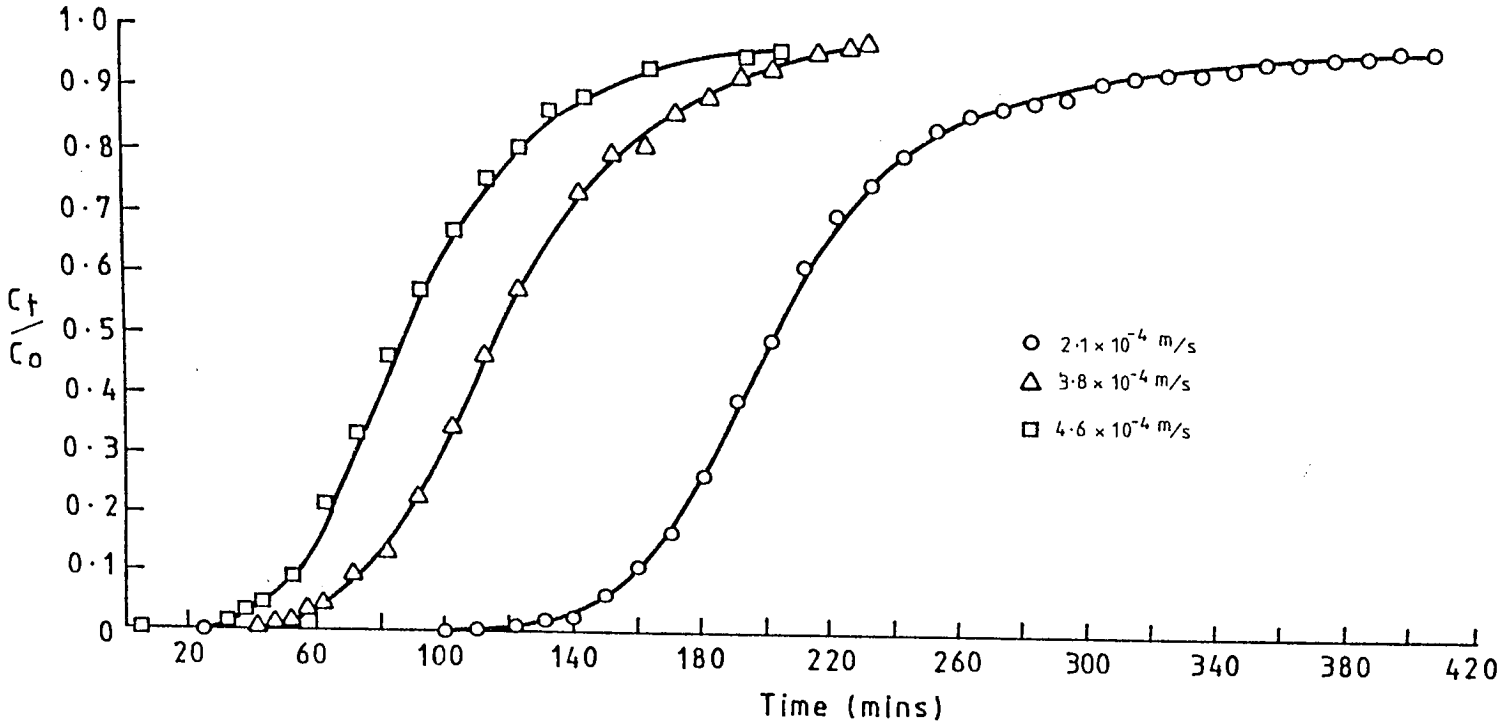

Figure 9.31 Effect of superficial velocity on breakthrough curve of n-eicosane

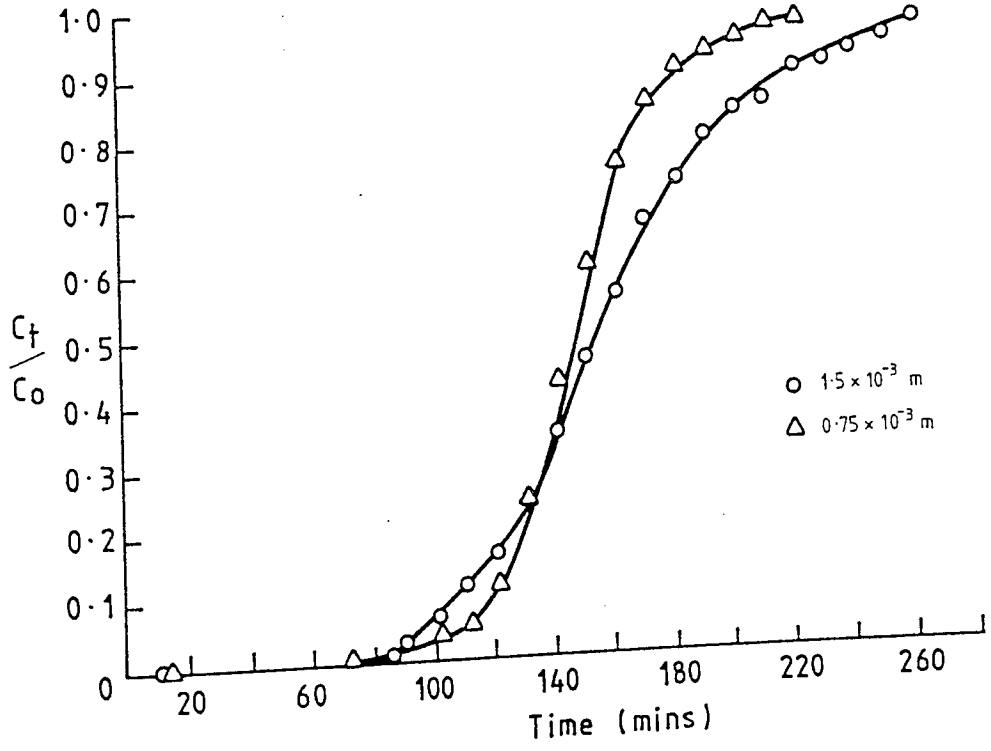

Figure 9.32 Effect of particle size (average diameter d_p) on breakthrough curve of n-hexadecane

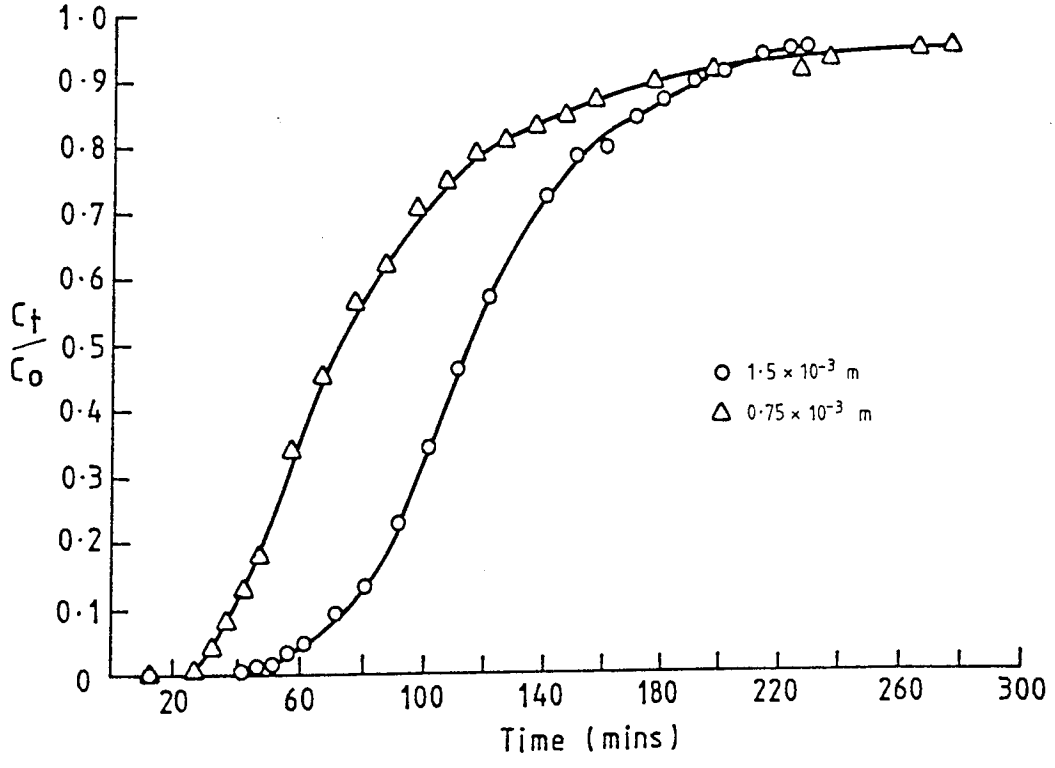

Figure 9.33 Effect of particle size (average diameter d_p) on breakthrough curve of n-eicosane

The increase in the percentage deviation of the f value from the normal dodecane system to the normal eicosane system was caused by an increased tendency for the trailing edge of the curve to flatten out as saturation approached in the case of the normal eicosane system, as shown in Figure 9.19. This can be attributed to the time to reach equilibrium being longer for higher normal paraffins than for lower normal paraffins as confirmed by the results obtained in batch experiments, Table 9.1.

The approach to ideality of the breakthrough curves of normal paraffins was affected by temperature as shown in Figures 9.20 to 9.22. The values of f and their percentage deviations for normal dodecane were,

Temperature °K	f	Percentage deviation %
303	0.47	6
323	0.48	4
343	0.49	2

It is clear from Figures 9.20-9.22, and from the above data, that the breakthrough curve approached close to ideality as the temperature was increased. This can be attributed to the increase in the diffusivity, and consequently of the mass transfer rate, of molecules to be adsorbed with increased temperature as illustrated in Table 9.3.

The effect of other operating parameters, namely bed height, feed concentration, superficial velocity, and particle size, on the breakthrough curves

and dynamic properties of adsorption of normal paraffins are shown in Figures 9.23 to 9.33 and discussed in the following sections.

9.3.2 Adsorption Zone Height

The height of the adsorption zone is arbitrarily defined as that portion of the bed over which the concentration changes from 5% to 95% of the feed concentration. This height was calculated using Equations 5.1 and 5.2. The values of height of mass transfer zone for various runs are listed in Table 9.11. Comparison of the values obtained by the two methods, mentioned in Chapter 5, demonstrates very good agreement with the average variation between corresponding values being < 0.007m. This indicates that the assumption of a constant width, constant speed, adsorption zone is justified.

The variation of the adsorption zone height with superficial velocity is shown in Figure 9.34 over a range of superficial velocity from 2.1×10^{-4} to 4.6×10^{-4} m/sec. The zone height was proportional to approximately the 0.65 power of superficial velocity for normal dodecane, and to approximately the 0.8 power for normal eicosane. For a feed containing 5% normal hexane, Schumacher (43), reported that the zone height was proportional to approximately the 0.7 power of the superficial velocity over a velocity range of 6.8×10^{-4} to 5.08×10^{-3} m/sec. This agreed well with the velocity dependence of zone heights calculated, by Schumacher, from the breakthrough data of Ziegenhain (79), who studied the adsorption of normal heptane from toluene flowing up through a bed of 1/16 inch, Type 5A molecular sieves. The Ziegenhain zone heights were proportional to the

0.65 power of velocity over a velocity range of 1.3×10^{-4} - 5.9×10^{-4} m/sec.

Theoretically, the liquid-phase zone height would be proportional to the first power of superficial velocity if the mass transfer was controlled by an internal diffusion resistance and to about the 0.6 power if external diffusion was controlling (33). The experimental velocity dependance fell between the 0.6 and 1.0 power over the entire flow-rate range. This indicates that the overall resistance is made up of a combination of internal and external resistances.

The effect of adsorption temperature on the zone height is demonstrated in Figure 9.35 for the three normal paraffins. In all cases the height of adsorption zone decreased with an increase in the adsorption temperature. The decrease was of the order of 0.05m as the adsorption temperature was increased from 303°K to 343°K. Schumacher (43) observed a similar trend for the adsorption of n-hexane.

In theory, any increase in temperature should have two counteracting effects on the zone height. The effect of temperature on the equilibrium isotherm is to decrease the adsorbate capacity of the sieves at higher temperatures. This will result in an increase in the number of transfer units, for a given separation and contribute to an increase in the zone height. The opposing effect of increased temperature is a tendency for a reduction in zone height resulting from an increase in the overall mass transfer coefficient. The first effect was observed to be a minor one, since the equilibrium loadings of the sieve at 303°K and 343°K were 0.77 mole/kg and 0.61 mole/kg respectively for normal dodecane, indicating a decrease in equilibrium loading of 25%. For the other two normal paraffins the percentage decrease was lower. The increase in the experimental overall mass transfer coefficient for a temperature

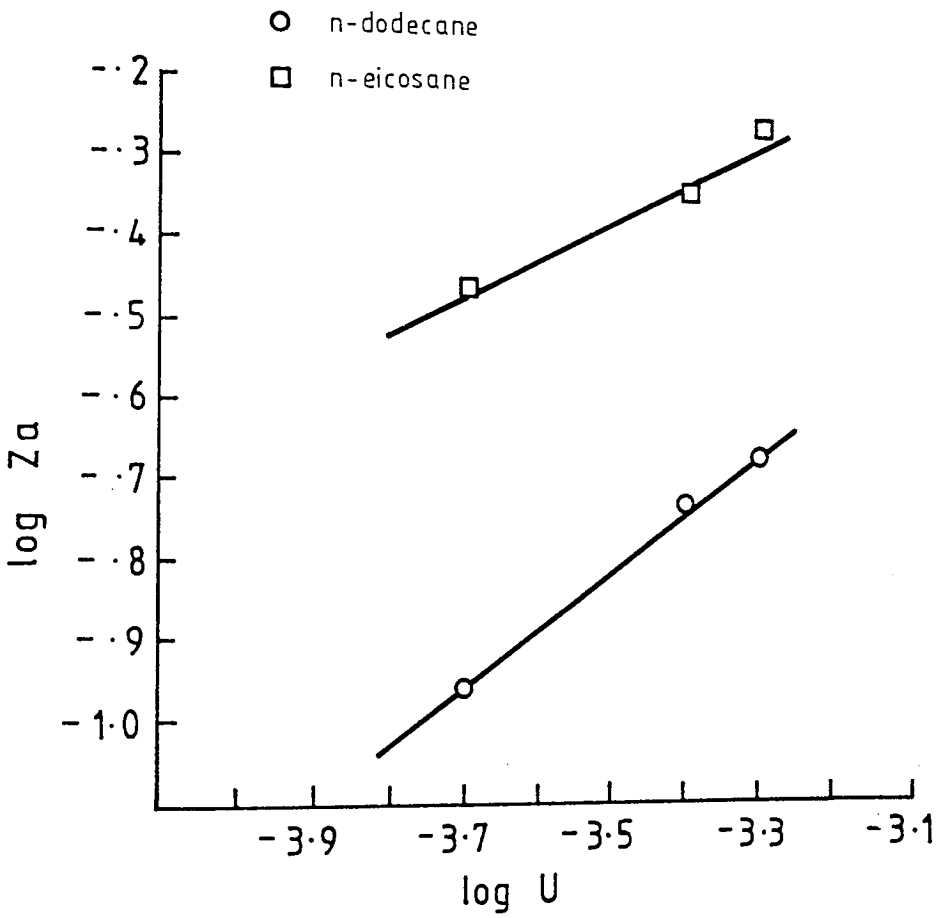

Figure 9.34 Effect of superficial velocity on adsorption zone height

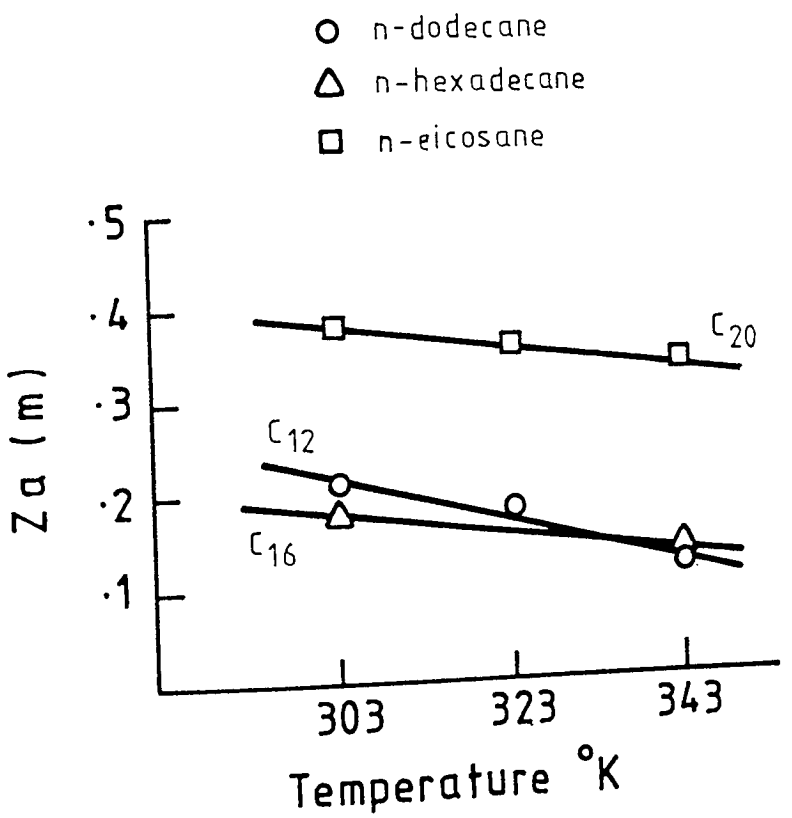

Figure 9.35 Effect of temperature on adsorption zone height

TABLE 9.11 Dynamic properties and equilibrium constants

Run	Za (method 1) m	Za (Method 2) m	Degree of Sat. %	Dyn Capacity kg/kg	f	LUB m	Equilibrium Constar K
1	0.185	0.185	77.1	0.114	0.48	0.07	12.3
2	0.121	0.121	84.7	0.120	0.49	0.06	10.9
3	0.210	0.200	74.6	0.113	0.47	0.09	13.6
4	0.248	0.248	71.8	0.090	0.45	0.10	12.5
5	0.109	0.107	88.3	0.114	0.42	0.04	12.3
6	0.187	0.186	77.0	0.114	0.46	0.08	12.3
7	0.274	0.276	66.4	0.085	0.48	0.12	13.3
8	0.167	0.162	77.6	0.111	0.52	0.07	5.9
9	0.175	0.182	78.8	0.117	0.47	0.07	3.5
15	0.379	0.374	56.0	0.097	0.45	0.16	9.1
16	0.391	0.397	61.2	0.040	0.39	0.13	9.1
17	0.497	0.477	43.0	0.066	0.45	0.20	9.1
19	0.250	0.251	68.3	0.083	0.48	0.10	9.2
23	0.460	0.450	52.6	0.078	0.40	0.19	9.7
24	0.563	0.542	45.1	0.081	0.38	0.17	9.7
26	0.830	0.829	28.1	0.052	0.31	0.22	9.8
28	0.348	0.333	70.2	0.079	0.33	0.11	9.7

increase from 303°K to 343°K was 86% for the normal dodecane system. The increase in theoretical overall mass transfer coefficient for the same temperature rise was 55%. Therefore an increase of temperature in the range 303 to 343°K will improve the adsorption process. Thus an optimum temperature will exist in industrial applications involving a balance between equilibrium loading and mass transfer rate.

9.33. Total Dynamic Capacity (TDC)

The total dynamic capacity is defined as the amount of adsorbate, n-paraffin, adsorbed per unit weight of molecular sieves in a dynamic system just after the effluent concentration has reached the feed concentration. It was calculated according to Equation 5.4 and using graphical integration as illustrated in the sample calculation in Appendix B.

The values of dynamic capacity were listed in Table 9.11. These values varied with the molecular weight of normal paraffin; being 0.114, 0.097 and 0.078 kg/kg sieve for normal dodecane, normal hexadecane, and normal eicosane respectively in the comparable Runs 1, 15 and 23. This can be attributed to the effects of two factors. The equilibrium loading capacity decreased for higher molecular weight of normal paraffin as observed in equilibrium experiments (Figure 9.4). The overall mass transfer coefficients, also decreased with increase in the molecular weight of the normal paraffin, as shown in Table 9.12.

Within the feed flow range of 2.78×10^{-8} to 5×10^{-8} m^3/sec the values

of the dynamic capacity were independent of flow rate, as illustrated by the following data:

Flow rate ($\times 10^8$) m^3/sec	Dynamic capacity kg/kg sieves	
	n-C_{12}	n-C_{20}
2.78	0.114	0.079
5.0	0.114	0.078
6.1	0.114	0.080

Values of dynamic capacity increased with temperature elevation. For example in normal dodecane adsorption the values of dynamic capacity were 0.113, 0.114 and 0.12 kg/kg sieves at temperatures of 303°K, 323°K and 343°K respectively, and were 0.076 and 0.09 kg/kg sieve for n-hexadecane and 0.065 and 0.081 kg/kg sieve for n-eicosane at temperatures of 303°K and 343°K respectively. This trend corresponds with the increase in mass transfer coefficient with temperature. The effect of particle size of molecular sieves on the values of dynamic capacity is illustrated in the data below:

Particle size d_p ($\times 10^3$)m	Dynamic capacity kg/kg sieve		
	n-C_{12}	n-C_{16}	n-C_{20}
0.266	0.085	-	-
0.75	0.09	.083	.052
1.5	0.114	.097	.078

The decrease in dynamic capacity with particle size is an unusual trend, since a reduction of particle size would be expected to increase the adsorption area and consequently result in an increase in the dynamic capacity. However the decrease in dynamic capacity with reduced particle size may be explained by the following effects.

(a) The effect of grinding on the crystals of molecular sieves being to decrease their adsorption efficiency. Whilst the pores cannot be disrupted because their diameter is so much smaller than the crystals, 5Å for the pore and 25000Å for the crystal, this effect could be due to the packing of small particles effectively "sealing-off" useful areas in crystals.

(b) An increase in the proportion of binding material in the small diameter size fraction from the screening operation. The clay inert binder tended to be soft and to produce dust on grinding.

9.3.4 Degree of Saturation

The values of degree of saturation calculated in accordance with Equation 5.7 are listed in Table 9.11.

For example degrees of saturation of C_{12}, C_{16} and C_{20} normal paraffins, at a flow rate of 5.0×10^{-8} m^3/sec, temperature 323°K, molecular sieves weight 0.066 kg, and of particle size 1.5×10^{-3} m, were 77.1%, 56.0% and 52.6% respectively.

The higher degrees of saturation in the cases of the lighter normal paraffins can be attributed to the higher equilibrium loadings and to the higher mass transfer coefficients. An increase in temperature increased the degree of saturation of normal paraffins. For examaple with normal dodecane the values of saturation were 74.6%, 77.1%, and 84.7% at temperatures of 303°K, 323°K and 343°K respectively, and were 79%, 83% at temperatures 303°K and 343°K for n-hexadecane and 17.6%, 23.9% and 27% at temperatures 303°K, 323°K and 343°K respectively for n-eicosane. This would be expected due to the increase of overall mass transfer with temperature.

An example of the increases of saturation percentage and overall mass transfer coefficients with an increase in temperature is shown below for the adsorption of normal dodecane:

	303 to 323°K
Saturation %	9.8
Exp overall MTC	3.1
Theo overall MTC	2.4

The values of degree of saturation for normal paraffin at different flow rates were:

Flow rate	Degree of saturation %		
(x 10^8)m^3/sec	C_{12}	C_{16}	C_{20}
2.78	88.3	61.2	70.2
5.0	77.1	56.0	52.6
6.1	77.0	43.0	45.1

The decrease of degree of saturation with increase in flow rate can be explained since at high flow rates the residence time is insufficient for the equilibrium loading to be attained, causing a reduction in the degree of saturation. However since in a practical application operation at a low flow rate will decrease the throughput of the process, optimisation is necessary between the degree of saturation achievable and throughput.

9.3.5 Mass Transfer Coefficients

The values of the external, pore, experimental overall, and theoretical overall mass transfer coefficients are represented in Table 9.12. These coefficients are based upon a weight-ratio driving force in the fluid phase and are expressed in units of kg of n-paraffin/(sec) (m^3) (kg n-paraffin/kg iso octane), abbreviated to kg iso octane/(sec) (m^3).

The experimental overall mass transfer coefficient was calculated from the following form of equation 5.3

$$K_y a = \frac{G_s N_t}{Z_a}$$

where

$$N_t = \int_{Y_b}^{Y_e} \frac{dY}{(Y - Y^*)} = \text{number of transfer units}$$

G_S = solute-free fluid mass velocity, kg solvent/(sec) (m^2)

Z_a = adsorption zone height, m

TABLE 9.12 Mass transfer coefficients (M.T.C.)

Run	External MTC kya kg/sec.m^3	Pore MTC k_pa kg/sec.m^3	Exp. Overall MTC Kya kg/sec.m^3	Theo. Overall MTC Kya kg/sec.m^3	Number of Transfer Unit N_t
1	16.9	7.4	3.9	5.1	2.81
2	20.0	9.2	6.7	6.3	3.09
3	13.9	5.4	3.6	3.9	2.88
4	57.3	29.5	3.0	19.5	2.81
5	14.0	7.4	3.7	4.8	2.81
6	18.1	7.4	4.7	5.3	2.81
7	332.0	234.3	2.7	137.4	2.81
8	17.0	7.4	4.8	5.4	3.13
9	17.0	7.4	4.6	5.4	3.20
15	16.6	6.5	2.1	4.7	3.07
16	12.9	6.5	1.1	4.3	3.07
17	16.7	6.5	1.9	4.7	3.07
19	52.8	26.1	3.2	17.4	3.07
23	15.1	6.2	1.9	4.4	3.48
24	16.1	6.1	1.9	4.4	3.48
26	50.7	24.6	1.1	16.6	3.48
28	12.4	6.2	1.4	4.1	3.48

A sample calculation is shown in Appendix B.

The external mass transfer coefficient was calculated from the Wilson and Geankpolis correlation 5.12 for liquids. The pore mass transfer coefficient was calculated from Equation 5.18 as illustrated in Appendix B. A theoretical $K_y a$ was calculated assuming that the overall resistance to mass transfer may be expressed as the sum of an external film resistance and a solid phase resistance. The area, a, on which the theoretical coefficient was based, is the outer surface interfacial area of the sorbent particles per unit volume of contacting system (solid plus fluid), or $6(1-\varepsilon)/d_p$ where d_p is the average particle diameter. Comparative values of mass transfer coefficients of the normal paraffin systems under similar operating conditions were:

n-paraffin	Mass transfer coefficient				Molecular diffusivity
	Ext kg/sec m^3	Pore kg/sec m^3	Expr kg/sec m^3	Theor kg/sec m^3	$D_m x10^8$ $(x10^8) m^2/sec$
n-dodecane	16.9	7.4	3.9	5.1	0.2507
n-hexadecane	16.6	6.5	2.1	4.7	0.2217
n-eicosane	15.1	6.2	1.9	4.4	0.2091

As shown by the above data the values of mass transfer coefficients for light n-paraffin were higher than those for heavy n-paraffin. This is reasonable because of the values of molecular diffusivity of these fluids. Theoretically the overall mass

transfer coefficient is proportional to the molecular diffusivity to the power 0.66 as shown in Appendix B. The calculated values of external mass transfer coefficient are at least twice the corresponding values of pore mass transfer coefficient for all systems. Thus an internal resistance controls the rate of mass transfer.

Variation of up to 134.7 kg/sec m^3 is apparent between the values of experimental and theoretical overall mass transfer coefficients listed in Table 9.12. Such a variation was also observed in Schumacher's work (33) on the adsorption of n-hexane in a column packed with 5A molecular sieves. It can be explained by a combination of factors:

(a) Convection currents in the column

The values of mass transfer coefficients at different flow rates were:

Flow rate	Mass transfer coefficient								
$(x10^8)m^3/sec$	n-C_{12}			n-C_{16}			n-C_{20}		
	Ext	Exper	Theo	Ext	Exper	Theo	Ext	Exper	Theo
2.78	14.0	3.7	4.8	12.9	1.1	4.3	12.4	1.4	4.1
5.0	16.9	3.9	5.1	16.6	2.1	4.7	15.1	1.9	4.4
6.1	18.1	4.7	5.3	16.7	1.9	4.7	16.1	1.9	4.4

Since the magnitudes of the external mass transfer coefficient are considerably greater than the measured coefficients, an external resistance is unlikely to be a

major cause of the observed dependence of overall coefficients on flow rate.

According to Schumacher (33) this effect may be partly attributed to convection currents set up in the column because of the different densities of the feed and the solute-free effluent. Such behaviour would tend to broaden the adsorption zone and reduce the experimental mass transfer coefficient. However whether the effect of density difference was, in fact, significant in either Schumacher's or the present work appears doubtful. For example the differences here were,

System	Feed density kg/m^3	Solute-free effluent density kg/m^3	Difference
$n\text{-}C_{12}$	668.7	668.0	0.7
$n\text{-}C_{16}$	668.9	668.0	0.9
$n\text{-}C_{20}$	669.0	668.0	1.0

The effect of convection would tend however to be more marked at low fluid flow rates since any relatively mild convection currents would be of no importance at higher bulk flow rates. This is confirmed by comparing the differences between the values of theoretical and experimental overall mass transfer coefficients at flow rates of 2.78×10^{-8} and 6.1×10^{-8} m^3/sec for the three normal paraffins.

Flow rate m^3/sec	Difference in experimental and theoretical MTC kg/sec m^3		
	n-C_{12}	n-C_{16}	n-C_{20}
2.78×10^{-8}	1.1	3.2	2.7
6.1×10^{-8}	0.5	2.8	2.5

(b) The assumption of a constant internal pore diffusion resistance in the calculation of the theoretical coefficients. In fact the internal resistance is some combination of a resistance to pore diffusion, a resistance to transfer through the apertures of the sieve crystal, and a resistance to intracrystalline diffusion. Moreover, this internal resistance is unlikely to be constant but probably increases as a pellet becomes more and more saturated, such that any solute molecule is eventually required to diffuse far into the pellet before finding an available adsorption site.

(c) The values of experimental and theoretical overall mass transfer coefficient at different average particle diameter are listed below:

Average particle diameter d_p ($\times 10^3$)m	Overall mass transfer coefficient kg/sec m^3					
	n-C_{12}		n-C_{16}		n-C_{20}	
	Exp	Theo	Exp	Theo	Exp	Theo
1.5	3.9	5.1	2.1	4.7	1.9	4.4
0.75	3.0	19.5	3.2	17.4	1.1	16.6
0.266	2.7	137.4	-	-	-	-

It is apparent from the above data that:

(i) The experimental mass transfer coefficient decreased with a decrease in the particle size, which is contrary to the expectation from theory, ie. that a decrease in particle size would increase the adsorption area and hence the overall mass transfer coefficient, a trend shown by the theoretical values.

(ii) The deviation between the theoretical and experimental overall mass transfer coefficients increased with a decrease in particle diameter. This may be attributed to the following causes:

- The effect of grinding on the crystals of molecular sieves being to decrease their adsorption properties.

- An increase in the proportion of inert binding material in the small diameter size

fraction from the screening operation. Several studies have been done by other authors (66,67) using crushing. However it is recommended that in future manufactured molecular sieve of different diameter sizes should be used instead of reducing the size by crushing to avoid the above effects which would not, of course, arise in an industrial adsorption operation.

9.3.6 Comparison Between Experimental and Predicted Breakthrough Curves using Treybal's Method and Graphical Evaluation of the Integrals

According to Treybal's method (42), Equation A.8

$$\frac{Z \text{ at } Y}{Z_a} = \frac{W - W_b}{W_a} = \frac{\int_{Y_b}^{Y} \frac{dY}{Y - Y^*}}{\int_{Y_b}^{Y_e} \frac{dY}{Y - Y^*}} \qquad \text{A.8}$$

should enable the breakthrough curve to be plotted by graphical evaluation of the integrals. The derivation of Equation A.8 is shown in Appendix A.

The predicted and experimental curves were calculated as illustrated in the Sample Calculation in Appendix B. Values of Y/Y_0 were plotted versus values of

$$\frac{W - W_b}{W_a}$$

in Figures 9.36 to 9.38 for comparing the experimental and predicted breakthrough curves of adsorption of n-dodecane, n-hexadecane, and n-eicosane

respectively with Type 5A molecular sieves of average particle diameter 1.5 x 10^{-3} m, feed concentration 0.01 mole fraction, flow rate of 5 x 10^{-8} m^3/sec and at a temperature of 323°K.

Comparison of the predicted and experimental curves in Figures 9.36 to 9.38 indicates considerable discrepancy between them. This may be attributed to the following effects.

(a) The assumption of constant overall mass transfer coefficient for the concentration within the adsorption zone.

(b) The consequences of the size range of molecular sieves particles used in the dynamic systems, whereas 1/8 inch size pellets of molecular sieves were used in batch experiments and hence in the calculation of predicted breakthrough curves.

9.3.7 Comparison Between Experimental and Predicted Breakthrough Curves using the Mathematical Model Derived in Chapter 8

The mathematical model developed in Chapter 8 is applied in this Section to predict breakthrough curves for the adsorption of normal paraffin systems, n-dodecane, n-hexadecane, and n-eicosane under similar operating conditions, represented in Runs 1, 15 and 23 respectively. This facilitated comparison of predicted and experimental breakthrough curves.

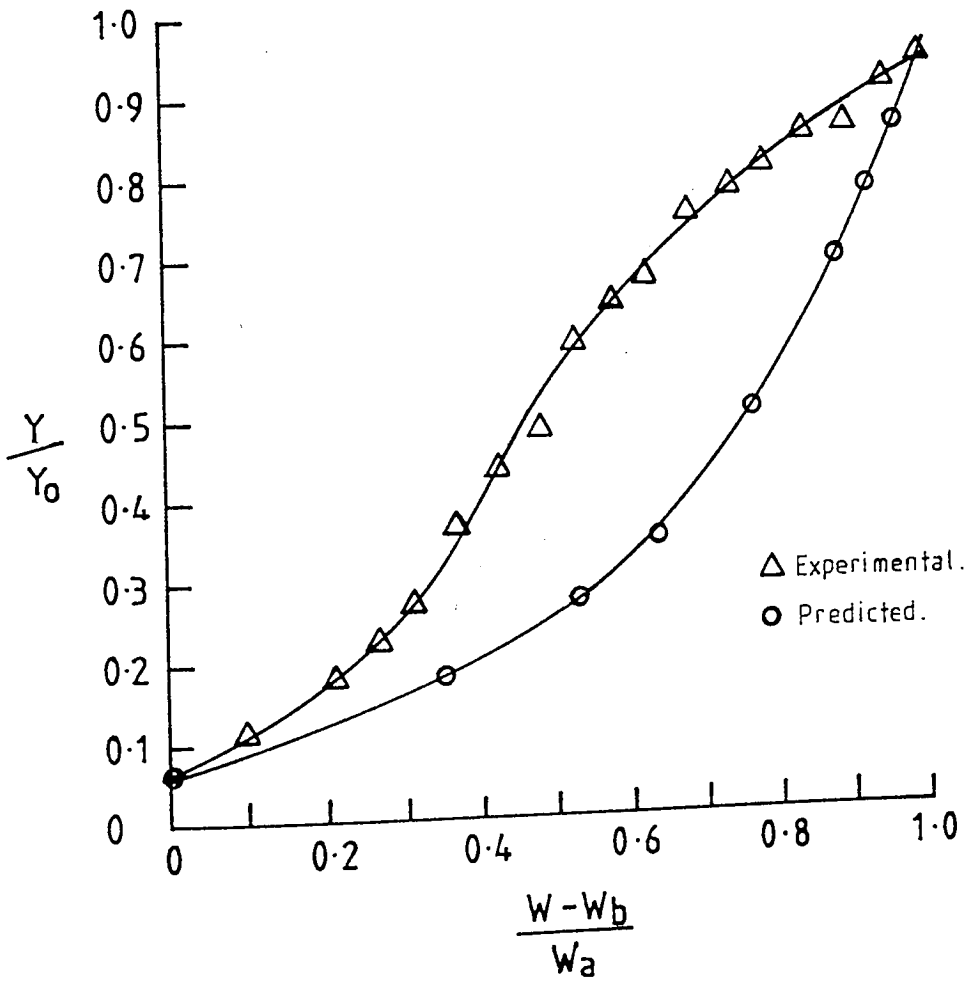

Figure 9.36 Comparison between experimental and predicted curves using Treybal's method (42) for adsorption of n-dodecane at 323°K with Type 5A molecular sieves

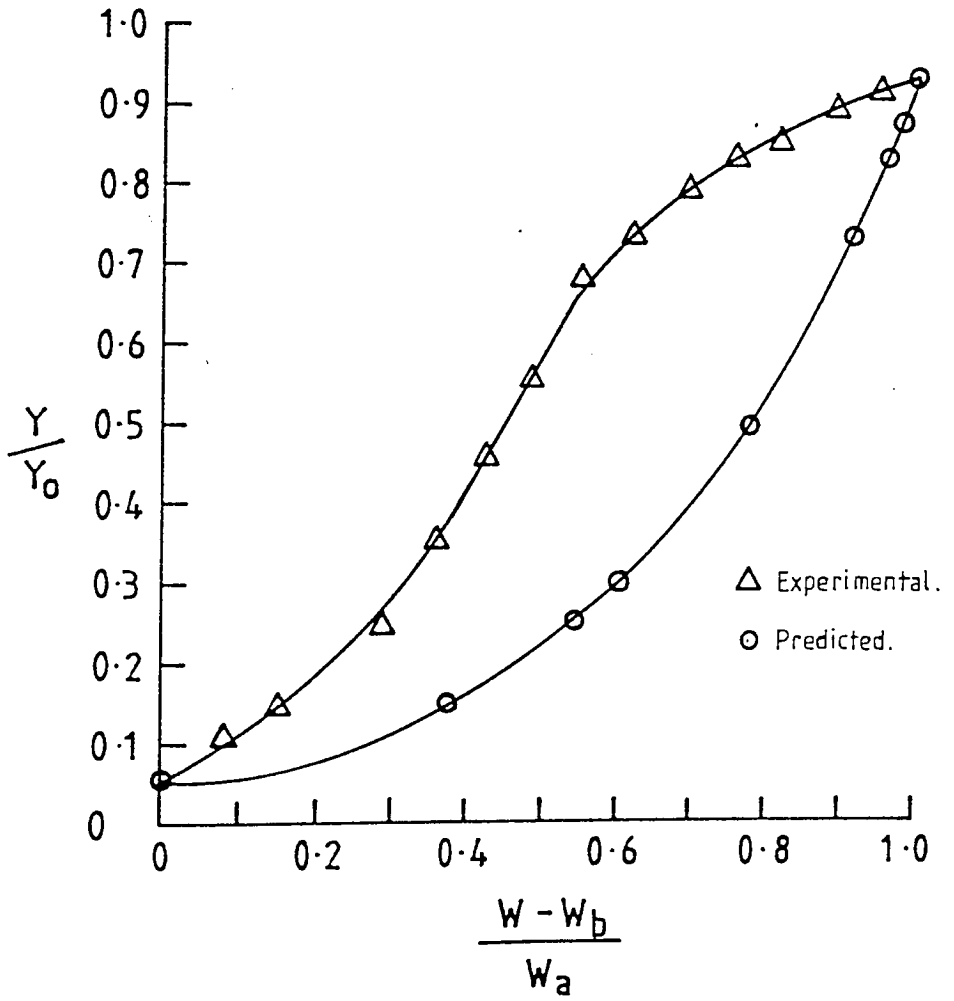

Figure 9.37 Comparison between experimental and predicted curves using Treybals method (42) for adsorption of n-hexadecane at 323°K with type 5A molecular sieves

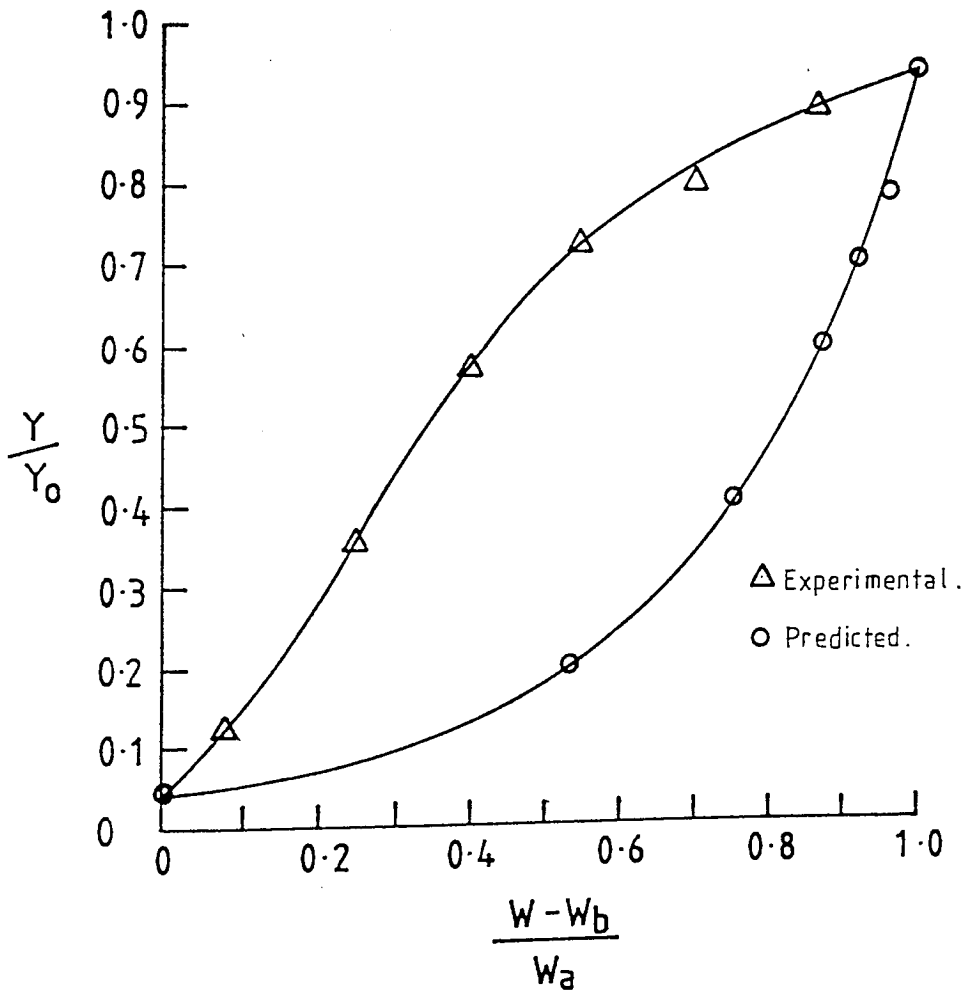

Figure 9.38 Comparison between experimental and predicted curves, using Treybals method (42) for adsorption of n-hexadecane at 323°K with type 5A molecular sieves

The applicability of any model to any real system may be tested by comparison of experimental and theoretical breakthrough curves and determination of consistent model parameters.

In the present study there were initially two unknown parameters, the equilibrium distribution coefficient K and the external film mass transfer coefficient k_f. Both may be evaluated using the experimental batch system data to draw equilibrium adsorption isotherm, calculating the equilibrium distribution coefficient (K), and using an empirical equation for estimating the mass transfer coefficient (k_f). The estimation of these parameters are illustrated in the Sample Calculation in Appendix B, and their values are listed in Tables 9.11 and 9.8 respectively.

Computation of Equation 8.34, which describes the concentration profile of the effluent of the adsorption column as a function of time and column height, was accomplished by means of SPERRY UNIVAC 1100 MAINFRAME COMPUTER and using FORTRAN 77 high level language.

The program used to produce the predicted data for breakthrough curves is illustrated in Appendix B. The integral which constitutes the solution has been solved numerically by the Trapezoidal method. The column space increments used were 0.0195 cm. It was verified that smaller increments did not change the results. The computed data for the predicted curves are shown in Appendix B.

The mean relative percent deviation (MRPD) is defined as:

$$\text{MRPD} = \frac{1}{N} \sum_{i=1}^{N} 100 \times \left| \frac{t_{Theo} - t_{Exp}}{t_{Theo}} \right|$$

where N is the number of experimental points.

Figures 9.39 to 9.41 represent the experimental and predicted breakthrough curves of adsorption of n-dodecane, n-hexadecane, and n-eicosane respectively. The values of mean relative percent deviation (MRPD), averaged over the eight values of time (t) at values of C/C_O, from 0.2 to 0.9, are 26, 22 and 13 for n-dodecane, n-hexadecane, n-eicosane breakthrough curves respectively.

These values indicate that the model provides a better fit with the n-eicosane system than with the other two systems. The variation of experimental and predicted breakthrough curves may be attributed to the assumption of linear isotherm and the external film mass transfer rate equilibrium in developing the model. In practice the real systems were of non-linear isotherm type and both external and internal mass transfer resistances were significant.

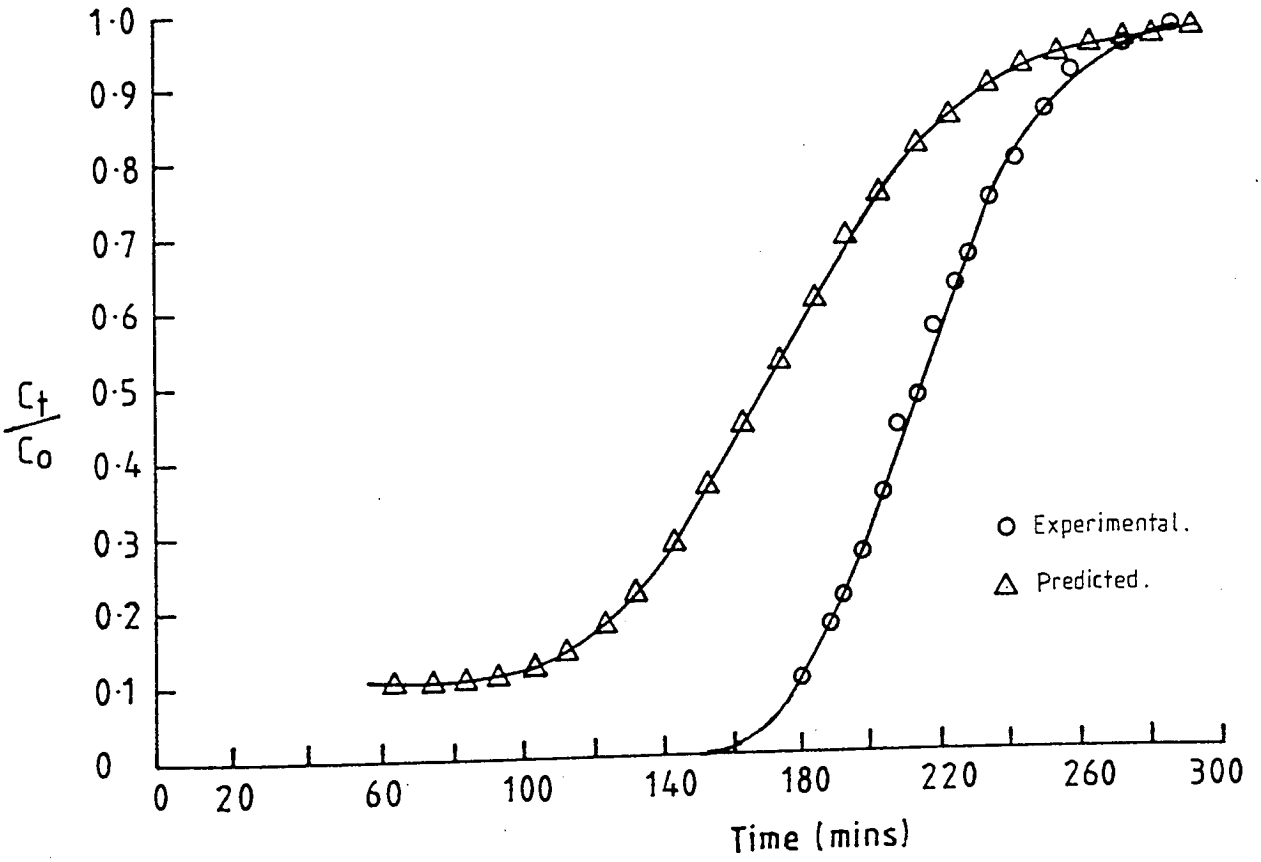

Figure 9.39 Experimental and Predicted breakthrough curves using the derived model, for adsorption of n-dodecane with type 5A molecular sieves in Run 1

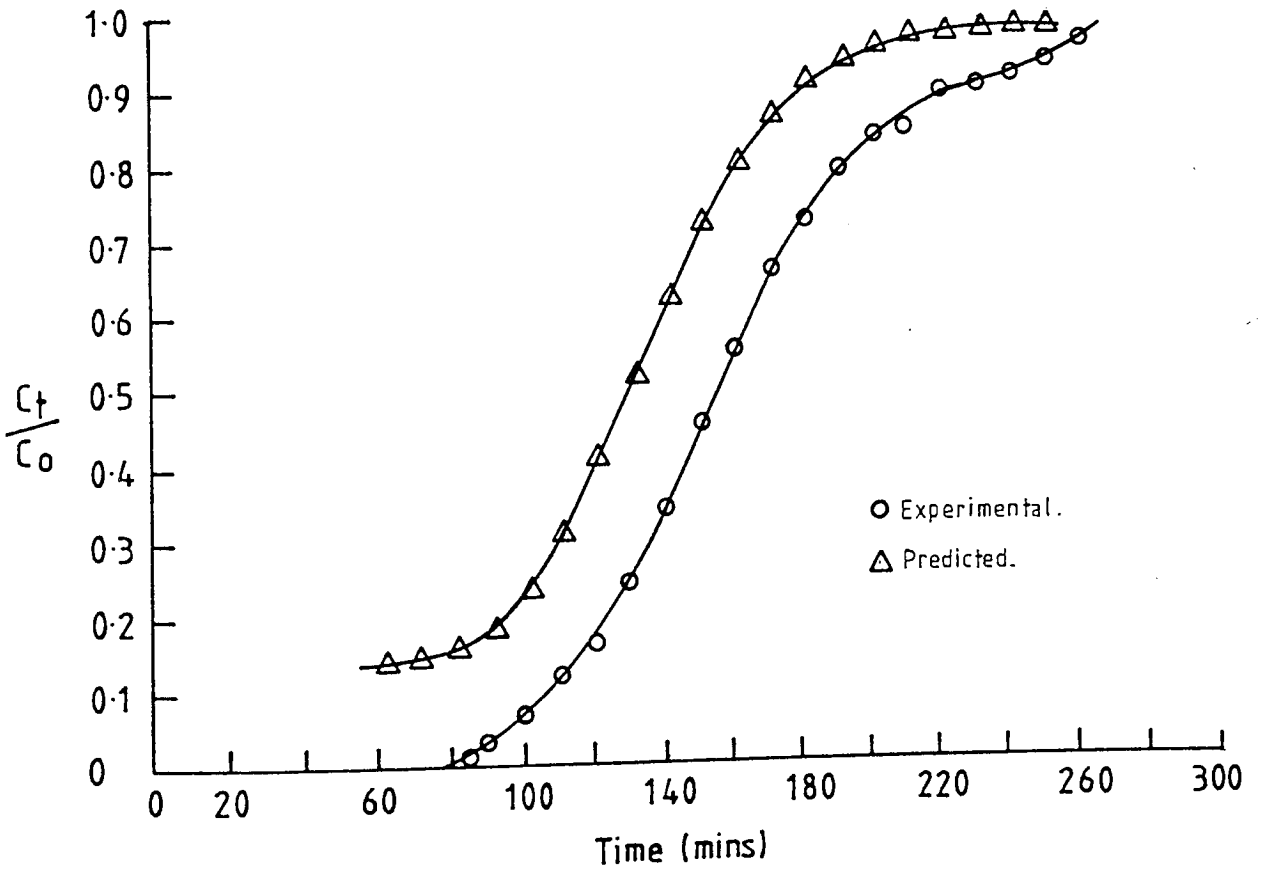

Figure 9.40 Experimental and Predicted breakthrough curves using the derived model, for adsorption of n-hexadecane with type 5A molecular sieves in Run 15

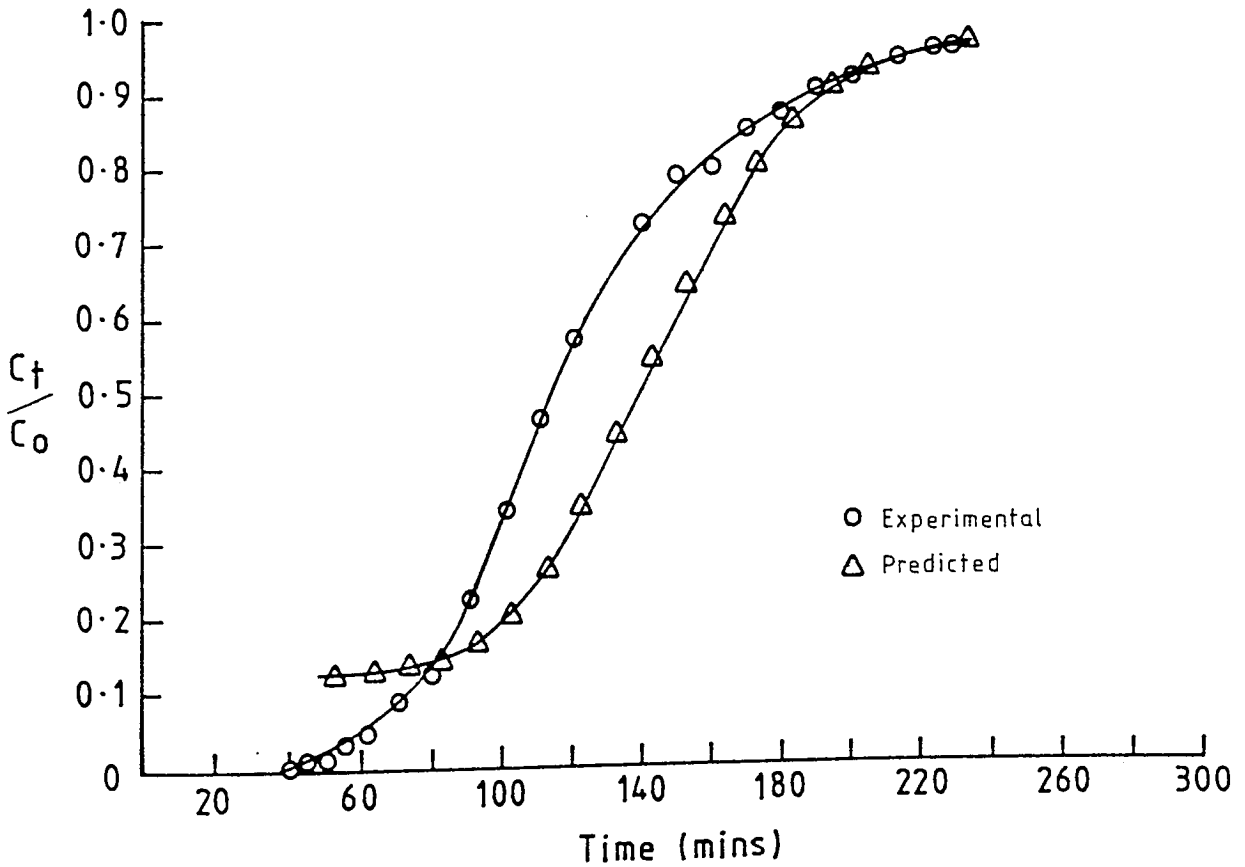

Figure 9.41 Experimental and Predicted breakthrough curves using the derived model, for adsorption of n-eicosane with type 5A molecular sieves in Run 23

CHAPTER 10

CONCLUSIONS AND RECOMMENDATIONS FOR FUTURE WORk

10.1 CONCLUSIONS

It may be concluded that high purity n-paraffins can be effectively separated from hydrocarbon mixtures by selective adsorption on 5A molecular sieves. The adsorption of n-paraffins in the range C_{12} - C_{20} on 5A molecular sieves is of non-linear isotherm and of favourable type. The modified BET equation produces a reasonable fit to the experimental equilibrium isotherms. The range of the logarithm of the separation coefficient was between 3.5 and 4.7 indicating that normal paraffin molecules are strongly adsorbed by type 5A molecular sieves.

Examination of the results from dynamic experiments demonstrated the justification of the assumption of a constant pattern behaviour of the mass transfer zone. This is considered to be a very useful design tool since the calculation of the form of the mass transfer front under constant pattern conditions is then very simple.

Comparison between the relative values of the external mass transfer coefficient and pore mass transfer coefficient indicated that the internal resistance was the major one tending to control the adsorption rate.

Comparison between predicted and experimental breakthrough curves revealed considerable discrepancies, which are explained by some inaccurate assumptions (e.g. linear isotherm, external M.T.C.) in the methods used. Other models, which could in future be tested and compared with the available data for various systems, are suggested in Section 10.2.

10.1.1 Batch System

The following detailed conclusions may be drawn from the results of batch experiments.

a) The experimental equilibrium adsorption isotherms of the three normal paraffins investigated were non-linear and of favourable type, approaching irreversible adsorption. Hence a constant pattern behaviour of the mass transfer zone may be anticipated through the adsorption column. The adsorption zone approach proposed by Michaels[40] can therefore be applied for the design of a practical adsorber. The proposed equation by Eltekov and Kiselev[36], Equation 4.4, fitted the experimental adsorption isotherms satisfactorily, and can therefore be applied to aid in qualitative interpretation of experimental isotherms of adsorption from n-paraffin systems within the range C_{12} to C_{20}.

b) An increase in the temperature of adsorption decreased the equilibrium loading of 5A molecular sieves. This effect was greater for normal dodecane and reduced for the higher paraffins.

c) The results of equilibrium loading for normal dodecane are in good agreement with those of Sundstrom and Krautz[46] confirming the reproducibility of the experimental techniques.

d) Under similar conditions of adsorption temperature and liquid concentration, the equilibrium loading decreased with an increase in molecular weight of the normal paraffin under investigation. This confirmed the violation of Traub's rule, previously reported by Gupta et. al.[57], that higher molecular weight

adsorbate should be preferentially adsorbed.

e) The values of the logarithm of the separation coefficient ($\log_{10}$ f) for the three normal paraffins were >2 , which indicates a high selectivity of adsorption of these normal paraffins by Type 5A molecular sieves.

f) The values of limiting amount of adsorbate filling the cavities of 1gm of molecular sieve (a_m), separation coefficient (f), and equilibrium adsorption time (t) decreased with an increase in temperature for the three normal paraffins as discussed in Chapter 9.

g) The values of heat of adsorption of each normal paraffin (C_{12}, C_{16}, and C_{20}) were calculated. A decrease of heat of adsorption was observed to correspond with an increase in molecular weight. A similar trend has been observed by Burgess et. al.(62) with 5A sieve for normal paraffins in the molecular weight region (C_{10} - C_{20}) at a temperature of 623°K.

h) The heat of adsorption increased with coverage for each of the three normal paraffins. This confirmed the major trends reported by Burgess et. al. (62), that the dependence of heat of adsorption on loading is increasingly steep in progressing from C_9 - C_{20} for 5A sieves.

i) From the results of kinetic experiments it is concluded that the rate of adsorption of the normal paraffins C_{12}, C_{16}, and C_{20} increased with an increase in temperature. The equilibrium time decreased from 17 to 8 hours; from 20 to 10 hours, and from 28 to 11 hours for n-dodecane, n-hexadecane, and n-eicosane respectively with an increase in temperature from 303°K to 343°K.

j) Effective diffusivity increased from 0.084×10^{-10} to 0.101×10^{-10} m^2/sec, from 0.074×10^{-10} to 0.098×10^{-10} m^2/sec., and from 0.067×10^{-10} to 0.081×10^{-10} m^2/sec for n-dodecane, n-hexadecane, and n-eicosane respectively

with an increase in temperature from 303°K to 343°K, which is in agreement with the published results from other studies(65).

k) The values of activation energy determined in the present study were 2 to 4 kcal/mole, in good agreement with the results reported (37) for the adsorption of normal paraffins C_{10}, C_{14}, C_{16}, and C_{18} on particular granules of CaA zeolite at moderate temperature in the range 300 - 340°K.

In the high temperature range 380 - 425°K, Falkovich et. al.(37) reported a range of 10 - 15 kcal/mole, indicating a change in the controlling mechanism of internal diffusion.

10.1.2 Dynamic Flow System

The conclusions arising from the results of the dynamic experiments are as follows,

a) The shape of each individual breakthrough curve for each system approximated to a smooth S-shaped curve.

The deviation of any curve from ideality increased with an increase in the molecular weight of the n-paraffin. This was caused by a tendency of the trailing edge of the curve to flatten out as saturation approached. The deviation decreased with an increase in temperature indicative of more efficient saturation of the adsorbent.

b) The assumption of a constant width adsorption zone, with a constant rate of travel, was justified by the agreement between the values of the height of adsorption zone calculated by the two Equations 5.1 and 5.2. This indicates the feasibility of using the mass transfer zone concept, originally suggested by

Michaels for fixed-bed ion-exchange columns, to describe the rate of adsorption of n-paraffins on Type 5A molecular sieves and to provide a simple design procedure.

c) The adsorption zone height was found to vary in proportion to approximately the 0.65 and 0.8 power of superficial velocity for normal dodecane and normal eicosane respectively. This was in reasonable agreement with the results of Schumacher[33] with normal hexane, and Ziegenhain[79] with normal heptane in which the powers were reported as approximately 0.7 and 0.65 respectively. It also gave an indication of the relative contributions of internal and external resistances to the overall resistance.

d) For the three systems of normal paraffins, n-dodecane, n-hexadecane, and n-eicosane the height of the adsorption zone decreased with an increase in the adsorption temperature, indicative of a lower resistance to mass transfer and hence elevation of adsorption temperature in the range up to 345°K will improve the rate of practical adsorption of n-paraffins with Type 5A molecular sieves.

e) The dynamic capacity of the sieves for the heavy n-paraffin, n-eicosanse, was lower by 0.036 kg/kg sieve than that for the lighter n-paraffin, n-dodecane. This could be explained in terms of changes in the equilibrium loading capacity and overall mass transfer coefficients as discussed in Chapter 9.

f) The dynamic capacity of 5A molecular sieve was increased by, on average, 6%, 18%, and 24% for normal dodecane, normal hexadecane, and normal eicosane respectively with an increase in temperature from 303°K to 343°K.

g) A decrease in dynamic capacity with reduction in particle size of molecular sieves was observed instead of an increase in dynamic capacity which was expected to accompany an increase in adsorption surface area. This could have

arisen due to a combination of factors, i.e.

i) The effect of grinding on the crystals.

ii) An increase in the proportion of inert binding material present in the small diameter size fraction obtained by screening.

h) The values of all the mass-transfer coefficients of light n-paraffin were higher than the values of the heavy n-paraffin as shown in Table 9.12, which would be expected because of the higher molecular diffusivity of these fluids.

i) The values of external mass-transfer coefficient were at least twice the corresponding values of pore mass-transfer coefficient in all the n-paraffin systems studied. Thus the internal resistance was a major factor controlling adsoption rate for the 5A molecular sieve.

j) The discrepancies shown in Table 9.12 between values of experimental mass-transfer coefficient and corresponding values of theoretical coefficient were explainable as due to a combination of the following factors:

i) The assumption of a constant internal pore diffusion resistance in the calculation of the theoretical coefficients.

ii) The effect of grinding on the crystals of molecular sieves and an increased proportion of inert binding material in the finer fractions of molecular sieves.

k) A comparison was made between experimental and predicted breakthrough curves, for the adsorption of n-paraffins with 5A molecular sieves, using Treybal's method[42] and graphical evaluation of the integral. The discrepancy demonstrated between the experimental and predicted breakthrough curves, could relate to the following factors:

i) The assumption of a constant overall mass transfer coefficient within the adsorption zone.

ii) The influence of crushing and particle size distribution differences in the molecular sieves used to obtain dynamic experimental data, for plotting the experimental breakthrough curve, and that used to obtain the batch experimental data for predictions.

l) A mathematical model has been developed for an isothermal plug flow system with one adsorbable component in an inert carrier, assuming a linear adsorption isotherm and an external film rate equation. The predicted breakthrough data for the n-paraffin systems, n-dodecane, n-hexadecane, and n-eicosane were calculated from this by a computer programme. A comparison of the experimental and predicted breakthrough curves showed mean relative percent deviation of 26, 22, and 13% for the n-dodecane, n-hexadecane and n-eicosane systems respectively. These deviations may be attributed to the assumption of a linear adsorption isotherm and fluid linear driving force rate expression with an external mass transfer coefficient in developing the model. In reality the systems exihibited non-linear equilibrium isotherms, and a combination of external and internal resistances contributed to the overall resistance to mass transfer.

10.2 SUGGESTIONS AND RECOMMENDATIONS FOR FUTURE WORK

Several suggestions for future work are presented in this section.

a) The present study was concerned with the investigation of adsorption of only one normal paraffin solute. Clearly, it is necessary to study the adsorption of n-paraffins from a feed stream of the composition likely to exist in a commercial

unit, which is normally a mixture of hydrocarbons with a range of 8 - 15 wt% of normal paraffin content. Such a study would determine the validity of applying the results of laboratory studies of pure binary systems to multicomponent, commercial mixtures. In addition such a study of adsorption from a commercial feed would provide information about the nature and extent of sieve deactivation by low-level impurities such as sulfur compounds, and by non-desorbable components of the feed.

b) It would be of value to use molecular sieves of different manufactured sizes, instead of crushing and screening, to avoid the effects observed in the present study and to work on a specific diameter of sieve particle instead of with a certain diameter range.

c) The use of a thermostatically-controlled digital density meter is recommended for analysis of binary systems for its accuracy, and ease and rapid analysis. For multicomponent adsorption studies the use of gas-liquid chromatography (GLC) is advised. The analysis of normal paraffin systems can be carried out with GLC (Intersmat IGC 16 equipped with flame ionization detector) on a fused silica column SE30 of 5m long and 0.35×10^{-3} in I.D.(67).

d) The method applied in the present study for the activation of molecular sieves can be used for dynamic adsorption studies because of its high efficiency of activation and ease of application compared with other methods (66, 67, 80).

e) It is recommended that higher sieve bed heights should be used, for adsorption of high molecular weight normal paraffins (C_{16^+}) with adjustments of the corresponding operating conditions to avoid the proximity of height of adsorption zone to the length of sieve bed. (Since where the height of adsorption

zone increases with increase in molecular weight of n-paraffin, as observed in the results of the present study, the increase of the height of adsorption zone over the length of the sieve bed will lead to unreliable breakthrough curve data).

f) As an extension to the present work the following studies may prove useful,

i) Adsorption of normal paraffins may be performed using various 5A molecular sieves commercially available with different types and percentages of clay binder, and various size of crystals, e.g. Davison 5A sieves, Regular (C-525 and C-625) and Z-100 (C-625 and C-626), Brand R, and Brand W to compare their efficiency with the Linde 5A molecular sieve used in the present study.

ii) Investigation of the desorption step of the n-paraffin systems used in the present work with different types of displacing agents (or desorbents) such as n-hexane, steam, and ammonia to determine which is the most efficient for desorption of n-paraffin systems.

iii) Comparison of the experimental breakthrough curves with the predicted curves calculated by mathematical models which account for the non-linear behaviour of the isotherm e.g. Langmuir, Freundlich isotherm, or the generalized and more flexible isotherm equation proposed by Radke and Prausnitz[81] and based on the assumption that the rate of mass transfer from the fluid phase to the fixed solid particle is controlled by one, or a combination of, the following mechanisms:

(1) external resistance due to diffusion of the adsorbate molecules through a stagnant liquid film surrounding the particles,

(2) internal transfer through the fluid phase occupying the pores of the

adsorbent, and

(3) diffusion of the adsorbate molecules along the surface of the pores of the adsorbent. Hasanain et. al.,[74], developed a new model based on diffusion through the solid particle and included the isotherm equation proposed by Radke and Prausnitz, which can be used for testing the present breakthrough data.

APPENDIX A

ADSORPTION ZONE APPROACH

Consider the idealized breakthrough curve shown in Figure 5.1. This results from the flow of a solvent fluid through an adsorbent bed at the rate of G_s kg/(hr)(sq m), entering with an initial solute concentration Y_o kgsolute/kg solvent. The total solute-free effluent after any time is W kg/sq m of bed cross section. The total effluent accumulated during the appearance of the breakthrough curve is $W_a = W_e - W_b$. The adsorption zone, of constant height Z_a m, is that part of the bed in which the concentration change from Y_b to Y_e is occurring at any time.

Let θ_a be the time required for the adsorption zone to move its own height down the column, after the zone has been established. Then

$$\theta_a = \frac{W_a}{G_s}$$

Let θ_E be the time required for the adsorption zone to establish itself and move out of the bed. Then

$$\theta_E = \frac{W_e}{G_s}$$

If the height of the adsorbent bed is Z m, and if θ_F is the time required for formation of the adsorption zone,

$$Z_a = Z \frac{\theta_a}{\theta_E - \theta_F} \qquad \text{A.1}$$

The quantity of solute removed from the fluid in the adsorption zone from the breakpoint to exhaustion is M k_g solute/sq m of bed cross section. This is given by the shaded area in Figure 5.1, which is,

$$M = \int_{W_b}^{W_e} (Y_o - Y)\, dw \qquad \text{A.2}$$

If, however, all the adsorbent in the zone were saturated with solute, it would contain Y_O W_a k_g solute/sq m. Consequently at the breakpoint, when the zone is still within the column, the fractional ability of the adsorbent in the zone still to adsorb solute is

$$f = \frac{M}{Y_o W_a} = \frac{\int_{W_b}^{W_e} (Y_o - Y)\, dw}{Y_o W_a} = \int_o^{1.0} (1 - \frac{Y}{Y_o})\, d\left(\frac{W - W_b}{W_a}\right) \qquad \text{A.3}$$

If f = o, so that the adsorbent in the zone is essentially saturated, the time of formation of the zone at the top of the bed θ_F should be substantially the same as the time required for the zone to travel a distance equal to its own height, θ_a. On

the other hand, if f = 1.0, so that the solid in the zone contains essentially no adsorbate, the zone-fromation time should be very short, essentially zero. These limiting conditions, at least, are described by

$$\theta_F = (1 - f)\,\theta_a \qquad \text{A.4}$$

Equation A.1 and A.4 provide

$$Z_a = Z\frac{\theta_a}{\theta_E - (1 - f)\,\theta_a} = Z\,\frac{W_a}{W_E - (1 - f)\,W_a} \qquad \text{A.5}$$

Assume that an adsorption zone has been established and is moving through the bed at a constant velocity. The adsorbent downstream from the adsorption zone is free of solute whilst that upstream from the zone is completely saturated with X_S kg of adsorbate/kg of adsorbent. The adsorbent is being saturated with solute at the rate of L_S kg of adsorbate/(hr.)(sq. m.). It can be imagined that the adsorption zone is held at a constant position within the bed by moving the adsorbent bed counter to the feed at a rate of L_S kg/(hr.)(sq. m.), as shown in Figure A.1a. The operating line over the entire tower is

$$G_S\,(Y_O - O) = L_S\,(X_S - O)$$

At any point in the tower, the concentration of solute in the fluid phase, Y, is related to the concentration of solute on the adsorbent X by $G_S\,Y = L_S\,X$ or

$$Y = \frac{L_s\,X}{G_s}$$

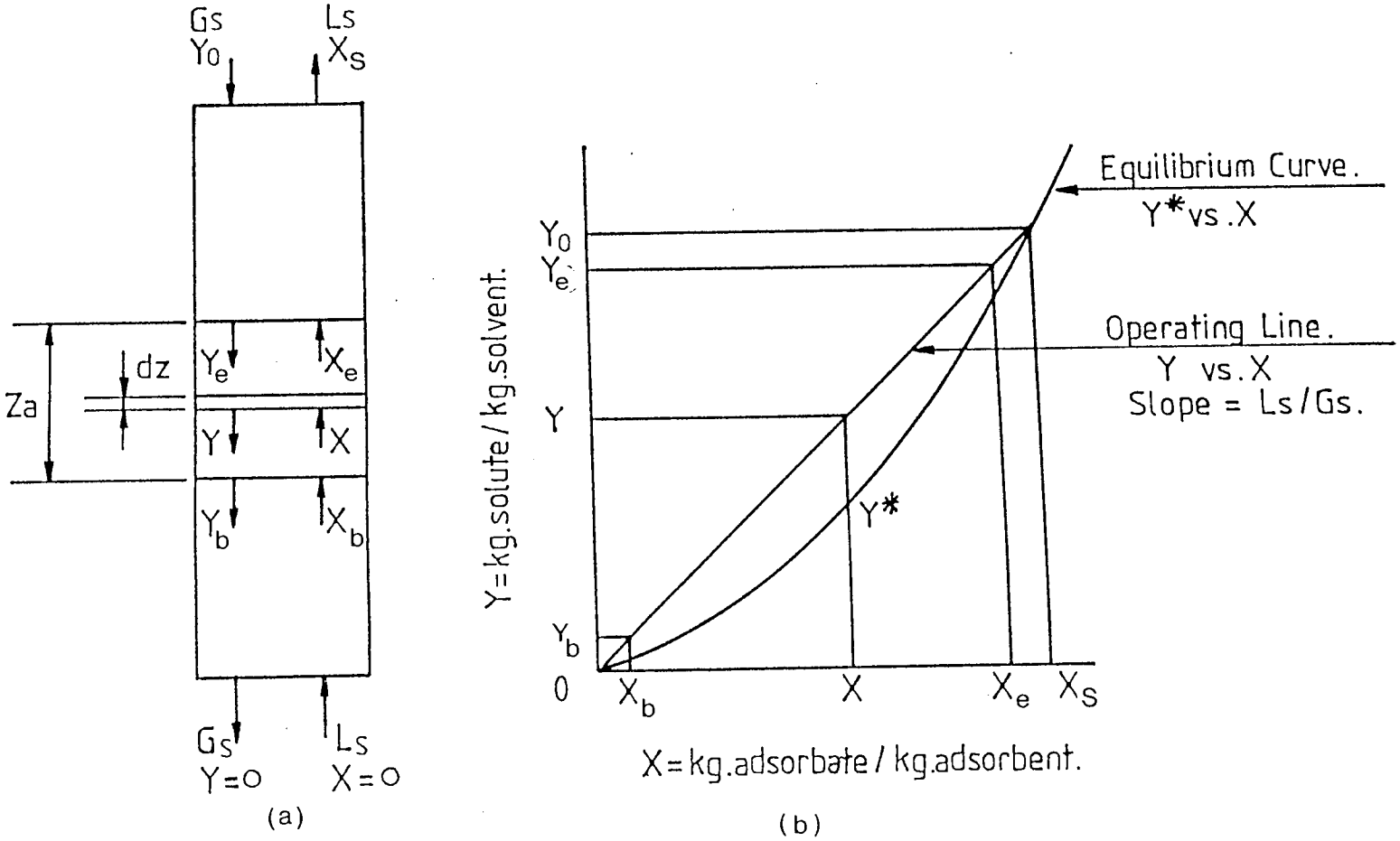

Figure A.1 The adsorption zone

Adapted from: Treybal, R,E., "Mass Transfer Operations", P.553, Figure 11.42

A typical operating line and equilibrium curve are shown in Figure A.1b.

Over the differential height, dZ, of the adsorption zone, the rate of adsorption is,

$$G_S \, dY = K_y \, a \, (Y - Y^*) \, dZ$$

Assuming that the overall mass-transfer coefficient, K_y a, is constant within the adsorption zone, the height of the adsorption zone is given by,

$$Z_a = \frac{G_s}{K_y \, a} \int_{Y_b}^{Y_e} \frac{dY}{Y - Y^*} = \frac{G_s}{K_y \, a} N_t \qquad \text{A.6}$$

where N_t is the number of overall transfer units in the adsorption zone.

For a value of Z less than Z_a at a point where the solute concentration has risen to Y,

$$Z = \frac{G_s}{K_y \, a} \int_{Y_b}^{Y} \frac{dY}{Y - Y^*} \qquad \text{A.7}$$

Since the zone height is proportional to the amount of effluent collected during breakthrough, the breakthrough curve can be calculated by a ratio of equation A.6 and A.7.

$$\frac{Z}{Z_a} = \frac{W - W_b}{W_a} = \frac{\int_{Y_b}^{Y} \frac{dY}{Y - Y^*}}{\int_{Y_b}^{Y_e} \frac{dY}{Y - Y^*}} \qquad \text{A.8}$$

Length of Unused Bed LUB

Equation A.8 should permit plotting the breakthrough curve by graphical evaluation of the integrals.

When breakthrough occurs, the position of the leading edge of the mass transfer front relative to the stoichiometric front is given by (L_o - L_s), where L_o is the length of the adsorbent bed, and L_s is the length of equilibrium section. The length (L_o - L_s) is termed the equivalent length of unused bed, or LUB. The equivalent equilibrium section is specified in terms of the length of equivalent equilibrium section, LES.

Local mass transfer rates within the front have no effect on the front velocity, although they do affect the shape of the front. At any time, θ, the position of the stoichiometric front is given by

$$L_s = U\theta$$

where U is the velocity of a steady-state mass-transfer wave.

By definition, at time θ_B:

$$L_s = LES$$

Therefore:

$$LES = U\theta_B \qquad \text{A.9}$$

By definition, at time θ_s:

$$L_s = L_o$$

Therefore:

$$L_O = U\theta_S \qquad \text{A.10}$$

From A.9 and A.10

$$L_O - L_S = U(\theta_S - \theta_B)$$

or

$$LUB = U(\theta_S - \theta_B) \qquad \text{A.11}$$

Combining Equation A.10 and A.11 by eliminating U,

$$LUB = \frac{(\theta_s - \theta_B)}{(\theta_s)} L_o \qquad \text{A.12}$$

APPENDIX B

SAMPLE CALCULATIONS

B.1 Equilibrium Loading Experiments

Example Run 2

System: n-dodecane, isooctane at 50°C, Molecular sieve type 5A 1/8 inch pellets Molecular Wt. of n.C_{12} = 170.34, Molecular Wt. of isoC_8 = 114.23

Prepared Solutions Data Table

Sample	Wt. of C_{12} gm	Wt of isoC_8 gm	Mmoles of C_{12} mmole	Mmoles of isoC_8 mmole	X_o mole fraction	Mmoles/gm solution mmole/gm
1	0.2972	27.5671	1.7447	241.3298	.00718	8.7235
2	0.4548	27.6651	2.67	242.1877	.0690	8.7076
3	0.5973	27.6443	3.5065	242.0056	.01428	8.6933
4	0.8843	27.6078	5.1914	241.6861	.02103	8.6648
5	1.1098	27.6284	6.5152	241.8664	.02623	8.6428
6	1.2683	27.7320	7.4457	242.7734	.02976	8.6282
7	1.4095	27.5474	8.2746	241.1573	.03317	8.6139

Adsorption Data Table:

Sample	Wt. of solution gm	m_s gm	n mmole	Oscillation Time	X mole-fraction	G mmole/gm	$\frac{X(1-X)}{G}$
1	7.7106	1.1013	67.2634	39935.7	0.00018	0.4275	0.00042
2	7.6387	1.1199	66.5150	39936.5	0.00104	0.5862	0.00176
3	7.5939	1.0708	66.0165	39938.5	0.00315	0.6863	0.00458
4	7.4130	1.1182	64.2320	39943.6	0.00945	0.6651	0.01407
5	7.4988	1.1136	64.8103	39948.3	0.01500	0.6536	0.02261
6	7.4262	1.0683	64.0744	39951.4	0.01848	0.6764	0.02682
7	7.4756	1.0943	64.3941	39954.4	0.02190	0.6634	0.03229

Sample 1:

X_o = initial concentration of n-dodecane in solution, mole-fraction

= 0.00718

m_S = weight of molecular sieve, gm

= 1.1013 gm

$$\text{mmole/gm solution} = \frac{1.7447 + 241.3298}{0.2972 + 27.5671}$$

= 8.7235 mmole/gm

n = number of total mmoles in solution, mmole

Wt. of solution x mmole/gm solution

= 7.7106 x 8.7235 = 67.2634 mmole

X = equilibrium concentration, mole fraction

using calibration curve in Figure C.1 in Appendix C.

X = 0.00018 mole fraction

Calculation of experimentally adsorbed amount of n-dodecane

G = Amount adsorbed of n-dodecane, mmole/gm

$$G = \frac{(X_o - X)n}{m_s} \qquad 4.5$$

$$= \frac{(.00718 - 0.00018)}{1.1013} \times 67.2634$$

= 0.4275 mmole/gm

Calculation of theoretically adsorbed amount of n-dodecane:

Theoretical value of adsorption was determined by modified B.E.T. equation, equation 4.4, by plotting values of

$$\frac{X(1-X)}{G} \quad \text{versus } X$$

to give a straight line as shown in Figure B.1

$$\frac{X(1-X)}{G} = \frac{0.00018\ (1-0.00018)}{0.4275} = 0.00042$$

The equilibrium equation in linear form will be:

$$\frac{X(1-X)}{G} = \frac{1}{a_m(f-1)} + \frac{X}{a_m}$$

The slope of a straight line in Figure B.1 represents a value

$$\frac{1}{a_m},$$

and the intercept represents a value of

$$\frac{1}{a_m(f-1)}$$

$$\text{slope} = 1.4414 = \frac{1}{a_m}$$

$$\text{intercept} = 0.00023 = \frac{1}{a_m(f-1)}$$

$$a_m = 0.69375$$

$$f = 6161.01$$

$$G\ (\text{theoretical}) = \frac{X(1-X)}{0.00023 + 1.4414\ X}$$

First assumption for values of X were established and values for G were calculated.

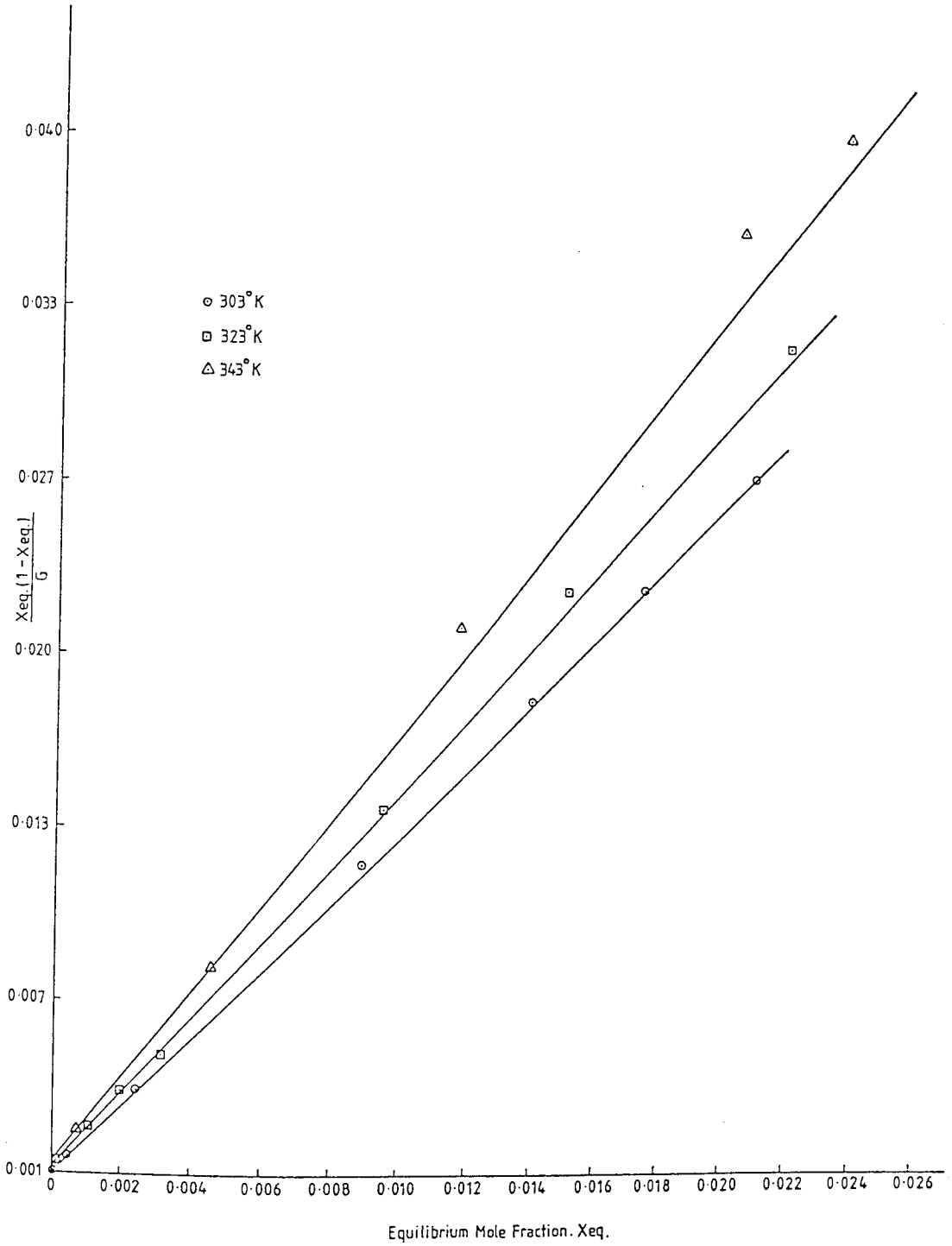

Figure B.1 n-Dodecane systems

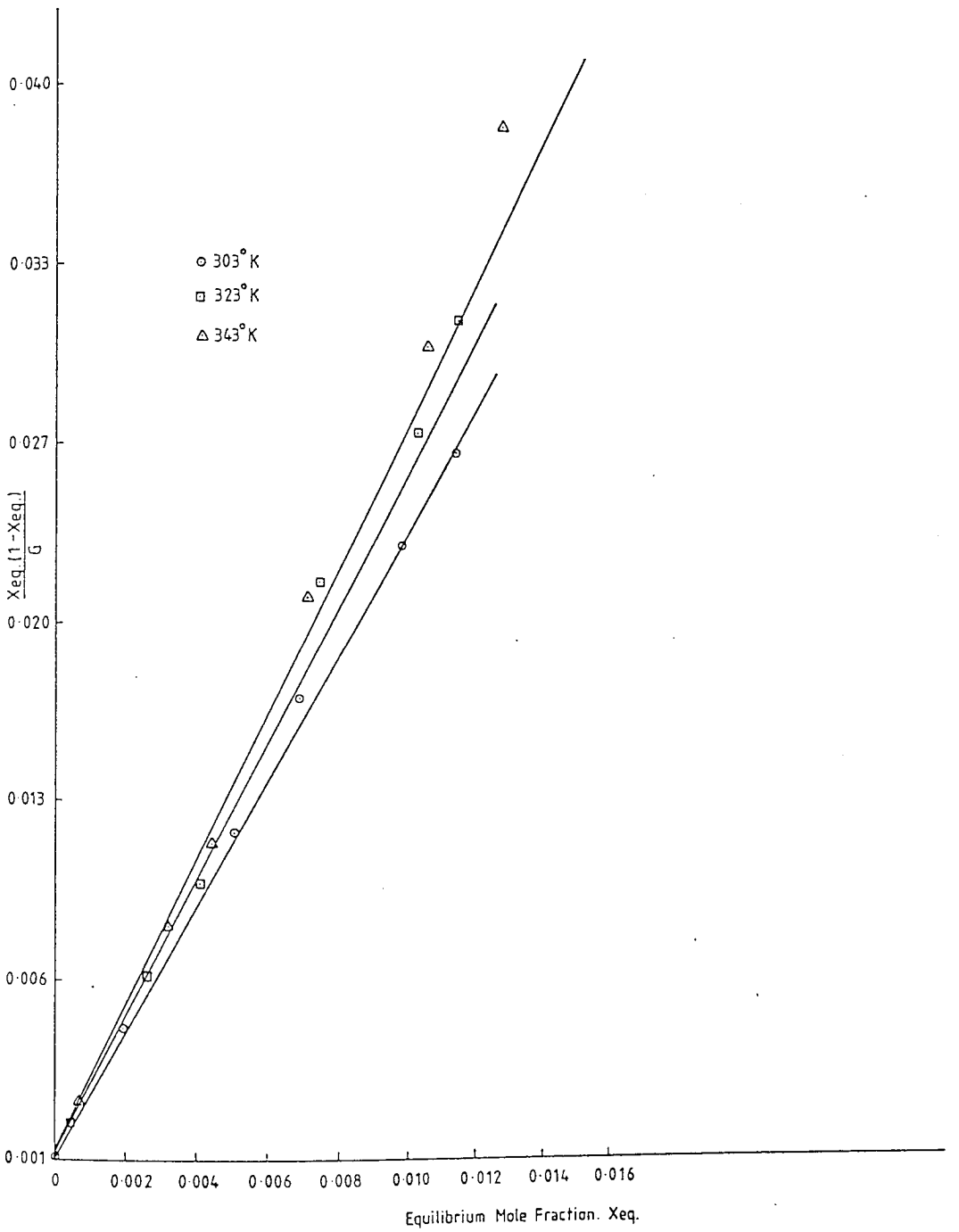

Figure B.2. n-Hexadecane systems

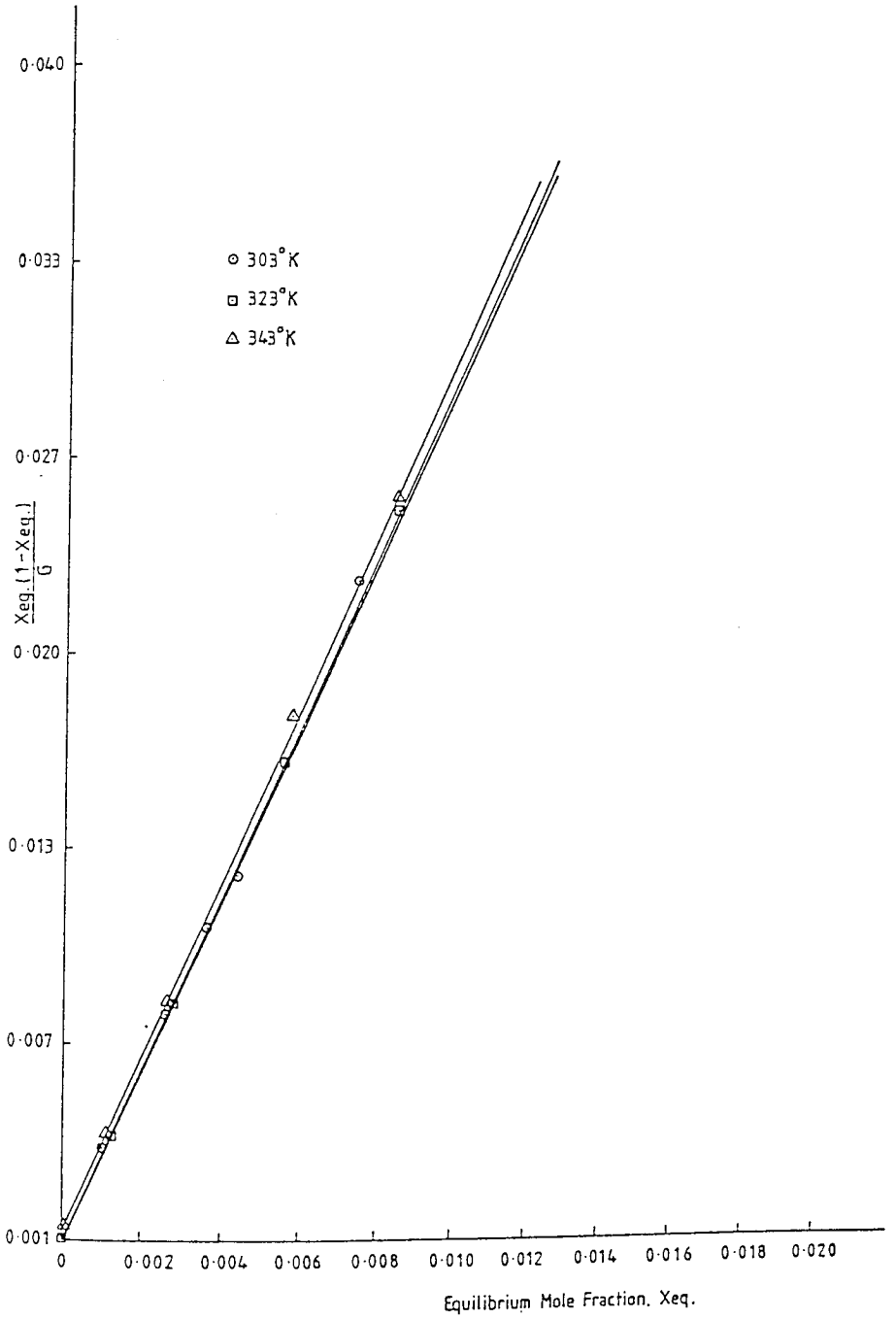

Figure B.3 n-Eicosane systems

X	G
0.0001	0.2644
0.0005	0.5235
0.001	0.5963
0.0015	0.6251
0.002	0.6404
0.003	0.6562
0.005	0.6686
0.007	0.6733
0.01	0.6758
0.02	0.6744

The theoretical and experimental adsorption equilibrium isotherm curve for n-dodecane at 303°K are shown in Figure 9.1.

Heats of Adsorption

Application of Equation 4.9 to the systems under investigation at two different temperatures and constant adsorbate loading G produces heat of adsorption.

For n-dodecane system at temperatures 303°K and 343°K and adsorbate loading of 0.4 mmole/gm.

From Figure 9.1

$$X_1 = 0.0001$$

$$X_2 = 0.00052$$

$$q_{iso}^{0.4} = 4.58 \quad \frac{303 \times 343}{343 - 303} \log \frac{0.00052}{0.0001}$$

$$= 8520 \quad \text{cal/mole}$$

$$= 8.52 \quad \text{kcal/mole}$$

$$= 8.52 \times 4.18 = 35.6 \quad \text{kJ/mole}$$

Heat of adsorption for various levels of adsorbate loading of n-dodecane are shown

below:

G	$\theta = \frac{G}{G_{max}}$	q_{iso}	
mmole/gm		k cal/mole	kJ/mole
0.25	0.36	6.5	27.2
0.3	0.43	7.5	31.4
0.4	0.58	8.5	35.6
0.5	0.72	12.8	53.6
0.55	0.79	15.9	66.6
0.575	0.83	19.0	79.5

The isosteres were plotted according to the following data:

1/Temp	G n-dodecane mole/kg						G n-hexadecane mole/kg						G n-eicosane mole/kg					
(x 10^3)	0.3		0.4		0.55		0.2		0.3		0.35		0.25		0.3		0.31	
K^{-1}	x	logx	x	logx	x	logx	x	logx	x	logx	x	logx	x	logx	x	logx	x	log
3.3	.00007	-4.1	0.0001	-4.0	0.00012	-3.9	0.00008	-4.1	.0001	-4.0	.00015	-3.8	0.00007	-4.2	0.0001	-4.0	0.00014	-3.8
3.09	0.00013	-3.9	0.00023	-3.6	0.00059	-3.2	0.00008	-4.1	.00029	-3.5	.0008	-3.1	0.00012	-3.9	0.00016	-3.8	0.00019	-3.7
2.91	.0003	-3.5	0.00052	-3.3	.0026	-2.6	0.00019	-3.7	.00062	-3.2	.0025	-2.6	0.00021	-3.7	0.0004	-3.4	0.00052	-3.3

The slope of isostere in case of n-dodecane at G = 0.3 is equal to 1522.3

$$\therefore \quad q_{iso}^{0.3} = 1522.3 \times 4.53 = 7.0 \text{ kcal/mole}$$

$$= 29.0 \text{ kJ/mole}$$

B.2. Kinetics Experiments

Example Run 3.

System: n-dodecane, isooctane at 343°K

Initial concentration = 0.01 mole fraction

Molecular sieve Type 5A in the form of 1/8 inch Pellets.

Sample	Time (t) hr	$\sqrt{t}$ $\sqrt{hr}$	Amount Adsorbed G_t mmole/gm	Relative Adsorption G_t/G_∞	D_e $(x10^{10})m^2/sec$
1	0.25	0.5	0.130	0.214	0.154
2	0.50	0.71	0.217	0.356	0.213
3	1.00	1.0	0.302	0.495	0.205
4	2.00	1.41	0.470	0.772	0.25
5	3.00	1.73	0.428	0.703	0.138
6	3.83	1.96	0.463	0.760	0.126
7	11.00	3.32	0.552	0.906	0.063
8	15.00	3.87	0.609	1.0	0.056

Kinetics of relative adsorption was illustrated by plotting values of G_t/G_∞ versus values of $\sqrt{t}$ as shown in Figure 9.9.

Effective Diffusion Coefficient D_e:

The equation given by Barrer and Brook(75) was used to calculate the effective diffusion coefficient

$$D_e = \frac{\pi}{4t} \left(\frac{V}{A}\right)^2 \left(\frac{G_t}{G\infty}\right)^2 \qquad 4.10$$

where,

$\frac{A}{V}$ = the ratio of the external surface area of granual to its total volume

For molecular sieve Type 5A - $\frac{1}{8}$ inch pellet [69]:

$\frac{V}{A}$ = 0.062 cm.

Sample 1:

$$D_e = \frac{\pi}{4 \times .25} \times (.062)^2 \ (0.214)^2 \times \frac{1}{36000000}$$

$$= 0.154 \times 10^{-10} \ m^2/sec.$$

Activation Energy E:

In accordance with Equation 4.15, and using Figure 9.9

At G/G_∞ = 0.25

T_1 = 303°K

T_2 = 343°K

t_1 = 0.5929 hr

t_2 = 0.283 hr

$$E = 4.58 \frac{T_1 \ T_2}{T_2 - T_1} \log \frac{t_1}{t_2}$$

$$E = 4.58 \frac{303 \times 343}{343 - 303} \log \frac{.5929}{.283}$$

= 3822 cal/mole

= 3.822 kcal/mole

= 3.822 x 4.186 = 16.0 kJ/mole

B.3. Dynamic Experiments

Adsorption Condition Run 1

Feed concentration wt%, mole-fraction of C_{12}		1.8, 0.012
Temperature	^oK	323
Feed rate	m^3/sec	5×10^{-3}
Particle size (d)	m	1.5×10^{-3}
Sieve weight, height	kg,m	0.0662, 0.388

Experimental Data

Sample No.	Oscillation Time[1] at 25°C	n-dodecane mole fraction (x)	Time[2] min.	W[3] kg	Y[4] kg/kg	Y/Y_o	$\frac{W-W_b}{W_a}$
1	39935.5	0	10	0.0205	0	0	-
2	39935.5	0	140	0.2849	0	0	-
3	39936.0	0.0006	145	0.2950	0.001	0.054	-
4	39936.4	0.0009	155	0.3154	0.0015	0.081	0.002
5	39936.7	0.0012	165	0.3357	0.002	0.108	0.106
6	39937.5	0.0021	175	0.356	0.0032	0.173	0.210
7	39938.0	0.0026	180	0.3662	0.004	0.216	0.263
8	39938.5	0.0033	185	0.3764	0.005	0.270	0.315
9	39939.5	0.0043	190	0.3866	0.0068	0.368	0.367
10	39940.4	0.0053	195	0.3968	0.008	0.432	0.42
11	39940.8	0.0058	200	0.4069	0.009	0.487	0.471
12	39941.6	0.0071	205	0.4171	0.0109	0.589	0.524
13	39942.3	0.0079	210	0.4273	0.012	0.649	0.576
14	39942.6	0.0083	215	0.4375	0.0125	0.676	0.628
15	39943.4	0.0092	220	0.4476	0.014	0.757	0.68
16	39943.6	0.0094	225	0.4578	0.0143	0.773	0.732
17	39944.0	0.0099	230	0.468	0.015	0.811	0.785
18	39944.4	0.0103	235	0.4782	0.0158	0.854	0.837
19	39944.9	0.0109	245	0.4985	0.0169	0.914	0.941
20	39945.4	0.0116	260	0.529	0.018	0.973	-
21	39945.8	0.012	279	0.5677	0.0185	1.0	-

Feed concentration (Y_o) = 0.0185

(1) the figure displayed by Density meter

(2) measured from first appearance of effluent at sample tap.

(3) solute-free effluent

(4) kg solute/kg solvent, Y estimated using mole fraction and Figure B8. The mole fraction was estimated using calibration curve Figure C.1 and oscillation time.

For sample number 7:

W = (feed rate) (feed density) (wt% solvent in feed) (time)

feed rate = $5 \times 10^{-8} \times 60$ m^3/min

feed density = 690.69 kg/m^3

wt% solvent in feed = 0.982

time = 180 min

W = $5 \times 10^{-8} \times 60 \times 690.69 \times 0.982 \times 180$ = 0.3662 kg of solute-free effluent

Experimental breakthrough data were plotted as Y/Y_o versus W in Figure B.4

From Figure B.4

Breakthrough point (W_b) = 0.315

Exhaustion point (W_e) = 0.51

Zone width (W_a) = $W_e - W_b$ = 0.195

$$\frac{W - W_b}{W_a} = \frac{0.3662 - 0.315}{0.195} = 0.263$$

The experimental breakthrough data were plotted as Y/Y_o versus

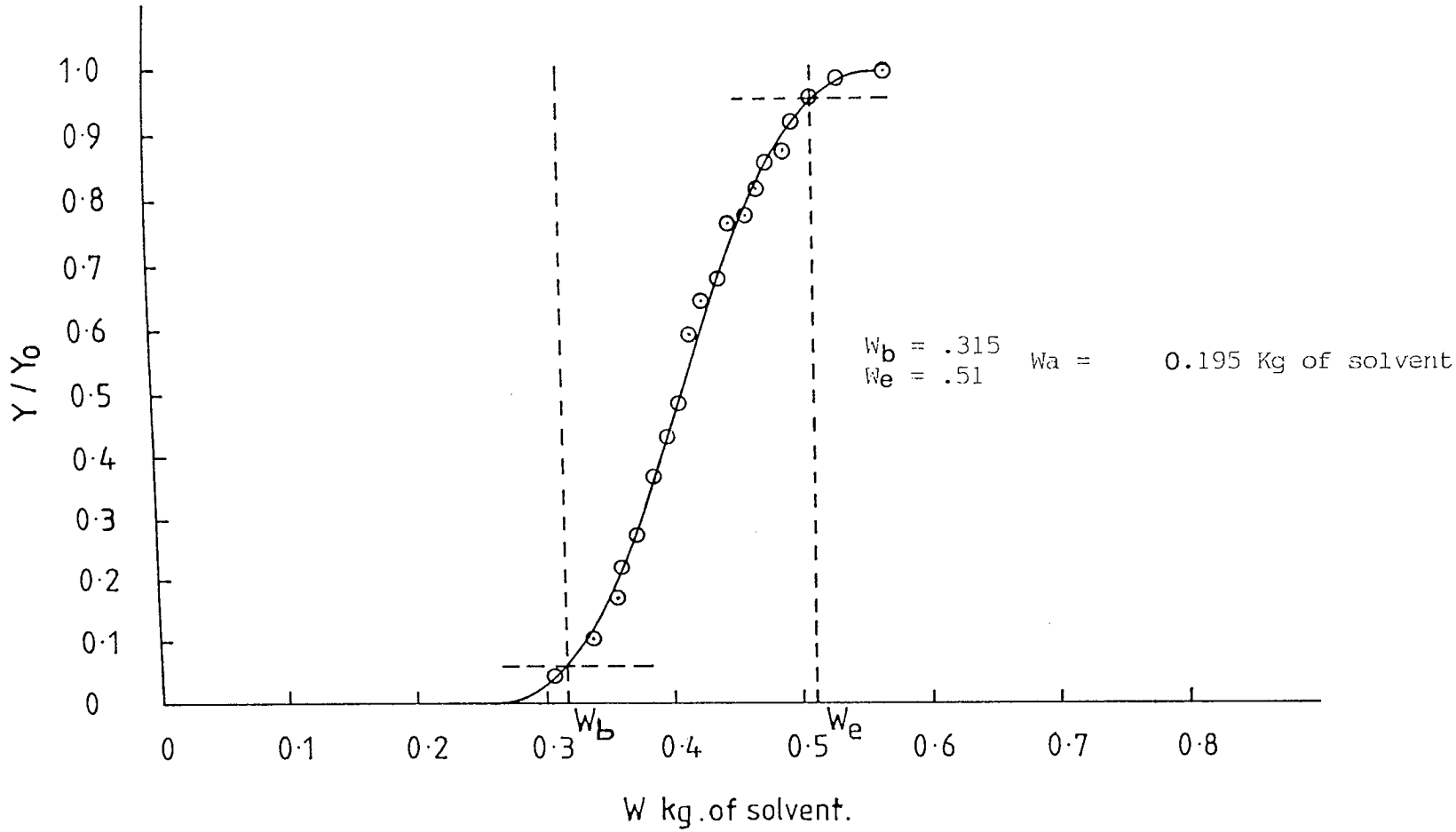

Figure B.4 Breakthrough curve, Run 1

Figure B.8 Mole fraction versus kg solute / kg isooctane

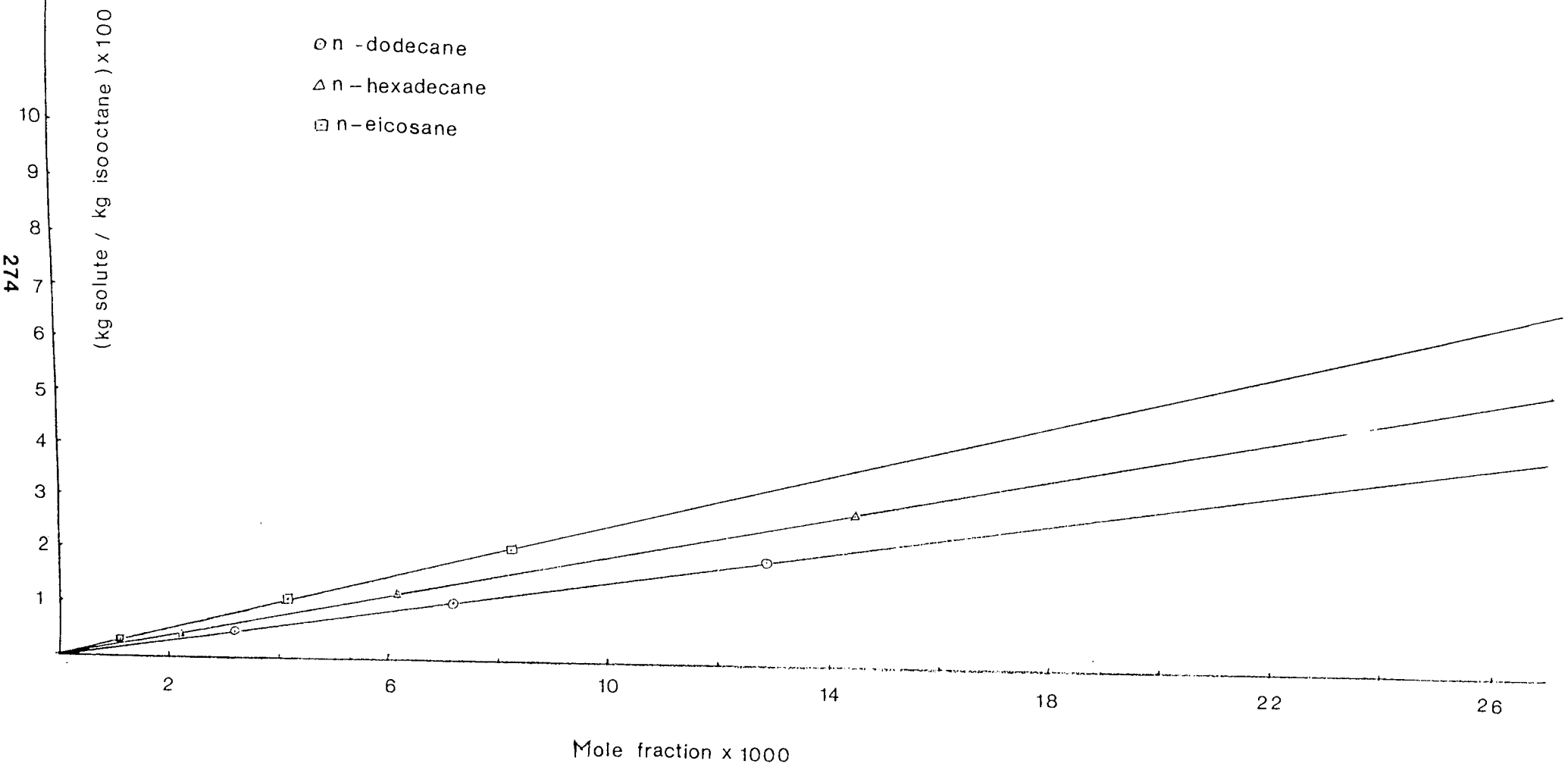

$$\frac{W - W_b}{W_a}$$

in Figure 9.36.

Calculation of breakthrough curve using equilibrium isotherm data

Point	mole fraction x	amount adsorbed G mmole/gm adsorbent	amount adsorbed X kg/kg adsorbent	Y kg solute/ kg solvent
1	0.0003	0.400	0.068	0.0004
2	0.0005	0.535	0.091	0.0009
3	0.001	0.600	0.102	0.0017
4	0.0015	0.630	0.107	0.0023
5	0.004	0.664	0.113	0.0061
6	0.006	0.670	0.114	0.0092
7	0.008	0.675	0.115	0.0122
8	0.01	0.678	0.1155	0.0153

The data in the first two columns in the above table are from the n-dodecane isotherm at 50°C in Figure 9.1.

$$\text{Amount adsorbed } X = G \times \frac{\text{Molecular weight}}{1000}$$

$$X \text{ at point } 3 = 0.6 \times \frac{170.34}{1000} = 0.102 \text{ kg solute/kg adsorbent}$$

The equilibrium data were plotted as Y versus X in Figure B.5.

The operating line was drawn passing through the origin, where the molecular sieve, was free of solute, to intersect the equilibrium curve at $Y_o = 0.0185$ as shown in Figure B.5.

X	Y	Y*	$\frac{1}{Y - Y^*}$	$\int_{Y_b}^{Y} \frac{dy}{Y - Y^*}$	$\frac{W - W_b}{W_a}$	Y/Y_o
(1)	(2)	(3)	(4)	(5)	(6)	(7)
kg/kg ads.	kg/kg solv.	kg/kg solv.				
0.006	0.001	0.00004	1041.7	0.0	0.0	0.054
0.02	0.0032	0.00011	323.6	1.0	0.356	0.173
0.03	0.0048	0.0002	217.4	1.486	0.528	0.259
0.04	0.0064	0.00023	162.9	1.784	0.634	0.344
0.06	0.0095	0.00036	109.4	2.139	0.760	0.514
0.08	0.0128	0.0006	82.0	2.453	0.872	0.692
0.09	0.0144	0.00085	73.8	2.578	0.916	0.778
0.1	0.016	0.0015	69.0	2.69	0.956	0.865
0.11	0.0176	0.003	68.5	2.8	0.995	0.951
0.111	0.0178	0.0034	68.4	2.813	1.0	0.962

In the above Table, the second column lists values of Y on the operating line between $Y_b = 0.001$ and $Y_e = .0178$ and the third column the corresponding values of Y* taken from the equilibrium curve at the same value of X.

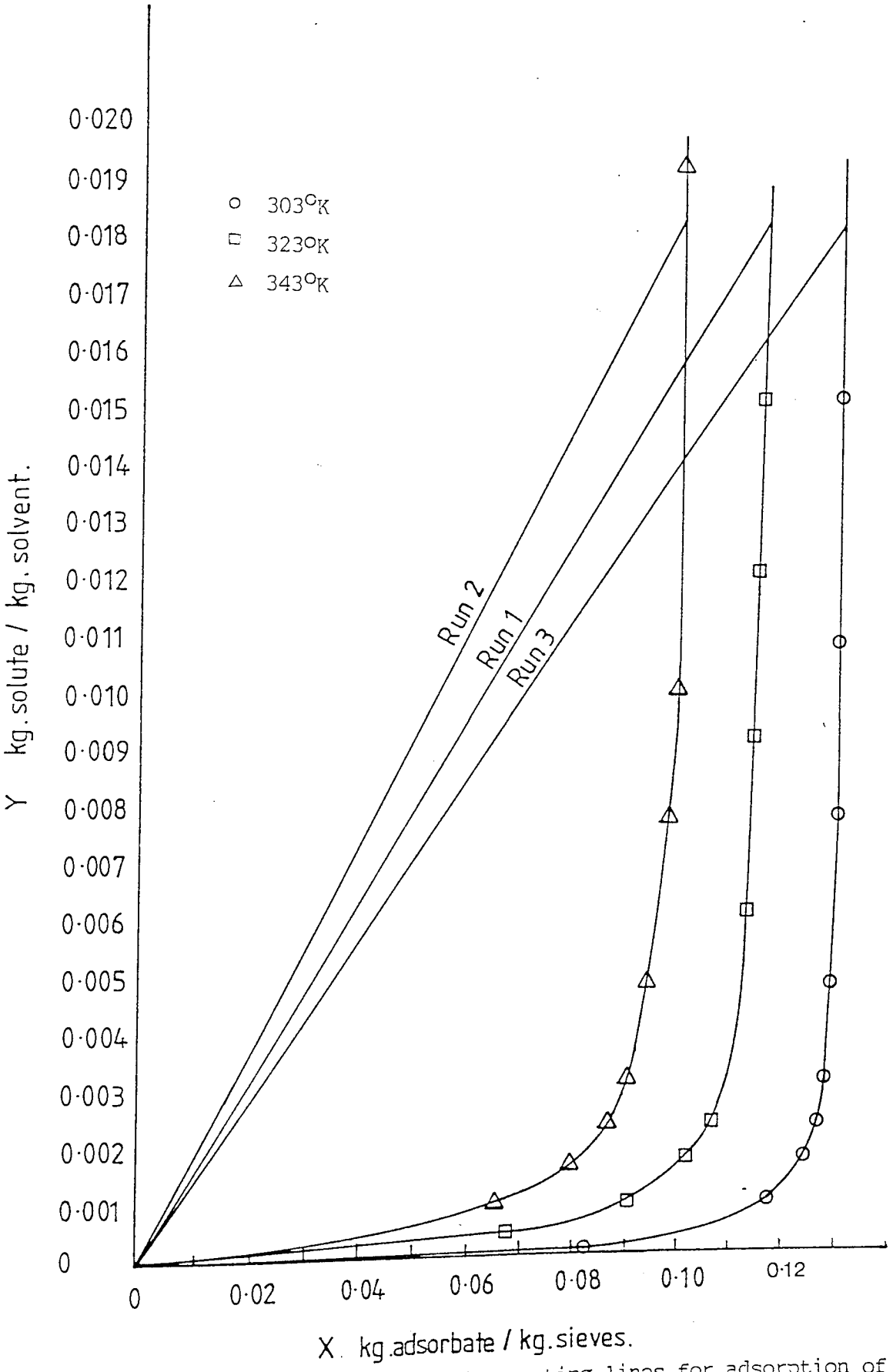

Figure B.5 Equilibrium curves and operating lines for adsorption of n-dodecane

The values of breakthrough point Y_b and exhaustion point Y_e were calculated as 0.05% and 0.95% respectively, where Y_o is the initial concentration of the feed = 0.0185 kg/kg solvent.

Figure B.6 illustrates a curve plotted from the data in columns 2 and 4.

Integrating graphically between each value of Y and Y_b in Figure B.6 would produce the number of transfer units corresponding to each value of Y as shown in column 5. The total number of transfer units corresponding to the adsorption zone was hence,

$$N_t = \int_{Y_b}^{Y_e} \frac{dY}{Y - Y^*} = 2.813 \qquad \text{A.6}$$

In accordance with Equation A.8, division of each entry in column 5 by 2.813 yielded the values in column 6. The calculated breakthrough data were plotted in Figure 9.36 using values of Y/Y_o from column 7 versus values of

$$\frac{W - Wb}{Wa}$$

from column 6.

Estimation of fractional ability of the adsorbent to adsorb additional solute within the adsorption zone (f)

From Equation A.3

$$f = \int_{o}^{1.0} \left(1 - \frac{Y}{Y_c}\right) d\left(\frac{W - Wb}{Wa}\right)$$

Hence f equals the entire area above the curve of Figure 9.36 (experimental curve) up to $Y/Y_O = 1.0$.

By graphical integration, $f = 0.48$.

Determination of Total Dynamic Capacity (T.D.C.)

According to Equation 5.4 the total dynamic capacity of the adsorption bed may be calculated.

$$\text{T.D.C.} = \frac{Y_o}{m_s} \text{ (area above breakthrough curve between W=0 and W=} \bullet \text{ in Figure B.4)}$$

where:

m_S = weight of molecular sieve

$$\text{T.D.C.} = \frac{.0185}{.0662} \times 0.4087 = 0.1142 \text{ kg n-dodecane/kg sieve}$$

Adsorption Zone Height (Method 1)

$$Z_a = Z \frac{W_a}{W_e - (1-f)W_a} \qquad 5.1$$

$$Z_a = 0.388 \left[\frac{0.195}{0.51 - (1-0.48)\ 0.195} \right] = 0.185 \text{ m}$$

where

$Z = 0.388$ m

$f = 0.48$

$W_a = 0.195$ kg of solute - free effluent

$W_e = 0.51$ kg of solute free effluent

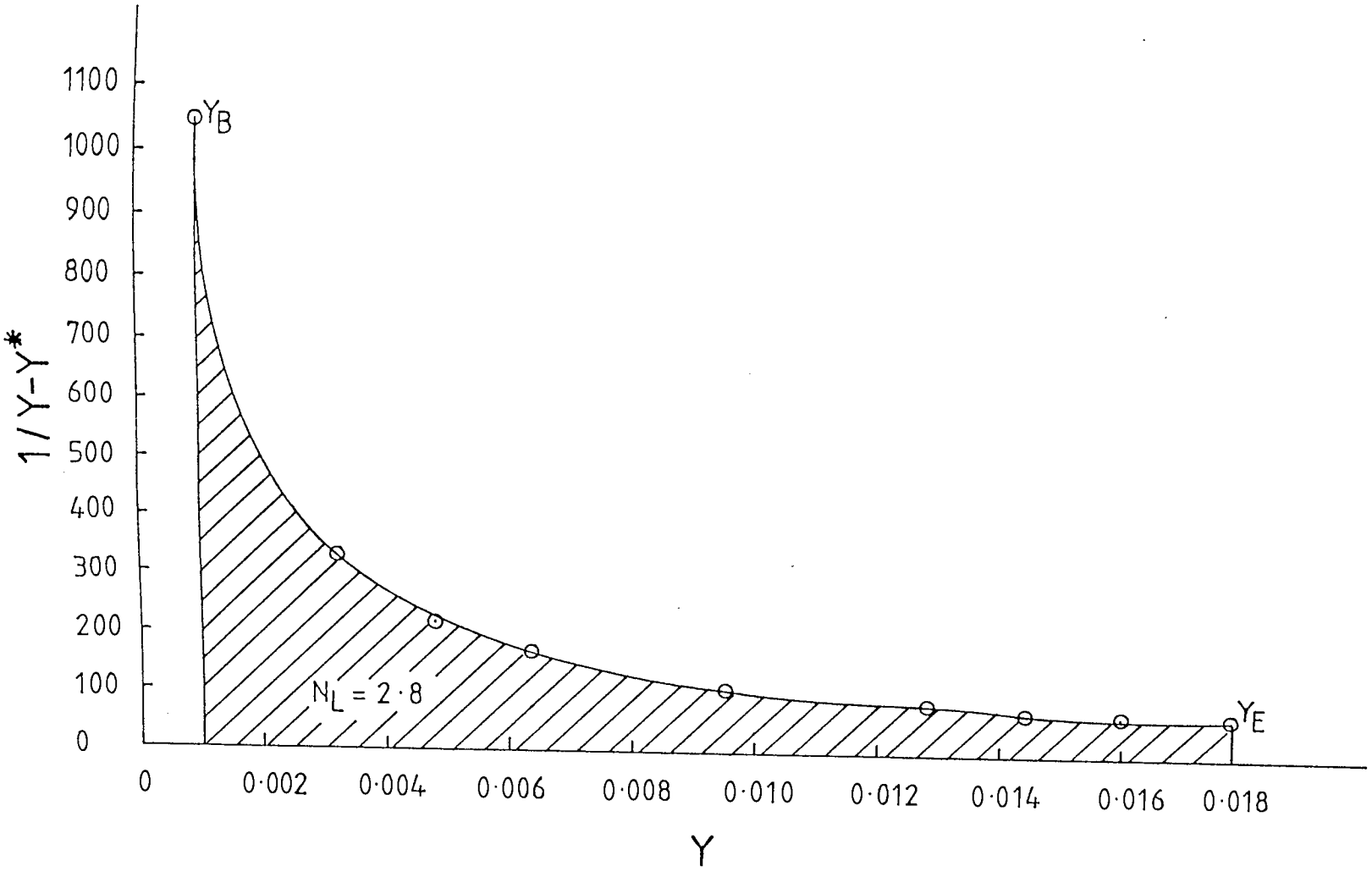

Figure B.6 Estimation of the number of transfer units, Run 1.

Adsorption Zone Height (Method 2)

$$Z_a = \frac{Q_a}{A\,\rho_b\,f\,(T.D.C.)} \qquad 5.2$$

where

Q_a = quantity of solute adsorbed between the breakthrough and exhaustion points, kg

$$= Y_o \int_{W_b}^{W_e} \frac{Y_o - Y}{Y_o}\,dw$$

= Y_o (area above breakthrough curve between W_b and W_e in Figure B.4)

= .0185 x 0.0936 = 0.00173 kg n-dodecane

$A = 2.243 \times 10^{-4}\ m^2$

$$\rho_b = \text{bed density} = \frac{m_s}{A \times Z} = \frac{.0662}{2.243 \times 10^{-4} \times 0.388} = 760.7\ \frac{\text{kg sieve}}{m^3}$$

T.D.C. = 0.1142 kg/kg sieve

$$Z_a = \frac{0.00173}{2.243 \times 10^{-4} \times 760.7 \times 0.48 \times 0.1142} = 0.185\ m$$

Degree of Saturation

$$\text{Degree of Saturation} = \frac{Z - f Z_a}{Z} \qquad 5.7$$

$$= \left[\frac{0.388 - 0.48 \times 0.185}{0.388}\right] \times 100 = 77.1\%$$

Length of Unused Bed (LUB)

$$LUB = \left[\frac{\theta_s - \theta_b}{\theta_s}\right] Z \qquad 5.6$$

From Figure 9.18

θ_b = 177 minutes $\quad \theta_s$ = 216 minutes

$$LUB = \left[\frac{216 - 177}{216}\right] .388 = 0.07 \text{ m}$$

Experimental Overall Mass Transfer Coefficient ($K_y a$)

From Equation 5.20

$$K_y a = \frac{N_t G_s}{Z_a}$$

where

G_s = solute free fluid mass velocity

= $U \rho_f$ x wt% solvent

$$U = \frac{V_t}{\varepsilon A}$$

V_t = feed volumetric flow rate = 5×10^{-8} m^3/sec

ε = voidage of adsorbent bed = 0.59

ρ_f = density of fluid feed = $\rho_{n\text{-}c12}\, x_{n\text{-}c12} + \rho_{iso\text{-}c8}\, x_{iso\text{-}c8}$

= $748.0 \times 0.012 + 690 \times 0.988 = 690.7$ kg/m^3

$$U = \frac{5 \times 10^{-8}}{0.59 \times 2.243 \times 10^{-4}} = 3.778 \times 10^{-4} \text{ m/sec}$$

$$\text{wt\% solvent} = \frac{100 - 1.8}{100} = 0.982$$

$$G_s = 3.778 \times 10^{-4} \times 690.7 \times 0.982 = .2562 \text{ kg/m}^2\text{sec}$$

$$Z_a = 0.185 \text{ m}$$

$$N_t = 2.813$$

$$K_y a = \frac{2.813 \times .2562}{0.185} = 3.9 \text{ kg/m}^3\text{sec}$$

External Film Mass Transfer Coefficient ($k_y a$)

$$Sh = \frac{1.09}{\varepsilon} (R_e)^{0.33} (S_c)^{0.33} \qquad .0015<R_e<55 \qquad 5.11$$

$$Sh = \frac{2 k_f R_p}{D_m}$$

R_p = average radius of sieve particles

$$= \frac{(1+2)}{4} 10^{-3} \text{ m}$$

D_m = molecular diffusivity m^2/sec

k_f = effective mass transfer coefficient m/sec

Scheibal proposed the following correlation(76)

$$D_{AB} = \frac{K T}{\mu_B V_A^{\frac{1}{3}}}$$

where,

D_{AB} = mutual diffusion coefficient of solute A at low concentration in solvent B, cm^2/s

T = absolute temperature, ^oK

μ_B = viscosity of solvent B, cp.

V_A = molal volume of solute A at its normal boiling temperature, cm^3/g-mole

K = constant = 17.5×10^{-8} for solvents other than water and benzene and where $V_A > 2.5\ V_B$

To estimate the liquid molal volume at normal boiling point for the systems under investigation, which are of weakly associated liquids, it is convenient to use Schroeder rule(76).

$V_{c_{12}}$ = 252 cm^3/g-mole

Vc_{16} = 364 cm^3/g-mole

$V_{c_{20}}$ = 434 cm^3/gm-mole

$V_{iso\text{-}c_8}$ = 182 cm^3/gm-mole

$V_A > 2.5\ V_B$ in all systems under investigation

$\therefore$ K = 17.5×10^{-8}

The viscosities of the solutes and solvent were taken from reference(77).

	303°K	323°K	343°K
$\mu_{c_{12}}$ cp	1.248	0.9215	0.7099
$\mu_{c_{16}}$ cp	2.748	1.840	1.326
$\mu_{c_{20}}$ cp	4.704	3.275	2.215
$\mu_{iso\text{-}c_8}$ cp	0.465	0.357	0.295

$$D_m = \frac{17.5 \times 10^{-8} \times 323}{0.357 \times (252)^{1/3}} = 0.2507 \times 10^{-4} \text{ cm}^2/\text{s}$$

$$= 0.2507 \times 10^{-8} \text{ m}^2/\text{s}$$

$$R_\epsilon = \frac{\rho_f U \varepsilon (2 Rp)}{\mu}$$

The densities of the solutes and solvent were taken from reference(78).

	303°K	323°K	343°K
$\rho_{c_{12}}$ gm/cm^3	0.7424	0.7274	0.7125
$\rho_{c_{16}}$ gm/cm^3	0.7683	0.7544	0.7405
$\rho_{c_{20}}$ gm/cm^3	0.7777	0.7642	0.7507
$\rho_{iso\text{-}c_8}$ gm/cm^3	0.6837	0.6680	0.6498

ρ_f = ($\rho_{c_{12}}$ at 50°C) x mole fraction + (ρ_{c_8} at 50°C) x mole fraction

ρ_f = 727.4 x .012 + 668.0 x .988 = 668.7 kg/m^3

μ_f = $\mu_{c_{12}}$ at 50°C x mole fraction + μ_{c_8} at 50°C x mole fraction

= .9215 x .012 + 0.357 x 0.988 = 0.364 cp

= .364 x 10^{-3}

$$\frac{\text{N sec}}{\text{m}^2}$$

$$R_\epsilon = \frac{668.7 \times 3.778 \times 10^{-4} \times 0.59 \times 2 \times \frac{1.5}{2} \times 10^{-3}}{0.364 \times 10^{-3}}$$

= 0.614

$$Sc = \frac{\mu}{\rho_f D_m} = \frac{0.364 \times 10^{-3}}{668.7 \times 0.2507 \times 10^{-8}} = 217$$

$$Sh = \frac{2 k_f R_p}{D_m} = \frac{2 k_f \times \frac{1.5}{2} \times 10^{-3}}{0.2507 \times 10^{-8}}$$

$$k_f = \frac{1.09 \times 0.2507 \times 10^{-8}}{1.5 \times 10^{-3} \times .59} R_e^{.33} Sc^{.33}$$

$$R_e^{0.33} = 0.8513$$

$$Sc^{0.33} = 5.902$$

$$k_f = \frac{1.09 \times 0.2507 \times 10^{-8} \times 0.8513 \times 5.902}{1.5 \times 10^{-3} \times .59} = 155.1 \times 10^{-7} \text{ m/sec}$$

The specific solid surface (a) for fixed beds was calculated from the following relation proposed by Treybal[42]

$$a = \frac{6 (1 - \varepsilon)}{d_p}$$

where

a = the specific solid surface, m^2 surface/m^3 bed

ε = voidage of the bed

d_p = diameter of a sphere m

Sieve particle size range (m)	a (m^2/m^3)
$(1 - 2) \times 10^{-3}$	1640
$(0.5 - 1) \times 10^{-3}$	3392
$(0.032 - 0.5) \times 10^{-3}$	9699

$k_y a = k_f \times \rho_{iso\text{-}c_8} \times a = 155.1 \times 10^{-7} \times 668.0 \times 1640 = 16.9 kg/sec\ m^3$

Solid-Phase Mass Transfer Coefficient ($k_p a$)

$$k_p a = \frac{60\, D_m\, \varepsilon_p}{d_p^2\, \tau}\, \rho_{iso\text{-}c_8} \qquad 5.18$$

$\tau = 2$ (33)

$\varepsilon_p = 0.33$ (33)

$$k_p a = \frac{60 \times 0.2507 \times 10^{-8} \times .33 \times 668}{(1.5)^2 \times 10^{-6} \times 2} = 7.37\ kg/sec\ m^3$$

Theoretical Overall Mass Transfer Coefficient (Ky a)

$$K_y a = \left[\frac{1}{ky\, a} + \frac{1}{kp\, a}\right]^{-1}$$

$$= \left[\frac{1}{16.9} + \frac{1}{7.37}\right]^{-1} = 5.1\ kg/sec\ m^3$$

Equilibrium Constant K

The slope of the isotherm, Figure B.7, between its origin and the point corresponding to the inlet concentration = 67.8 mole/kg sieve,

$$K = 67.8 \times \frac{\text{m.wt.}}{1000} \times \frac{\rho_b}{\rho_{c_{12}}}$$

$$K = 67.8 \times \frac{170.39}{1000} \times \frac{775.9}{727.4} = 12.3$$

Theoretical relation between the overall mass transfer coefficient and the molecular diffusivity

According with Wilson and Geankpolis correlation 5.12 :

$$Sh = \frac{1.09}{\varepsilon} (Re)^{0.33} (Sc)^{0.33}$$

$$\frac{2 k_y R_p}{D_m} = \frac{1.09}{\varepsilon} \left(\frac{2 \rho_f U R_p \varepsilon}{\mu} \right)^{0.33} \left(\frac{\mu}{\rho_f D_m} \right)^{0.33}$$

$$k_y = \frac{1.09 D_m^{0.66}}{2 \varepsilon R_p^{0.66}} (2 U \varepsilon)^{0.33}$$

$$\frac{1}{K_y a} = \frac{1}{k_p a} + \frac{1}{k_y a}$$

In systems studied $k_p a \simeq 0.5 k_y a$

$$\therefore \quad \frac{1}{K_y a} = \frac{3}{k_y a}$$

$$\therefore \quad K_y a = \frac{k_y a}{3} = \frac{1.09\, D_m^{0.66}}{6\varepsilon\, R_p^{0.66}} \, (2U\varepsilon)^{0.33}$$

$$\therefore \; K_y \propto D_m^{0.6}$$

The overall mass transfer coefficient is proportional to the molecular diffusivity to the power of 0.66.

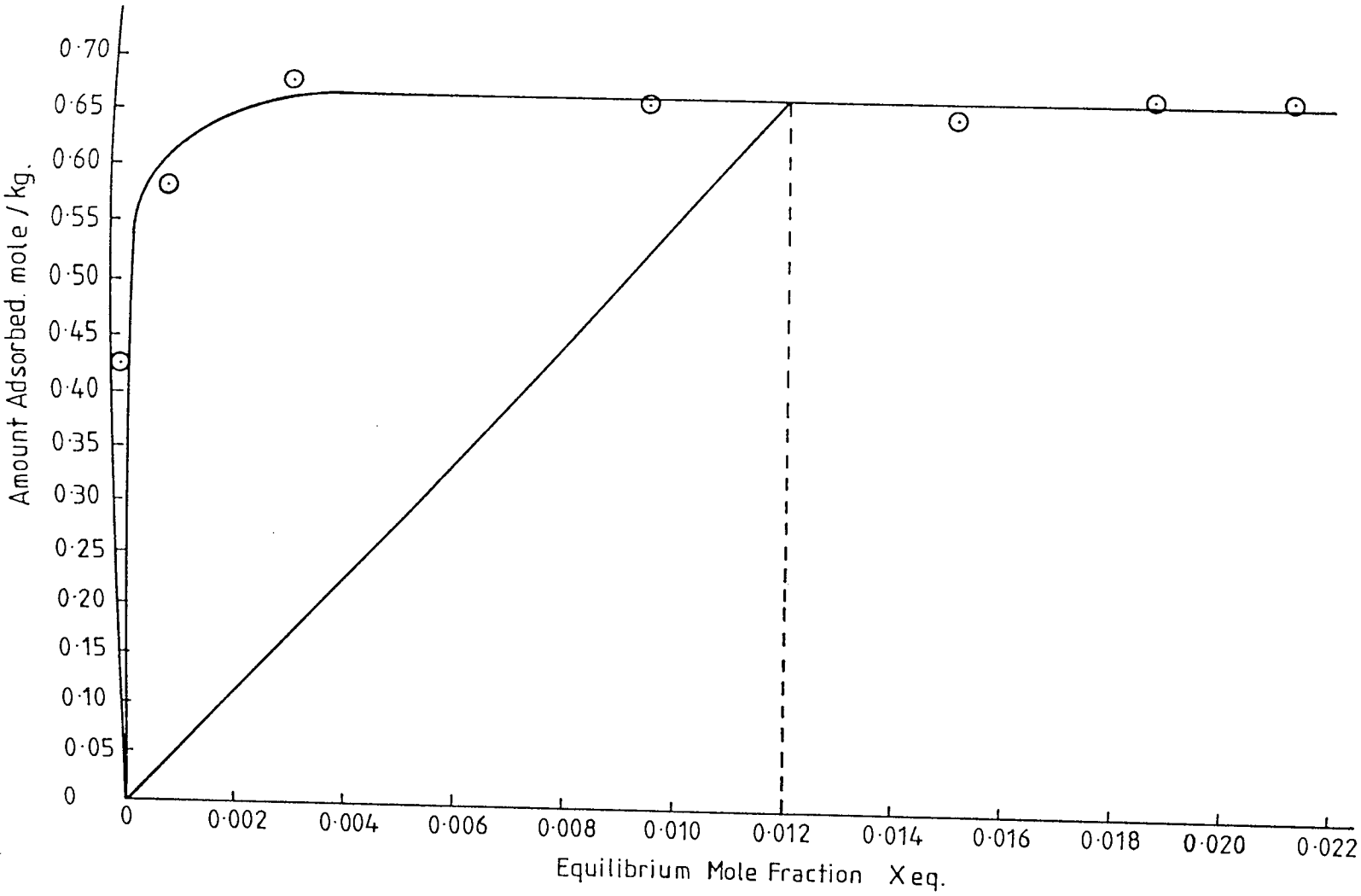

Figure B.7 Estimation of Equilibrium constant (K), Run 1

Program for solution of the mathematical model
proposed in chapter 8

```
@ED,U TEST.BSL
CASE UPPER ASSUMED
ED 1.P1C. SAT-06/20/87-18:22:52-(54,55)
EDIT
C:
      1:          DIMENSION A(2)
      2:          COMMON XL,XK,XKF,V,B,XM,COF
      3:          EXTERNAL FTR
      4:          TI=20.*60.0
      5:          TF=300.*60.0
      6:          TINC=10.*60.0
      7:          N=(TF-TI)/TINC
      8:  9     PRINT*,' KF , L , B , K , V , M '
      9:        READ(5,*)XKF,XL,B,XK,V,XM
     10:        IF (XK.EQ.0 .OR. XKF.EQ.0 ) GO TO 100
     11:         COF=3.*XKF/(V*B*XM)
     12:         A(1)=0.0
     13:         A(2)=     XL
     14:        M=2000
     15:        PRINT 11,XKF,XL,B,XK,V,XM
     16:    11 FORMAT(5X,' DATA ENTERED ARE AS FOLLOWS :',//
     17:       &  ,20X,'KF = ',E15.9,/
     18:       &  ,20X,'L  = ',F7.3,/
     19:       &  ,20X,'B  = ',E15.9,/
     20:       &  ,20X,'K  = ',F7.3,/
     21:       &  ,20X,'V  = ',E15.9,/
     22:       &  ,20X,'M  = ',F5.2,//,5X,'PREDICTED CURVE :'/)
     23:        DX=(A(2)-A(1))/REAL(M)
     24:         DO 20 I=1,N+1
     25:         FK=1
     26:         T=TI+(I-1)*TINC
     27:        SUM=0.0
     28:        X=A(1)
     29:        Y1=FTR(T,X)
     30:        YN=FTR(T,A(2))
     31:        DO 5 J=2,M-1
     32:        X=A(1)+(J-1)*DX
     33:        SUM=SUM+2*(FTR(T,X))
     34:  5     CONTINUE
     35:        FX=DX/2.0 *( Y1+SUM+YN)
     36:C       F=1.-EXP((3.*XKF/(L*XK))*((XL/V)-T))*FX
     37:          F=1.-COF*FX
     38:        WRITE(6,*)T,F
     39:    20  CONTINUE
     40:        GO TO 9
     41:  100  STOP
     42:        END
     43:        FUNCTION FTR(T,X)
     44:        COMMON XL,XK,XKF,V,B,XM,COF
     45:C       PRINT*,X,T,X/V,XKF**2,B**2,V,XM,XK
     46:        Y=2.0*SQRT((9.*X*(T-(X/V))*XKF**2)/(B**2.*V*XM*XK))
     47:        BSL=BSSL(Y,2)
     48:        FTR=EXP((-3.*XKF/B)*((T-X/V)/XK + X/(V*XM) ) )* BSL
     49:        RETURN
     50:        END
EOF:50
0:
```

Predicted breakthrough data

Experimental Run 1

```
@XQT TEST.ESL
  KF  ,  L  ,  B  ,  K  ,  V  ,  M
     DATA ENTERED ARE AS FOLLOWS :

                        KF =  .9149999 98-0 05
                        L  =    .390
                        B  =  .7499999 99-0 03
                        K  =  12.300
                        V  =  .3780000 01-0 03
                        M  =  1.44
    PREDICTED CURVE :

 1200.0000        .1 0474746
 1800.0000        .1 0474798
 2400.0000        .1 0475373
 3000.0000        .1 0482484
 3600.0000        .1 0523409
 4200.0000        .1 0679697
 4800.0000        .1 1126038
 5400.0000        .1 2147468
 6000.0000        .1 4106819
 6600.0000        .1 7358455
 7200.0000        .2 2136486
 7800.0000        .2 8463282
 8400.0000        .3 6117052
 9000.0000        .4 4669253
 9600.0000        .5 3574745
 10200.000        .6 2280595
 10800.000        .7 0319785
 11400.000        .7 7368763
 12000.000        .8 3263907
 12600.000        .8 7984456
 13200.000        .9 1615911
 13800.000        .9 4307688
 14400.000        .9 6235208
 15000.000        .9 7571693
 15600.000        .9 8470844
 16200.000        .9 9058686
 16800.000        .9 9433355
 17400.000        .9 9665906
 18000.000        .9 9806932
```

Predicted breakthrough data

experimental Run 15

KF , L , S , K , V , M
DATA ENTERED ARE AS FOLLOWS :

KF = .84299998-005
L = .390
S = .74999998-003
K = 9.100
V = .37800001-003
M = 1.44

PREDICTED CURVE :

1200.0000	.13654877
1800.0000	.13655126
2400.0000	.13663980
3000.0000	.13747101
3600.0000	.14149275
4200.0000	.15409093
4800.0000	.18294172
5400.0000	.23493786
6000.0000	.31237163
6600.0000	.41097541
7200.0000	.52106953
7800.0000	.63092352
8400.0000	.73035005
9000.0000	.81294814
9600.0000	.87654035
10200.000	.92227626
10800.000	.95320936
11400.000	.97299506
12000.000	.98502150
12600.000	.99199726
13200.000	.99587242
13800.000	.99794073
14400.000	.99900438
15000.000	.99953271
15600.000	.99978675
16200.000	.99990524
16800.000	.99995095
17400.000	.99998264
18000.000	.99999383

Predicted breakthrough data

experimental Run 23

```
KF , L , B , K , V , M
   DATA ENTERED ARE AS FOLLOWS :

                    KF =  .8139999 98-005
                    L  =    .390
                    B  =  .7499999 99-003
                    K  =   9.700
                    V  =  .3780000 01-003
                    M  =  1.44
  PREDICTED CURVE :

1200.0000       .1 2919410
1800.0000       .1 2919705
2400.0000       .1 2927553
3000.0000       .1 2995291
3600.0000       .1 3307652
4200.0000       .1 4268459
4800.0000       .1 6475856
5400.0000       .2 0533367
6000.0000       .2 6777990
6600.0000       .3 5085158
7200.0000       .4 4863005
7800.0000       .5 5228360
8400.0000       .6 5262087
9000.0000       .7 4230054
9600.0000       .8 1697188
10200.000       .8 7532482
10800.000       .9 1838837
11400.000       .9 4855842
12000.000       .9 6871480
12600.000       .9 8160632
13200.000       .9 8952620
13800.000       .9 9421372
14400.000       .9 9689357
15000.000       .9 9837691
15600.000       .9 9917348
16200.000       .9 9958926
16800.000       .9 9980056
17400.000       .9 9990529
18000.000       .9 9995595
```

APPENDIX C

CALIBRATION CURVES

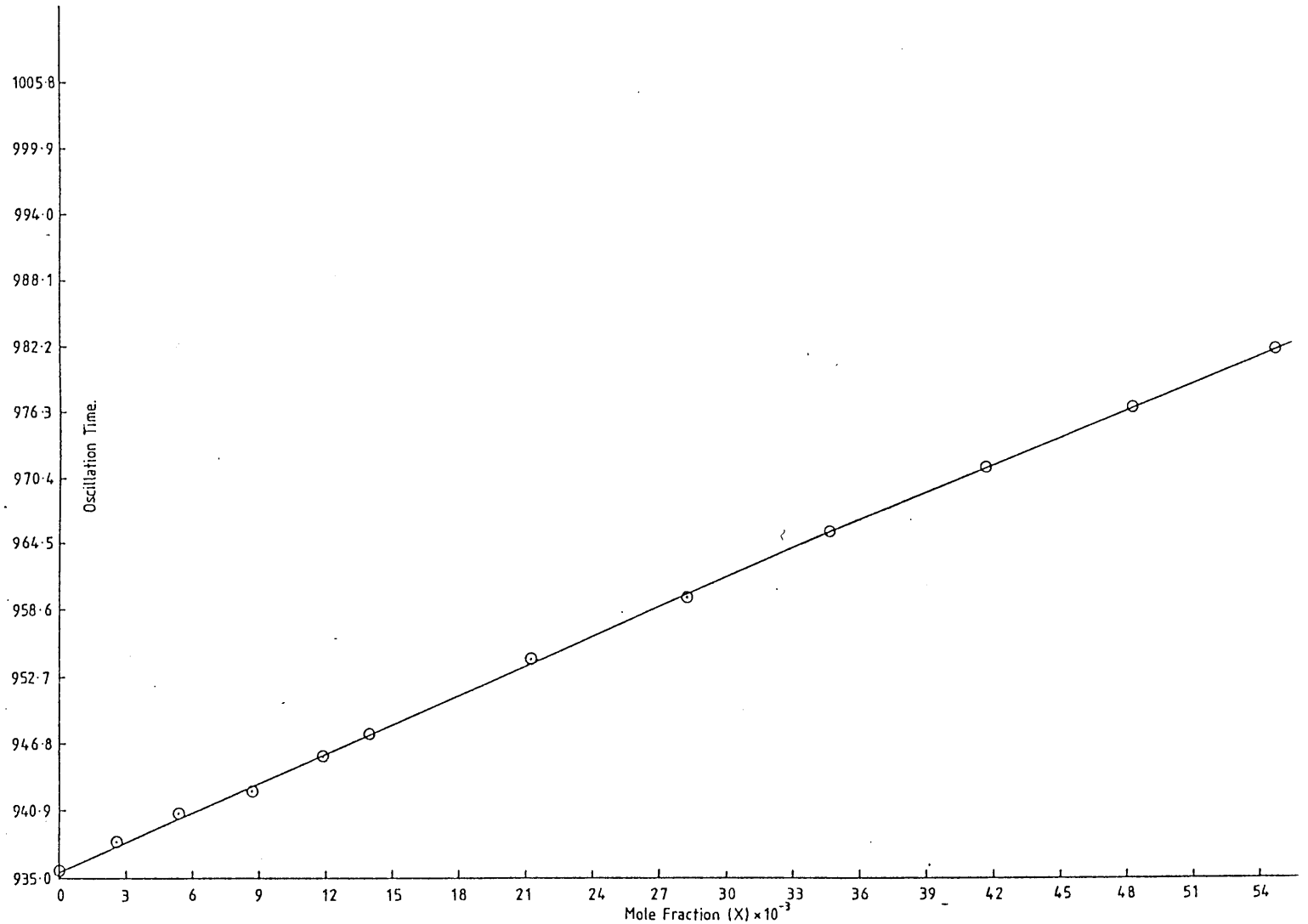

Figure C.1. Calibration curve for n-dodecane - isooctane solution using density meter at 25°C

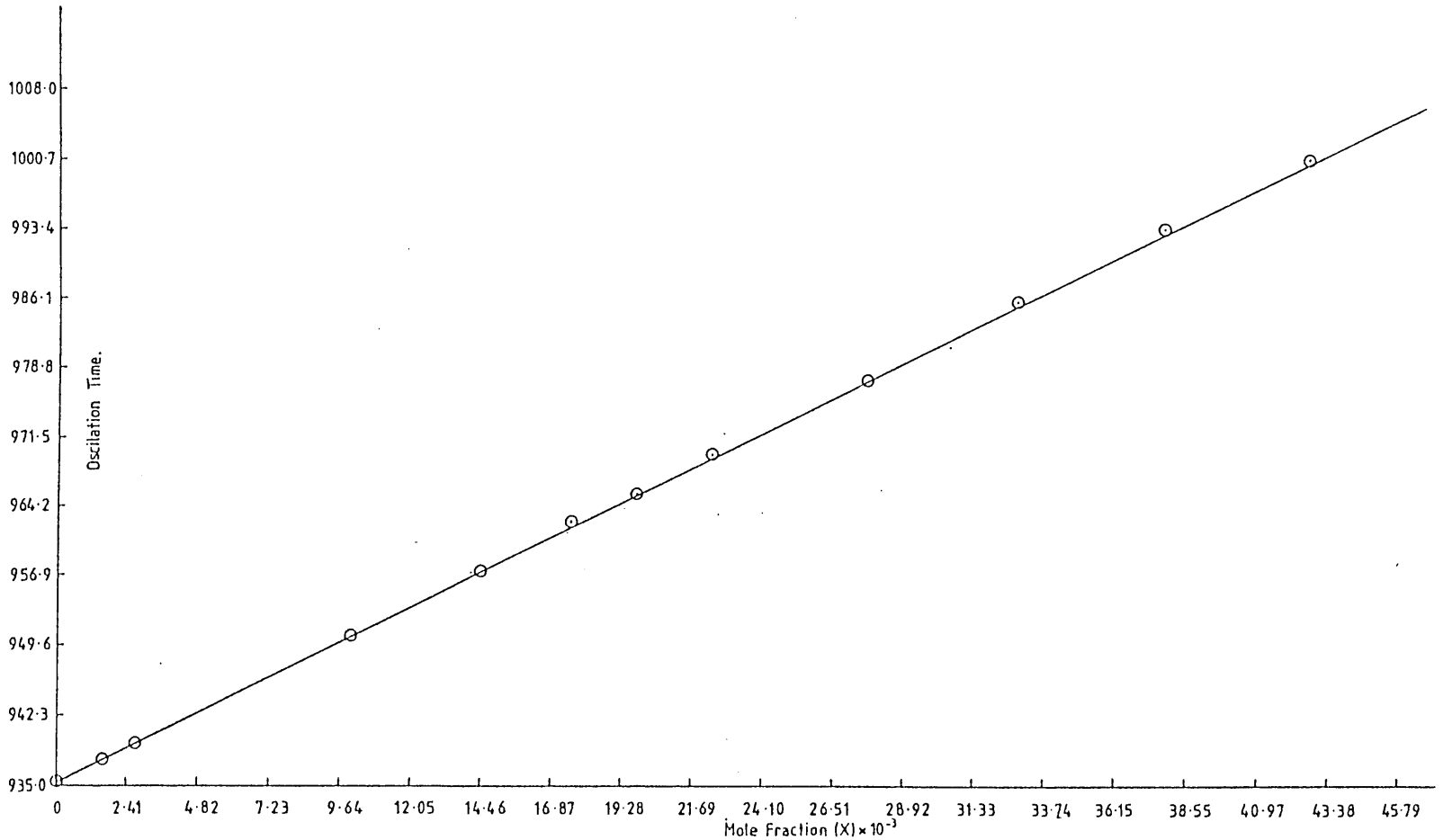

Figure C.2 Calibration curve for n-hexadecane - isooctane solution using density meter ar 25^{O}C

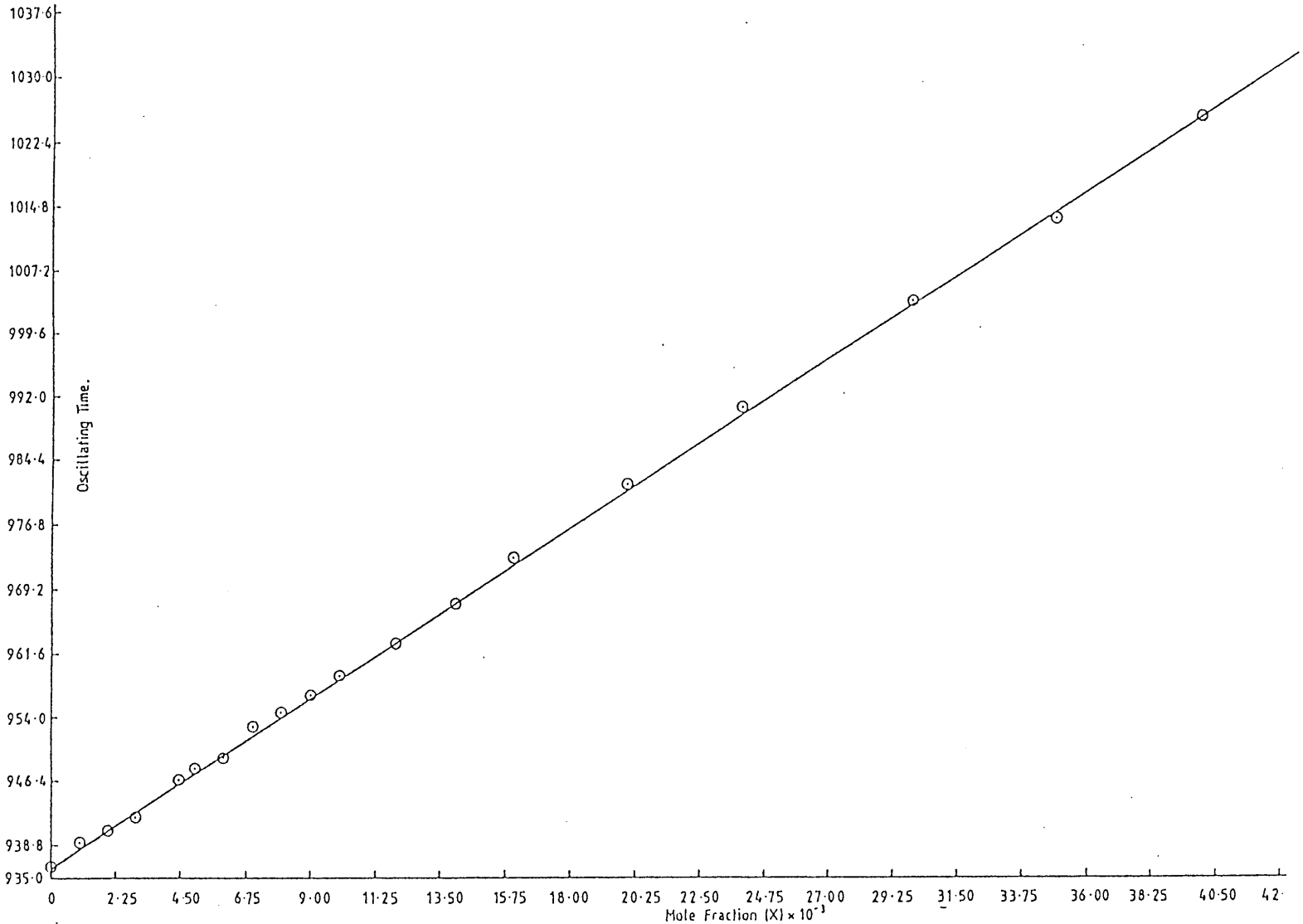

Figure C.3. Calibration curve for n-eicosane — isooctane solution using density meter at 25°C

NOMENCLATURE

A	Cross-sectional area, m^2
a_m	Maximum amount of component adsorbed filling the cavities of 1gm of zeolite
a	External surface area per unit particle volume, $^{m^2}/_{m3}$
b	Langmuir energy term, $^{m^3}/_{mol}$
β	Coefficient of mutual displacement
C	Concentration of solute in solution, $^{mole}/_{m3}$
C_S	Saturation concentration of solute in solution, $^{mole}/_{m3}$
C*	Fluid concentration at the external surface of the solid
C_o	Initial concentration, $^{mole}/_{m3}$
D_e	Effective diffusivity, $^{m^2}/_s$
D_m	Molecular diffusivity, $^{m^2}/_s$
D	Diffusivity, $^{m^2}/_s$
D_o	Constant
d_p	Particle diameter, m
E	Activation energy, $^{kJ}/_{mole}$
f	Fractional ability of adsorbent within the adsorption zone to adsorbe additional solute (dynamic study)
f	Separation function, a function characterizing the collective interactions occurring in zeolite-solution system (batch study)

ΔF	Free energy change, $^{kJ}/_{mole}$
G	Adsorption value, $^{mole}/_{kg}$
G_t	Adsorption value at time t, $^{mole}/_{kg}$
G_∞	Adsorption value at equilibrium , $^{mole}/_{kg}$
G_o	Adsorption value at time 0, $^{mole}/_{kg}$
G_m	Experimental limiting adsorption value, $^{mole}/_{kg}$
G_{t/G_∞}	Relative adsorption
G_s	Superficial mass flow rate of solute-free solvent $^{kg}/_{hr.\ m2}$
ΔH	Enthalpy change, $^{kJ}/_{mol}$
K	Equilibrium constant
K_ya	Overall mass transfer coefficient, $^{kg}/_{hr.\ m3}$
k_ya	External mass transfer coefficient, $^{kg}/_{hr.\ m3}$
k_pa	Solid-phase mass transfer coefficient, $^{kg}/_{hr.\ m3}$
k_f	External fluid film mass transfer coefficient $^{m}/_{s}$
LUB	Length of unused bed, m
L_s	Length of equilibrium section , m
L_o	Length of the adsorbent bed, m
M	Molecular weight, g/mole
m_s	Weight of molecular sieves, kg
MRPD	Mean relative percent deviation
n	Total number of moles in solution, mole
N_t	Number of overall mass transfer units
q	Concentration of sorbate in the solid, mole/kg

$\bar{q}$	Average concentration of sorbate in the particle, mole/kg
q^*	Concentration of sorbate in the solid in equilibrium with C
q_{iso}	Isosteric heat of adsorption, kJ/kg^{o}K
Q_a	Quantity of solute adsorbed between the breakthrough and exhaustion points, kg
R	Gas constant
R_p	Average radius of particles, m
Re	Reynolds number
ΔS	Entropy change, kJ/mole ^{o}K
Sc	Schmidt number
Sh	Sherwood number
T	Absolute temperature, ^{o}K
t	Time, hr
TDC	Total dynamic capacity, kg solute/kg adsorbent
U	Interstitial velocity of the fluid, m/s
V_t	Volumetric flow rate, m^3/s
W_a	Solute-free effluent collected between the breakthrough and the exhaustion points, kg.
W_e	Total solute-free effluent collected up to the exhaustion point, kg
X	Concentration, mole fraction
X_o	Initial mole fraction
Y	Concentration of fluid at any point in the adsorption zone,

kg solute/kg solvent

Y_b Concentration of fluid at breakthrough point, kg solute/kg solvent

Y_e Concentration of fluid at exhaustion point, kg solute/kg solvent

Y^* Concentration of fluid at equilibrium with adsorbent at any point in the adsorption zone, kg solute/kg solvent

Y_o Feed concentration, kg solute/kg solvent

Z Bed height, m

Z_a Height of adsorption zone, m

μ Viscosity, cp

ε Voidage of adsorbent bed

ε_p Internal porosity of the particle

τ Tortuosity

ρ Density, kg/m^3

ρ_b Bed density, kg/m^3

θ_a Time required for the adsorption zone to move it's own height down the column

θ_b Breakthrough time, s

θ_E Time required for the adsorption zone to establish itself and move out of the bed

θ_s Stoichiometric breakthrough time, s

θ_F Time required for formation of the adsorption zone

REFERENCES

1. Freund M, Csikos R, Keszthelyi S and Moses GY, Paraffin Products, Properties, Technologies, Applications, Elsevier Scientific Publishing Company, N.Y. (1982).

2. Report No. 55, by the Process Economics Program., St. Res. Inst., Menlo Park, California, Oct. 1969.

3. Shukla RP, Singhal AK, Saraf DN, Indian Chemical Engineer, XXI(2), 13 (1979).

4. Thomas TL, Molecular Sieves in Petroleum and Natural Gas Processing, World Petrol. Congress, 6th Frankfurt/Main, June 26, 1963.

5. Bennett H, Industrial Waxes, Chemical Publishing Comp., New York, (1975).

6. Al-Ameeri RS, Owaysi FA, Ind. Eng. Chem. Prod. Res. Dev., 23 (4), 634 (1984).

7. Hassan AM, The Adsorption of Straight Chain Hydrocarbons from Ternary Liquid Solution by 5A Molecular Sieves Crystals, PhD Thesis, Cornell University (1975).

8. Collins JJ, Chem Eng. Progr., 64, 8, (1968).

9. Sodhi JS, Chandra D, Petroleum and Hydrocarbons 4, (4), (1970).

10. Hirsch CK, Molecular Sieves, Reinhold Publishing Corp., N.Y., (1961).

11. Norman NL, Recent Development in Separation Science, Chemical Rubber Company Press, New Jersey (1976).

12. Hiester NK and Vermeulen T, Chem. Eng. Prog., 48, 505, (1952).

13. Ruthven DM, Loughlin KF, Chem. Eng. Sci., Vol. 26, (1971).

14. Breck DW, Zeolite Molecular Sieves Structure Chemistry and Use, John Wiley Interscience (1974), New York, USA.

15. Gorring RL, J. of Catalysis 31, 13-26 (1973).

16. Breck DM, Eversole WG, Milton RM, Reed TB, Thomas TL, J. Amer. Chem. Soc., (1956) 78, 5963.

17. Reed TB, Breck DW, J. Amer. Soc., (1956), 78, 5972.

18. Union Carbide Molecular Sieves, Distributed by Fluka AG Chemische Fabrik.

19. Roberts PV, York R, Ind. Eng. Chem., Process Design Develop., 6, (1967).

20. Myers HS, Hipkin HG, Petroleum Refiner, 35, (7), 175, (1956).

21. Pavlyuchenko KV, Dokl. Akad. Nauk Belorussk. SSSR, 8, 8, (1964).

22. Fleck RN, Union Oil, US 2, 925, 379, (Feb. 16, 1960).

23. Ebdon JF, Gas, 41, 8, p.79, (1965).

24. Clark EL, Oil & Gas J., 57, 120-123, (Apr. 1959).

25. Miab JN, Chen NY, Weisz PB, J. Catalysts, 6, 2, 278-287 (1966).

26. Stormount DN, Oil & Gas J, 62, 50-53, (Nov. 1964).

27. Stormount DN, Oil & Gas J., 65, 15, 149-175 (1967).

28. Cheadle GD, Welsh CJ, Lappin TA, Dana PM, Oil & Gas J., 64, 29, 76, (1966).

29. Ruthven DM, Principles of Adsorption and Adsorption Processes, Wiley - Interscience Publication, (1984).

30. Satterfield CN, Cheng CS, A.I.Ch.E.J., 18, 4, July (1972).

31. Vermeulen T, Advances in Chemical Engineering, 2, (1958).

32. Gleuckauf E, Coates JJ, J. Chem. Soc., 149, (1947).

33. Schumacher WH, The Separation of Hydrocarbons by Adsorption in Fixed-Beds of Molecular Sieves, PhD Thesis, Cornell University, (1975).

34. Langmuir I, J. Amer. Chem. Soc., 38, 2221, (1916).

35. Keinath TM & Wanielista MP, Mathematical Modelling for Water Pollution Control Processes, Ann Arbor, Mich. Ann Arbor Science Publishers (1975).

36. Eltekov YA, Kiselev AV, Molecular Sieves Series, University of London, UK, (1967).

37. Falkovich MI, Eltekov YA, Chernozhukov NI, Translated from Khimiya Technologiya Tapliv i Masel, No.12, December (1968).

38. Hattori T, Akizuki I, Kamogawa K and Murakami Y, Fifth International Conference on Zeolite, Naples, Italy, June, (1980).

39. Eberly PE, Zeolites Chemistry and Catalysis, Rabo JA, Editor, A.C.S. Monograph 171 (7), 392 (1976).

40. Michaels AS, Ind. Eng. Chem., 44, 1922 (1952).

41. Collins JJ, Chem. Eng. Prog., Symp. Series No. 74, 63 (1967), 31.

42. Treybal RE, Mass Transfer Operations, McGraw-Hill, 3rd Ed., N.Y. (1980).

43 Schumacher WT, York R, I & EC Process Design and Development Vol. 6, No. 3, July (1967).

44. Satterfield CN, Mass Transfer in Hetrogeneous Catalysis, M.I.T., (1970).

45. Weigel O, Steinhoff EZ, Z. Kristallogr. Kristallgeometric. Kristallphys. Kristallchem., 61, 125 (1924).

46 Sundstrom DW, Krautz FG, J. Chem. Eng. Data, 13, 223, (1968).

47. Satterfield CN, Smeets JK, A.I.Ch.E.J., Vol. 20, 31, p.618, (1974).

48. Asher WJ, Campbell ML, Hydrocarbon processing, Vol. 48, No.1 (1969).

49. Phillips JR, Chem. Eng. Prog. Symp. Series, Vol. 65, No. 96, (1969)

50. Ruthven DM, Loughlin KF, J. Chem. Soc., Faraday Trans., 68, 696, (1972).

51. Ruthven DM, Vaulitis AP, Loughlin KF, J. of Colloid and Interface Science, Vol. 84, No. 2, (1981).

52. Falkovich MI, El'tekov YA, Chernozhukov NI, Translated from Khimiya Technologiya Topliv i Masel, Feb. (1969).

53. Nelson KH, Walker RD J. Appl. Chem., 11, 358 (1961).

54. Kehat, E, Rosenkranz Z, Ind. Eng. Chem, Proc. Des. Dev., 4, 217, (1965).

55. O'Connor JG, Brurow FH, Norris MS, Analytical Chem., Vol. 29, No. 7,

July, (1957).

56. Kehat E, Heineman M, Ind. Eng. Chem. Process Des. Develp. Vol 9, No.1 (1970).

57. Gupta RK, Kunzru D, Saraf DN, J. Chem. Data, 25, (1980).

58. Satterfield CN, Cheng CS, A.I.Ch.E.J., 18, 720, (1972).

59. Ruthven DM, A.I.Ch.E.J., 22, 753, (1976).

60. Peterson DL, Redlich O, J. Chem. Eng. Data, 7, 570, (1962).

61. O'Connor JG, Norris MS, Anal. Chem., 32, 701, (1960).

62. Burgess CG, Duffett GJ, Minkoff, Taylor RG, J. Appl. Chem., 14, Aug., (1964).

63. Barrer RM, Ibbitson DA, Trans. Faraday Soc., 40, 195, (1944).

64. Satterfield CN, Cheng CS, A.I.Ch.E. Sym. Ser., No. 117, Vol. 67, (1971).

65. Yakimova AV, Astakhov VA, Lokin VD, Jon. of Applied Chem. of the USSR, Vol. 54, No. 10, 2316-18, (1981).

66. Al-Zaid KA, The Adsorptive Separation of Aromatic Hydrocarbon Mixtures, PhD Thesis, Univ. of Aston in Birmingham, UK, (1987).

67. Al-Damkhi AM, Separation of n-Paraffins by Selective Adsorption, PhD Thesis, Univ. of Aston in Birmingham UK, (1986).

68. Antonson CR, Dranoff JS, Chem. Eng. Prog. Sym. Ser., Vol. 63, No. 74, (1967).

69. Antonson CR, Dranoff JS, Chem. Eng. Prog. Sym. Ser., Vol. 65, No. 96,

(1969), p.27.

70. Rosen JB, J. Chem. Phys., 20, 387, (1952).

71. Thomas HC, J. Am. Chem. Soc., 66, (1944).

72. Hougen OA, Marshall WR, Che. Eng. Prog., 43, (1947).

73. Antonson CR, Dranoff JS, Chem. Eng. Prog. Sym. Ser., Vol. 65, 96, (1969), p.20.

74. Hasanain MA, Hines AL, Cooney DO, A.I.Ch.E. Sym. Ser., No. 230, Vol. 79, (1983), p.60.

75. Barrer RM, Brook DW, Trans. Faraday Soc., 49, 1049 (1953).

76. Reid RC, Praunitz JM, Sherwood TK, The Properties of Gases and Liquids, 3rd ed., McGraw-Hill, N.Y. (1977).

77. American Pet. Inst., Selected Values of Physical and Thermodynamic Properties of Hydrocarbons and Related Compounds, Project 44, Carnegie Press, Pittsburgh, Pa. (1953).

78. Egloff G, American Chem. Soc. Monograph Ser., Vol. 1, Reinhold Publ. Corp.

79. Ziegenhain WC, Refining Engr. 29, C-6-C-12, (Aug. 1957).

80. Chi CW, Lee H, Chem. Eng. Prog. Sym. Ser., No. 96, Vol. 65, (1969), p.65.

81. Radke CJ, Prausnitz JM, Ind. Eng. Chem. Fund., 11, 445, (1972).